

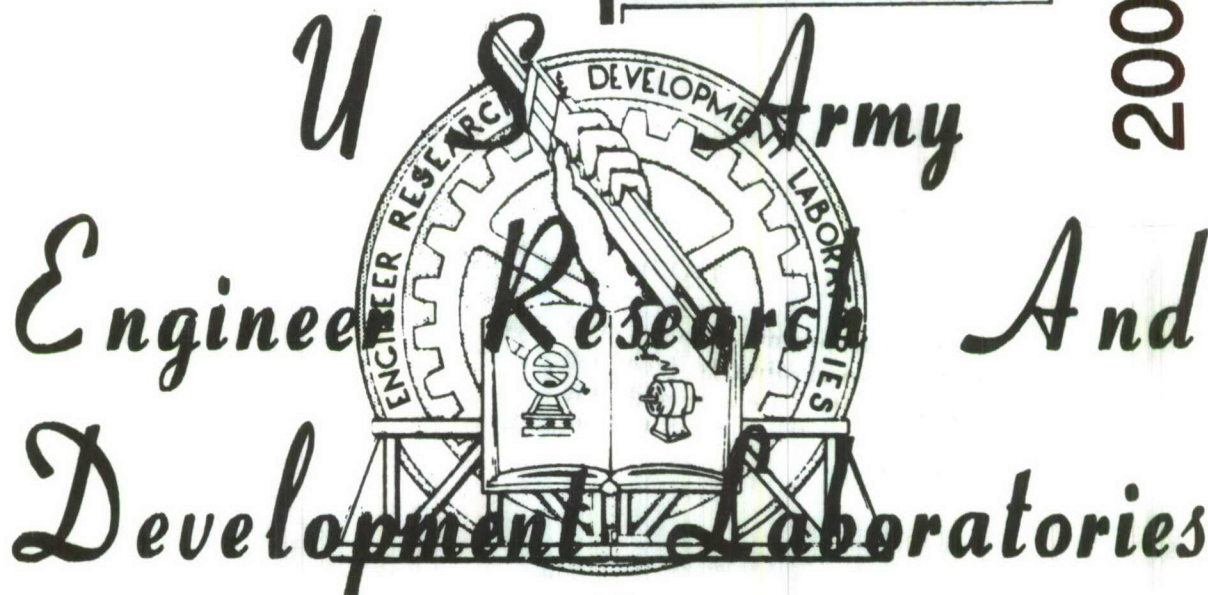
DEPARTMENT OF THE ARMY
U. S. ARMY MOBILITY COMMAND

*not in DTIC
29 Jan 82*

**PROCEEDINGS OF THE
TWELFTH BASIC RESEARCH GROUP
CONTRACTORS' CONFERENCE
and
SYMPOSIUM**

6 - 8 November 1963

20080710 002



FORT BELVOIR, VIRGINIA

DDC AVAILABILITY NOTICE

U. S. Government agencies may obtain copies of this report directly from DDC. Other qualified DDC users should request thru Commanding Officer, USAERDL, Ft. Belvoir, Virginia.

AD 613076

PROCEEDINGS OF THE
TWELFTH BASIC RESEARCH GROUP
CONTRACTORS' CONFERENCE
and
SYMPOSIUM

6-8 November 1963

U. S. Army Engineer Research and Development Laboratories
Fort Belvoir, Virginia

Sponsored by

Project 8X99-25-001-41
U. S. Army Engineer Research and Development Laboratories
Fort Belvoir, Virginia

Prepared by

M. D. Kemp
Basic Research Group, USAERDL

THE VIEWS CONTAINED HEREIN REPRESENT
ONLY THE VIEWS OF THE PREPARING AGENCY
AND HAVE NOT BEEN APPROVED BY THE
DEPARTMENT OF THE ARMY.

INTRODUCTION

The Twelfth Basic Research Laboratory Contractors' Conference and Symposium was held on 6-8 November 1963 at USAERDL, Fort Belvoir, Virginia. The proceedings of this conference are issued in order to afford government agencies and laboratories the benefit of its transactions.

Although the majority of the papers presented at this year's conference were contributed by staff members of the Basic Research Laboratory and their contractors, several scientists working in allied areas were asked to present invited papers. It is considered appropriate to extend our thanks to the authors and to those who contributed to the discussions of the symposium. Thanks also go to the authors of the invited papers because their contributions enhanced the value of the symposium.

In order to gain more time for discussions, preprints of the papers or their extended abstracts were solicited from the contributors to the symposium and placed at the disposal of all attendees of the conference prior to the opening date. Thus, the issue of the preprints permitted the presentation of additional papers and more time for discussion. It was suggested to the authors that they read a synopsis rather than the whole paper. From the comments of the number of attendees, it can be concluded that this procedure was very successful.

With a few exceptions, all papers presented at the symposium appear in these proceedings as full-length papers. Those who preferred to publish their work elsewhere submitted extended abstracts for inclusion in this volume. As in the past, the discussions that followed each paper were not tape-recorded and, therefore, not included in this volume.

It was tentatively decided to hold the Thirteenth Basic Research Laboratory Contractors' Conference and Symposium in the Fall of 1964, again at USAERDL, Fort Belvoir, Virginia. It seems advantageous to hold the conference at Fort Belvoir since many participants come from the Washington, D. C., area and from the Eastern Seaboard.

An informal expression of opinion from all participants of this conference would be very much appreciated so that we can improve the conference next year. Especially desirable would be comments concerning the inclusion of the discussions into next year's proceedings.

Z. V. HARVALIK
Director
Basic Research Group

CONTENTS

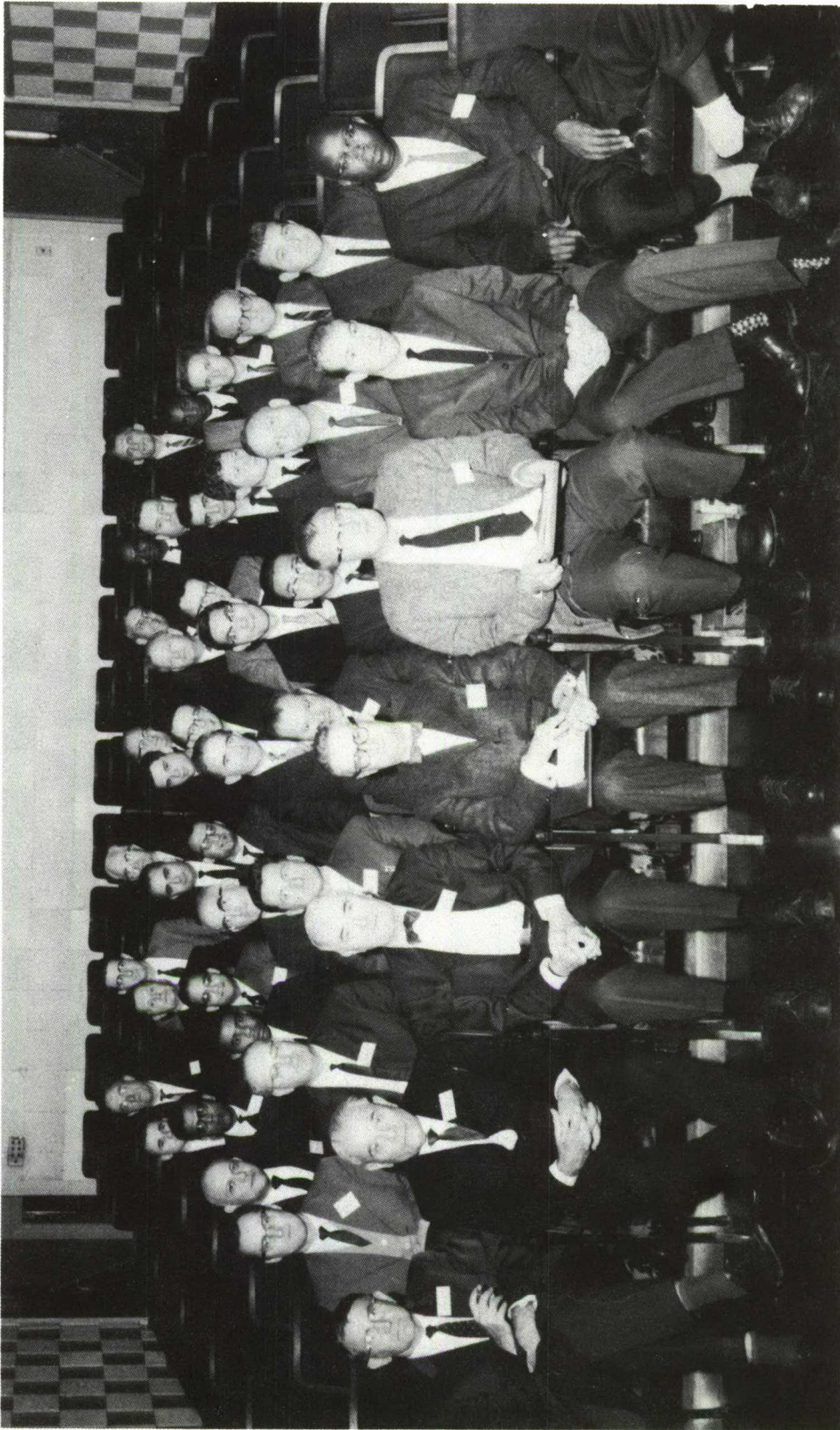
	<u>Page</u>
THE IMPACT OF ARMY RESEARCH by Dr Harold C. Weber	1
STUDY OF PREPARATION AND PROPERTIES OF AZIDES by A. Forsyth, P. J. Kemmey, R. Manno and V. R. Pai-Verneker	5
PROPERTIES AND REACTIVITIES OF DIFFERENTLY PREPARED NaN_3 AND $\text{Ba}(\text{N}_3)_2$ by K. Torkar	11
THE PREPARATION AND PROPERTIES OF SOME NOVEL LIGHT METAL AZIDES by K. Terada, A. J. Erbel, and F. M. Brower	21
FURTHER STUDIES ON THE THREE COMPONENT SYSTEM IN PURIFICATION by James L. Taylor	39
FURTHER OBSERVATIONS ON THE GROWTH OF ALPHA LEAD AZIDE CRYSTALS by M. D. Kemp	49
THE MECHANISM OF UPTAKE OF IMPURITIES BY AZIDE CRYSTALS by M. Blais and V. R. Pai-Verneker	65
AN ELECTRON MICROSCOPIC INVESTIGATION OF THE THERMAL DECOMPOSITION OF NaN_3 AND KN_3 CRYSTALS by J. A. Joebstl	73
THE GAS PHASE DECOMPOSITION OF SIMPLE ORGANIC AZIDES by M. S. O'Dell and B. deB. Darwent	89
DECOMPOSITION OF ALKALINE EARTH AZIDES UNDER ORGANIC SOLVENTS by Y. Okamoto, J. C. Goswami and W. Brenner	91
KINETIC STUDIES ON THE REACTION BETWEEN AZIDES AND METAL IONS by Heinrich C. Egghart	95
PROPERTIES OF MOLTEN AZIDES: DATA ON BINARY SYSTEMS OF MONOVALENT INORGANIC AZIDES by H. J. Mueller and J. A. Joebstl	103

CONTENTS (cont'd)

	<u>Page</u>
SOME COMMENTS ON THE AZIDE REACTION by Henry Eyring	109
THE CRYSTAL STRUCTURE OF α -LEAD AZIDE by Gerald L. Glen	113
CRYSTAL STRUCTURE CHANGE OF SODIUM AZIDE AT 19° C by B. S. Miller and G. J. King	125
NITROGEN NMR CHEMICAL SHIFTS IN THE AZIDE ION by R. A. Forman	129
THE PHOTOCHEMICAL DECOMPOSITION OF SODIUM AZIDE by P. W. M. Jacobs, A. R. T. Kureishy and F. C. Tompkins	131
PARAMAGNETIC RESONANCE OF Mn^{++} IN SODIUM AZIDE by G. J. King and B. S. Miller	145
ELECTRON PARAMAGNETIC RESONANCE OF NITROGEN ATOMS IN ALKALI METAL AZIDES by Frederick F. Carlson	151
ELECTRON SPIN RESONANCE OF POTASSIUM COLLOIDS IN KN_3 by Robert C. McMillan	157
THE STUDY OF TRANSIENT ABSORPTION SPECTRA OF AZIDES BY MEANS OF A FAST RECORDING SPECTROMETER by G. D. Singer and H. J. Mueller	163
AZIDE RESEARCH AT ARKANSAS POLYTECHNIC COLLEGE by Jack G. Dodd	173
EXCITATION OF LATTICE VIBRATIONS BY IMPACT by Masataka Mizushima	181
FURTHER DEVELOPMENTS IN THE STATISTICAL THEORY OF EXPLOSION INITIATION by Daniel S. Ling, Jr	205
SOME FACTORS AFFECTING IMPACT SENSITIVITY by W. C. McCrone	219

CONTENTS (cont'd)

	<u>Page</u>
INFRARED STUDIES OF ORGANIC AZIDES by Eugene Lieber and C. N. R. Rao	225
AZIDO-COMPLEXES IN NON-AQUEOUS SOLUTIONS by V. Gutmann, G. Hampel and O. Leitmann	235
INFRARED SPECTROSCOPIC EVIDENCE FOR THE SPECIES NH by Dolphus E. Milligan and Marilyn E. Jacox	247
GROUP THEORETICAL ANALYSIS OF THE VIBRATIONAL SPECTRUM OF IMPURITIES IN CRYSTALS by L. A. Veguilla-Berdecía and George C. Turrell	251
MOLECULAR SPECTROSCOPY IN THE BASIC RESEARCH LABORATORY by James I. Bryant	257
APPENDIX I Attendance List	273
APPENDIX II Program	275
AUTHOR LIST	279
DISTRIBUTION LIST	281



Attendants at Basic Research Laboratory Twelfth Contractors' Conference and Symposium, Motion Picture Laboratory, 6 November 1963 (left to right):

1st Row: Z. V. Harvalik, H. P. Kallmann, H. C. Weber, E. Lieber, C. J. Cook, F. F. Carlson,
M. D. Kemp

2nd Row: H. Egghart, K. Torkar, V. Gutmann, H. Rosenwasser, K. Terada, F. M. Brower,
F. E. Wawner

3rd Row: H. J. Mueller, A. J. Coleman, R. McGill, D. G. Burkhard, Y. Okamoto, P. L. Kronick,
W. Jorgensen

4th Row: A. R. T. Kureishy, S. K. Deb, V. R. Pai-Verneker, P. Marinkas, G. L. Glen, R. Manno,
P. J. Kemney

5th Row: G. Singer, H. Fisher, D. Mergerian, R. C. Forman, H. D. Poole, A. Forsyth,
J. L. Taylor

6th Row: G. J. King, S. J. Magrum, W. I. Grieve, E. Gelerinter, V. M. Davis, M. S. O'Dell,
R. C. McMillan

THE IMPACT OF ARMY RESEARCH

by

Dr. Harold C. Weber
Chief Scientific Advisor
U. S. Army, OCRD
Washington, D. C.

I hardly believe it necessary to inform this audience of the value of research. Research might be defined as "any critical or exhaustive investigation having as its aim the uncovering of new facts and their interpretation." All knowledge can be useful and as far as the Army is concerned, all knowledge is useful. I know of no organization or group where the search for new knowledge covers such a wide spectrum as does that of Army research. We of the Army are interested in what is new in space, in the atmosphere, on the earth and under the earth. We want to know all about how different people react to different conditions, how disease, both physical and mental, effects humans. We are vitally interested in education and educational methods since we have a staggering problem on our hands of educating our men not only to operate and maintain our ever more complex equipment but also to cope successfully language-wise and custom-wise with the peoples of almost any part of the world, not to mention the more prosaic role of the Army as an operating fighting unit with its multitude of modern equipment.

You provide us with new information in any field and we will have a use for it -- we may not have the money to put your idea to use -- repeatedly, we find it necessary to at least temporarily forego the application of new information because of a limited amount of money; but this is as it should be. We must choose first things first.

The Army has always had a deep-rooted interest in Research. The U. S. Military Academy was the first and for many years the only engineering school in the country. The story of its many graduates who became professors and Presidents of our Universities is most interesting. Even today, its graduates are found throughout the administrative staffs of many of our leading educational and research institutions. As early as 1798, Eli Whitney was awarded a contract by the U. S. Government to develop a system for manufacturing interchangeable parts for the production of firearms in Army arsenals. The results of this work were fundamental to developing the industrial revolution and thus were a start in the growth of our modern mass production concepts. The reputation in research made by various Army research centers, such as Picatinny Arsenal, Watertown Arsenal, and the Walter Reed Institute, to mention but three out of many, was

and is outstanding, particularly when we remember these centers were already engaged in research during an early period when industry as a whole was not too strongly research oriented.

As was true in so many industries, it was the second World War that really focused the Army's attention on the outstanding importance of uncovering new information. Probably, this interest was sparked by the signal success of the Manhattan Project's work on atomic energy and the Radiation Laboratories' advances in electronics. Very quickly research was recognized as a most important segment of Army activity and an organization was built to assure Army's position as a leader in all areas of research activity. Not only was the number and scope of the Army laboratories greatly expanded but in addition, the important and authoritative positions of Assistant Secretary of the Army for Research and Development, Chief of Research and Development (a position carrying the rank of a 3-star general) and the various positions of Chief Scientist were established.

Today, the Army is spending a total of one billion, four hundred and sixty-nine million, nine hundred thousand dollars on research and development in 38 Army operated laboratories, as well as in a very large number of industrial and educational centers.

I can assure you, the Army laboratories are supplied with the most modern equipment and are staffed with more than their share of outstanding leaders in the various scientific fields. Such an organization, working as it does in close cooperation with your research centers, cannot fail in keeping us in the forefront.

The money you, as taxpayers, spend on Army research and development pays dividends twice over. Of course, the first and most necessary job for the defense establishment is to provide for the defense and security of the United States. But, there are extra and often unexpected returns from defense research.

You are probably aware of many contributions Army R&D has made to all the sciences -- the life, environmental, physical and social sciences -- and the ultimate applications of these to society at large. Some Army firsts are less well known, such as the pressurized container which dispenses your shave cream, or the anti-icer you spray on your car's windshield -- even Metrecal.

A "first" I want to tell you about is the electronic digital computer. Scientists now wonder how they ever got along without it. As is so true of the many firsts, along the road of scientific and technological progress, the stimulus that produced and sustained the crucial effort was provided by the extraordinary demands of war. The problems of war are seldom essentially new problems. What is

different in wartime is the concentrated marshaling of available talent -- both government and private -- to meet old challenges that have come to assume life or death proportions.

Such an old challenge was the omni-present Army problem of the computation of firing and bombing tables for the Artillery and the Air Corps. This job had been the responsibility of a handful of skilled civilians at the Ballistic Research Laboratory at Aberdeen Proving Ground. The job was time-consuming and undoubtedly would have become unwieldy in the event of America's involvement in war with the Axis powers. Therefore, many avenues of potential improvement were explored from 1940 on; but the first positive step was taken in 1942 with the proposal of a contract to the Moore School of Electrical Engineering of the University of Pennsylvania.

The original \$61,700 contract called for six months of "research and development of an electronic numerical integrator and computer", from which was coined the acronym of the final product, ENIAC. The original contract called for a report only, but nine supplementary contracts and a grand total of \$486,804.22 produced a working pilot model of an electronic digital computer by 1946.

By today's standards, the ENIAC was an awkward monster. Its thirty separate units, plus power supply and forced-air cooling, weighed over thirty tons. Its 19,000 vacuum tubes, 1,500 relays, and hundreds of thousands of resistors, capacitors, and inductors consumed almost 200 kilowatts.

But ENIAC was the prototype from which most other modern computers evolved. The Army's original \$400,000 plus investment has had a pay-off to the civilian economy so large that one would need a modern high speed computer to calculate it. We do know that the present computer industry is a direct descendant of Army-sponsored research and we are proud of this. Parts of the original ENIAC were placed in the Smithsonian recently, to commemorate the Army's electronic marvel that became, thanks to the genius of our public-private partnership in research, an antique in 15 short years.

The advances made by Army medical research are widely known from the conquest of yellow fever to the development of a whole series of modern vaccines to control many of the diseases to which mankind is subject. For example, the new smallpox vaccine (based on both British and American Army research) can be stored for as long as 3 years at room temperature without loss in potency. In fact, if any of you have been vaccinated recently, you may have found the "take" more real than any of those you have experienced formerly. Some mustard gas derivatives are used to give increased life span to those suffering from leukemia. Most of the progress in development of artificial limbs is due largely to the continuing research the Army does in the field.

In the area of food processing, because of extensive research, the Army is ever in the forefront. The newer dried soups and other foods are based, in part, on work started by the Army years ago. Soon you may be eating "fresh" meats and vegetables which can be stored for years in plastic packages without refrigeration because of the work done by Army scientists in processing foods by nuclear radiation.

In communications, the Army has always been a leader. It pioneered in the use of the Armstrong regenerative circuit during the first World War (Armstrong was a Major during this conflict) and in the commercial development of the vacuum tube. These two made possible practical radio telephony and broadcasting. Later Army research funds aided in the development of transistors and the miniaturized receivers which some of you may be carrying in your pockets. Army money added to that from the defense establishment actually made possible present day television through the development of war-time radar equipment.

One can multiply the number of "spin-offs" to cover educational methods, pharmaceuticals, metallurgy and advances in materials of construction, to mention but a few.

Modern research has become so expensive and the tools needed, in many instances, so complex and cumbersome that no single company or indeed group of companies could afford to take the financial risk of the possible large expense and long term required for successful completion. Rocket and space research are areas in question. As technology progresses ever larger and more complex, developments are sure to appear. Thus, it would seem inevitable that government research should take an even greater and more important position in the country's research effort. Perhaps an ever greater number of patents will be issued to workers in government installations. Some sort of licensing procedure may have to be worked out. It has seemed to me that patents have become less important as technology has developed and perhaps in the future they will become even less important. At any rate, industry and government are irretrievably locked in a united technological effort. Without such a partnership the scientific progress we hope for is well nigh impossible. Such a partnership will make a lasting imprint on our economic system -- it already has. I see nothing alarming or startling in this. To me it is progress and progress is something we must have if we are to retain our leadership. I am sure we are entering an era of unprecedented technological and economic advancement.

STUDY OF PREPARATION AND PROPERTIES OF AZIDES

by

A. Forsyth, P. J. Kemmey, R. Manno and V. R. Pai-Verneker
Picatinny Arsenal
Dover, New Jersey

Physical and chemical properties of azides have been investigated by various schools^{1,2,3} and interesting results have been presented. A detailed review of the solid state effects, however, suggests that quite a number of the effects one observes in azides as in many other solids are primarily caused by the presence of impurities. It was, therefore, decided to make a comparative study of the different methods and then try to prepare extremely pure azides (wherein the impurity content would be less than one part per million). In this work we have studied the preparation of KN_3 , NaN_3 , BaN_6 and PbN_6 . Hydrazoic acid itself is prepared by several methods although the principle involved is the same. If one adds a solution of NaN_3 to sulphuric acid HN_3 is obtained. Preparation of HN_3 by ion exchange is also well known. Recently Reitzner and Manno⁴ have prepared azides using phosphoric acid instead of sulphuric acid, and they have discussed the advantages of their modification over the conventional method. In this work we have used their method to prepare HN_3 , unless otherwise stated.

Experimental

Preparation of KN_3 , NaN_3 and BaN_6 :

HN_3 gas is passed into an aqueous solution of the respective hydroxide until there is an excess of HN_3 . Absolute ethyl alcohol is then added with constant stirring until there is no further precipitation of the azide. Azide prepared in this way, in particular KN_3 and NaN_3 , comes out pinkish in color when reagent grade hydroxides are used. Alternatively we have repeated the procedure replacing the hydroxide by the carbonate. The azide thus obtained is white but may still contain many impurities. Replacing the reagent grade carbonates by carbonates of spectroscopic purity obtained from Johnson and Mathews, England, KN_3 , NaN_3 , BaN_6 and PbN_6 have been prepared. To precipitate the azides from their saturated aqueous solutions we have tried three different precipitating agents - ethanol, methanol and acetone. These azides are practically insoluble in any of the reagents tried and yet we find that methanol does not precipitate BaN_6 from its saturated solution. Ethanol gives a fine silky precipitate whereas with acetone the precipitate appears coarse. On the basis of recent experiments by Blais and Pai-Verneker⁵ ethanol is used to precipitate the azides from solutions of low pH

since, at least in the case of BaN_6 , the uptake of metal ion impurity is the smallest under these conditions.

Preparation of PbN_6 : - In order to understand to what extent the method of preparation affects the properties of PbN_6 we have prepared it in the following ways:

1) $\text{Pb}(\text{NO}_3)_2 + \text{NaN}_3$ in alcoholic solution.

2) $\text{Pb}(\text{AC})_2 + \text{NaN}_3$ in alcoholic solution.

3) $\text{PbO} \xrightarrow{\text{NO}_2} \text{Pb}(\text{NO}_2)_2$
 $\text{Pb}(\text{NO}_2)_2 + \text{alcoholic solution of } \text{HN}_3 \longrightarrow \text{PbN}_6$

The third method of preparation was introduced in the case of PbN_6 by Reitzner and Manno in order to avoid the incorporation of impurities like Na, Ac , NO_3^- , etc. The azide thus prepared comes out yellow in color even when the entire preparation is done in the dark and the strength of HN_3 alcoholic solution is more than 6%. This color is probably due to some impurity. We have, therefore, used PbO of spectroscopic grade obtained from the same source as above. The preparation yields white lead azide even when it is done in light. Even specpure PbN_6 when kept in light for a long time turns yellow.

Photolysis of lead azide: - The apparatus used was a usual conventional vacuum system and the pressures of N_2 gas built up due to the photolytic decomposition of PbN_6 were measured by a Pirani gauge. In each experiment a known amount of PbN_6 was put into a glass boat of a definite size so that in all cases the same surface area was exposed to the unfiltered radiation from the low pressure Hg lamp. Before doing the actual experiments, the reproducibility of the system was tested on identical samples and found to be within 1%. The following figures show the results.

Results and Discussion

Figure 1 shows how the photolytic rate changes with the time of irradiation. All the three samples 1) prepared from $\text{Pb}(\text{NO}_3)_2$, 2) prepared from reagent grade PbO and 3) prepared from specpure PbO , behave in the same way, i.e., initially the rate is high but as the irradiation proceeds the rate starts falling off till it reaches a constant value. The initial rates as one can see from Figure 1 are highest in the case of PbN_6 prepared from $\text{Pb}(\text{NO}_3)_2$ and is lowest in the "specpure" preparation. This is true for the final steady rate as well.

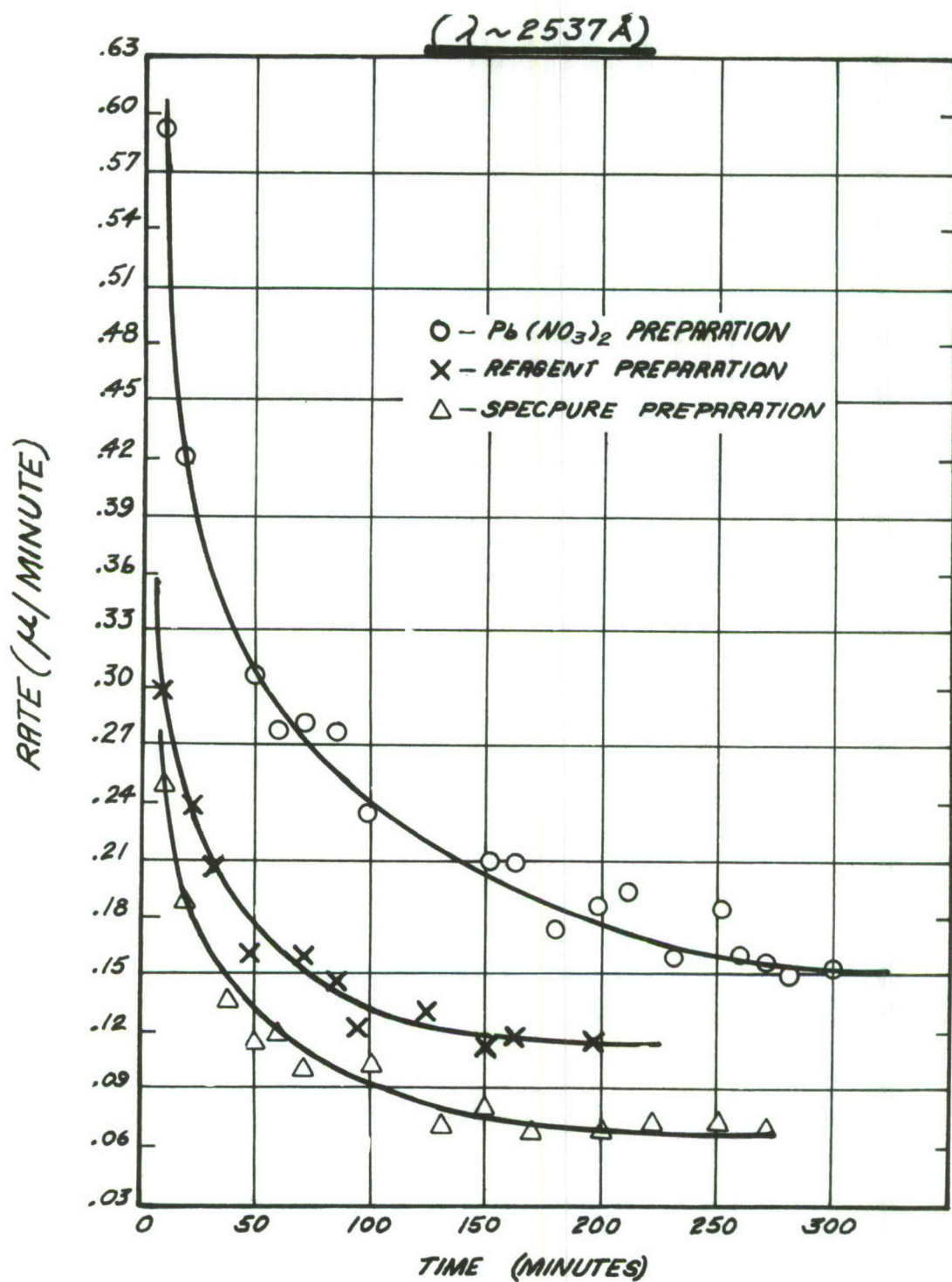


Figure 1. Rates of photolysis of various lead azides.

Figure 2 shows the rate intensity relationship studied during the constant rate period. As is evident from the figure, the rate of the photolytic decomposition is directly proportional to the intensity of the radiation source.

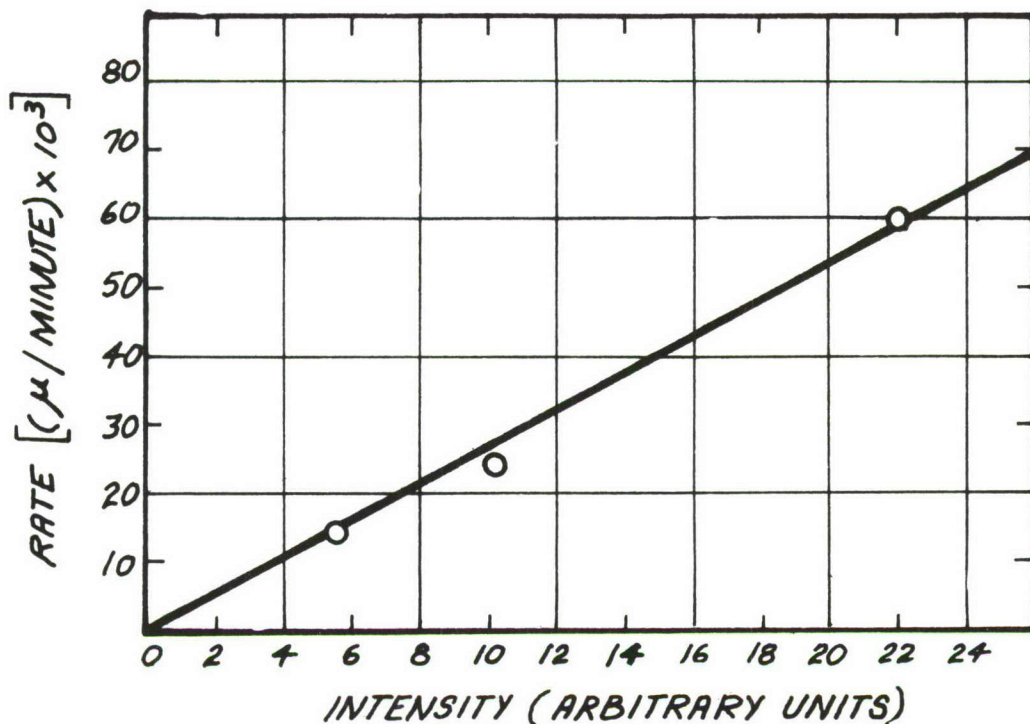


Figure 2. Rate as a function of intensity for specpure lead azide in the constant rate region.

Figure 3 is a plot of the photolytic rate versus time of irradiation in the case of PbN_6 prepared from $\text{Pb}(\text{AC})_2$. Here one finds the initial rate is the same as that for the "specpure" PbN_6 and yet the final constant rate is much higher.

We have also studied the way in which the photolytic rate varies with the temperature and have found that from 0°C to 100°C the rate is constant if the other factors are kept constant, i.e., the rate is temperature independent. We have further found that in the constant rate period no detectable dark rate was observed in any of the preparations except the $\text{Pb}(\text{NO}_3)_2$ preparation.

Earlier work on the photolysis of PbN_6 was carried out by Dodd⁶ on $\alpha\text{-PbN}_6$ and by Dumas⁷ on amorphous PbN_6 . In his work Dodd found that the rate of photolysis of $\alpha\text{-PbN}_6$ increased indefinitely with the time of irradiation. Dumas, on the other hand, worked on

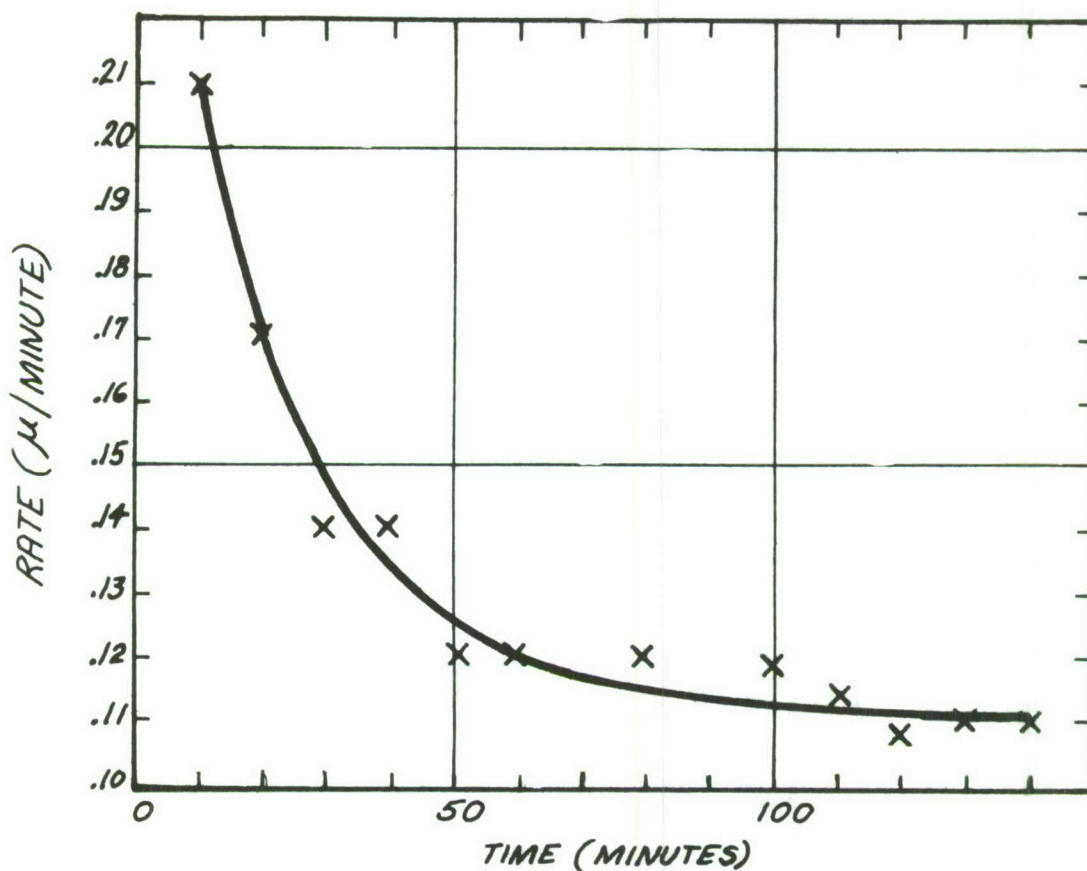


Figure 3. Rate of photolysis of lead azide prepared from lead acetate and sodium azide.

"amorphous" PbN_6 and found that after an initial rise the photolytic rate remained constant. Dumas studied the reaction for five to six minutes and Dodd for about fifteen minutes. We have studied the reaction for about 300 minutes measuring initially at one-minute intervals. It is not possible to compare these results without knowing the absolute intensities of the light sources used by the other workers. However, our results give rate curves which are distinctly different from theirs. It is possible to explain the decreasing rate shown in Figures 1 and 2 to a model involving the filling of electron traps in the bulk of the sample; however, further work is considered to be required before examining such models in detail.

Acknowledgment

We take pleasure in thanking Dr. H. J. Matsuguma for his encouragement in the progress of the work.

References

1. Yoffe, Evans & Deb: Nature 294, 180 (1957).
2. Jacobs, Tompkins, Pai-Verneker: J. Phys. Chem. (1962).
3. Reitzner, Kaufman & Bartell: J. Phys. Chem. 421, 66 (1962).
4. Reitzner & Manno: Nature, Vol. 198, No. 4884, p 991 (1963).
5. Blais & Pai-Verneker: Unpublished work.
6. Dodd: Tech. Rept. 9 Oct. 1956.
7. Dumas: Tech. Rept. 9 Oct. 1956.

PROPERTIES AND REACTIVITIES OF
DIFFERENTLY PREPARED NaN_3 AND $\text{Ba}(\text{N}_3)_2$

by

K. Torkar
Institute for Physical Chemistry
Technische Hochschule
Graz, Austria

Abstract

Our studies are concerned with the influence of the conditions of preparation on the reaction behavior of azides. Certain attention is paid to differences in the energy content in order to obtain statements concerning thermal data. Furthermore, we are interested in the influence of the preparation methods on the kinetics of the substances caused by them. Reports on decomposition enthalpies, heats of solution, and disorder energies are presented for the energetics, whereas decomposition tests, influences of different gas atmospheres, and conductivity tests were used for the kinetics.

These few examples will be given in order to show which problems arose at different stages of our investigations, and which results were obtained. Therefore, we divided the program into investigations concerning sodium azide and barium azide, resp.

Sodium Azide

Our considerations are concerned with the energy content and the surplus energies of differently prepared sodium azides. As an example tests with atomized sodium azide, a so-called "active" substance, characterized by small particle size and lattice distortions had been carried out. The substance was obtained by atomizing an alcoholic solution in dry nitrogen. As reference substance, we used a well-crystallized preparation which had been obtained by recrystallization from an aqueous solution of Merck azide.

After characterizing the two preparations by microscopic, electron-microscopic and X-ray methods, we determined first their heats of solution in water at room temperature. For the atomized preparation we obtained a surplus content of total enthalpy of about 100 cal/mole. In order to obtain further statements concerning the surplus energy and to find out which part is due to the entropic term and which is due to the free energy, we looked for a way of experimental determination of one of these two factors. For this purpose we determined the solubility which is connected with the free energy.

Knowledge of the activity coefficient of sodium azide solutions is also a prerequisite of this determination. Therefore we carried out vapor pressure measurements with sodium azide solutions of different concentrations from which all dissolved gases had been removed. For the atomized sample we found a solubility that is 0,2% higher than that for the stable reference material.

With this value one can calculate a surplus free enthalpy of about 2 cal/mole only for the atomized azide.

According to thermodynamics this would mean a surplus entropy of 0,37 cal/mole for the active sample and this is a relative high value.

In order to compare these values with surface properties we tried to calculate the surface energy of sodium azide. For this purpose we had to know the lattice energy. Hojendahl (ref. 1) found a value of 149 kcal/mole having used an idealized spherosymmetric azide ion for his calculation.

For our calculations we assumed an azide ion similar to a spheroid in which a point charge is superimposed on a quadrupole. Considering the quadrupole term we obtained a value of 172 kcal/mole as lattice energy. This value corresponds better to that of 175 kcal obtained on the basis of thermochemical data. Using this calculation method one finds a mean surface tension of about 600 erg/cm². This value is similar to those found for alkali halides.

The next step was the determination of the surface area by krypton adsorption, which yielded a surface for the atomized azide of about 3000 cm²/g. Since the surface energy is equivalent to a free energy, one gets the result, that the free surface enthalpy of the atomized sodium azide lies also in the range of 2 to 3 kcal/mole. Therefore, the essential points are:

- 1) The measurements of solubility make it possible to determine a surplus of free energy, which is in agreement with the calculated surface energy.
- 2) Even for the atomized product, having a very small particle size, one finds that the contribution of the surface energy to the total enthalpy is very small.
- 3) The entropic part of energy is a big one and is related to the strong lattice distortions.
- 4) If we are able to compare these values with the entropic and enthalpic terms of the rate equation, we can understand, that the reaction rate is more dependent on the entropic term, than on

the activation enthalpy. The same conclusion comes out of all kinetic measurements, facts on which we have already reported last year.

Surface properties and impurity atoms are among the reasons for changes of the reaction temperature of thermal decomposition of sodium azide preparations. Generally, fine dispersed particles decompose at lower temperatures than coarse crystals. The atomized sample, however, shows a shifting to higher temperatures of decomposition. The assumption, that this effect is due to gases chemically adsorbed, is confirmed by decomposition tests in the presence of different gases at various pressures. We assume that formation of nuclei takes place at surfaces at first. If the decomposition occurs in different atmospheres, a reaction of these gases will occur with the surface nuclei. Certainly, the reaction will depend on the nature of the gas and the nuclei, resp. This process will be favored with an electrophile gas, in which case the nuclei growth on the surface will be stopped to a more or less amount. Due to capturing of surface-nuclei and the further increasing of temperature of the sample decomposition will be shifted to higher values consequently. Therefore, the decay period starts after a retardation-time.

When temperature increases, formation and growth of nuclei begins also in the crystal bulk at lattice imperfections, but this process is not influenced by the atmosphere. Experimental results are presented in Figure 1.

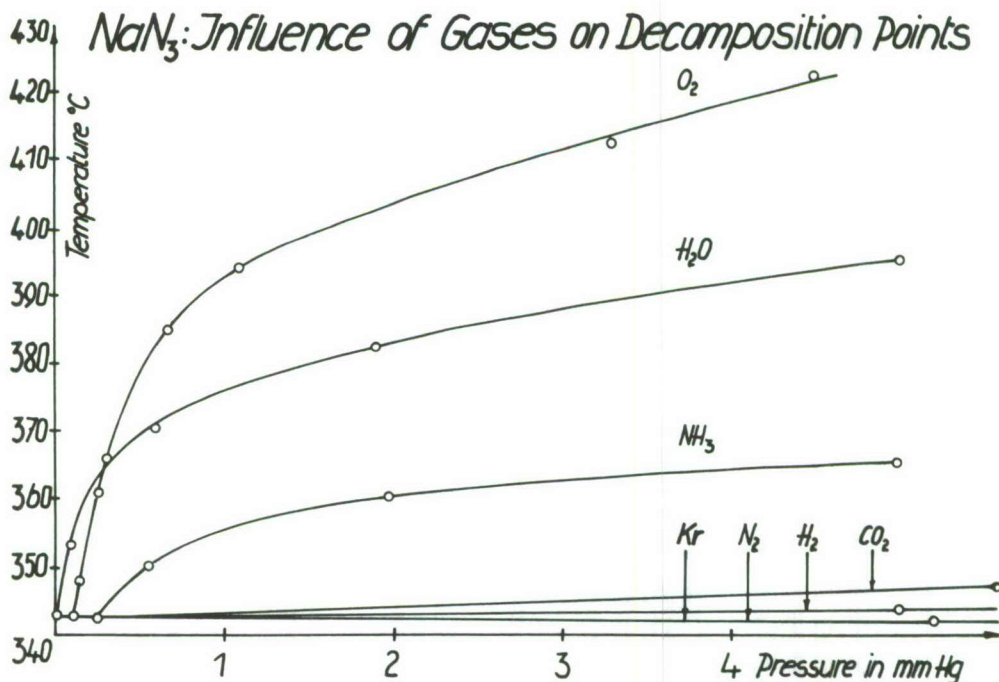


Figure 1

Decomposition points are plotted versus pressure of different gases. Our tests show that the decomposition temperature is affected in the above stated way by the electrophile oxygen. Water-vapor and ammonia behave in a similar manner with a smaller effect. Inert gases or noble gases (nitrogen, carbon dioxide, and krypton) show no influence. Hydrogen shows no changing of reaction temperature under these conditions.

The later beginning of the decay period is connected with a higher reaction rate, because of the higher reaction temperature. The different duration of the reaction must therefore be proportional to the decomposition temperature in a reciprocal manner. This is confirmed by the experiments presented in Figure 2.

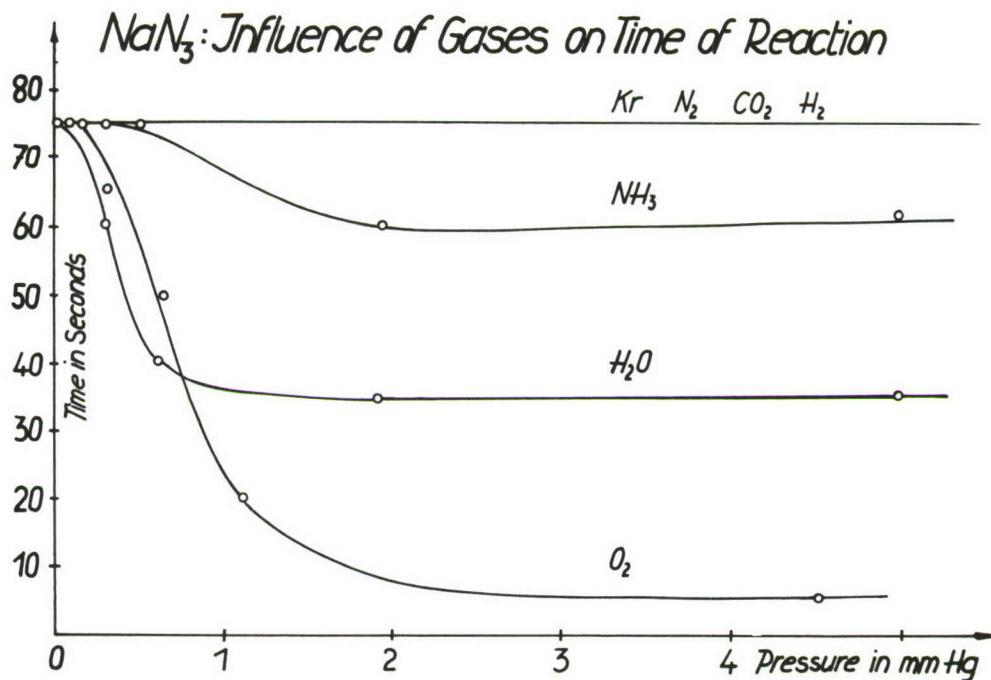


Figure 2

Not only the energetics of the substances and the conditions at the surface affect the thermal decomposition, but we have also to consider the influence of lattice defects. In this connection foreign atoms play an important role. Therefore, we started investigations with preparations of sodium azide doped with calcium. The situation is shown in Figure 3 which presents typical decomposition curves. Analytical data have been obtained by mass-spectrometric technique.

Decomposition-Curves $P(t)$ of Pure and Ca-Doped NaN_3 at 356°C

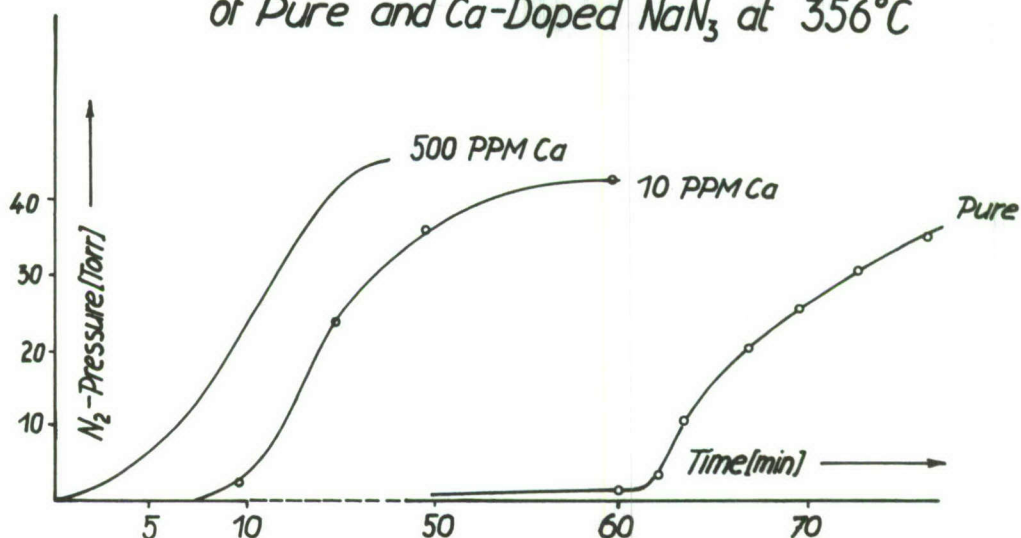


Figure 3

The sample with the highest content of Ca has the shortest induction period. This is comparable with a decomposition of the so-called "black azide" on which we have reported last year.

In order to find out in which way Ca influences the decomposition mechanism, firstly we ought to have a better knowledge of the decomposition mechanism of pure sodium azide. Therefore we started measurements on the temperature dependence of ionic conductivity. Measurements of single crystals doped with Ca are still under way. Here, only results on pure sodium azide single crystals will be presented. In Figure 4 the logarithm of conductivity is plotted versus reciprocal absolute temperature.

We can divide the whole range into four sections:

- Low temperature ionic (extrinsic) conductivity
- High temperature ionic (intrinsic) conductivity
- Nuclei formation
- Nuclei growth

Most experiments have been executed merely in the low temperature part with pellets (ref. 2).

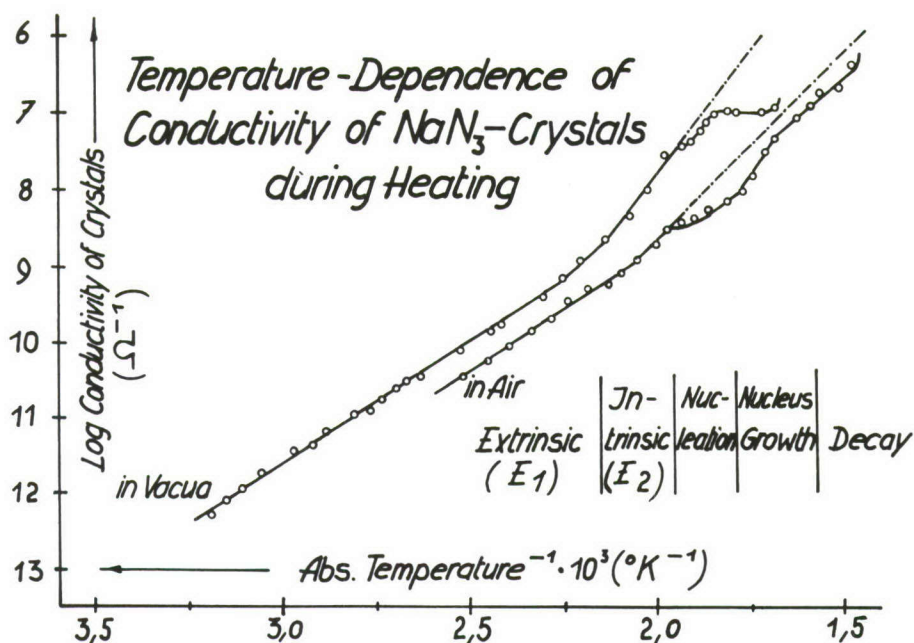


Figure 4

According to the theory of ionic conduction, we found an activation energy of about 0,65 eV for the low temperature section, and about 1,2 eV for the high temperature section. From these values we can determine an energy of defect formation of about 1,1 eV. This is probably due to Frenkel disorder. With Schottky disorder the energy of defect formation should be much higher as in the case of alkali halides.

The third part in Figure 4 is due to nuclei formation. This process is connected with a blocking up of conducting sodium interstitials and vacancies, forming centres, so that the exponential increase in conductivity will be retarded.

The last period is due to nuclei growth. At this stage macroscopically developing nitrogen can be noticed for the first time. The situation is different in air and in vacuo. In electrophile gas atmosphere conduction corresponds practically to ion migration; in vacuo, however, it is constant and independent of temperature.

On the basis of Mott's theory (ref. 3) of nuclei growth, we interpret these results with the additional assumption in the following way: Sodium azide behaves like a semiconductor at its boundary to sodium. This requires the existence of donor terms. This situation is illustrated qualitatively in Figure 5 showing the band scheme of levels. From these terms electrons transfer into the

conduction band of sodium metal may occur until the Fermi levels of the metal and of the boundary layer of the azides are equal. This would stop the electron transfer. If however, the charged metal boundary layer will be discharged by sodium ions, further decay of the azide is possible. According to this interpretation, the reaction of nuclei growth ought to be controlled by the diffusion of sodium ions.

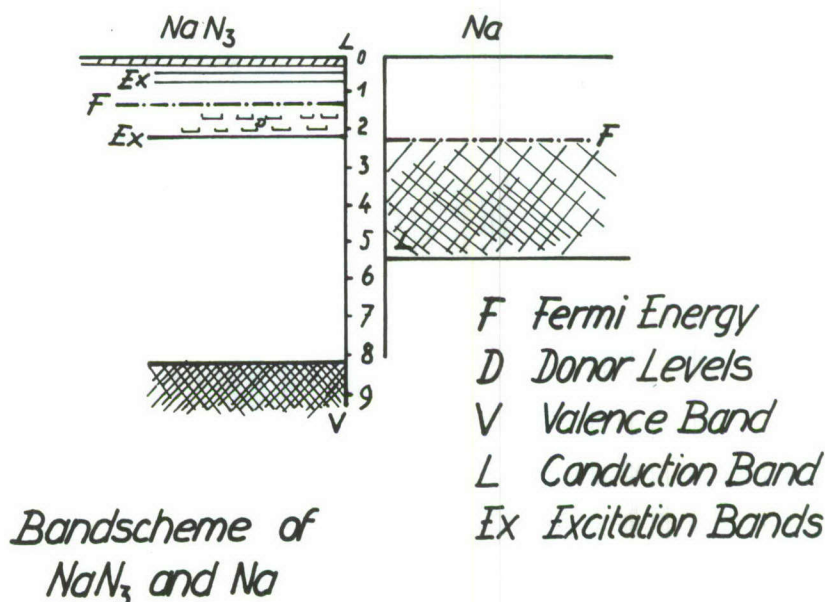


Figure 5

This explains also the difference in conductivity occurring in air and in vacuo. Discharge of the boundary layer between sodium azide and metallic sodium in vacuo obviously occurs by sodium ions, which are thus eliminated from conduction. Consequently there is no longer any exponential temperature dependence.

In presence of oxygen as an electrophile gas, however, discharge takes place by electron transfer to the oxygen. In this way the sodium ions remain free for conduction which will again show an exponential increase with temperature.

These experiments are in agreement with above-mentioned decomposition test carried out in different gas atmospheres, for it follows from conductivity tests too, that O₂ is retarding nuclei growth.

In the course of nuclei growth there will be one point, where conductivity increases so rapidly, that practically a short circuit is produced. The reason is simple: the nuclei will grow together.

In summary the following conclusions from conductivity measurements came out:

- 1) We assume a Frenkel disorder
- 2) A modified Mott's theory holds for the explanation of nuclei growth
- 3) Electrophile gases react with surface nuclei, thereby influencing conductivity and decomposition temperature.

Barium Azide

Starting investigations concerning barium azide it soon came out that, in this case, the problems are still more complicated than with NaN_3 .

Up to the present, we found three factors which are of influence on the reaction behavior of barium azide; factors which need not to be taken into consideration dealing with NaN_3 :

- 1) $\text{Ba}(\text{N}_3)_2$ can form a monohydrate which is only stable under special conditions. It can be prepared by slow crystallization from a saturated solution acidified with HN_3 . One obtains hexagonal prisms of some mm length with a nearly theoretical water content presenting a X-ray diagram different from that of the water free Barium azide. The monohydrate is loosing water very lightly, for instance, already by storing in air. The rate of dehydration depends certainly on particle size.

In this connection it is interesting to mention that, preparing barium azide by slow precipitation from an aqueous solution with acetone, one obtains needles of some cm length presenting a X-ray diagram showing lines of the monohydrate and of the water free $\text{Ba}(\text{N}_3)_2$. Thus, dealing with the monohydrate one must be aware of this tendency of dehydration. Therefore, often preparations will be obtained having a water content which is between that of the water free azide and the monohydrate.

Furthermore, it should be mentioned that the monohydrate has a heat of solution of about 7,7 kcal/mole, whereas for the water free substance we found about 5,4 kcal/mole. In literature, a value of 7,7 kcal is recorded for the water free substance.

- 2) Furthermore, it is difficult to work with barium azide according to the fact that there is an influence of storage time on its reaction behavior. For the water free substance prepared by dehydration of the monohydrate, a sample with a higher surface area and perhaps with lattice distortions will be obtained. The sample properties

are changing with the course of time and thereby are varying the energetics and kinetics until these become constant after a long time.

A number of experiments had been carried out to see the influence of storage time on the decomposition enthalpy. Simultaneously, we determined heats of solution of the same sample. These results are shown in Figure 6.

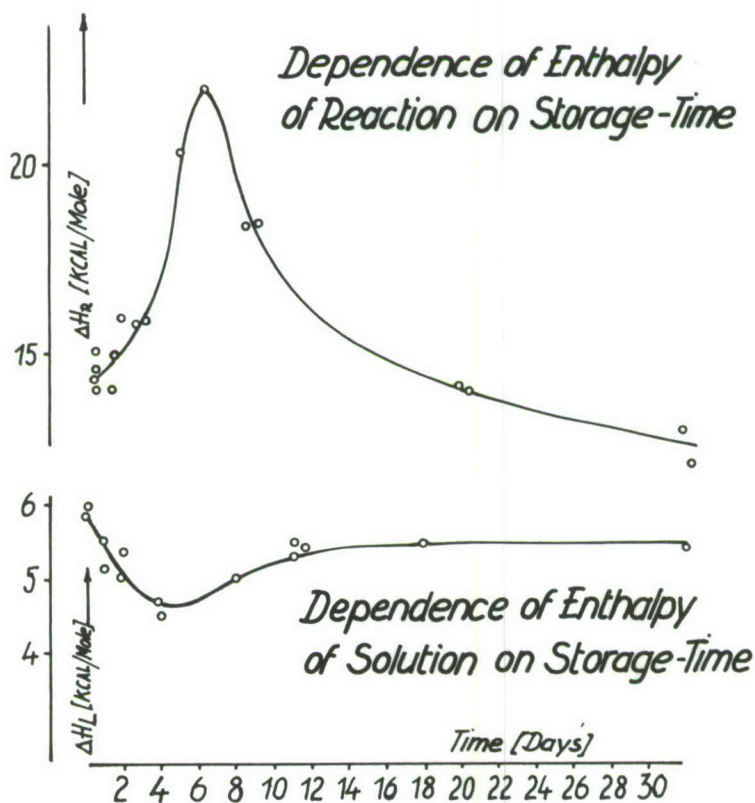


Figure 6

As using freshly prepared water free barium azide obtained by dehydration of the monohydrate, we had expected a function uniformly decreasing according to an aging process. But on the contrary, the curves are characterized by a pronounced maximum which is common to both curves and is occurring about the sixth day of storing.

3) Finally, there are different directions of decomposition possible. From a thermodynamic viewpoint, the reaction can go to barium metal, as well as to nitride. This implies different enthalpy values: an endothermal value of about 5 kcal for the reaction to metal and an

exothermal value of about 24 kcal for the reaction to nitride, both referred to one mole of azide. This situation may be the reason for the explanation of the maximas in Figure 6, namely, if there is a time-dependent factor which leads the reaction to more or few nitride, for instance, presence of nuclei.

Naturally, all these experiments are at the beginning, but we have the feeling, that many of the contradicting investigations being executed, especially in the field of barium azide, are related to questions of this kind.

References

1. K. Hojendahl, Kgl. Danske Vidensk. Selsk. 16, 135.
2. P. W. M. Jacobs and F. C. Tompkins, J. Chem. Phys. 23, 1445 (1955).
3. N. F. Mott and R. W. Gurney, Electronic Processes in Ionic Crystals, Clarendon Press, Oxford, 1948.

THE PREPARATION AND PROPERTIES OF SOME NOVEL LIGHT METAL AZIDES*

by

K. Terada, A. J. Erbel, and F. M. Brower
The Dow Chemical Company
Midland, Michigan

Metal azides have been known for several decades, but recent surveys^{1,2} of the chemical literature reveal that many of the theoretically possible azide compounds have not been synthesized. Several light metal azides of groups I, II and III of the periodic table have been reported³ but in some instances the compounds were not well characterized.

The azide synthesis effort described in this paper was a small part of another program and was terminated prematurely due to greater promise in other areas of investigation. Because of circumstances surrounding this work, some of the compounds described in this paper are incompletely characterized and only briefly mentioned, while others which received more attention are treated more elaborately.

Lithium Azides

Preparation of Lithium Azide

Several preparations of lithium azide are described in the literature⁴⁻⁷ but in our experience a higher purity product was more readily obtained by a novel reaction using n-butyl lithium and hydrazoic acid as starting materials as shown in the following equation:



Lithium azide was also prepared from sodium azide and lithium chloride in alcoholic solution⁴, but complete separation of the product from unreacted lithium chloride caused difficulty. When the above preparation was modified by the use of an ion exchange technique, a chloride-free product was obtained. This preparation was conducted in aqueous solution and removal of the water of solvation required additional manipulation. For this reason, the reaction of butyl lithium and hydrazoic acid is a preferred laboratory preparation and is described in more detail below.

* This research was supported by the Advanced Research Projects Agency and was monitored by the Air Force Systems Command, Research and Technology Division, Rocket Propulsion Laboratory, Edwards, California, under Contract Nrs. AF 33(616)-6149 and AF 04(611)-7554, with Mr. J. T. Edwards as project engineer.

Approximately 3 molar n-butyl lithium in heptane solution was added dropwise with stirring to approximately 1 molar hydrazoic acid in anhydrous ethyl ether solution. A slight elevation in temperature was noted, gas (presumably butane) was evolved, and simultaneously a white precipitate formed. The precipitated lithium azide was washed with diethyl ether, filtered and dried. Elemental analyses were:

Calc. for LiN_3 : Li, 14.2%; N, 85.8%
 Found: Li, 15.6%; N, 85.7%

The X-ray diffraction pattern (Table I) was identical to that of lithium azide prepared by a literature method⁷. Figure 1 shows the infrared spectrum of this compound. Lithium azide is quite hygroscopic and must be handled entirely in an inert atmosphere. Short exposure to the atmosphere causes the formation of the hydrated forms of the azide. However, the water of hydration can be removed under high vacuum.

Lithium azide is also soluble in anhydrous hydrazine to the extent of 20-30 g. per 100 g. of hydrazine with no apparent decomposition of either compound even at 50° C. The impact sensitivity of LiN_3 was 108.1 cm. (50% fire level, 2 kg. wt.) and spark sensitivity was 0.003 joules.

Table I

X-Ray Powder Diffraction Data for Lithium Azide

<u>d</u>	<u>I/I₀</u>	<u>d</u>	<u>I/I₀</u>
4.73	37	1.410	8.3
2.815	100	1.351	3.3
2.700	50	1.291	2.0
2.601	100	1.207	1.3
2.365	5.3	1.182	4.0
2.117	4.0	1.081	0.7
2.077	5.3	1.069	1.3
1.971	2.0	1.050	2.0
1.681	1.3	1.039	0.7
1.653	10	0.990	2.0
1.625	22	0.976~	0.7
1.583	1.3	0.961~	0.7
1.561	1.3	0.950~	0.7
1.506	4.0	0.944~	0.7

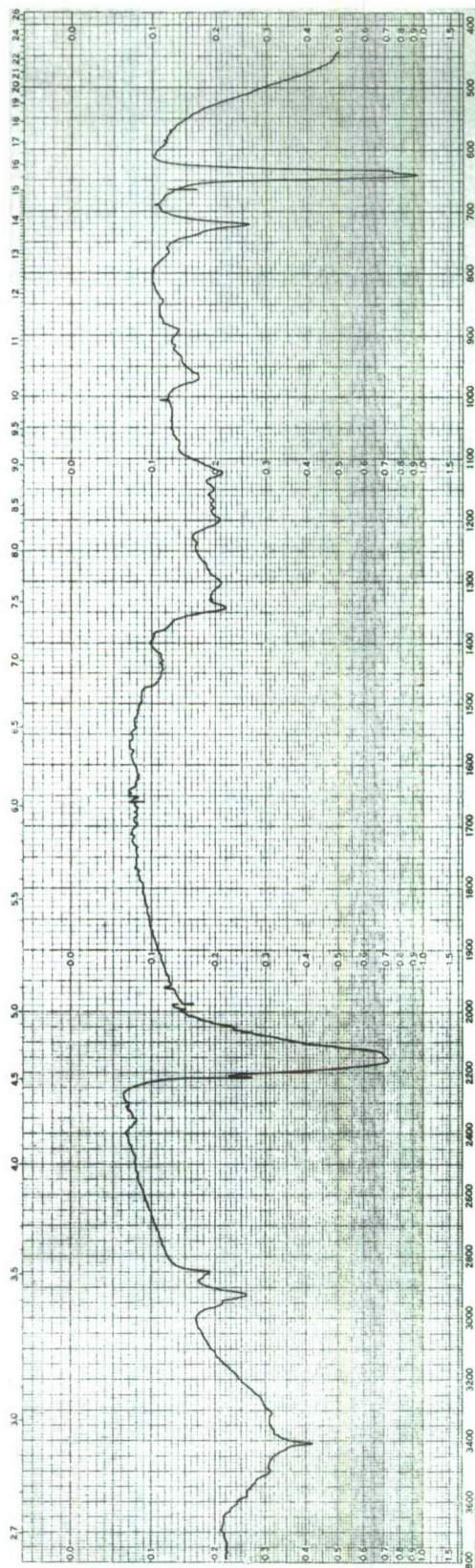


Figure 1. Infrared spectrum of lithium azide.

Lithium Azide - Hydrazine Adduct

The preparation of the lithium azide - hydrazine complex was attempted by the following methods:

- (i) To a solution of LiN_3 in 60:40 ethyl ether-ethanol mixture, hydrazine was added dropwise. A white precipitate formed which was shown by X-ray diffraction (Table II) analysis to have an unknown crystal pattern. The infrared spectrum (Figure 2) indicated the presence of both hydrazine and azide groups.
- (ii) Lithium azide was prepared, and its reaction with hydrazine investigated. A 20% solution of this compound in dry hydrazine formed a solution which was allowed to stand for 2 days before the excess hydrazine was removed by distillation under vacuum at about 50°C . The white product gave the same X-ray diffraction pattern obtained in procedure (i).

Table II

X-Ray Powder Diffraction Data for
Lithium Azide - Hydrazine Adduct

<u>d</u>	<u>I/I₀</u>	<u>d</u>	<u>I/I₀</u>
5.1	2.5	1.915	3.0
4.97	2.0	1.85	1.2
4.41	5.0	1.82	1.2
4.26	5.0	1.77	2.0
4.00	10.0	1.73	1.6
3.50	60	1.71	1.2
3.21	16	1.67	0.8
3.11	100	1.63	0.8
2.95	60	1.58	4.0
2.76	10	1.52	1.2
2.62	16	1.490	0.4
2.38	16	1.461	0.4
2.35	4.0	1.453	0.8
2.27	1.2	1.382	0.8
2.20	1.2	1.350	1.2
2.04	1.2	1.300	0.8
1.99	6.0		

- (iii) Lithium hydrazide, prepared by treating butyl lithium with hydrazine, reacted with hydrazoic acid as shown in the following equation:



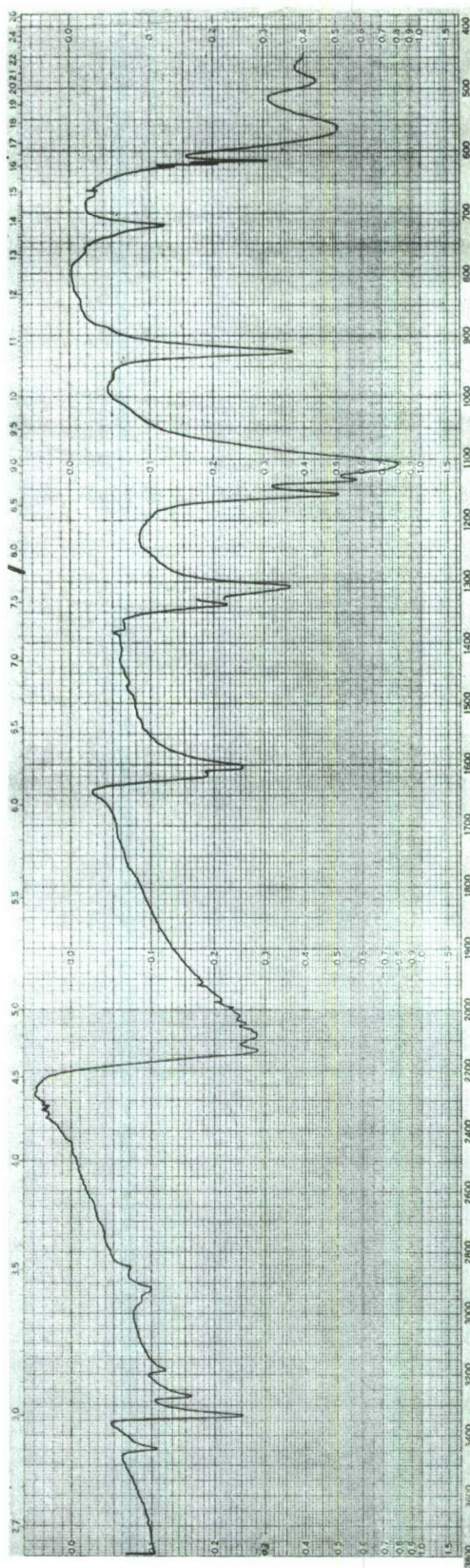


Figure 2. Infrared spectrum of lithium azide-hydrazine adduct.

This reaction was quite vigorous and a white flocculent product resulted. X-Ray showed the presence of the novel phase of what may be $\text{Li}(\text{N}_2\text{H}_4)\text{N}_3$. The infrared spectrum was similar to that obtained for the product in process (i).

- (iv) Hydrazinium azide did not react with lithium hydrazide to give the desired product.

On the basis of these experiments it was concluded that only one $\text{LiN}_3\text{-N}_2\text{H}_4$ complex forms at room temperature.

Lithium azide - hydrazine adduct is hygroscopic. Differential thermal analysis of the compound showed an endotherm at about 150°C ., when liquid condensate began to form on the cooler part of the tube. The remainder of the DTA curve was identical to that obtained for LiN_3 which flashed at 249°C .

Analysis of samples for hydrazine indicated the compound was $\text{Li}(\text{N}_2\text{H}_4)\text{N}_3$. Difficulty in obtaining total nitrogen and hydrogen prevented a complete analysis of this material.

Magnesium Azide

Synthesis in Tetrahydrofuran

The preparation of magnesium azide from diethyl magnesium in ether-dioxane solution has been described³. In our work, the procedure was modified to permit starting with commercially available bis(cyclopentadienyl)magnesium in tetrahydrofuran. A solution of this reagent was added dropwise to a diethyl ether solution of hydrazoic acid which had been previously chilled to -80°C . A precipitate formed at once. After warming to room temperature, the mixture was filtered in an inert atmosphere glove box. Elemental analysis for magnesium, carbon and hydrogen gave good agreement with the formula $\text{Mg}(\text{N}_3)\cdot 2\text{C}_4\text{H}_8\text{O}$.

Differential thermal analysis of the products disclosed an endotherm which began at 135°C ., reached a maximum at 160°C ., and crossed over at 200°C . to a very small exotherm which persisted to 300°C . without showing a minimum. There was no sign of melting or sudden decomposition.

A portion of the product was devolatilized at 100°C . and 10^{-4} mm. for six days. Tetrahydrofuran was evolved and identified by the vapor pressure. The resulting solid residue contained 85.9% of the amount of Mg calculated for $\text{Mg}(\text{N}_3)_2$. Two extractions with dry benzene raised the Mg content to approximately 92% of theory for $\text{Mg}(\text{N}_3)_2$.

Synthesis in Hydrazine

Anhydrous hydrazine was condensed onto a mixture of magnesium turnings and hydrazinium azide hydrazinate, $N_2H_5N_3 \cdot N_2H_4$. The mixture was warmed slowly to room temperature. Gas evolution began soon after the hydrazine melted and ceased after 15 minutes; an insoluble white solid formed and all the magnesium had disappeared.

The liquid was condensed into a pumped trap and a small amount of hydrazinium azide hydrazinate was removed by sublimation. The white solid residue was not sensitive to mechanical shock.

From the volatile liquid, a small amount of ammonia was separated by distillation through a trap at -80°C ., at pressure of 38 mm. Hg.

A sample of the white residue weighing 0.30 g. was hydrolyzed with excess aqueous sodium hydroxide on the vacuum line. The volatile products were distilled through two -80°C . traps into a -196°C . trap, thereby separating 0.022 mmole of a volatile material, presumably ammonia. The contents of the -80°C . trap were removed and found by titration to contain 2.07 mmoles of hydrazine and, as a check, 1.98 meq. of weak base. The hydrolysis residue was found by titration to contain 2.6-2.8 meq. of anion of a weak acid, the azide ion.

The above results indicate that the reaction produced 85% of $Mg(N_3)_2 \cdot N_2H_4$ and 15% of $Mg(N_2H_3)_2 \cdot N_2H_4$.

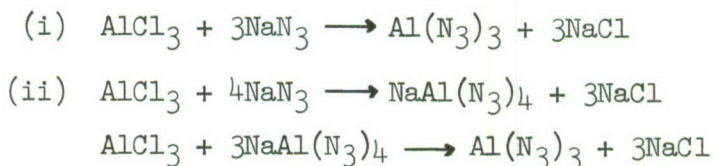
Aluminum Azides

Wiberg and Michaud³ reported the preparation of aluminum triazide from aluminum hydride and hydrazoic acid, and some evidence to show that NaN_3 reacted with aluminum chloride to form aluminum triazide was also presented.

In addition methyl aluminum diazide was prepared from trimethyl aluminum and hydrazoic acid. In the present work, these reactions have been re-examined and in some cases novel compounds were obtained.

Aluminum Triazide

Aluminum triazide was prepared by three different methods as shown in the following equations:



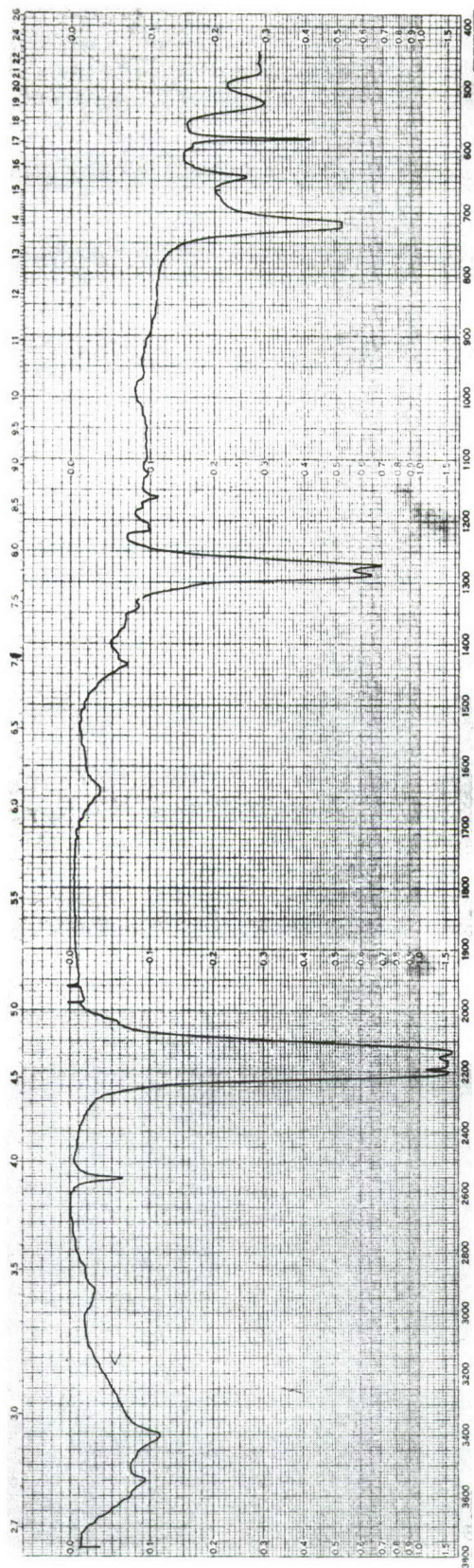
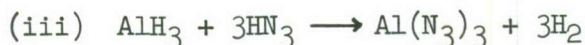


Figure 3. Infrared spectrum of aluminum triazide.

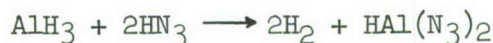


In every case the main product was shown by elemental analysis and infrared spectra (Figure 3) to be $Al(N_3)_3$. Methods (i) and (ii) were more workable processes and gave higher purity products. Even so, the product was not completely pure, containing a few percent of solvent and free NaN_3 . The preparation of sodium aluminum tetraazide as shown in method (ii) will be discussed more fully in a subsequent section.

Aluminum azide is shock-sensitive and detonates above 3000° C. It is soluble in both hydrazine and tetrahydrofuran.

Hydrogen Aluminum Azides

This work was directed toward the preparation of hydrogen aluminum diazide and dihydrogen aluminum azide by variation of the stoichiometry of the reactants in equation (iii) in the preceding section.



An ether solution of hydrazoic acid was added to a freshly prepared frozen solution of aluminum hydride in each of two experiments designed to carry out the reactions shown in the above equations. In both cases, hydrogen was evolved when the ether solution melted. When gas evolution had ceased, the ether was removed under vacuum to give white solids. Infrared spectra showed these materials both to have Al-H bonds (absorption $\sim 1850 \text{ cm.}^{-1}$) and azide groups (absorption $\sim 2150 \text{ cm.}^{-1}$).

The relative intensities of the two absorption bands are reversed in the two samples, the azide absorption being stronger in the case where two moles of hydrazoic acid were used. The products were solvated with 10-20 wt. % ether, but desolvation attempts were not emphasized. Both of the above products were shown by X-ray diffraction to be amorphous.

Ethyl Chloroaluminum Azide

The preparation of chloroaluminum diazide was attempted using the following reaction:



The rapid addition of hydrazoic acid in diethyl ether to 1 M diethyl aluminum chloride in the same solvent gave a slight reaction

at once as indicated by gas evolution; the solution slowly became cloudy and a white precipitate settled out. After one-half hour the ether was removed under vacuum leaving a white powder. The elemental analyses indicate that perhaps only one of the ethyl groups had been replaced. The product may have contained some ether.

Calc. for $\text{ClAlC}_2\text{H}_5\text{N}_3$: Cl, 26.6%; Al, 20.2%; N, 31.4%; C, 18.0%; H, 3.8%

Found: Cl, 21.3%; Al, 16.0%; N, 32.9%; C, 19.8%; H, 4.1%

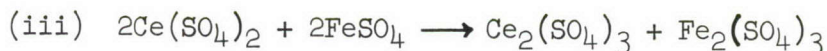
The infrared spectrum indicated the presence of the azide group.

Methyl Aluminum Diazide

Methyl aluminum diazide has been reported to form when trimethyl aluminum is reacted with excess hydrazoic acid in ether solution.



This work was repeated in our laboratory and elemental analyses, as well as infrared spectra (Figure 4), indicated that the compound is probably the reported methyl aluminum diazide. Consistent nitrogen analyses by any of the known methods either gave explosions during analysis or inconsistent results. It was found that if the methyl aluminum diazide was hydrolyzed with a dilute solution of sodium hydroxide, the resulting solution containing sodium azide could be quantitatively titrated with standard ceric sulfate to get a measure of the azide nitrogen present. The reactions are as follows:



The method has a precision of $\pm 0.8\%$ and an accuracy of $\pm 1.0\%$.

Some preparations gave fairly good analytical results and data from such a sample are as follows:

Calc. for CH_3AlN_6 : C, 9.5%; H, 2.4%; Al, 21.4%; N, 66.7%

Found: C, 10.5%; H, 2.4%; Al, 19.8%; N, 66.5%

Other samples prepared under slightly different conditions gave data which can best be interpreted by postulating that the third methyl group can also be replaced but at a slower rate. It appears

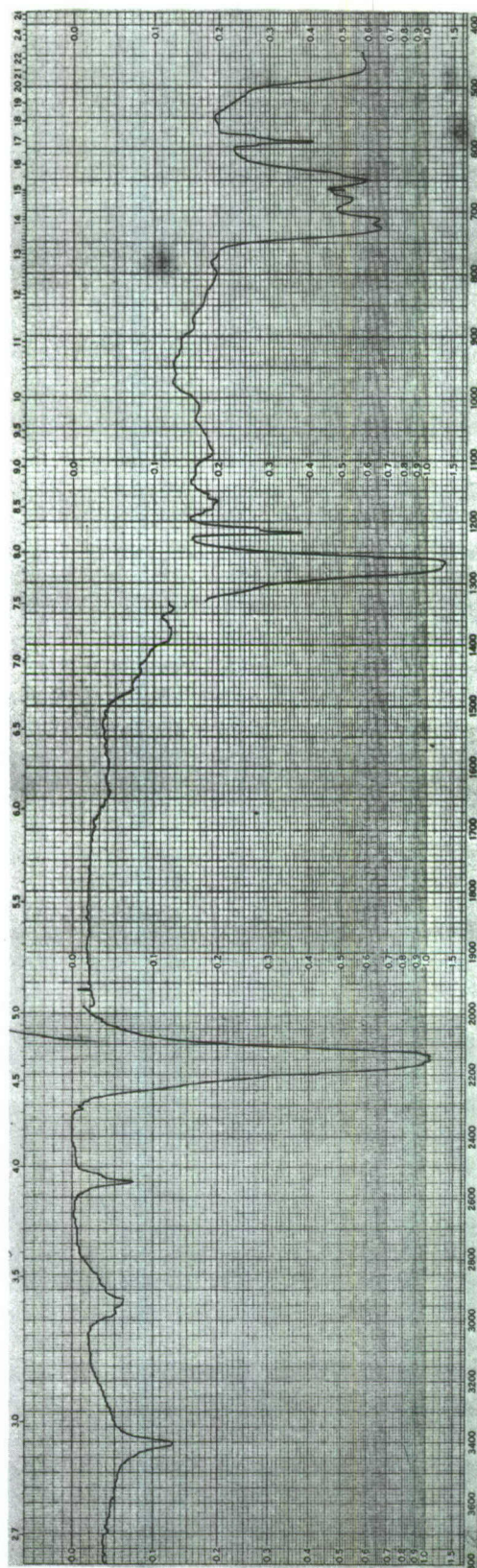


Figure 4. Infrared spectrum of methyl aluminum diazide.

from elemental analysis that some samples are mixtures of the various methyl azides and X-ray diffraction data shows at least two distinct novel patterns, one of which (Table III) is believed to be methyl aluminum diazide. Data obtained on the higher purity samples of methyl aluminum diazide show it to be a white crystalline solid. The solid had an impact sensitivity of 4.7 cm. (50% fire level, 2 kg. wt.) and exploded during DTA analysis between 250°-300° C. The density was 1.2 g./cc. Methyl aluminum diazide is soluble in tetrahydrofuran and in hydrazine with which it reacts to form an adduct.

Table III
X-Ray Powder Diffraction Data for
Methyl Aluminum Diazide

<u>d</u>	<u>I/I₀</u>	<u>d</u>	<u>I/I₀</u>
10.0	23	2.65	0.6
8.0	100	2.62	0.6
6.6	17	2.53	2.5
5.26	2.5	2.45	2.5
4.97~	1.8	2.33	1.8
4.29	6.9	2.22	0.6
3.98	1.2	2.176	2.5
3.63	3.8	2.140	2.5
3.51	3.1	2.070	0.9
3.41	0.6	2.040	1.2
3.29	18	1.930	1.2
3.17~	3.1	1.898	1.2
3.10	15	1.839	1.2
2.97	3.1	1.733	0.6
2.90	7.7	1.699	1.8
2.80	6.9	1.647	1.5
2.70	6.2	1.580	0.6

Complex Metal Azides

Wiberg and Michaud³ reported the preparation of lithium borozide and sodium hexazidostannate. This work was not repeated but the analogous compounds, sodium aluminum tetraazide and lithium aluminum tetraazide were prepared.

Sodium Aluminum Tetraazide

The equation for the preparation of sodium aluminum azide from sodium azide and aluminum chloride was given earlier in this paper. The reaction was carried out by bringing together a solution of

aluminum chloride in benzene and one of sodium azide in tetrahydrofuran. After stirring overnight at room temperature, the solids were allowed to settle and the liquid was decanted. The liquid portion was subjected to distillation until the approximate original volume of benzene remained. Further dilution of the residue with benzene and additional distillation to remove all tetrahydrofuran gave a solid which was washed with diethyl ether and dried under vacuum at 100° C. for 3 hours.

The white product analyzed as follows:

Calc. for NaAlN_{12} : Azide N, 77.2%; Al, 12.4%; Na, 10.4%

Found: Azide N, 77.5%; Al, 12.0%; Na, 10.1%

Sodium aluminum azide of 99.6% purity (by elemental analysis) is a white crystalline solid. The infrared spectrum (Figure 5) shows the presence of the azide group and the X-ray diffraction pattern (Table IV) is novel. The impact sensitivity is 6.5 cm. (50% fire level, 2 kg. wt.); the spark sensitivity is less than 0.0013 joules, and in the autoignition tests, there was no fire through 300° C.

Differential thermal analysis gave no detonation but there was evidence of decomposition above 150° C. The density of sodium aluminum azide was measured by weighing a sample submerged in ether and was found to be 1.59 g./ml. Sodium aluminum azide is very soluble in hydrazine. A solution containing 17 wt. % did not appear to be saturated. In tetrahydrofuran, the material was largely dissolved but the undissolved material was sodium azide. Apparently in this solvent there is rapid dissociation of sodium aluminum azide to sodium azide and aluminum azide. Sodium aluminum azide slowly loses the azide group when exposed to moist air.

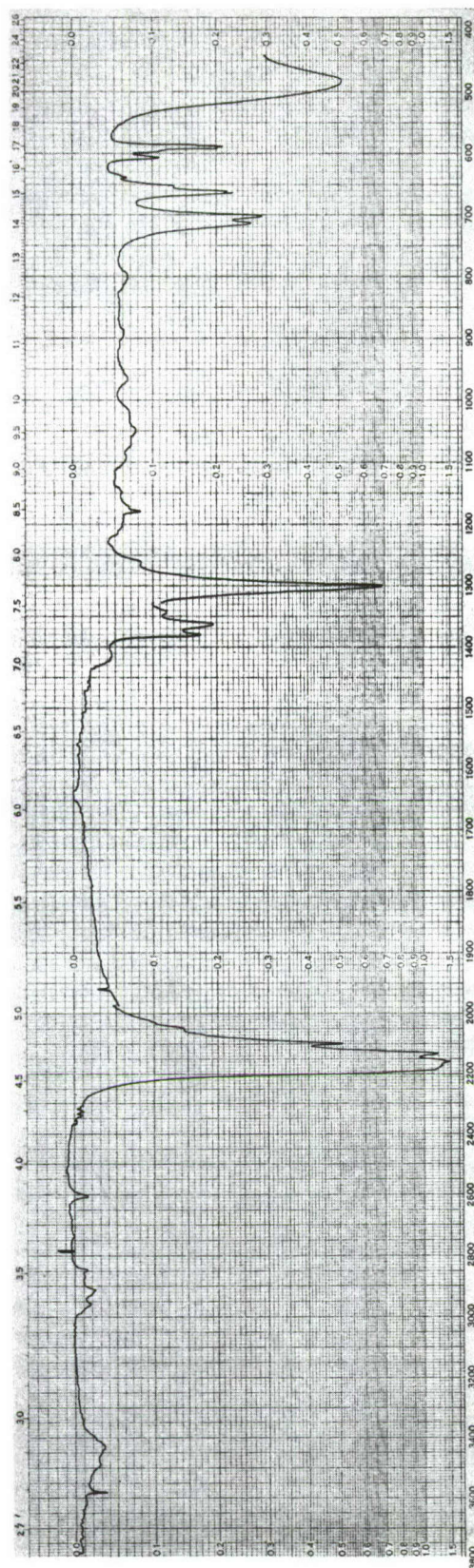


Figure 5. Infrared spectrum of sodium aluminum tetraazide.

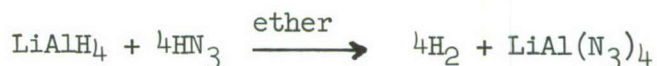
Table IV

X-Ray Powder Diffraction Data for
Sodium Aluminum Tetraazide

<u>d</u>	<u>I/I₀</u>	<u>d</u>	<u>I/I₀</u>
8.8	100	2.47	10
8.1	75	2.36	8
6.7	25	2.30	15
5.3	8	2.20	2
4.98	18	2.15	2
4.62	13	2.10	2
3.98	6	2.06	3
3.90	25	1.95	2
3.59	6	1.93	3
3.50	6	1.86	3
3.37	7	1.825	3
3.20	13	1.79	1
3.09	5	1.745	3
2.97	17	1.715	1
2.93	30	1.67	2
2.79	5	1.635	1
2.74	7	1.60	2
2.70	15	1.555	2
2.62	10	1.51	
2.60	10	1.471	11
2.53	7		

Lithium Aluminum Tetraazide

Lithium aluminum azide was prepared from the reaction of lithium aluminum hydride and hydrazoic acid in ethyl ether.



The reaction was carried out at room temperature. Hydrogen gas evolved and a white precipitate settled out. After drying under vacuum overnight, the material was analyzed but the sensitivity of the compound prevented adequate characterization. Elemental analyses were as follows:

Calc. for LiAlN_{12} : Li, 3.4%; Al, 13.3%

Found: Li, 3.1%; Al, 12.4%

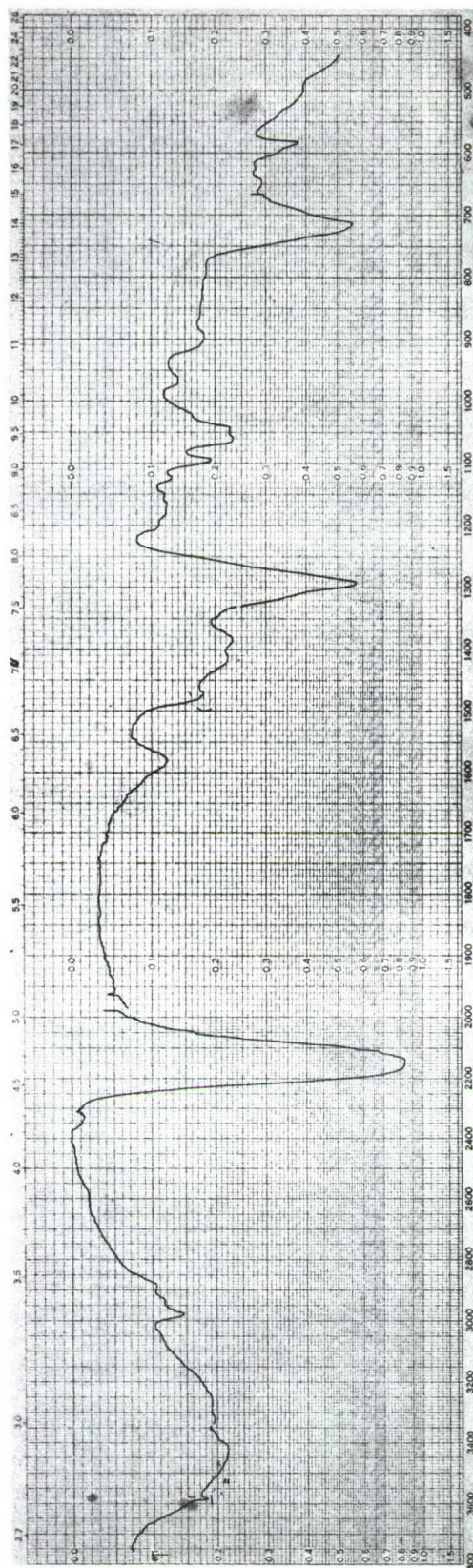


Figure 6. Infrared spectrum of lithium aluminum tetraazide.

The infrared spectrum shown in Figure 6 indicates the presence of the azide group and the absence of Al-H bonds. The product was found to be shock-sensitive and detonated with a red flash above 300° C.

Conclusion

Several simple and complex azides of the metals of groups I thru III of the periodic table were prepared. Physical and chemical properties were examined, but in most cases further work will be required to completely characterize the compounds.

Acknowledgments

The authors wish to thank the coworkers at The Dow Chemical Company for their assistance. J. Krueger and B. L. York made valuable contributions in the preparation of many of the compounds described. Paul F. Reigler developed new analytical procedures for the azide nitrogen and hydrazine. R. B. Nunemaker carried out most of our elemental analysis and H. W. Rinn did all of our X-ray diffraction work.

References

1. H. Rosenwasser, "Hydrazoic Acid and Metal Azides", (A Literature Survey), Project 8-07-11-440, Report 1551-TR (Oct. 1958 - Dec. 1959). Army Engineer Research and Development Laboratories, Fort Belvoir, Virginia.
2. B. L. Evans, A. D. Yoffe, and P. Gray, Chem. Rev., 59, 515-68 (1959).
3. E. Wiberg and H. Z. Michaud, Z. Naturforsch., 9b, 497-503 (1954).
4. A. W. Browne, "Inorganic Syntheses", Vol. I, McGraw-Hill Book Company, Inc., N. Y., 1939, p. 79.
5. M. W. Miller and L. F. Audrieth, *ibid.*, Vol. II, 1946, p. 139.
6. N. Hoffman-Bang, Acta Chem. Scand., 11, 581 (1957).
7. "Gmelin's Handbuch der anorganischen Chemie", Vol. 20, Verlag Chemie, G.m.b.H., Berlin, 8th Ed., 1960, p. 277.

FURTHER STUDIES ON THE THREE COMPONENT SYSTEM IN PURIFICATION

by

James L. Taylor
Basic Research Laboratory
U. S. Army Engineer Research and Development Laboratories
Fort Belvoir, Virginia

At the previous conference¹ reference was made to a method of purification for a selected series of alkali azides. The experimental results reported at that time indicated that the method was highly efficient, and they indicated that the proper selection of specific solvent combinations results in the separation and improved qualities, purity-wise, of the selected series of alkali azides. It was evident at that time that the success or failure in applying this method to other series of azides had a dependency upon the cationic portions of the respective azides (Table I). And even in the selected alkali series there existed a wide variation in the solvent combinations utilized (Table II). Recent studies along these lines indicated that this method in its presently devised state was not applicable to other series of azides.

Table I
Spectrograph Analysis of Selected Azides

Substance							
Impure Azide				Purified Azide			
NaN ₃	KN ₃	RbN ₃ Metal	CsN ₃	NaN ₃	KN ₃ Metal	RbN ₃	CsN ₃
Fe	Fe	Fe	Fe	Fe*	Ca	Ca	Ca
Si	Si	Si	Si	Ca	Mg	Mg	Mg
Mg	Mg	Mg	Mg	Mg		K*	
Al	AL	AL	Al				
Ca	Ca	Ca	Ca				
Cu	Cu	Cu	Cu				
K	Na	Na	K				

* Only faint lines were observed for these elements, indicating negligible concentration.

The work reported at the last conference has been extended and the emphases in the more recent months have been on identifying the cationic contaminants existing in selected materials.

Table II
Proportions by Volumes of Water, Ethanol, and Ethyl Ether
in the Purification of Selected Alkali Azides

Substance*	Solvent (volume)			Percentage Yields**
	Water	Ethanol (abs)	Ethyl Ether (anhyd)	
NaN ₃	1	2.0	1	36
KN ₃	1	2.5	1	45
RbN ₃	1	4.0	1	48
CsN ₃	1	6.0	1	40

* The alkali azides were subjected to one purification.

** Percentage yields of the alkali azides at the points of miscibilities of water and ethyl ether.

Spectrographic analyses have been made of various azide compounds from different sources where various methods of preparations are utilized (Table III, Table IV, Table V, Table VI)

Table III
Spectrograph Analysis of Selected Azides

NaN ₃ ^a		NaN ₃ ^b		Substance		Purified Azide	
				Impure Azide		NaN ₃ ^{c,d}	
Metal	% Wt.	Metal	% Wt.	Metal	% Wt.	Metal	% Wt.
Ag	0.001	Ba	0.001	Ba	0.1	Ba	0.01
Al	0.001	Ca	0.001	Ca	0.1	Ca	0.01
Ba	0.1	Cu	0.0001	Cr	0.0001	Cu	0.0001
Ca	10.0	K	1.0	Cu	0.0001	K	0.1
Cr	0.01	Mg	0.001	K	0.1	Na	Present
Cu	0.01	Na	Present	Mg	0.001		
Fe	0.001			Na	Present		
K	0.1			Sr	0.01		
Mg	1.0						
Na	Present						
Rb	0.1						
Si	0.001						
Sn	0.001						
Sr	0.1						

^aSodium Azide; commercial, Fisher Products. Washed.

^bSodium Azide, crystal, BRL preparation. Fisher Products, commercial.

^cSodium Azide; commercial, McKay Products.

^{c,d}Sodium Azide; BRL purification, Three Component System Method.

Table IV
Spectrograph Analysis of Azides

KN ^a ₃		Substance		KN ^c ₃		KN ^d ₃	
Metal	% Impurity	Metal	% Impurity	Metal	% Impurity	Metal	% Impurity
Al	0.01	Al	0.01	Al	0.01	Al	0.1
Ba	0.1	Ba	0.1	Ba	0.1	Ba	0.1
Ca	0.1	Ca	0.1	Ca	1.0	Ca	1.0
Cu	0.01	Cu	0.001	Cu	0.01	Cu	0.01
Fe	0.001	Fe	0.0001	Fe	0.001	Fe	0.001
K	Present	K	Present	K	Present	K	Present
Mg	0.001	Mg	0.001	Mg	0.001	Mg	0.1
Na	0.1	Na	0.1	Na	10.0	Na	10.0
Si	0.001	Si	0.001	Ni	0.01	Si	0.01
				Si	0.01		

^aPotassium Azide; commercial, Distillation Products Industries. Lot No. 8427.
Reactants: NH_2NH_2 , HNO_2 , KOH

^bPotassium Azide; commercial, Distillation Products Industries. Lot No. 8427.
Reactants: NH_2NH_2 , HNO_2 , KOH

^cPotassium Azide; ERDL preparation, McCrone's method.
Reactants: KOH, NaN_3 , Alcohol

^dPotassium Azide; ERDL preparation, McCrone's method.
Reactants: KOH, NaN_3 , Alcohol

Table V
Spectrograph Analysis of Azides

CsN ₃ ^a		Substance CsN ₃ ^a		CsN ₃ ^b	
Metal	% Purity	Metal	% Purity	Metal	% Purity
Ag	0.0001	Ag	0.0001	Ag	0.0001
Al	0.01	Al	0.01	Al	0.01
Ca	1.0	Ca	0.1	Ca	1.0
Cr	0.1	Cr	1.0	Cd	0.001
Cs	Present	Cs	Present	Cs	Present
Cu	0.001	Cu	0.1	Cu	0.01
Fe	1.0	Fe	1.0	Fe	0.1
Mg	1.0	Mn	0.1	Mg	0.1
Na	1.0	Mg	1.0	Na	10.0
Ni	0.1	Na	1.0	Si	0.1
Si	1.0	Ni	0.1	Sn	0.01
Sn	0.1	Si	1.0		
		Sn	0.1		

^aCesium Azide, commercial, Distillation Products Industries.
Reactants: NH₂NH₂, HNO₂, CsOH or Cs₂CO₃

^bCesium Azide; ERDL preparation.
Reactants: Cs₂CO₃, HN₃ (ion exchange)

Table VI
Spectrograph Analysis of Azides

TlN ₃ ^a		Substance Ba(N ₃) ₂ ^b	
Metal	% Impurity	Metal	% Impurity
Ag	0.01	Ag	0.0001
Al	0.001	Al	0.001
Ca	0.1	Ba	Present
Cu	0.001	Ca	0.01
Fe	0.01	Cu	0.01
In	1.0	K	0.1
Mg	0.1	Mg	0.0001
Pb	1.0	Na	0.1
Si	0.01	Si	0.001
Sr	0.001	Sr	0.01

^aThallium Azide; BRL preparation. Reactants: NaN₃, Tl₂SO₄

^bBarium Azide; ERDL preparation. Reactants: HN₃, BaCO₃, (ion exchange)

The results of these analyses indicate that the cationic contaminant contents of the respective azides have a definite dependency upon the methods of preparation.

Purified samples of sodium azide have been extensively utilized here in our research on lead azide crystal preparations (Table VII).

Table VII
Spectrograph Analysis of Selected Azides

Impure Azide NaN ₃ ^a		Substance	Purified Azide NaN ₃ ^b	
Metal	% Wt.		Metal	% Wt.
Ba	0.1		Ba	0.01
Ca	0.1		Ca	0.01
Cr	0.0001		Cu	0.0001
Cu	0.0001		K	0.1
K	0.1		Na	Present
Mg	0.001			
Na	Present			
Sr	0.01			

^aSodium Azide; commercial, McKay Products

^bSodium Azide; commercial, McKay Products, BRL purification, Three Component System Method

It has been observed here that when alpha lead azide crystals are grown the distribution of good crystals in a given batch varies as the purity of the reagent materials and the frequency of explosion is considerably reduced. (In relation to these experiments, experiments on radical processes in alpha lead azide at very low temperature were initiated by King et al² and it was reported that high order detonation occurred in good crystals as compared to weak crystal glow for bad crystals of alpha lead azide prepared from raw reagent material.)

This indicates that in order to continually improve products and to keep the growing products substantially detonation free an experiment needs to be devised whereby the raw reagent materials for the preparations of the azides should be as free from contaminants as possible.

In an effort to elucidate solution structures for the subsequent purifications of the various series of azides, nuclear magnetic resonance spectra were obtained for the alkali azide series (Figs. 1, 2, 3, and 4). The smaller peak at the side of the main

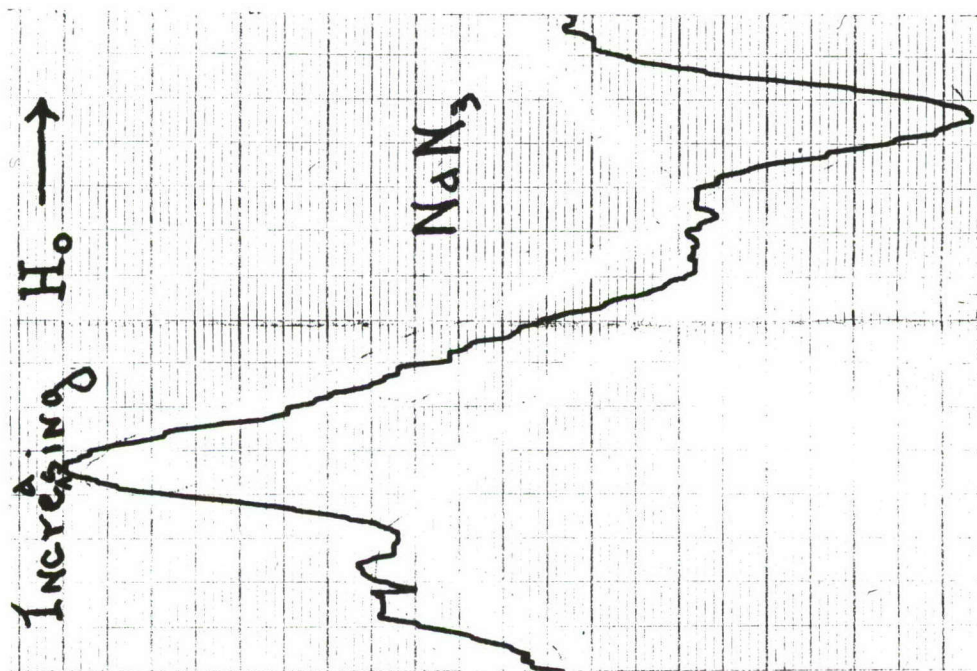


Figure 1. Nuclear magnetic N^{14} resonance spectra of sodium azide (aqueous solution). Reference scales are in parts per million. 2.74-Mc Oscillator.

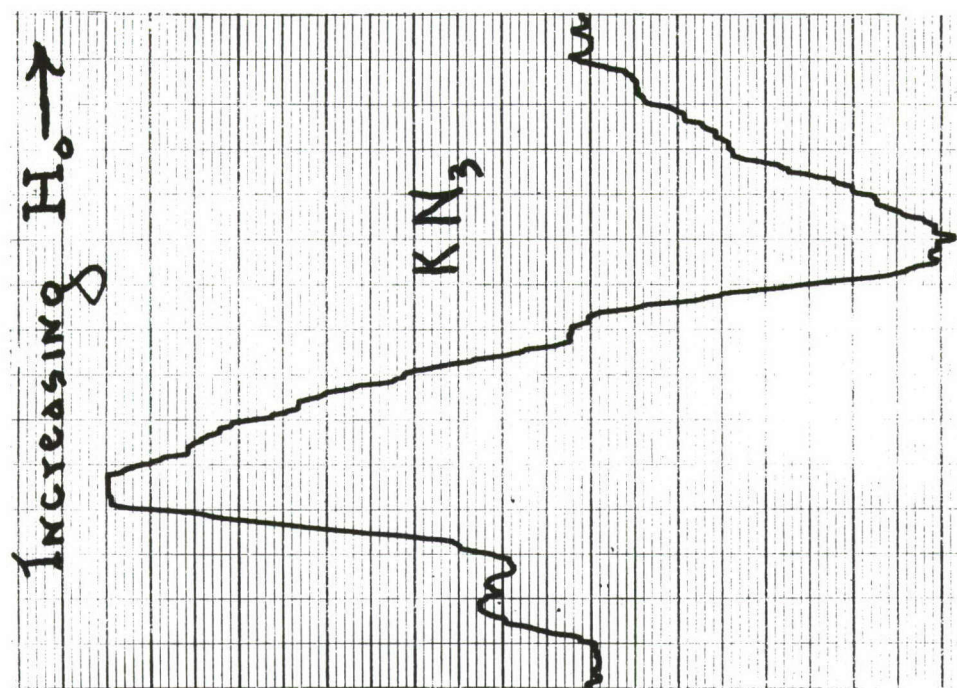


Figure 2. Nuclear magnetic N^{14} resonance spectra of potassium azide (aqueous solution). Reference scales are in parts per million. 2.74-Mc Oscillator.

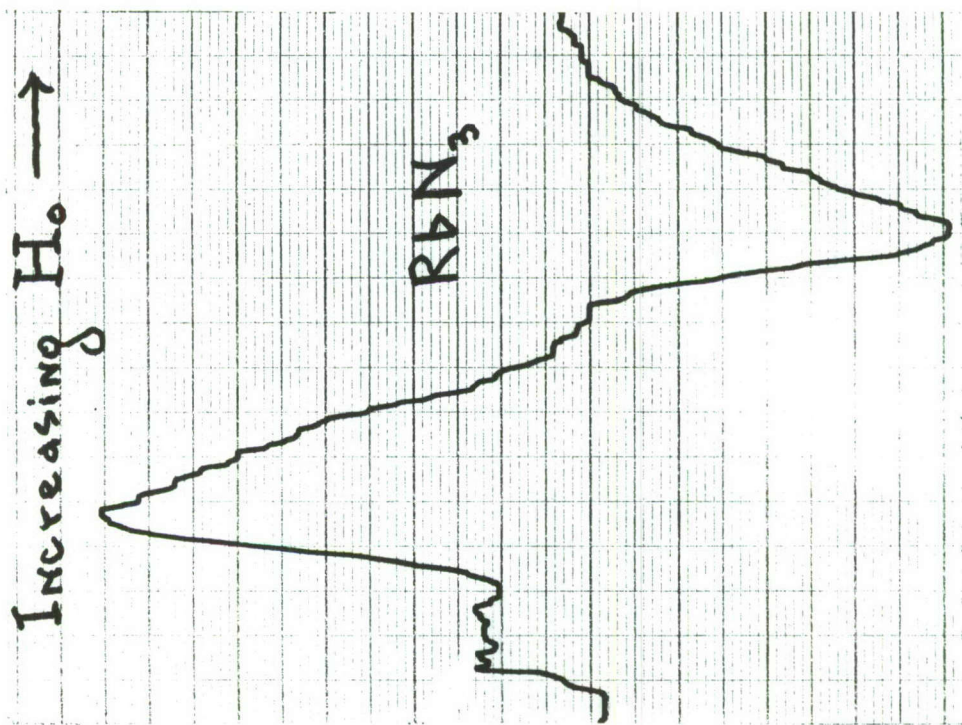


Figure 3. Nuclear magnetic N^{14} resonance spectra of rubidium azide (aqueous solution). Reference scales are in parts per million. 2.74-Mc Oscillator.

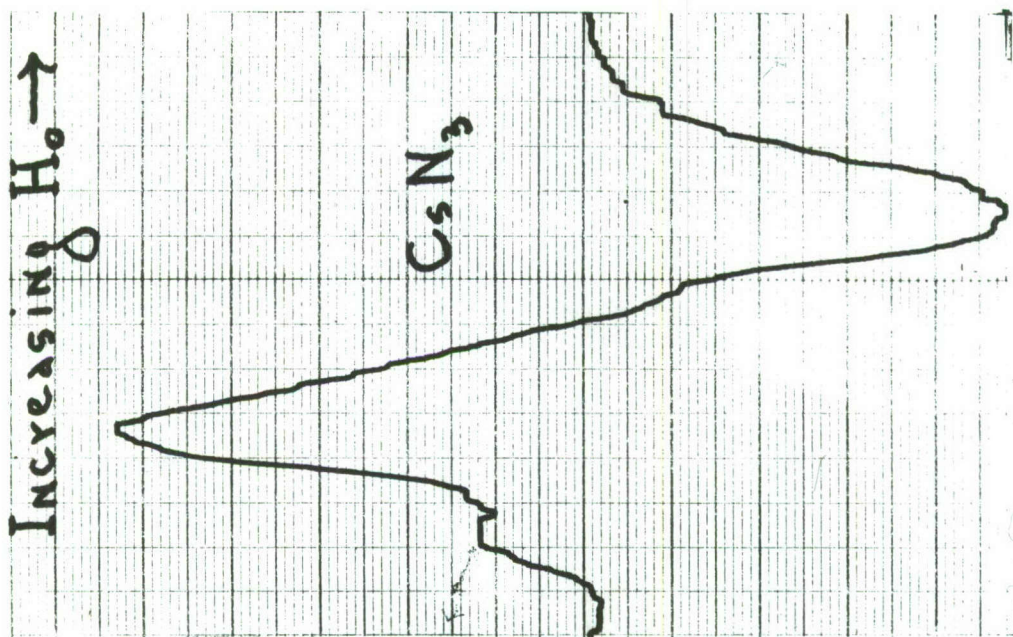


Figure 4. Nuclear magnetic N^{14} resonance spectra of cesium azide (aqueous solution). Reference scales are in parts per million. 2.74-Mc Oscillator.

peak at the alkali azides is attributable to the central nitrogen in the azido group of the molecule. The chemical shift between the central nitrogen and the terminal nitrogens is decreasing as we proceed down the series (Table VIII).

Table VIII
Nitrogen¹⁴ Wide-Line Studies

Substance	Nitrogens	
	Line-width Central-Terminal	Line-width Terminal-Terminal
NaN ₃	125 ppm	255 ppm
KN ₃	82.5 ppm	210 ppm
RbN ₃	59.0 ppm	195 ppm
CsN ₃	47.0 ppm	187 ppm

This indicates a tendency towards covalency in the particular solvent. This means that the difference in molecular environment between nitrogens is becoming smaller. The line width of the peak at half-height also seems to be decreasing as we proceed down the series of the alkali metals. This is normally a function of the charge distribution about the molecule. Symmetrical distribution gives sharp lines (i.e. NH₄ is very sharp) and less symmetry of charge broadens the lines. The line width of the peak attributable to the central nitrogen seems to be smaller than the line width of the line assigned to the terminal nitrogens. This would indicate that the central nitrogens are in a more symmetrical environment than the terminal nitrogens.

Relative to the growth of lead azide crystals, studies have been initiated to elucidate the structures of the respective growth solutions of alpha lead azide and the new polymorphic form of alpha lead azide reported by Kemp³. Nuclear magnetic resonance spectra have been made of the respective growth solutions. Growth solution for old and new habits are Fig. 5 and Fig. 6, respectively. Significant differences are not readily apparent. The smaller peak is no longer observable in lead azide and this would indicate that the azide nitrogens are exchanging more rapidly with each other and that the single time-averaged peak results.

Further study in relation to these parameters is contemplated. It is believed that a knowledge of the effects of such parameters will allow the subsequent development of purification solvent systems for other series of azides and furnish information useful to explain the reason for the stability of alpha lead azide grown in one solution in preference to another, and perhaps the nature of the new polymorph of alpha lead azide.

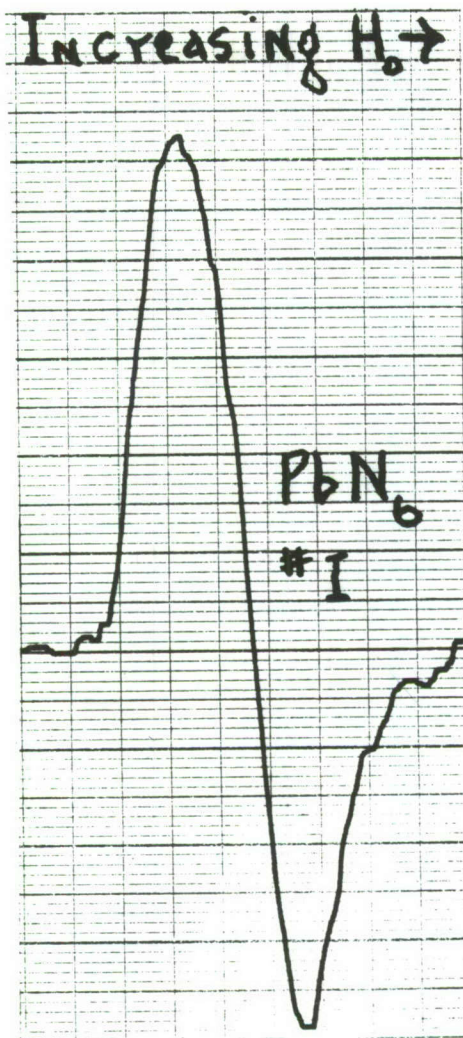


Figure 5. Nuclear magnetic N^{14} resonance spectra of lead azide growth solution. Sample No. I. Reference scales are in parts per million. 2.74-Mc Oscillator.

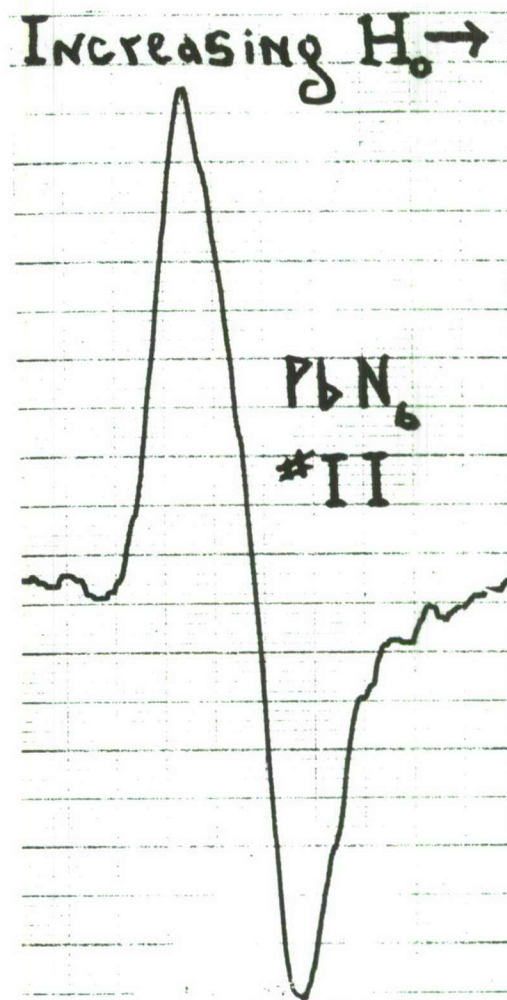


Figure 6. Nuclear magnetic N^{14} resonance spectra of lead azide growth solution. Sample No. II. Reference scales are in parts per million. 2.74-Mc Oscillator.

References

1. J. L. Taylor, Proceedings of the Eleventh Basic Research Group Contractors' Conference and Symposium, 31 October - 2 November 1962, pp. 307.
2. King, et al., unpublished data.
3. M. D. Kemp, Proceedings of the Twelfth Basic Research Laboratory Contractors' Conference and Symposium, 6-8 November 1963.

FURTHER OBSERVATIONS ON THE GROWTH OF ALPHA LEAD AZIDE CRYSTALS

by

M. D. Kemp

Basic Research Laboratory

U. S. Army Engineer Research and Development Laboratories
Fort Belvoir, Virginia

Substantially all basic materials of modern technology are made of crystals. It follows that a knowledge of how crystals are formed, how they grow, what parameters affect their growth is a most vital aspect of the science of materials. In common with most other observations, the construction and growth of a crystal is not as neat and orderly and simple as it looked at first sight. Around 1930, scientists thought that they had a reasonable explanation of the means by which crystals grow but subsequent extensive researchers have uncovered a multitude of new information which has made the older information not only obsolete but broadly inaccurate. We do have today a vast new still incomplete source of information and discoveries relating to crystals and parameters affecting their formation.

The chemistry of crystal growth had for a long time been a neglected field of study during the time that solid state physics had moved to the front of physics research. The imbalance is largely unnoticed during the time that new advances continue to come from the physicists. My area of concern has been materials and all the requisite chemistry related thereto such as preparation, standardization, purification, crystal growth, etc. It has been restricted, however, during this report period due to the urgent requirement for lead azide crystals. This report then relates some additional experiments and observations on the growth of alpha lead azide crystals.

It has been known for a long time that lead azide exists in two polymorphic forms. An alpha (orthorhombic form $\rho^{4.71}$) and a beta (monoclinic form $\rho^{4.93}$)¹. Other forms have been reported from time to time, notably an amorphous form by Z. V. Harvalik and co-workers² at the University of Arkansas, and a gamma or thin fragile hexagonal plate form by some British workers³.

None of these polymorphs adequately served our purpose and too, the two crystalline forms detonate spontaneously during growth from solution. The beginning of the work involved looking at the solubility and compatibility of lead azide in selected solvent systems based on certain theoretical considerations. The ultimate purpose of the work in chemistry at the Basic Research Laboratory was to

Table I. Variation in Number of Mortalities

H ₂ O - GLYCOL	0.5C	C	1.5C
1-0		00000000 00000000 00000000	
15-1		000000 000000	
11-1	00000	000000000 000000000 000000000 00	00000
10-1	00000	00000	00000
9-1	00000	00 000000000 000000000 000000000	00000
8-1	00000000	00000000 00000000 0000	00000000
7-1	00000000	00000000 00000000 0000	00000000
6-1	0000	0000	0000
5-1	0000	0000	0000
4-1	0000	000	00000000 0000000
3-1	000	0000000 00000000	00000000 0000000
2-1	000	000	000
1-1		000000 000000	0000000 00000
0-1		00000000 0000	

grow crystals of lead azide of good, clear, large and continually improving optical properties for other studies. The definition and limitations of the words, "large and clear" were changing parameters affected primarily by the successes or failures of our experimental and theoretical approaches. A related purpose was to increase the basic information in the area of crystal growth including the related parameters of growth from solution. As a practical manner, the reduction or elimination of the spontaneous detonations probability was a necessity. The work commenced some six years ago.

The growth of lead azide crystals of any type and in any optical condition has always been dependent upon the extent to which a specimen could be obtained in any finite size free of spontaneous detonations during growth.

In a previous report⁴ it was shown that a choice of additives in large amounts to the growing solutions would reduce the probability of spontaneous detonations. The first report and the first observations made on both the alpha and beta forms of lead azide used glycol as an additive and the results of the first experiments indicate that for glycol as an additive the probability of spontaneous detonations increases with the ionic or total concentration of reacting material and also increases with a decrease in the amount of glycol in the system (Table I). At approximately 50% by volume of added glycol the probability of explosion was practically nonexistent for any concentration of reacting material. These results were obtained using the diffusion technique of Miles (Figure 1) for

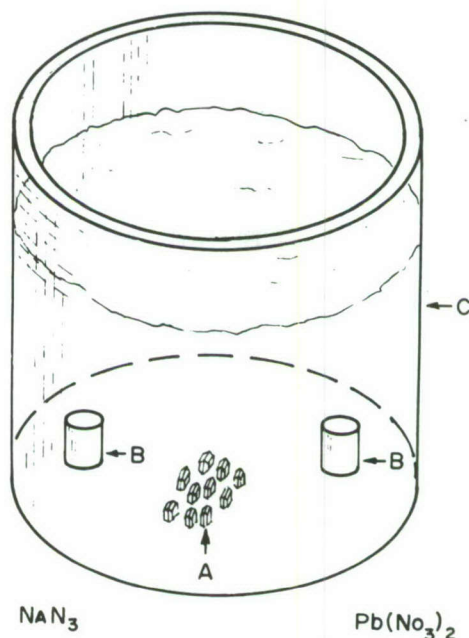


Figure 1. Growing assembly.

growing monoclinic crystals of lead azide. However, using the same ratio of glycol the absence of spontaneous detonations was also observed for the alpha modification. With the addition of glycol in large quantities one can observe an apparent large increase in the viscosity of the growing media. The effects of this viscosity increase could be expected to decrease the ionic mobility and the probability of the required particles reaching the surface of any growing crystal seed in order to cause the "size increasing" event. It has been realized for some time that the Gibbs-Thomson⁵ relation could be applied in a qualitative way to the increase in size of the incipient new phase. It would have an increased vapor pressure or solubility when first formed because of its minute size. It would, therefore, immediately disappear rather than grow to a larger size. The quantitative relation governing is given by the following equation for an isotropic nucleus

$$\ln \alpha = \frac{2 \sigma M}{\rho R T r}$$

r = radius

σ = interfacial tension

ρ = density

α = solubility ratio

σ and α in the above equation are obviously solvent dependent and σ is not determined with any ease and certainty. A feeling for the effect of the factor α on the growth of a nucleus can be obtained from the work of Ostwald⁶ in which the driving force in crystal growth is shown to be supersaturation (Figure 2).

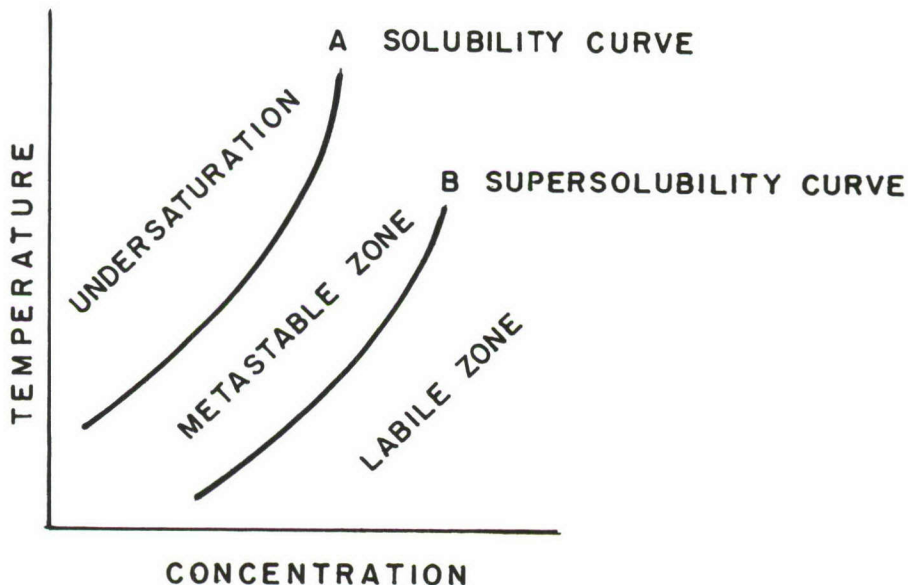


Figure 2

These considerations lead one to look at the effects of other solvents on the growth of lead azide and one obtains the following on the crystal growth parameters of lead azide as measured by the number of detonations (Table II).

Table II

<u>Solvent</u>	<u>No. of Samples</u>	<u>No. of Detonations</u>
Ethanol and Water	10	0
Methanol and Water	10	0
Acetone and Water	10	0
Glycol and Water	10	0

Samples obtained from each system were subjected to chemical and infrared analysis. The chemical determinations of lead from the first three samples are indistinguishable (Table III) and accordingly no sample is assigned to the respective determinations. The third determination of azide as silver azide detonated in the oven and delayed a re-determination during the process of replacing the oven. Infrared analysis performed on the samples are shown in the next series of figures where Figure 3 shows the characteristic azide bond from purely aqueous solution. Figure 4 shows the comparative samples from acetone. Samples from glycol and alcohol (Figure 5) also showed no anomalies. Sensitivity tests made on the crystals showed no change in the sensitivity of the crystals and after removal from solution the lead exhibits an indefinite shelf life.

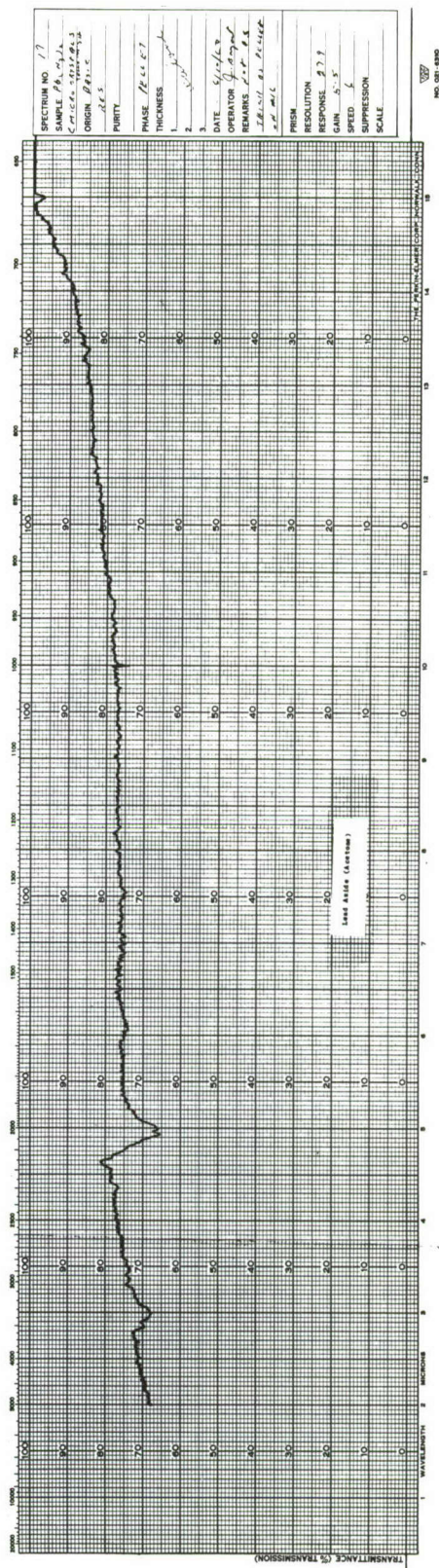
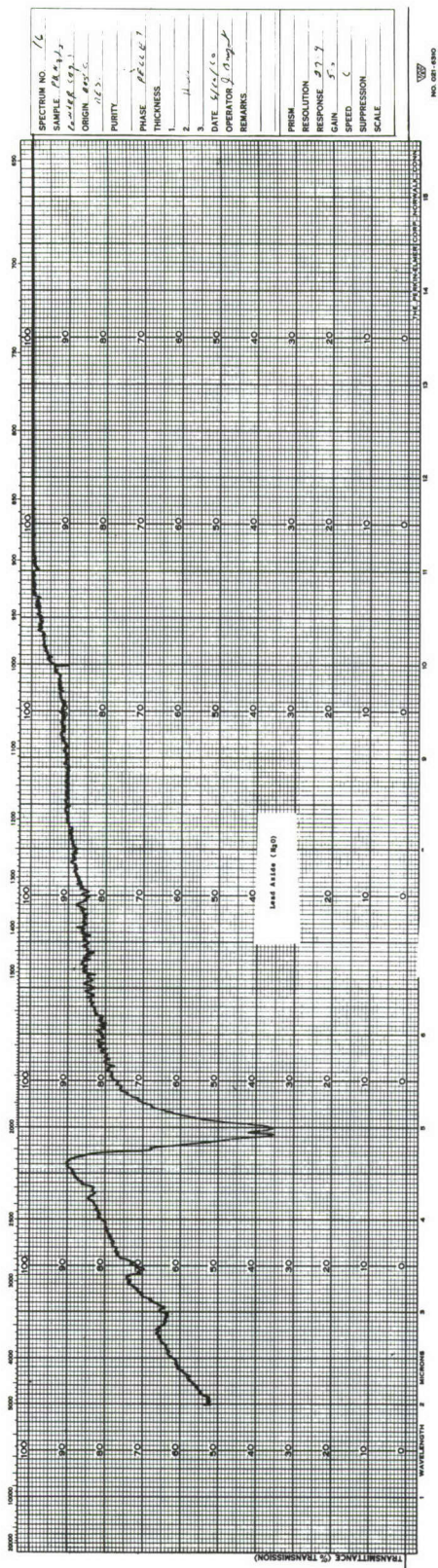
Table III

Azide Ion

<u>Theoretical AgN₃ Formed (grams)</u>	<u>Experimental AgN₃ Formed (grams)</u>	<u>Difference (grams)</u>
0.0075	0.0075	0.0000
0.0075	0.0076	0.0001

Lead Ion

<u>Sample Wt. (grams)</u>	<u>Theoretical PbSO₄ Formed (grams)</u>	<u>Experimental PbSO₄ Formed (grams)</u>	<u>Difference (grams)</u>
0.3014	0.3138	0.3133	0.0005
0.1467	0.1527	0.1523	0.0004
0.1480	0.1541	0.1538	0.0003



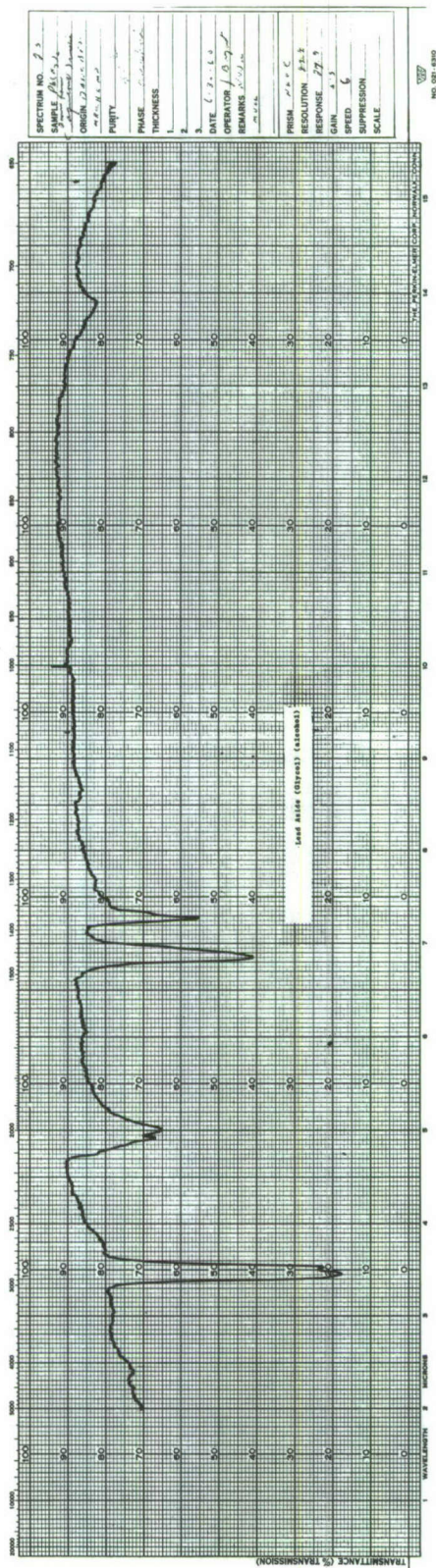


Figure 5

It can be concluded, then, that the spontaneous detonations have a great dependency upon solvent parameters and of immediate consideration is the effect of changing the solvent from water to something less polar. For the great majority of reactions which occur in solutions, the specific solvent properties determine not only the rate but the equilibrium. The chief property of reactions in aqueous solution is the formation of ions. We recognize in this situation a depletion of ions through the formation of the neutral azide molecule. An exact prediction of the total effect of the solvent and the ionic equilibrium is impossible. It should be expected, however, that as the solution becomes less polar, the dissociation should decrease and the dissociation constant should become progressively smaller. This is borne out by some data taken from the literature on acetic acid mixtures of dioxane and water (Figure 6).

IONIC EQUILIBRIA IN SOLUTIONS AT 25°C (CALORIES)



Solvent	F_1°	H_1°	$C_{p_1}^\circ$	S_1°
Water	6846	-92	-36.5	-22.1
Water + 20 percent Dioxane	7217	-52	-44.0	-24.4
Water + 45 percent Dioxane	8602	-442	-51.1	-30.3
Water + 70 percent Dioxane	11348	-610	-51.7	-40.1
Water + 82 percent Dioxane	13827	-1338	-124.5	-50.8

H. S. Harned and B. B. Owen, *The Physical Chemistry of Electrolytic Solutions*, Reinhold Publishing Corp., New York, 2nd Edition, 1950, Page 514.

Figure 6

The change in the ionization constant with the dielectric constant is very large. The results here are consistent with the observation that the spontaneous detonations are reacting particle concentration dependent. The dielectric constant of the solvents used as additives in the lead azide crystallization are water 80, glycol 41, alcohol 33, acetone 21, and for ethyl alcohol 23. It is known and shown in Figure 7 that the addition of a non-electrolyte as a rule lowers the dielectric constant. For the addition of electrolytes, the experimental data do not allow any definite conclusion to be drawn.

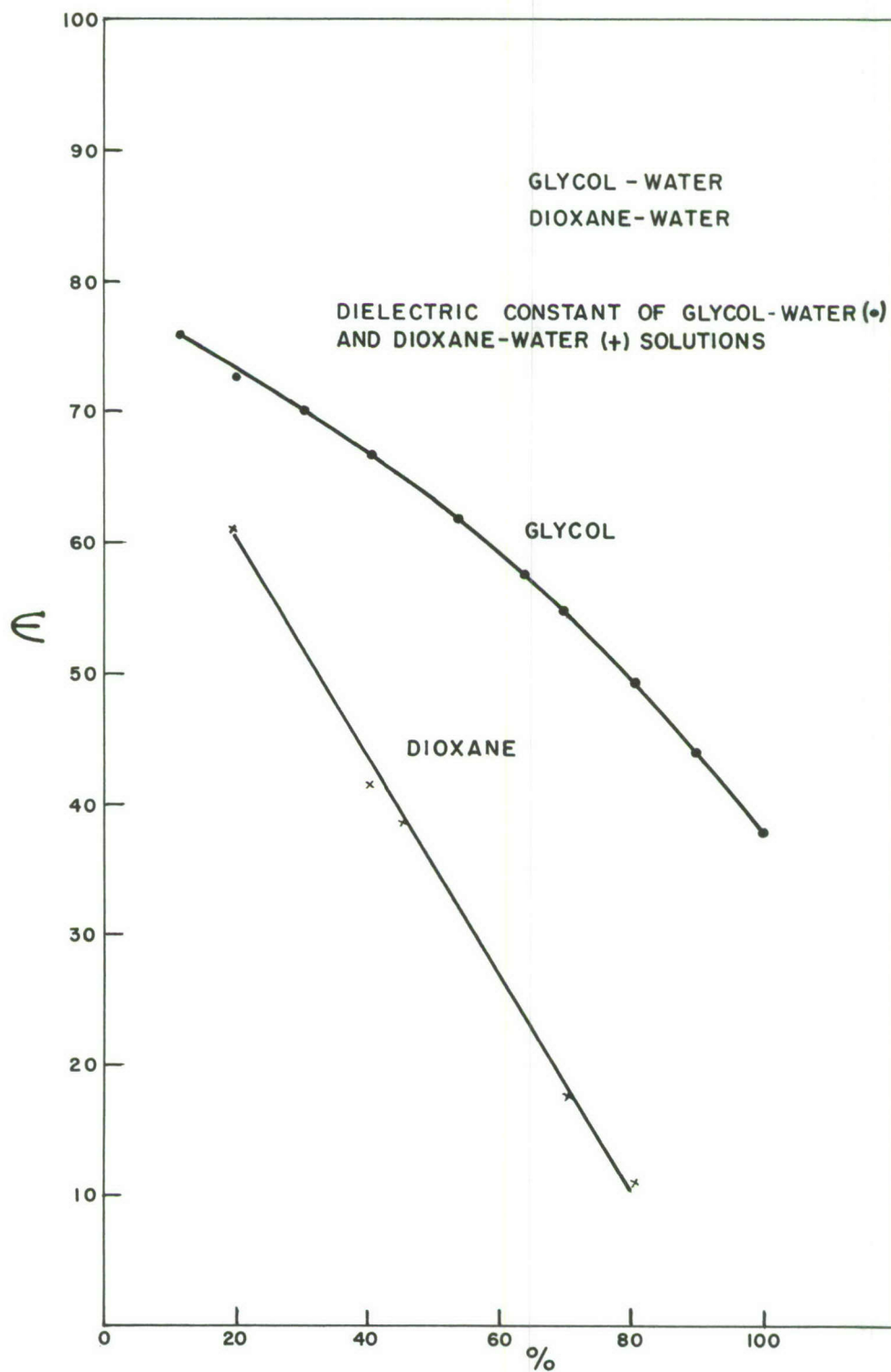


Figure 7

When a molecule is dissociated into a pair of ions the work done is stored as the mutual potential energy of the ions. If later the ions are allowed to approach each other, the stored potential energy becomes available and can be absorbed either by the solvent or the growing crystal. At the same time the dielectric becomes free of the ionic fields and when the dielectric consists of polar molecules, the liberations of the dipoles from the lead and azide ionic fields could result in cooling. If an oversimplified electrostatic analogy is used certain generalizations may be made. Considering the crystallization as the bringing two ions from infinite distance to the equilibrium distance of the neutral molecule in a medium of dielectric constant D , then the electrical work is given by Coulomb's law

$$W = \frac{Z_A Z_B e^2}{rD} = \Delta F$$

and can be equated to the corresponding change in free energy. From the thermodynamic relation

$$\left[\frac{\partial(\Delta F)}{\partial T} \right]_P = -\Delta S$$

the change in entropy can be obtained and is given by

$$\Delta S = \frac{Z_A Z_B e^2}{rD} \cdot \frac{\partial \ln D}{\partial T}$$

In all cases it is obvious that during the formation of the crystal, ΔF and $T\Delta S$ have different signs and jointly through

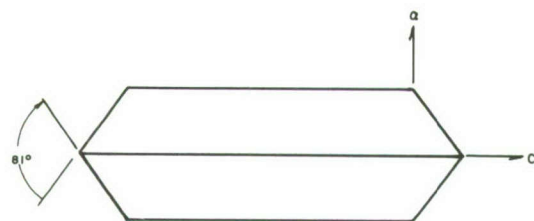
$$\Delta H = \Delta F + T\Delta S$$

determine the energy distribution in the system. We are able then, through the dielectric, to alter the magnitude of the heat change and the related equilibrium of the reactions.

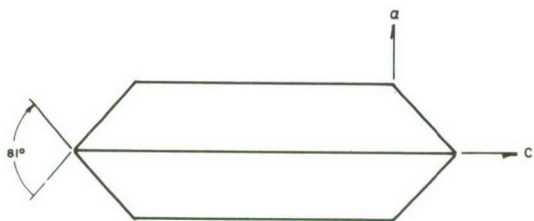
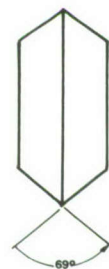
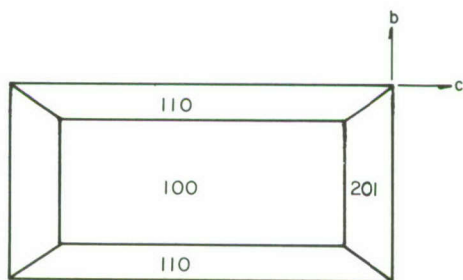
These considerations are not exact since the interaction of an ion with a molecular medium is not governed completely by the dielectric constant. They do, however, give a general trend of the effect of the solvent on the stability of independent ions in solutions.

The solution utilized at BRL for growth of crystals is a rather complicated one, consisting of the base, a buffered mixture of sodium acetate and acetic acid. To this base is added a number of solvents selected for a variety of theoretical reasons. During these studies with certain formamide derivatives a new habit of alpha lead azide has been prepared. Crystals of the size 4 to 6 mm taken from the

growing solution are of a new habit. The external appearance of the crystals has changed due to accelerated growth of the \bar{b} direction and retarded growth in the \bar{a} direction as compared with the reported alpha lead azide crystal. A comparatively large (100) face was observed as being characteristic for the new form. The (130) prism is replaced by the prism (110) but there may be seen an occasional (130) face. The macrodome (201) is still present. The features may be seen in Figure 8.



NEW HABIT
 α -Pb (N₃)₂



OLD HABIT
 α -Pb (N₃)₂

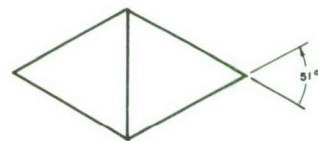
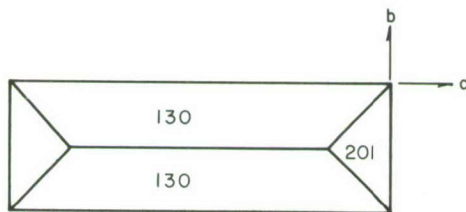


Figure 8

The interfacial angles were measured with an optical goniometer and are the same as those reported for lead azide by Hattori and McCrone⁷.

Insignificant variation in habit or optical quality was observed on crystals taken from several different lots. A comparison of the new crystal habit with the older reported habit is shown in Figure 9. The figure also shows the exceptional optical clarity of the new crystals. The extreme smoothness of the (100) face is seen from the interference photograph in Figure 10. The large area of this face greatly enhances optical, surface nucleation and x-ray studies of the new form.

Representative samples of the crystals were subjected to chemical and infrared analysis. The results were compared with lead azide grown from purely aqueous media. The chemical analysis are stoichiometric. The infrared data indicate no inclusions in the crystals. Infrared curves are shown for the aqueous lead azide sample (Figure 3), the new form (Figure 11), and the nujol sample background (Figure 12).



Figure 9

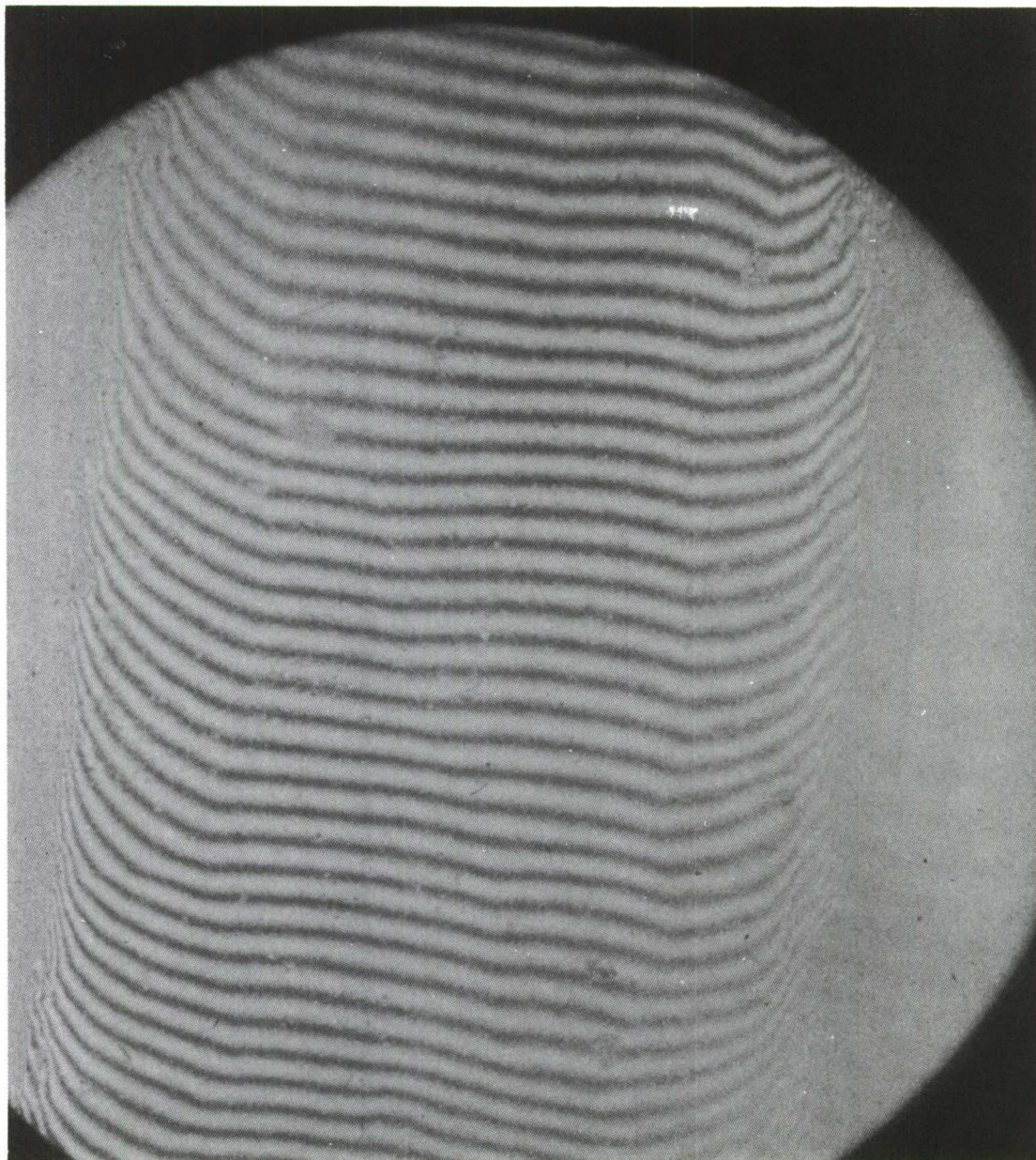


Figure 10

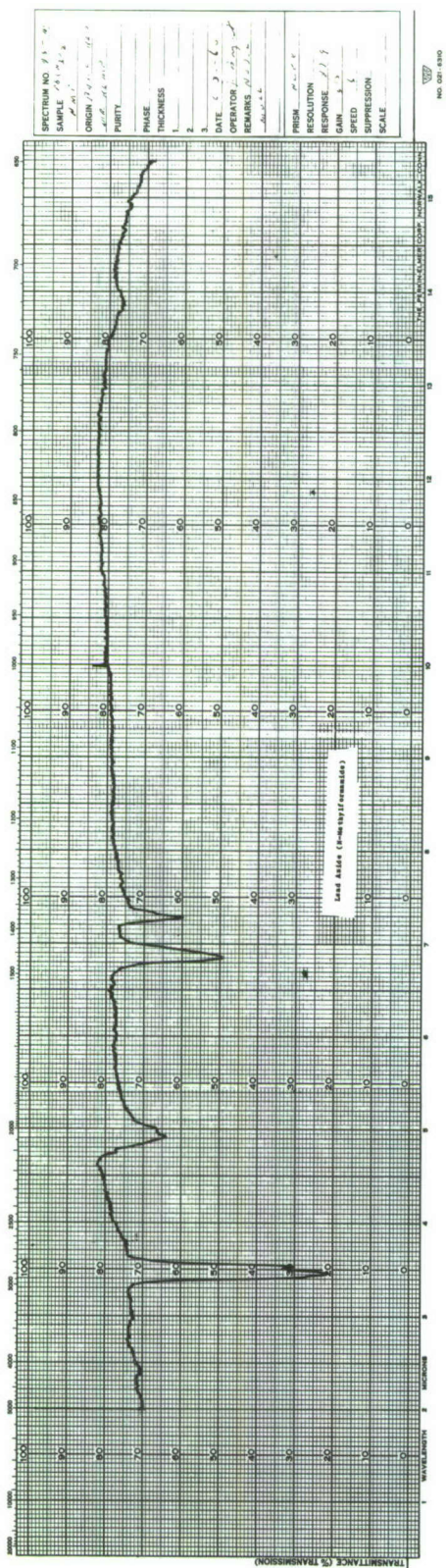


Figure 11

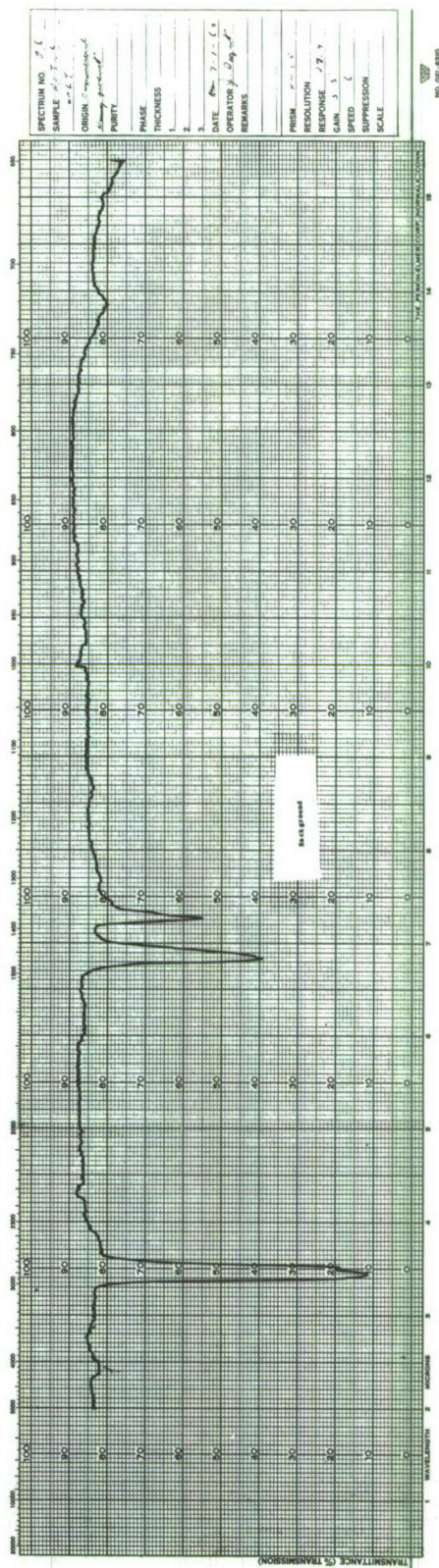


Figure 12

Acknowledgments

The crystallography and photographic work were performed by Mr. F. E. Wawner. Mr. O. Fred Kezer assisted with the experimental work.

References

1. Miles, J. Chem. Soc. 2532 (1931).
2. Harvalik, Informal Monthly Report, Contract DA-44-009-ENG-2439, 4-11-56 and 5-10-56.
3. ERDE Report #23/R/58, February 1959.
4. M. D. Kemp, Acta. Cryst. 13, 1080 (1960).
5. Lord Kelvin, Phil. Mag. 42, 448 (1881).
6. Wilhelm Ostwald, "Lehrbuch" Vol II Leipzig, Engelmann, 1896-1902.
7. K. Hattori and W. C. McCrone, Anal. Chem. 28, 1791 (1956).

THE MECHANISM OF UPTAKE OF IMPURITIES BY AZIDE CRYSTALS

by

M. Blais and V. R. Pai-Verneker
Picatinny Arsenal
Dover, New Jersey

Introduction

Photochemical and decomposition properties of inorganic azides have been extensively studied. Yoffe et al¹, Jacobs et al² and Reitzner et al³ have shown the role of impurities in the decomposition and it is unnecessary to mention how important it is to have extremely pure material. Different methods have, in the past, been tried to prepare pure azides. These methods have been based on trial and error. It was, therefore, felt that a systematic approach was necessary to study the mechanism of the uptake of impurities by azide crystals. No trace analysis of impurities in azides is yet reported. We have analyzed two samples of azides; the following table presents the list of the impurities which are found:

Table I

<u>Azide Analyzed</u>	<u>NaN₃</u>	<u>KN₃</u>	<u>Impurities Detected ppm (atomic)</u>
(The azides were prepared by passing HN ₃ in the metal carbonates.)	0.05	0.1	Bi
	0.3	8	Pb
	1.5	4	Ta
	2	6	Sn
	1	1	Cd
	0.1	0.3	Hg
	0.2	3	Rb
	2	3	Zn
	1	0.4	Cn
	5	0.4	Ni
	10	4	Fe
	0.5	3	Mn
	1	4	Cr
	0.5	0.4	Sc
	500	40	Ca
	1.5	---	K
	15	14	Cl
	3.5	14	S
	5	14	P
	15	280	Si
	5	14	Al
	15	14	Mg
	---	0.4	Na

In the present work uptake of iron by barium azide has been studied.

Barium azide was first prepared by Curtins and Rissam⁴. They reported that the azide is anhydrous. Since then several others Dennis, Benedict and Gill⁵, Günther, Andrew and Ringbam⁶ have reported the existence of one molecule of water of crystallization in barium azide. More recently Torkar⁷ has prepared barium azide in two ways: 1) crystallization from an aqueous HN_3 solution of barium azide and 2) precipitating from a slightly acidic solution by means of acetone. In both the preparations Torkar found a molecule of water of crystallization which could be driven off either by drying in a drying chamber at 80°C or over phosphorus pentoxide. In view of the presence of impurities in the azides and the disagreement over the results from different schools concerning the water of crystallization in barium azide we decided to undertake the study of the various methods of preparing barium azide. We have prepared barium azide by the following ways.

Experimental

Preparation and analysis of barium azide: HN_3 gas from the Reitzner generator was passed into a solution of barium carbonate in water till free of carbonate; the pH was between 3 and 4. The azide was then obtained from this solution by one of the following ways: 1) addition of acetone, 2) addition of ethanol and 3) by allowing the aqueous HN_3 solution of barium azide to evaporate in air. In case of precipitation, the azide was washed several times with the precipitating agent. After preparation, one part of the azide was kept in air for drying while the other was kept in a vacuum desiccator over phosphorus pentoxide. After leaving the samples for drying at room temperature for a week they were analyzed for barium and nitrogen. Results are presented in Table II.

Uptake of Fe^{59} by barium azide during precipitation: The following experiment will serve to describe how the uptake of Fe^{59} by barium azide was studied an aliquot portion of the barium azide stock solution was taken. A known amount of Fe^{59} (of the order of micro-micro curie) was added and stirred. The precipitating agent (alcohol or acetone as the case may be) was then added drop by drop with constant stirring until a fraction of barium azide was precipitated. It was then centrifuged and further washed. Barium azide was dried and weighed and Fe^{59} was estimated by a gamma ray spectrometer.

Stock solution of barium azide was prepared by dissolving a weighed amount of barium azide in doubly distilled water. The pH of such a solution was between 7 and 8. Another set of experiments was carried out in the pH range 4-5 or 5-6. For these experiments the stock solution was prepared by dissolving a weighed amount of barium azide in an aqueous HN_3 solution. Results are presented in Table III.

Results and Discussion

Table II

State of BaN ₆	% Ba Calculated	% N ₂ Calculated	
BaN ₆	61.98	38.01	
BaN ₆ $\frac{1}{2}$ H ₂ O	59.57	36.53	
BaN ₆ 1 H ₂ O	57.32	35.15	

Method of preparing	Drying	%Ba	%N ₂	Water of crystal
1) Acetone	Air	62.6 \pm 1%	37.8 \pm 1%	nil
	Vacuum	62.6 \pm 1%	37.7 \pm 1%	nil
2) Ethanol	Air	62.1 \pm 1%	38.15 \pm 1%	nil
	Vacuum	62.2 \pm 1%	37.6 \pm 1%	nil
3) Water	Air	59.20 \pm 1%	36.02 \pm 1%	$\frac{1}{2}$ H ₂ O
	Vacuum	62.37 \pm 1%	38.02 \pm 1%	nil

Table III

Precipitating Agent	Conditions	% BaN ₆ Precipitated	D	
a) Ethanol	pH 7-8	13.4	2.55	2.8
		39.2	2.83	2.09
		60.4	2.40	1.97
		66	2.57	1.66
		73.2	2.64	1.59
b) Ethanol	pH 4-5	21.2	2.01	1.81
		33.6	2.08	1.76
		56.4	2.65	1.79
		65.2	2.61	1.68
		73.6	2.19	1.47
c) Acetone	pH 7-8	54.4	5.77	2.63
		24	6.6	4.11
		61.2	8.0	2.76
		79.8	6.95	2.09
		82	8.11	2.12
		5.6	7.22	6.17
		12.4	5.84	4.55
		35	7.69	3.8
		65.4	---	1.43
		79.4	---	1.56
d) Acetone	pH 5-6	16.2	1.72	1.62
		47.2	1.90	1.55
		60.4	1.81	1.43
		73.2	1.87	1.37
		84.8	1.14	1.06

Our experiments on the preparation and analysis of barium azide clearly indicate as shown in Table II that barium azide can be prepared either in a hydrated state or in an anhydrous state by suitably choosing the method of preparation. During our study of the uptake of Fe^{59} by barium azide we have used ethanol and acetone as the precipitating agents and, therefore, we are throughout dealing with anhydrous barium azide. A close look at Table III and Figures 1 and 2 would reveal that of the distribution coefficients D and λ , D is constant whereas λ seems to decrease systematically with the increase in amount of barium azide precipitated. In the case of acetone precipitation in the pH range 7-8 one finds that there is a scatter in the D values but the λ 's are decreasing. The experimental conditions as one would see later were such that λ and not D should have been constant. One further notices that in the acetone precipitation in the pH range 7-8, the D values are round about 7 whereas in all other cases the D values are round about 2.

It is usually possible experimentally to differentiate between two general types of impurity uptake: 1) mixed crystal formation, i.e., incorporation of the impurity into the crystal lattice of the precipitate and 2) adsorption of the impurity on the surfaces of the

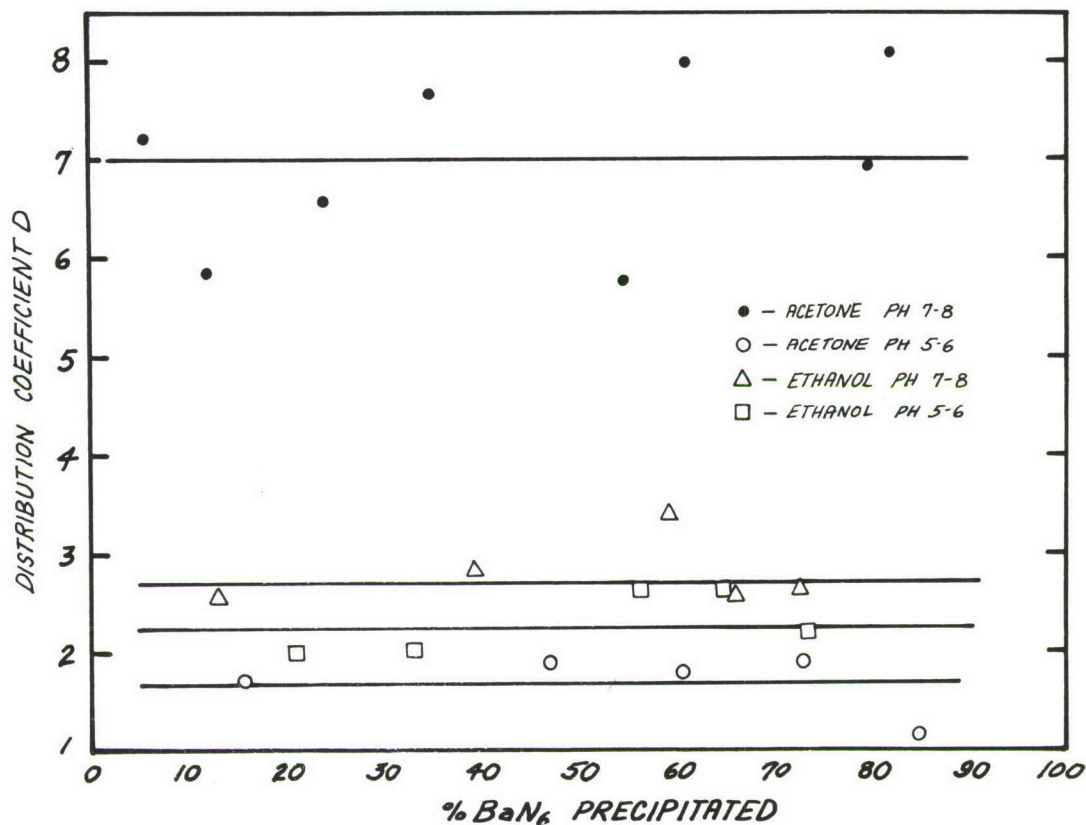


Figure 1. Distribution coefficient vs. % BaN₆ precipitated.

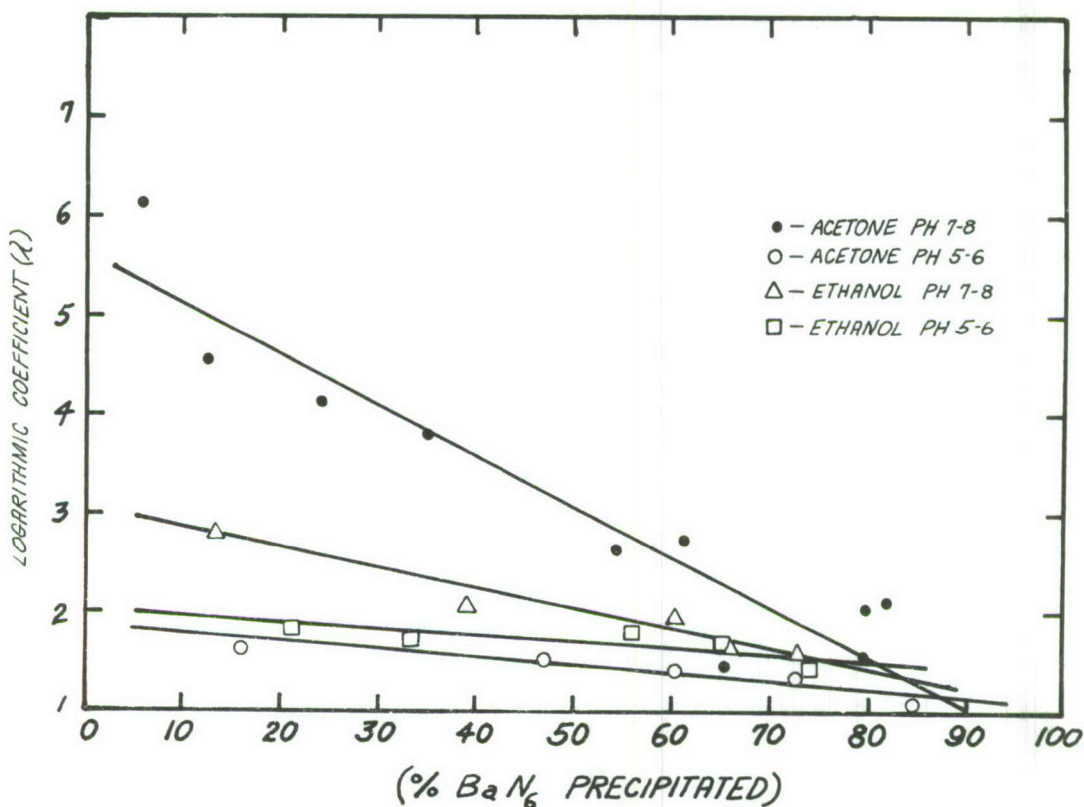


Figure 2. Logarithmic coefficient vs. % BaN₆ precipitated.

precipitate during or after its formation. When incorporation into the lattice occurs, the ratio of the fraction of impurity to the fraction of the precipitate removed from the solution is relatively independent of precipitating conditions such as the presence or absence of an excess of the precipitant or of highly charged ions. If the impurity is carried by means of an adsorption process, this ratio is usually very dependent on the precipitating conditions. When impurity is incorporated into the lattice (substitution) the distribution is continuous, though not necessarily homogeneous; whereas if the impurity is adsorbed, its distribution may be discontinuous, the impurity being distributed over the surface of the crystals or in some cases only on certain planes of the crystal. In the case of mixed crystal formation the distribution of the impurity between the precipitate and the solution can follow

1) Berthelot-Niernst law

$$\left(\frac{\text{Guest ions}}{\text{Host ions}} \right)_{\text{solid}} = D \left(\frac{\text{Guest ions}}{\text{Host ions}} \right)_{\text{solution}}$$

if equilibrium between the ions in the interior of the precipitate and the ions in solution is reached or 2) Logarithmic distribution law

$$\log \frac{\text{total guest ions}}{\text{guest ions in solution}} = \lambda \log \frac{\text{total host ions}}{\text{host ions in solution}}$$

if the distribution is inhomogeneous. Adsorption of impurities from solution generally follows Freundlich's adsorption isotherm.

Our experiments on the uptake of Fe^{59} by barium azide precipitated by alcohol clearly indicate that D is constant and that it is independent of the precipitating conditions. This, therefore, suggests that iron is carried through mixed crystal formation. It is true that the experimental conditions should have favored a constancy in the λ values rather than in the D values. It is, however, known that if the precipitate is fine then the diffusion through the crystal lattice becomes faster and D rather than λ comes out to be constant.⁸ Barium azide prepared in the above way is actually in the form of fine crystals. Acetone precipitated barium azide, on the other hand, carries iron, the mechanism of which depends on the experimental conditions. In an acidic solution where the pH is between 5-6, D in the case of acetone precipitation, is constant and the same as that precipitated by alcohol whereas in the pH range 7-8 it is about three times higher and although it is fairly constant its occasional variation suffices to suggest the mechanism of internal adsorption⁹. The causes of this type of behavior may be many-fold. The nature of the acetone precipitated barium azide varies according to the pH and the precipitate is coarse and not fine as in the case of alcohol precipitation. Hence, it is possible that the growth mechanism is different. One could have attributed the lower value of D in the pH range 5-6 to an excess of N_3^- ions if the complex ion carried by barium azide had a negative charge. It is known from the work of Ricca¹⁰ that the iron complex is $[\text{Fe}(\text{N}_3)]^{++}$. Accordingly, one is led to conclude that the high D value is either due to 1) a change in the nature of the growth of the azide crystal or 2) a change in the nature of the complex in the presence of acetone. Iron is known to form complexes like $[\text{Fe}(\text{NCS})_6]^-$. It has been shown that copper forms complexes with azide ions of the type $[\text{Cu}(\text{N}_3)_y]^{X-}$ where X can be 1, 2 or 4. There is, therefore, no reason why iron should not form complexes with azide ion bearing a negative sign. This then could easily explain the low D value in the pH range 5-6.

It seems, therefore, that if the other impurities behave in the same way as iron when barium azide is precipitated, the best method of preparation would involve precipitation of small fractions of barium azide by ethanol or acetone in the low pH range. Preparation by evaporation of aqueous solution of barium azide seems to result in barium azide which is not anhydrous.

Acknowledgment

The authors take pleasure in thanking Dr. H. J. Matsuguma, Chief of the Explosives Laboratory, Picatinny Arsenal, for encouragement in the progress of the work.

References

1. Yoffe, Evans & Deb: Nature 294, 180 (1957).
2. Jacobs, Tompkins & Pai-Verneker: J. Phys. Chem 66, 1113 (1962).
3. Reitzner, Kaufman & Bartell: J. Phys. Chem. 66, 421 (1962).
4. Curtins & Rissam: J. pr. Ch.: 58, 287 (1898).
5. Dennis, Benedict & Gill: J. Am. Soc. 20, 229 (1898); Z Anorg. Ch. 17, 22 (1898).
6. Günther, Andrew & Ringbom: Z. Elektroch 36, 217 (1930).
7. Torkar: Private Communication.
8. Purkayastha and Pai-Verneker: Anal. Chem. 31, 814 (1959).
9. Radioactivity Applied to Chemistry - Wahl and Bonner, p 123 6.1 (d).
10. Ricca: Gazz. Chim. ital 75, 71 (1945).

AN ELECTRON MICROSCOPIC INVESTIGATION OF THE THERMAL DECOMPOSITION OF NaN_3 AND KN_3 CRYSTALS

by

J. A. Joebstl

Basic Research Laboratory

U. S. Army Engineer Research and Development Laboratories
Fort Belvoir, Virginia

Abstract

The thermal decomposition of NaN_3 and KN_3 crystals has been studied by means of electron microscopy. The crystals were cleaved in a vacuum cleavage apparatus for preparation of clean surfaces. Subsequent heating decomposed the cleaved surfaces to a maximum depth of one micron. Replica techniques and the gold decoration technique after Bassett were then applied for examination of the surface decomposition. The thermal decomposition of the alkali azides results in the formation of alkali metal and nitrogen. Both decomposition products are volatile at the decomposition temperature. In the course of the decomposition, characteristic surface structures were observed which show evidence of a preferential decomposition at surface steps and surface imperfections. Similar decomposition studies on contaminated surfaces gave different results thus demonstrating the importance of the surface condition for the initial stage of decomposition of a metastable crystal.

It was reported in a previous paper¹ that during the initial surface decomposition of NaN_3 characteristic surface structures were observed, which seemed to indicate a preferential decomposition at sites of crystal imperfections. During the past year this study of the surface decomposition of alkali azide crystals was continued and the results of this investigation will be presented in the following report.

The decomposition studies were again carried out on cleavage planes of alkali azides, because naturally grown crystal faces are heavily contaminated and, therefore, unusable for such investigations. The crystals were cleaved in a vacuum cleavage apparatus² and the cleaved surfaces were subsequently thermally decomposed to a maximum depth of one micron. Replica techniques were then applied for an electron microscopic examination of the surface decomposition. Some crystals, however, were cleaved in a dry box containing dry nitrogen and subsequently transferred into the vacuum hot stage of the Reichert Metallographic Microscope "MeF", where the thermal decomposition was initiated. After the investigation of the surface changes

by means of optical microscopy (using the interference contrast technique) the crystals were transferred into an evaporation unit for the preparation of preshadowed replica. The thermal decomposition was carried out always in dynamic vacuum to avoid a formation of specks of alkali metal on the crystal surfaces. In all experiments the crystals were decomposed at 320°C and the length of heat treatment varied between 2 and 20 minutes. The induction period of NaN_3 at this temperature was between 40 and 60 minutes. Therefore, it can be assumed, that all of the observed surface changes are due to surface decomposition during the induction period.

The first sign of decomposition appeared after three minutes of heat treatment (Figure 1). Small pits developed along cleavage steps, whereas no changes were observed in areas free of surface imperfections. Further decomposition (after about five minutes of heat treatment) altered the appearance of cleavage steps considerably (Figure 2). Formerly straight steps fissured and split up in steps of smaller heights. Relatively large surface irregularities disappeared during this initial surface decomposition (Figure 3). The first part of the decomposition process consists, therefore, in a retreat of microscopic surface step formations and a leveling of the crystal surface. After ten minutes of heat treatment, decomposition could also be observed on surface areas free of visible imperfections. In the further course of decomposition a surface structure developed, which was very similar to that observed by other investigators on cleavage planes of ionic crystals after heat etching (Figure 4). Etch lines appeared along crystallographic directions and some crystals got covered with a network of these lines (Figure 5). Many of these etch lines exhibited an ideal V-shape (Figure 6). Simultaneously with these etch patterns a wavy step figuration appeared and soon covered large parts of the crystal surface (Figure 7). All of these observations indicate a preferential decomposition at sites of imperfections during this stage of thermal decomposition. Continuation of the decomposition process made the surface structure more and more irregular. Different crystallographic planes now clearly exhibited different thermal stabilities (Figure 8). Some crystals were cleaved in this stage of thermal decomposition after the heat treatment. The electron microscopic examination revealed that the thermal decomposition took place at this stage throughout the crystal along boundaries (Figure 9).

The following scheme of the initial decomposition process was the result of the above microscopical study of the thermal decomposition of NaN_3 . The thermal decomposition starts at surface irregularities like steps, etc. Further decomposition then occurs at sites of crystal imperfections. Until this stage the decomposition is a pure surface reaction. This decomposition on the external surface is followed by a spreading out of the decomposition process throughout the crystal along boundaries.

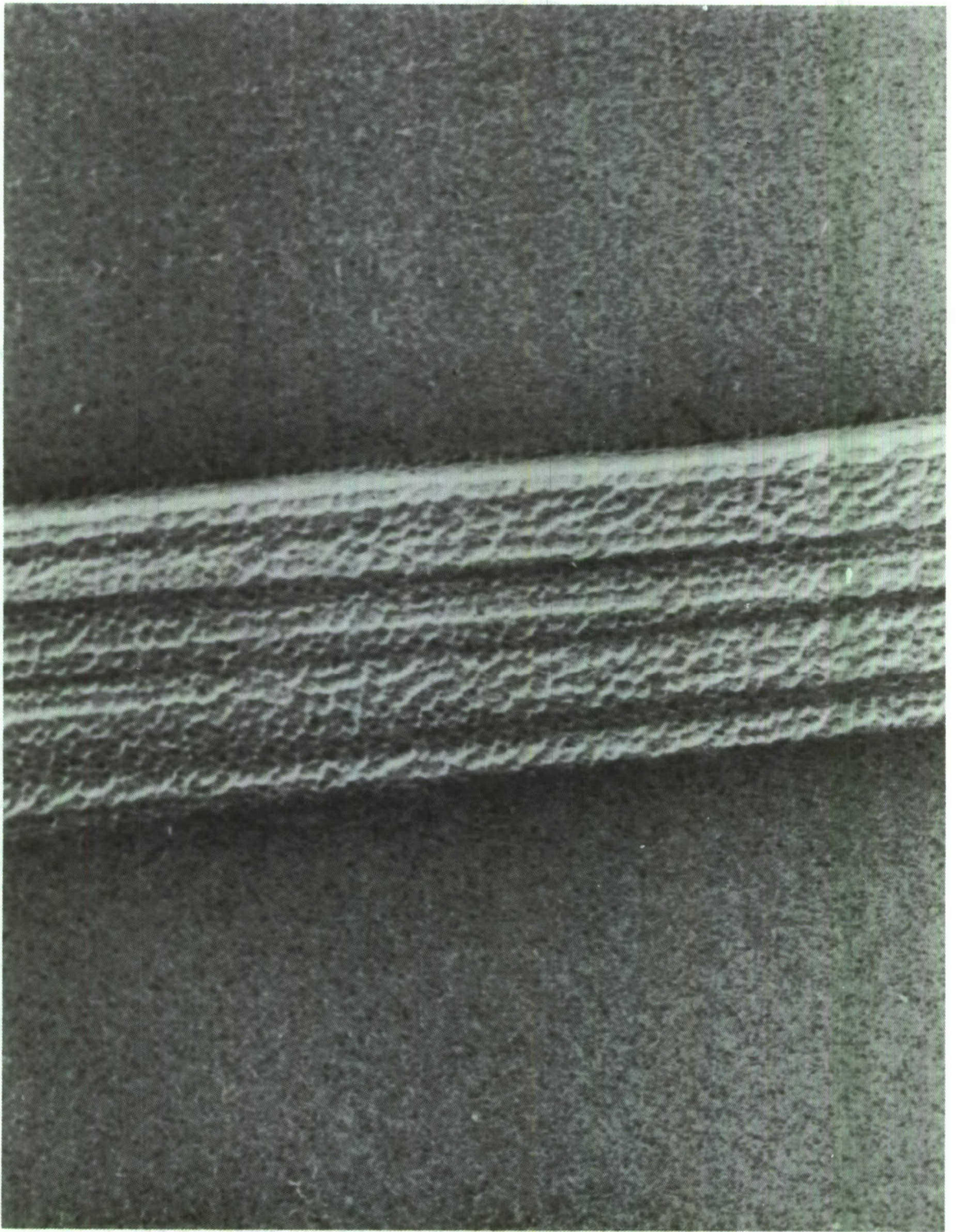


Figure 1

120,000X

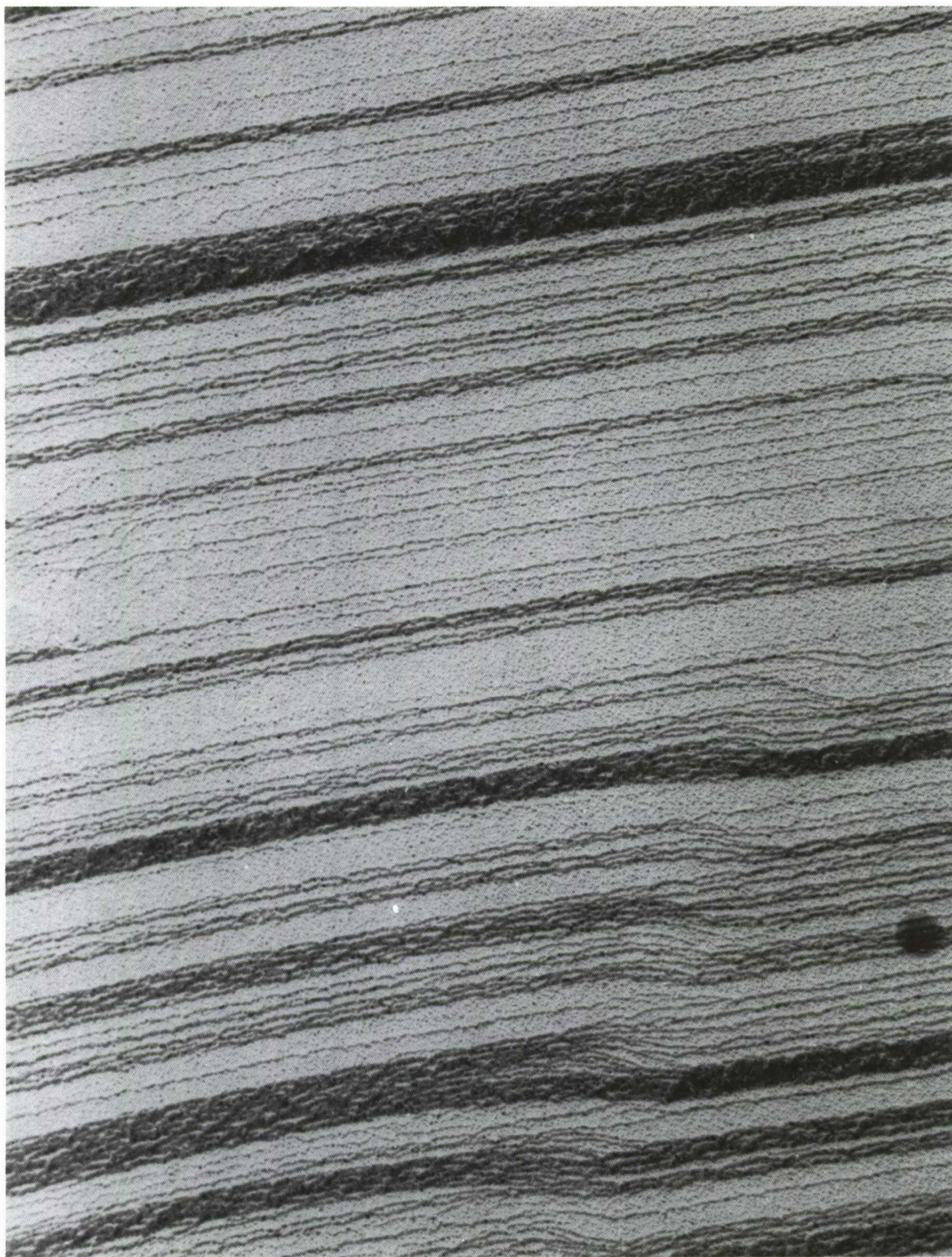


Figure 2

80,000X



Figure 3

50,000X

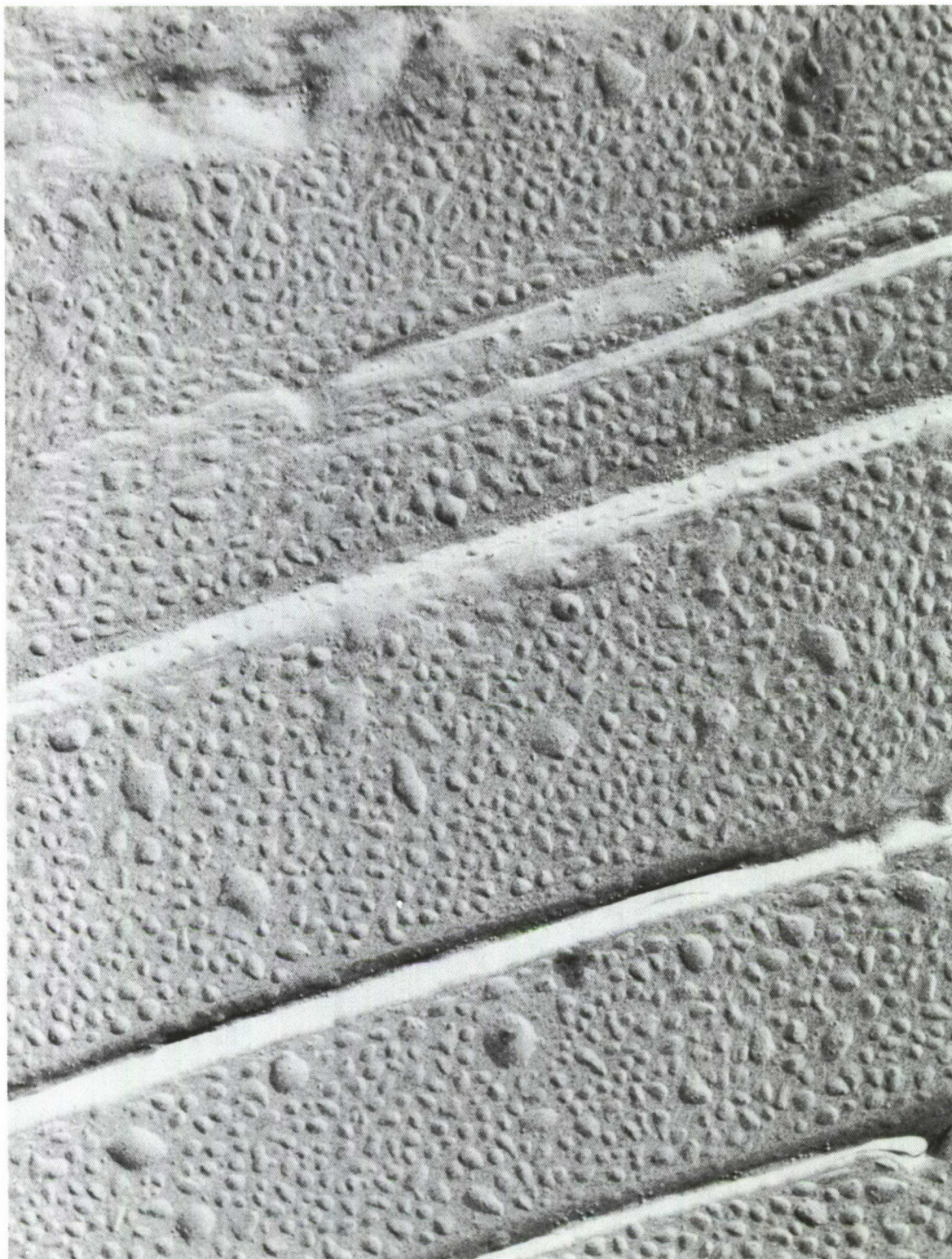


Figure 4

50,000X

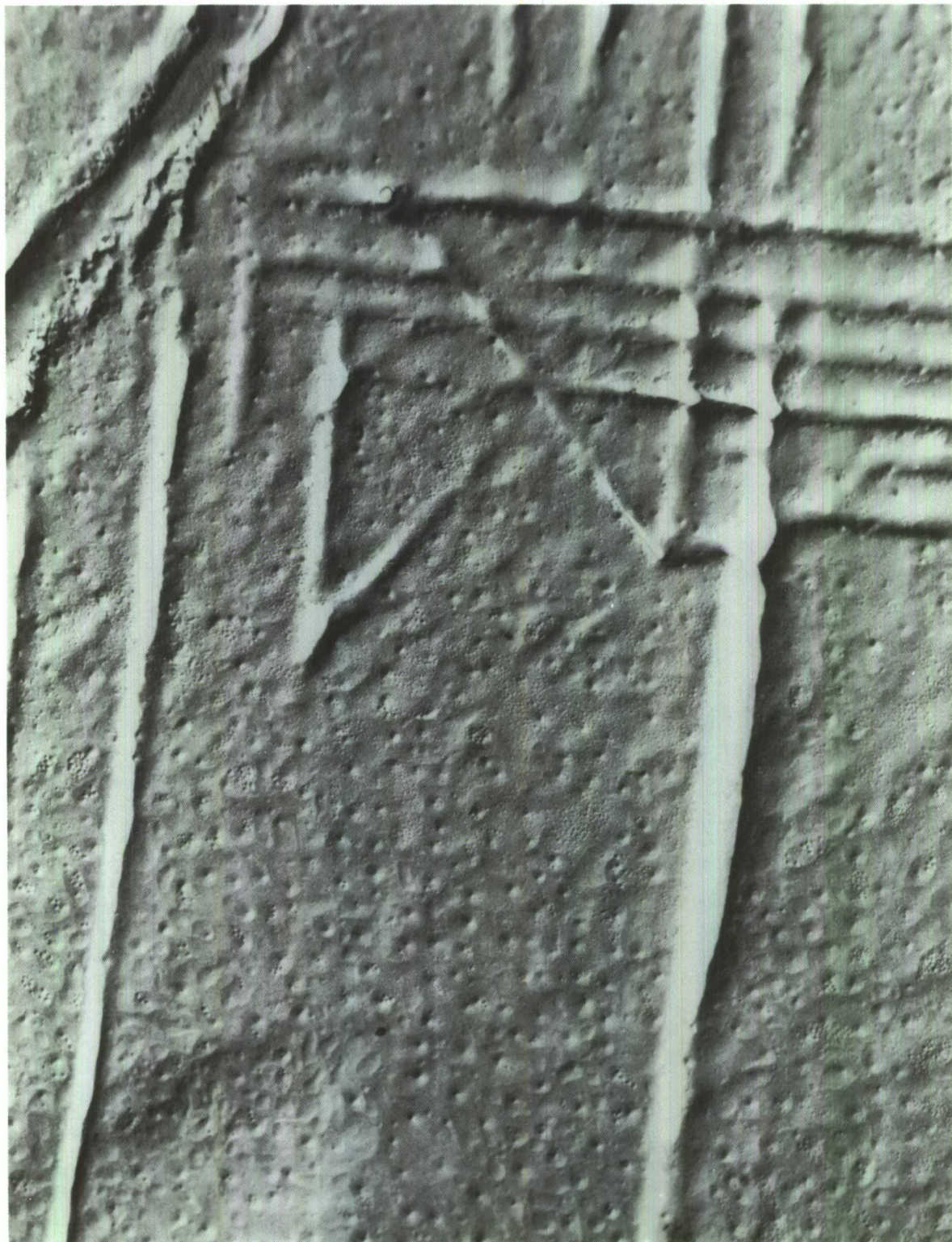


Figure 5

50,000X

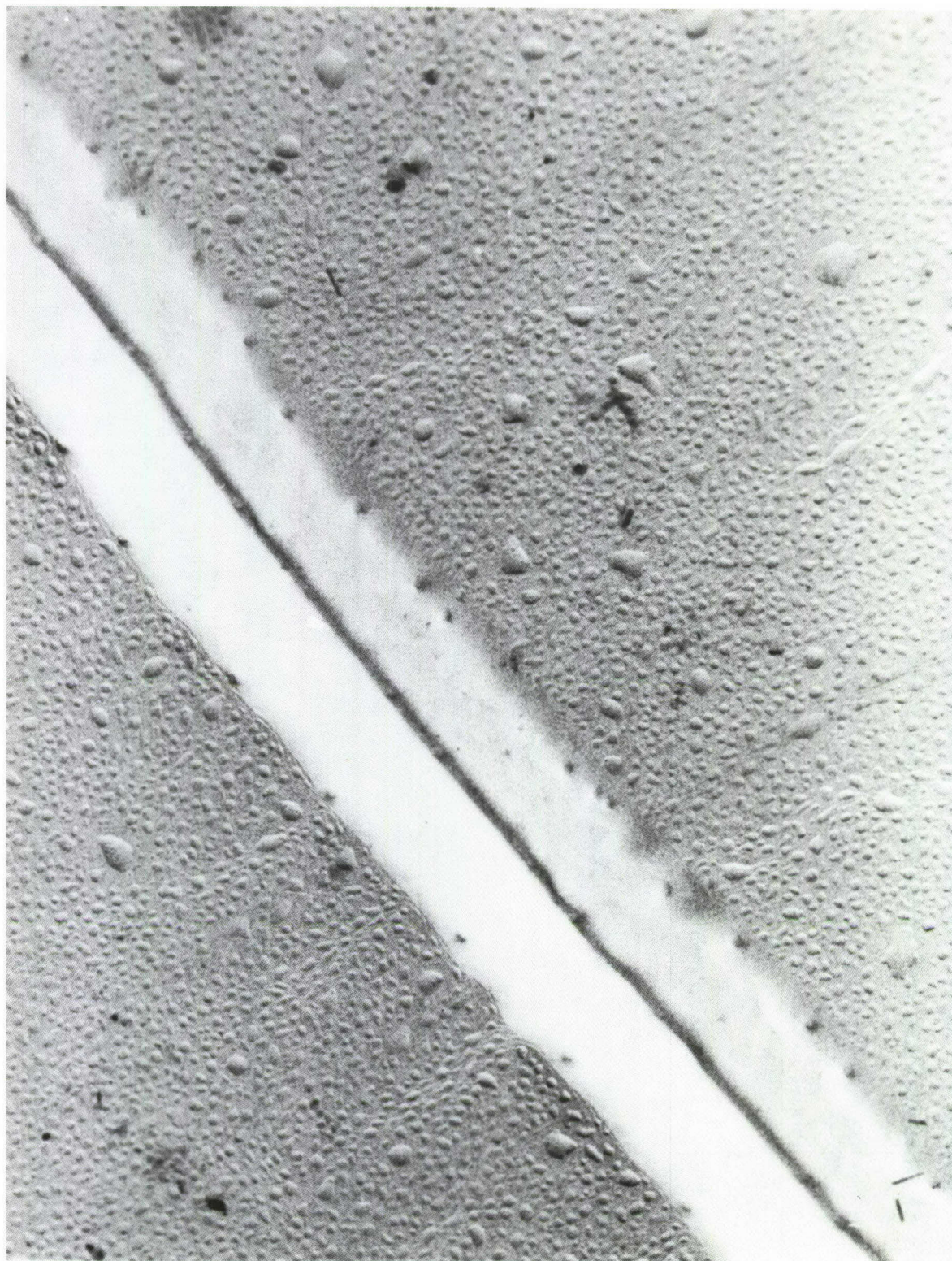


Figure 6

80,000X

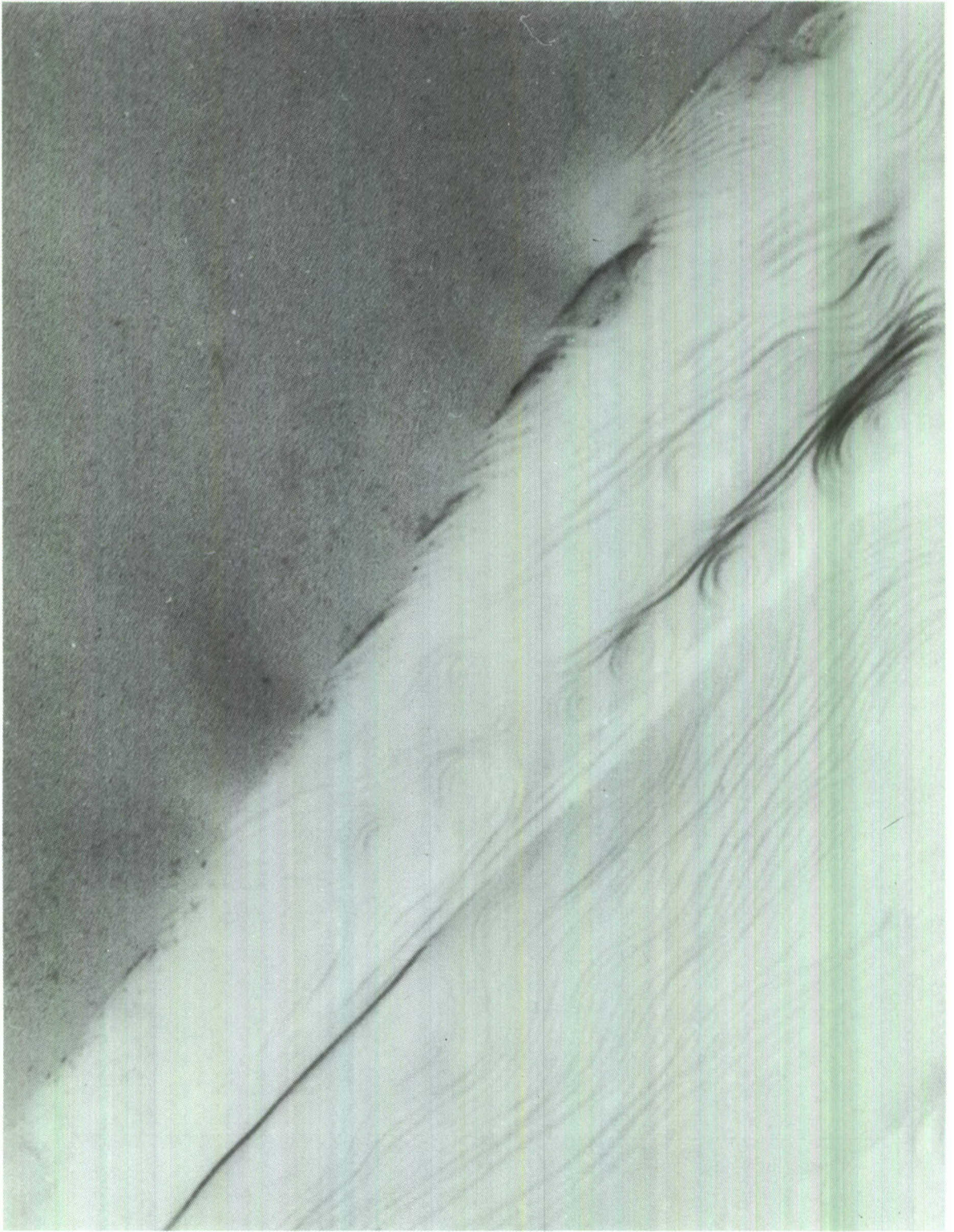


Figure 7

50,000X

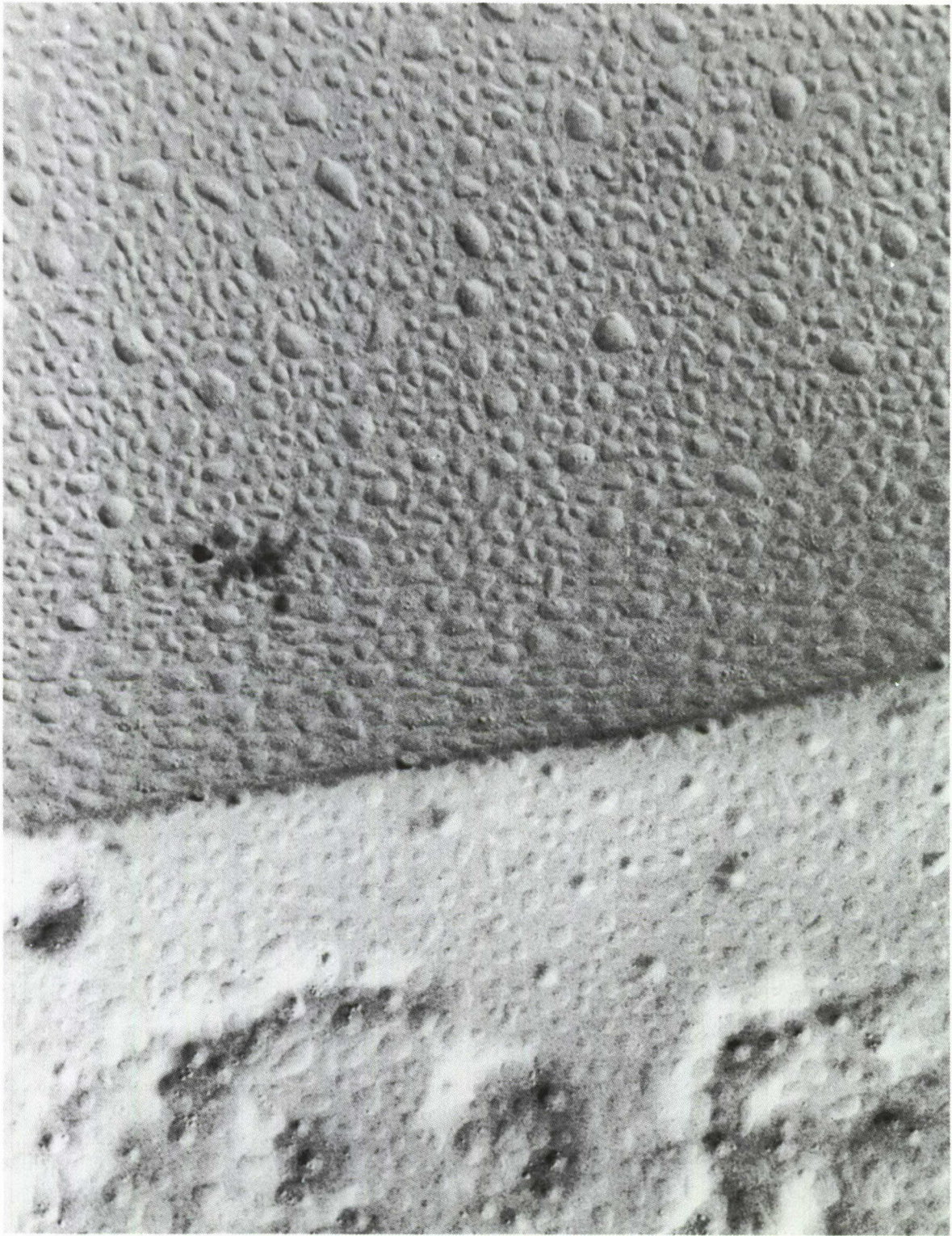


Figure 8

50,000X



Figure 9

50,000X

Similar decomposition studies were carried out with crystals which were exposed to air for several hours between the cleavage and the decomposition process. Electron microscopic examination proved that the cleavage planes were heavily contaminated after this treatment. It was very difficult to follow the thermal decomposition on these contaminated surfaces (Figure 10). But, nevertheless, it can be said that no etching was observed on these crystal surfaces during the decomposition process. Surface contamination seems to hinder the preferential decomposition at surface imperfections.

The decomposition studies on KN_3 were also carried out at the temperature of 320°C . The surface changes observed on these crystals were similar to those on NaN_3 . In the case of KN_3 , however, it was difficult to differentiate between the effect of preferential decomposition and the beginning of the melting at surface steps (melting point of $\text{KN}_3 = 345^\circ \text{C}$).

During the last months an attempt was made to reveal and to identify the defect structure of crystal surfaces of NaN_3 by means of controlled thermal decomposition. The gold decoration technique after Bassett³ was applied in these experiments for obtaining replica which can resolve monolayer steps. This technique consists in the decoration of surface irregularities (like monolayer steps) with gold nuclei. This method can resolve details of the micro structure of crystal surfaces, which cannot be revealed otherwise by conventional replica methods. With this decoration method surface structures were observed on cleavage planes of NaN_3 , which were too complex for simple cleavage structures (Figures 11 and 12). It was, therefore, concluded that these were already structures of slightly decomposed surfaces. This is probably due to the fact that surface decomposition on azide crystals can take place during the replication process initiated by the heat radiation from the evaporation source. This relatively uncontrolled surface decomposition during the evaporation of metal and carbon on the cleavage planes cannot be revealed with conventional replica methods because of their lower resolution. At the present time experiments are being carried out to exclude this heat radiation by using a heat filter, designed and constructed by H. Horn⁴. This filter acts as a speed selector; it prevents the heat and light rays originating from the evaporation source from arriving at the sample. This apparatus makes it possible to condense metal nuclei on metastable surfaces with a minimum of energy interaction. The application of this evaporation technique will certainly be a great step forward for the attempt to identify crystal defects in inorganic azides by means of preferential decomposition.



Figure 10

50,000X

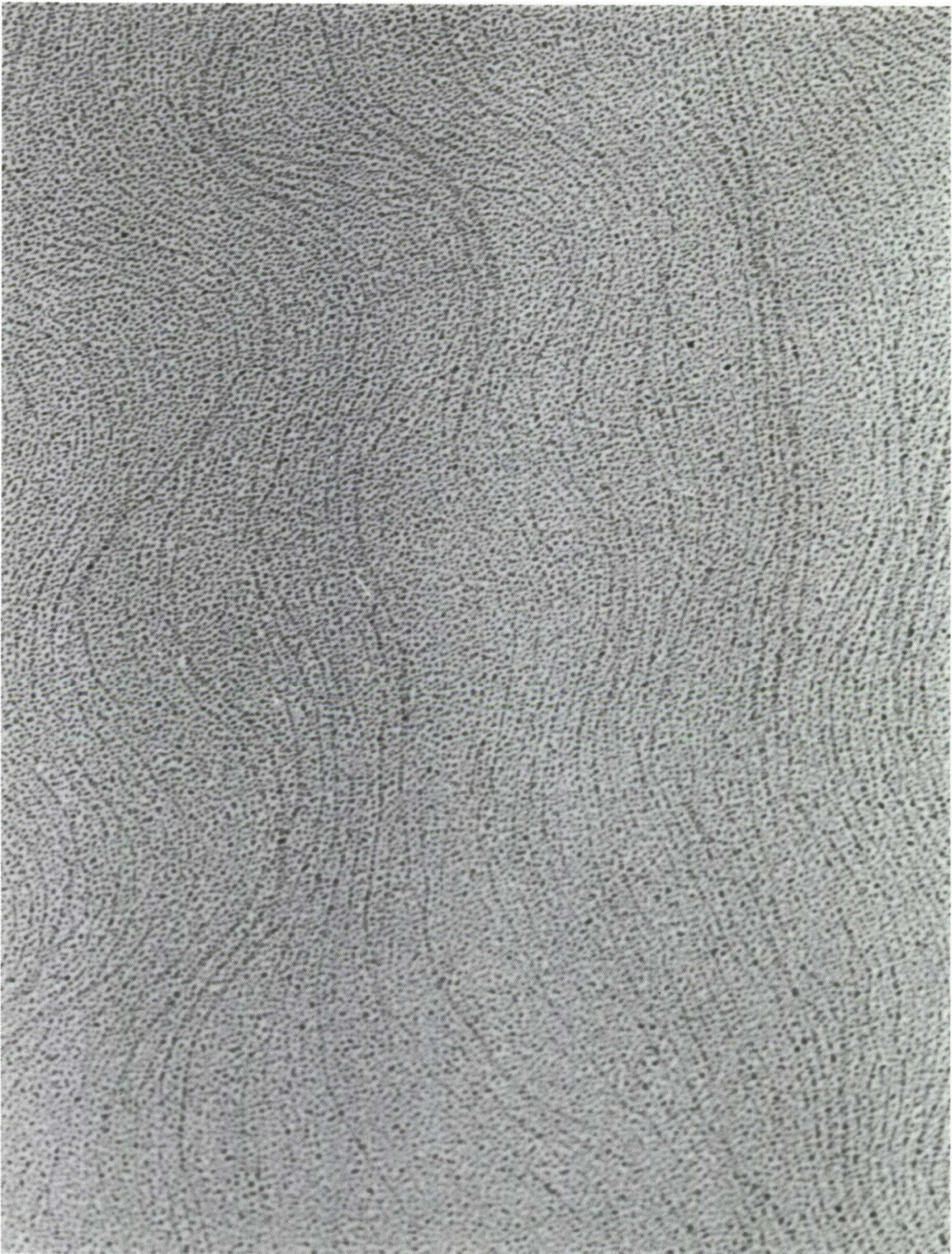


Figure 11

100,000X



Figure 12

100,000X

References

1. J. A. Joebstl, Proceedings of the Eleventh Basic Research Group Contractors' Conference and Symposium, 1962, pp. 185-206.
2. J. A. Joebstl, The Microscope and Crystal Front, 13, No. 10 (1963).
3. G. A. Bassett, Phil. Mag. 3, 1042 (1958).
4. H. R. F. Horn, Proceedings of the Fifth International Congress for Electron Microscopy, 1962, A-9.

THE GAS PHASE DECOMPOSITION OF
SIMPLE ORGANIC AZIDES

by

M. S. O'Dell and B. deB. Darwent
Department of Chemistry
The Catholic University of America
Washington, D. C.

The mechanism and kinetics of the photochemical and thermal decompositions of simple organic azides are reviewed and compared with the decomposition of similar compounds. In particular, the effect of alteration of the hydrocarbon portion of the compounds on their modes of decomposition are examined.

The proposed method of investigating the kinetics and mechanism of the thermal decomposition of methyl-, ethyl-, isopropyl-, and tertiary butyl azides is presented. Some attention is paid to surface reactions.

DECOMPOSITION OF ALKALINE EARTH AZIDES UNDER ORGANIC SOLVENTS

by

Y. Okamoto, J. C. Goswami and W. Brenner
Research Division, School of Engineering and Science
New York University
New York, N. Y.

The thermal decomposition of a number of inorganic azides, especially those of heavy metals, proceeds explosively and results in formation of corresponding metal and nitrogen gas according to the reaction:



During the decomposition of azides such as calcium azide, however, some nitride is also formed. The experiments of Tompkins and Young¹ suggest that the nitride is not an intermediate in the decomposition but arises from the reaction of metallic calcium with gaseous nitrogen formed during the decomposition.

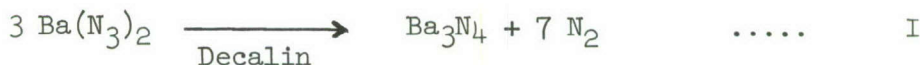
Barium azide was found to decompose smoothly in organic solvent such as decalin or xylene near the boiling point and produced a finely divided black powder and nitrogen gas.² The results of the elemental analysis of the product are shown in Table I.

Table I

Elemental Analysis of the Black Powder

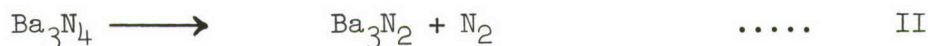
	Observed wt. %	Calculated wt. % as Ba ₃ N ₄
Nitrogen	12.49	11.95
	12.10	
	12.72	
Barium	86.0	88.05

The data suggest that the black powder corresponds to barium pernitride, Ba₃N₄. Therefore, this reaction is believed to take place as shown in the equation I:

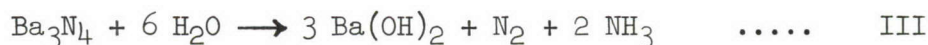


The x-ray analysis of this compound shows it has an hexagonal structure, $a = 5.22 \text{ \AA}$ and $c = 5.50 \text{ \AA}$.

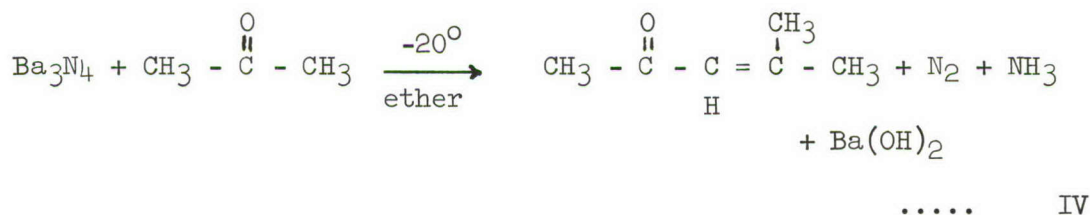
Upon further heating in nitrogen atmosphere, the barium pernitride decomposed into barium nitride and gave off additional nitrogen gas:



The compound was exceedingly reactive with water and air. With water, barium pernitride was rapidly converted to barium hydroxide and nitrogen gas and ammonia were also produced. The following equation (III) shows this reaction:

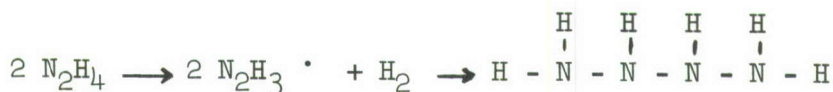


This material was also found to be highly active catalyst for the Aldol condensation.³ The compound exhibits much greater reactivity than that of aluminum tri-*t*-butyl alcoholate⁴ known as a powerful catalytic agent for this reaction. Barium pernitride reacts with acetone at -15 to -20°C . Evolution of nitrogen and ammonia started immediately and diacetone alcohol was obtained as the main product:



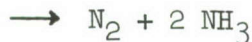
Calcium and strontium azide were also decomposed smoothly in decalin and produced their pernitrides. Hartmann and his coworkers⁴ have reported strontium and calcium pernitrides which were believed to be prepared from the corresponding amides by heating in high vacuum.

The constitution of these pernitrides has not yet been established. However, Rice and Scherber⁵ observed that, when hydrazine was pyrolyzed, a yellow material was condensed at 77°K . Upon raising the temperature to 95°K , the material decomposed into nitrogen and ammonia (mole ratio N_2 to NH_3 was 1 to 2). They suggested the yellow compound was tetrazane which formed during condensation at the low temperature by combination of two hydrazine radicals derived from the pyrolytic process:



at 77° K

Tetrazane



The alkaline earth pernitrides such as barium, strontium and calcium were also found to react with aqueous acid and formed nitrogen gas and ammonium salts (mole ratio 1 to 2). According to the results, these alkaline earth pernitrides might correspond to their tetrazane salts.



The mechanism of thermal decomposition of alkaline earth azides such as barium, strontium, and calcium azides has not yet been fully understood. However, the detailed investigations and isolation of the intermediate products (such as Ba_3N_4) from the decomposition of such azides under organic compounds may throw some light in the mechanism study of thermal decomposition of the alkaline azides.

References

1. F. C. Tompkins and D. A. Young; Discussions Faraday Soc. 23, 202 (1957).
2. Y. Okamoto, Reported at 141st American Chemical Society Meeting, Washington, D. C., March, 1962.
3. Y. Okamoto, Reported at New York and New Jersey ACS Regional Meeting, January, 1963.
4. H. Hartmann, H. J. Fröhlich and F. Ebert, Z. Anorg. Allgem. Chem. 218, 181 (1934).
5. F. O. Rice and F. Scherber, J. Am. Chem. Soc. 77, 291 (1955).

KINETIC STUDIES ON THE REACTION BETWEEN AZIDES AND METAL IONS

by

Heinrich C. Egghart
Basic Research Laboratory
U. S. Army Engineer Research and Development Laboratories
Fort Belvoir, Virginia

There are numerous investigations of inorganic azides as solids but very little work has been done with molten azides. Some years ago I became convinced that much information could be gained by studying the azides in the molten state. This approach appeared to be particularly important with regard to the theories that molten phases play an essential role in the explosion of solids. I had observed that pure potassium azide is quite stable above the melting point of 350°C and decomposes slowly even at temperatures considerably above 400°C . Therefore, much of the work was done with potassium azide melts.

There is evidence that purely thermal instability is a necessary but not sufficient condition for explosions to occur. Catalytic and autocatalytic effects are important factors which have to be considered also. Therefore, the decomposition of potassium azide melts on finely divided metal powders as catalysts was studied. It was found that transition metals like nickel, cobalt, iron and manganese lower the activation energy for potassium azide decomposition from 49 to 32 Kcal/mole, while the influence of copper was only moderate. It was concluded that holes in the d-band of the metals are important for adsorbing the azide ion by electron sharing. Two azide ions adsorbed on adjacent sites or one adsorbed azide ion and another azide ion might form the transition configuration leading to decomposition. The importance of the holes in the d-band was confirmed more recently by comparison of the catalytic properties of group VIII metals like palladium, rhodium and platinum (all of which have holes in d-bands) with the catalytic properties of the group Ib metals silver and gold which have full d-bands. Essentially, the same results were obtained as with nickel, cobalt, iron and manganese on one side and copper on the other.

After these investigations were completed, the influence of ionic impurities on the decomposition of potassium azide melts was studied. Doped samples were prepared by mixing potassium azide and metal halides or sulfates in a small agate vial of a mixer mill. The decomposition of samples usually weighing less than one milligram was studied in a decomposition apparatus described in previous Contractors Conference Proceedings. The samples were dropped into

a reaction vessel which was held at a constant temperature. The increase in nitrogen pressure was measured by an alphanatron gage and recorded automatically.

The first step in the decomposition of these doped potassium azide samples is usually a reaction lasting not longer than a few seconds. In this initial reaction, a volume of nitrogen is evolved which is proportional to the amount of metal salt added and to the valency of the metal ion. During this reaction no potassium metal is formed and the overall change consists of an electron transfer from the azide ion to the impurity metal ion. With many metals, fast nucleation within the potassium azide melt can be observed and the catalytic decomposition of the potassium azide melt begins immediately after the metal is formed. Figure 1 is an example of this type. On an enlarged scale, a step of the curve at the fractional decomposition $\alpha = 0.044$ corresponding to 2.2 mole percent of two valent cobalt ions would be visible. Below this step, the nitrogen formed stems from the reaction $\text{Co}^{++} + 2\text{N}_3^- \rightarrow \text{Co} + 3\text{N}_2$. Above the step, the catalytic decomposition of potassium azide on cobalt metal particles occurs. The shape of the curve from $\alpha = 0.044$ on is typical for all metals of group VIII of the periodic table (except iron) regardless whether added as metal powder or produced from the metal salts within the potassium azide melt as described in this paper. The decrease of the reaction velocity after the beginning of the catalytic decomposition is caused by a change of the frequency

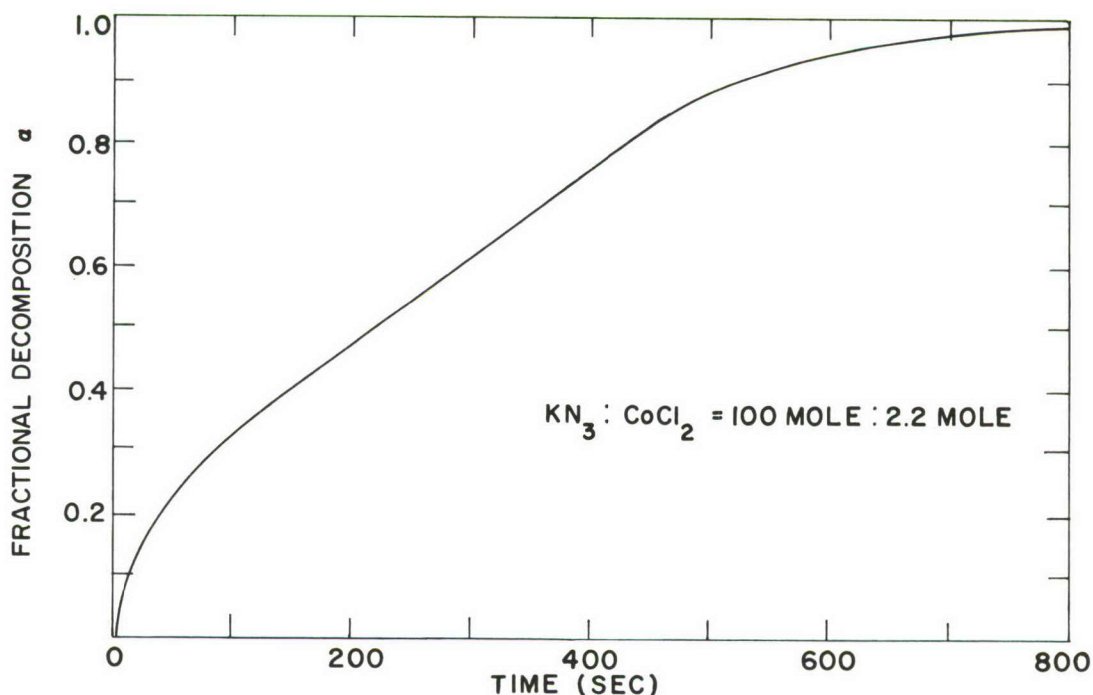


Figure 1

factor only. When potassium azide is decomposed on a metal previously used as catalyst, the curves are linear from the origin on indicating a zero order reaction. The activation energy for potassium azide decomposition on group VIII metals formed within the potassium azide melt is practically the same as with the respective metal powders, namely, around 31 Kcal/mole.

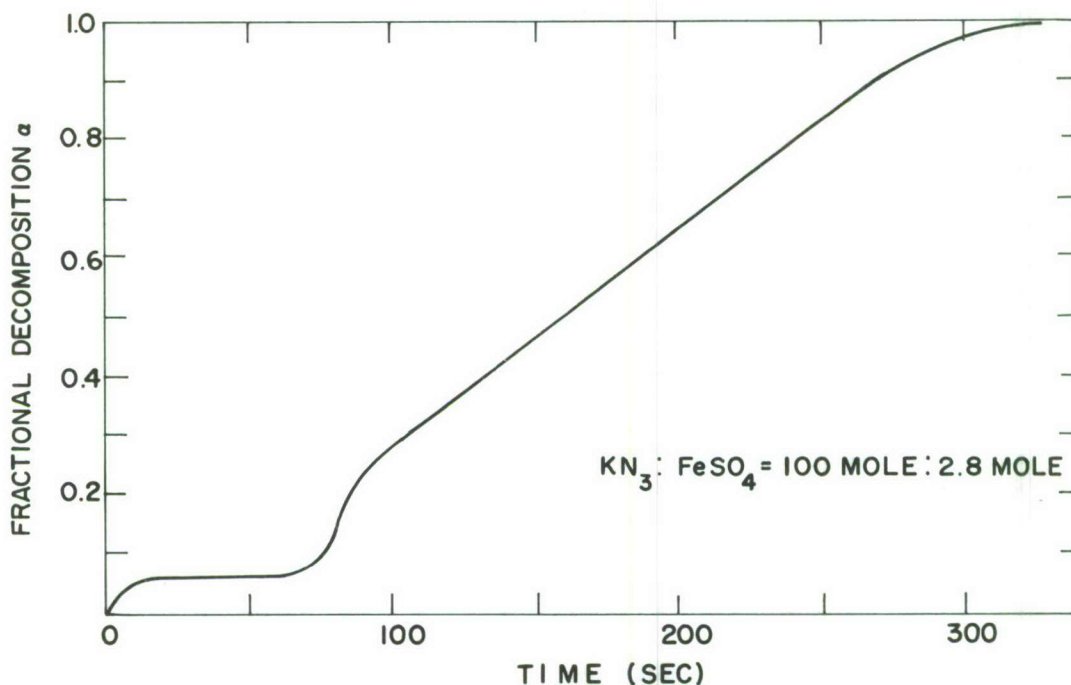


Figure 2

Figure 2 shows the case where the nitrogen volume evolved during the initial reaction indicates that the iron ions have been discharged. However, the metal nucleates only after an induction period. At the time when the iron particles finally appear, the catalytic decomposition with the formation of both nitrogen and potassium metal sets in. The activation energy, obtained in the usual way using different samples at different temperatures, was about 10 Kcal/mole higher as expected from the work with iron metal powder. Therefore, it was undertaken to obtain the activation energy from one and the same sample at different temperatures by using the so-called split-run technique. With this method, the expected result, namely, an activation energy of 31 Kcal/mole was obtained. The reason for the discrepancy between the results of the two methods seems to be clear. The length of the induction period was found to be dependent on the concentration of the metal salt added and also on the temperature. It appears reasonable to assume that the

size of the iron particles formed and herewith the specific surface of the iron present is also temperature dependent. Therefore, only the split-run technique can be expected to give reliable results in these cases.

When copper, silver and gold are formed from their halides within the potassium azide melt, their catalytic properties are somewhat better than as metal powders. An activation energy of 36 Kcal/mole was found for gold.

For chromium-chloride-doped potassium azide, the curves are similar to the one shown on Figure 2. However, with these samples no metal formation could be detected. The solid formed as chromium nitride. The activation energy required for decompositions of chromium salt doped samples was 35 Kcal/mole. The nitride formation can certainly be expected also when ions of the elements left of chromium in the periodic table are present in potassium azide melts.

After these studies on the impurity catalyzed potassium azide decomposition, investigations were performed on the reactions of azides and metal salts. This seems interesting because the impurity reactions are very likely able to influence the sensibility of azides and because the decomposition of any azide can be quite closely simulated by these reactions as far as thermo-chemistry is concerned.

Many of these reactions are too fast under the temperature and concentration conditions existing in molten potassium azide. Therefore, most of these reactions had to be carried out either in the solid state or in low melting fused salts which were both solvents and diluents. The molten salt media used were alkali halide mixtures, alkali nitrate mixtures, alkali thiocyanates and a potassium chloride copper chloride mixture. Using these media, a considerable amount of data on azide reactions was obtained. However, only some representative cases will be discussed here.

When cuprous chloride and potassium azide react, the reaction curves (nitrogen evolution curves) are very similar regardless of whether the experiments were performed in the solid state or in a molten salt medium. This can be seen in Figures 3 and 4. In the solid state as well as in the molten salt medium an activation energy of 18 Kcal/mole was found. In neither case did the reaction velocity depend on the reactant concentrations. All these observations indicate that the kinetics of these reactions is determined by the decomposition of one and the same intermediate species which is some kind of a copper azide. The mode of reaction described here is not the only way in which copper chloride and alkali azides react. If an alkali azide is added to a low melting potassium chloride/copper chloride mixture, the reaction curve corresponds very well to first order kinetics and the activation energy is not 18 but 35 Kcal/mole.

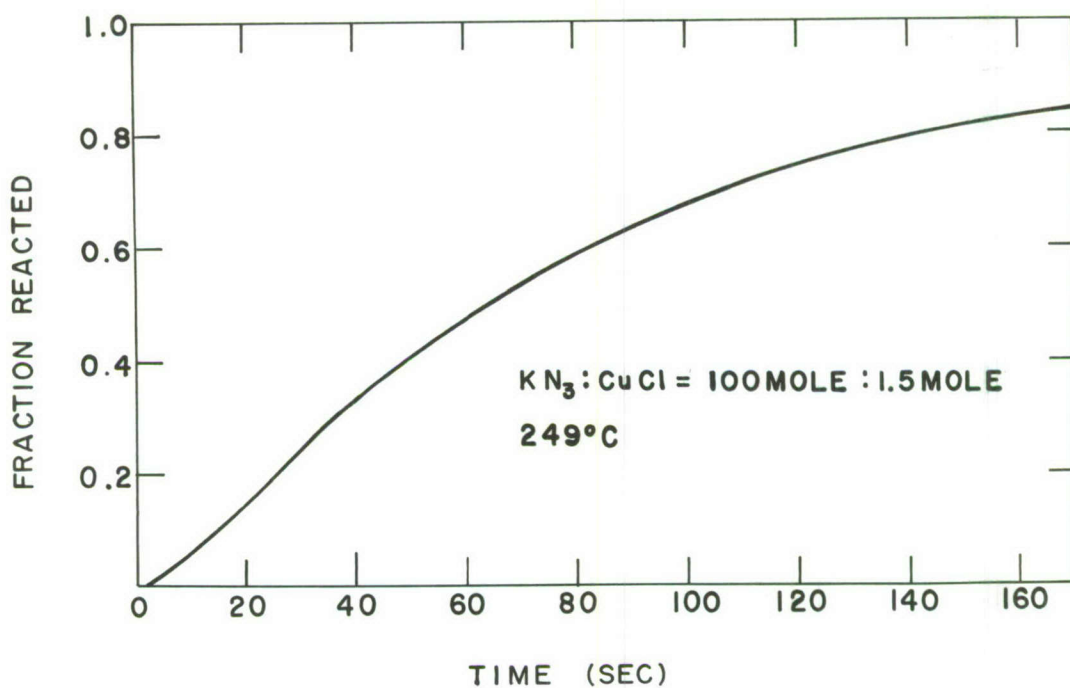


Figure 3

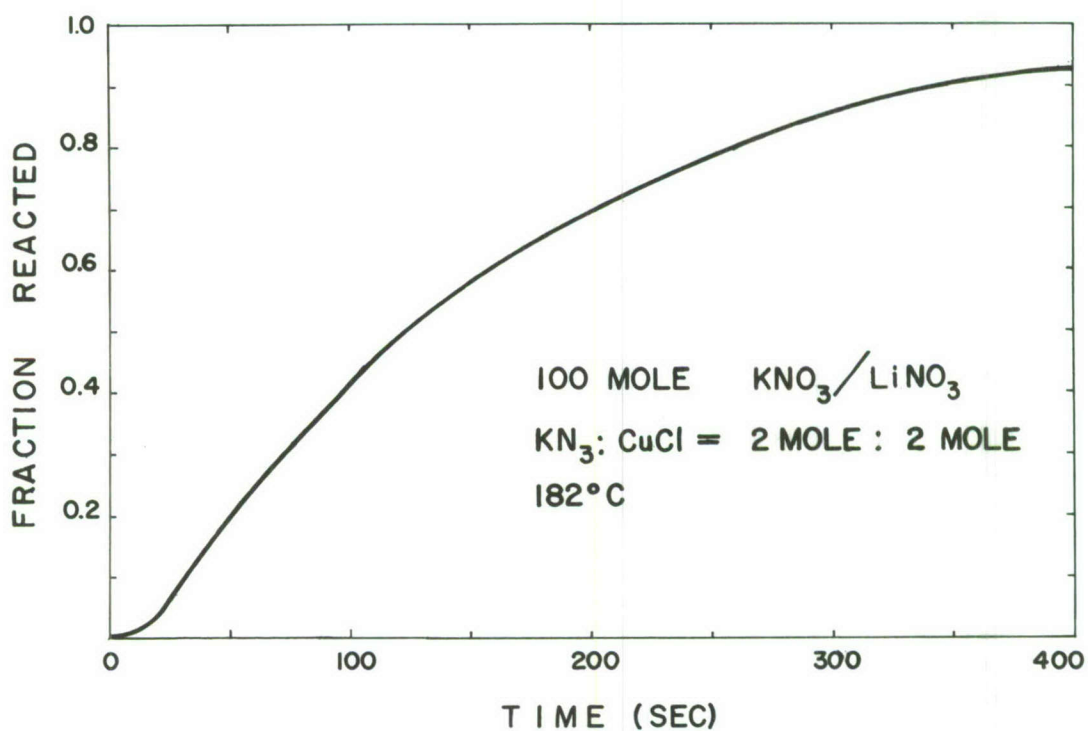


Figure 4

Figure 5 shows the curve for the reaction of cobalt chloride with potassium azide in the solid state. The shape of the curve as well as microscopic observations indicate an interface reaction. To avoid possible self-heating, these reactions were carried out at temperatures sufficiently low to permit the reaction to last up to 5 hours. The activation energy for this reaction was 45 Kcal/mole which is close to the activation energy required to decompose potassium azide itself.

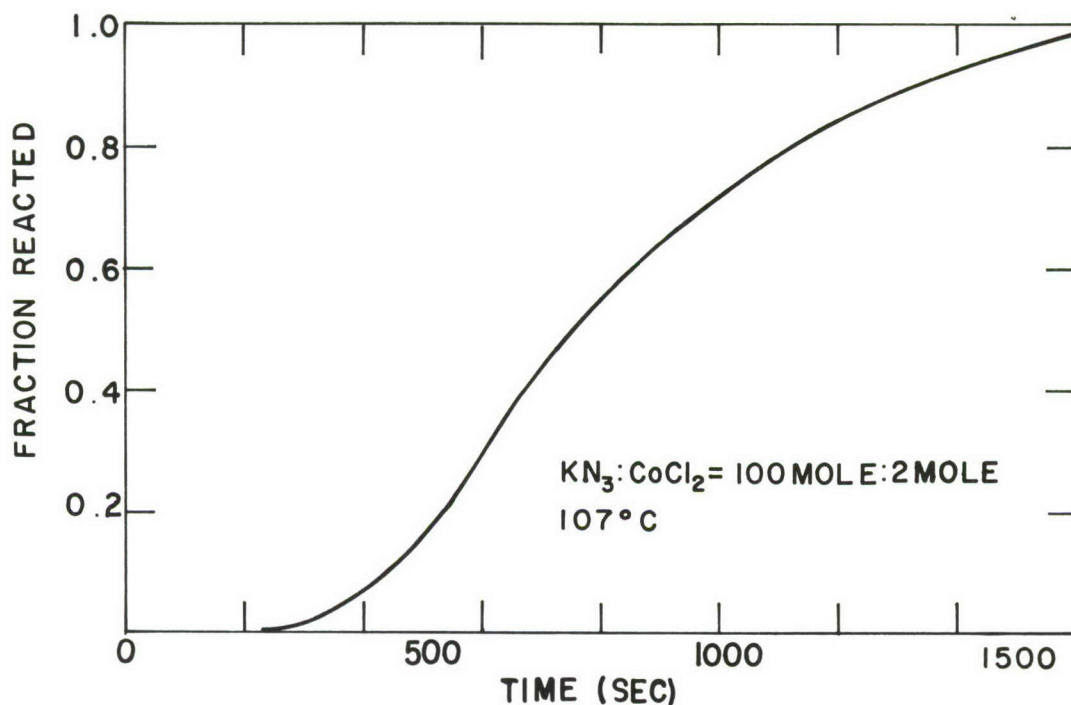


Figure 5

When cobalt ions react with azides in alkali nitrate medium, two modes of reaction can be observed differing in reaction velocity as much as four orders of magnitude. This is displayed in Figure 6. When the melt contains more cobalt ions than azide ions, a relatively slow reaction occurs. The activation energy of this process is 35 Kcal/mole. However, when more azide ions are present than cobalt ions, a fast reaction takes place requiring an activation energy of only about 12 Kcal/mole. In the fast process, cobalt metal formation occurs. In the slow one it does not. In the fast one, the reaction velocity depends on the concentration of the reactants (azide ions and cobalt ions). In the slow one it does not. Figure 7 shows that in the case of equimolarity of the reactants, both reaction paths have a chance to occur. (It should be noted here that the delay in the start of the fast reaction (Figures 6 and 7) is caused by

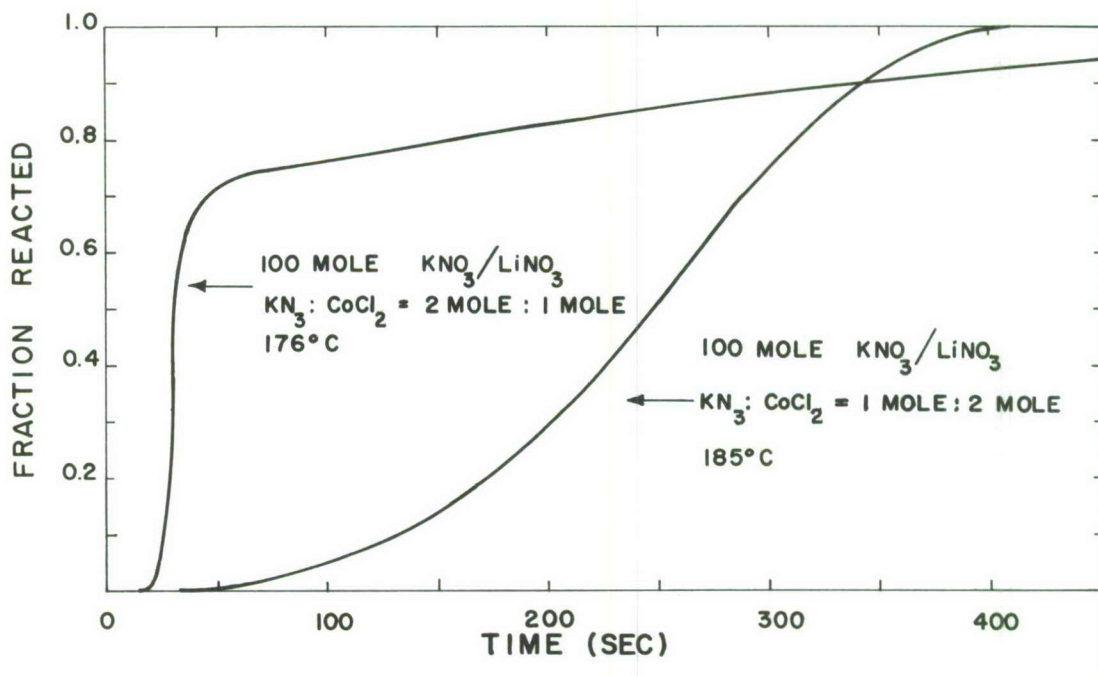


Figure 6

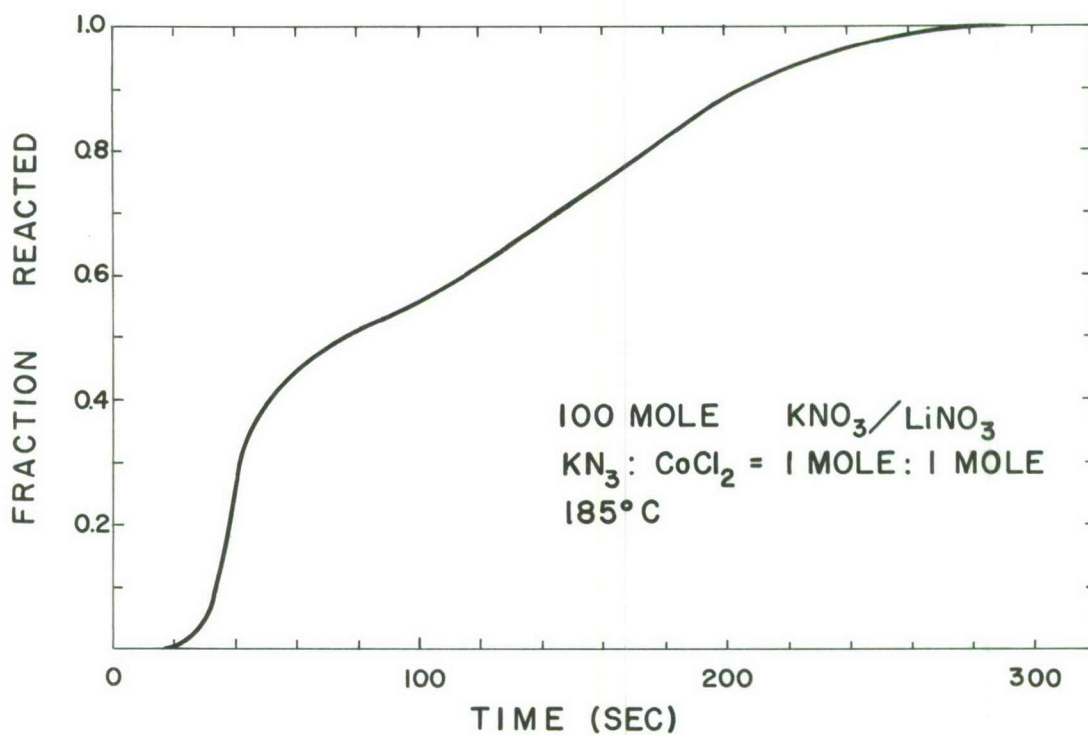


Figure 7

the time required for melting of the medium and is not a true induction period.)

All these observations indicate that in the case of azide ion deficiency, a comparatively stable species is formed, the decomposition of which is rate determining. When azide ions are in abundance, the transition state is of short lifetime and does not determine the velocity of the reaction. From these results and other considerations, it appears reasonable to assume an entity containing only one azide ion for one cobalt ion to be a comparatively stable species. However, a cobalt ion with two azide ions or an azide ion and an azide radical is likely to be a very unstable transition state.

The reactions of non transition metal halides like thallium chloride or lead chloride with alkali azides (leading to nitrogen and metal) are slow in molten salt media and slow even in molten potassium azide. Also here as described for the reaction of cuprous chloride with alkali azides, the increase of nitrogen pressure is independent of the concentration of the reactants, which indicates the formation of fairly stable thallium and lead azide type compounds. Whether these compounds are completely dissolved or present as particles in the molten salt medium, their decomposition is slow at 400° C or above, requiring an activation energy of more than 40 Kcal/mole.

PROPERTIES OF MOLTEN AZIDES: DATA ON BINARY
SYSTEMS OF MONOVALENT INORGANIC AZIDES

by

H. J. Mueller and J. A. Joebstl
Basic Research Laboratory
U. S. Army Engineer Research and Development Laboratories
Fort Belvoir, Virginia

Introduction:

The study of inorganic azides in the molten state is of particular interest for elucidating the nature of metastability of these compounds. Whereas the properties of a compound in the solid state are determined by three major factors, i.e., the character of the chemical bond, crystallographic structure, and structure defects, only the bond character is of importance in the molten state. Thus the question whether a correlation exists between the stability of an azide and its specific bond character should be studied preferentially on fused azides.

The investigation of molten azides is, furthermore, of great interest in view of the hypothesis promoted by Bowden's school¹ that an azide has to melt, at least locally, before it can explode. Some investigators claimed that they observed, on microscopic scale, the melting of heavy metal azides, for instance crystalline $\text{Pb}(\text{N}_3)_2$, preceding the explosion. We do not consider this to be sufficient evidence since we found that $\text{Pb}(\text{N}_3)_2$ may undergo contact fusion with suitable compounds at temperatures far below the explosion temperature. The possibility must be considered, therefore, that the reported melting might have been due to the local formation of a low melting binary mixture of the azide and certain surface contaminations (carbonates, hydroxides, etc.) rather than to a true melting of the pure azide. However, even in cases where a melting point determination by direct observation seems impossible due to the highly unstable character of the azide, these data can be easily calculated by extrapolating the liquidus curves of binary systems in which the explosive azide is one of the components. The knowledge of the accurate melting points of the explosive azides will certainly answer the question whether explosion coincides with melting of the azide.

In addition, valuable information on the mechanism of decomposition can be obtained by studying the electrolysis of azide melts. Depending on the experimental conditions, the decomposition rate can be drastically changed in electrolysis experiments. Our experiments showed that rapid decomposition can be achieved even with the otherwise rather stable melts of alkali azides.

The following report presents data on binary mixtures of monovalent inorganic azides. Low melting mixtures of ionic azides (eutectica) are of particular interest for the investigation of the relative thermal stability of various azides. These mixtures are also very suitable for decomposition studies by means of electrolysis.

Experimental:

The study of binary mixtures of inorganic azides was begun by establishing composition-temperature diagrams of various binary systems using thermal analysis, optical microscopy and x-ray diffraction techniques. The thermal analysis was carried out in high vacuum, in air, or in a nitrogen atmosphere. For these experiments an apparatus was constructed which registered simultaneously the temperature of the sample and the nitrogen evolution. For the microscopic investigations a Thomas-Kofler-Hotstage with thermistor attachment was used. More detailed observations of the melting process were made on the vacuum hotstage of the Reichert Metallographic Microscope "MeF". Usually the type of the composition-temperature diagram was at first determined microscopically by means of "contact preparations"²; the liquidus and solidus curves were then established by means of thermoanalysis. X-ray powder patterns were used for the examination of the solid phases. The thermal decomposition was studied either at constant temperature or while continuously raising the temperature. For the isothermic decomposition studies the conventional arrangement consisting of a static high vacuum system, a vacuum gauge, and a thermostat was employed.

Discussion of the Results:

The binary mixtures of azides can be divided as follows: Category 1: Both components have the same anion but different cations (azide-azide systems). Category 2: Both components have the same cation but different anions. This "anionic dilution" is necessary in order to stabilize various inorganic azides (for instance the explosive bivalent azides) in the molten state. Category 3: Both components have different cations and anions. These systems are the most complicated ones. Chemical reactions which are likely to occur between the components in the solid and molten state, as well as ion association and molecular aggregation in the fused mixtures render the evaluation of these systems rather difficult. Nevertheless, these systems seem to be of some importance for the preparation of azides from reversible systems.

So far, we have concerned ourselves with the systems of Category 1 (azide-azide mixtures). These systems are of particular interest because they include such binary mixtures of azides which are composed of components having different degrees of metastability.

The systems which have been studied are listed in Table I.

TABLE I

<u>System</u>	<u>Type</u>	<u>Minimum Melting Point (° C)</u>	<u>Melting Points of the Components (° C)</u>
$\text{KN}_3:\text{NaN}_3$	e	304	(345, 420)
$\text{RbN}_3:\text{NaN}_3$	e	268	(317, 420)
$\text{CsN}_3:\text{NaN}_3$	e	210	(323, 420)
$\text{KN}_3:\text{RbN}_3$	ss III	300	(345, 317)
$\text{KN}_3:\text{CsN}_3$	e	255	(345, 323)
$\text{RbN}_3:\text{CsN}_3$	ss I	-	(317, 323)
$\text{KN}_3:\text{AgN}_3$	e	220	(345, 300)
$\text{RbN}_3:\text{AgN}_3$	e	170	(317, 300)
$\text{CsN}_3:\text{AgN}_3$	e	135	(323, 300)
$\text{TLN}_3:\text{AgN}_3$	e	175	(315, 300)

e = Eutectic Type of binary system
 ss I = Roozeboom Type I solid solution
 ss III = Roozeboom Type III solid solution

The system $\text{KN}_3:\text{NaN}_3$ was investigated in particular. The eutectic mixture is composed of 25 mole % NaN_3 and 75 mole % KN_3 . Eutectic melting was observed on mixtures with a NaN_3 content as low as 1 mole %, however. If a partial solid solution of NaN_3 exists in KN_3 , the percentage of NaN_3 must be below this value. Molten mixtures with KN_3 in excess are very stable, mixtures with NaN_3 in excess easily undergo autocatalytic decomposition at temperatures slightly above the melting point. Dynamic decomposition studies showed that a strongly increased nitrogen evolution occurs during the cooling period while the temperature goes through the two-phase field between the liquidus and solidus line. This indicates that the presence of a second phase tends to increase the thermal instability. The isothermic decomposition of $\text{NaN}_3\text{-KN}_3$ mixtures in eutectic composition seems to proceed in two steps, namely a fairly rapid decomposition of the less stable NaN_3 followed by the slow decomposition of KN_3 . This interpretation is supported by

the observation that during repeated melting-solidification cycles of a eutectic mixture, the liquidus temperature increases gradually until a temperature of only 5°C less than the fusion temperature of pure KN_3 is reached. These results can be easily interpreted with the assumption that NaN_3 decomposes preferentially, thus shifting the composition of the sample continuously towards increasing KN_3 content. A more detailed evaluation of the isothermic decomposition studies, in view of determination of activation energies and dependence of the observed induction period from the gas pressure, is under way.

The melting point of NaN_3 is unknown because NaN_3 decomposes before melting occurs. Using the binary systems KN_3 - NaN_3 and RbN_3 - NaN_3 , the theoretical melting point of pure NaN_3 was calculated as $420 \pm 10^{\circ}\text{C}$, using the well-known approximation formula³. At the present time an attempt is being made to determine, by the same method, the theoretical melting point of $\text{Pb}(\text{N}_3)_2$.

Besides these azides-azides mixtures a large number of binary systems of Category 2 and 3 were tentatively investigated. The investigation of these more complicated systems indicated, in particular, that for a full understanding of the properties of single or composite melts of azides it is necessary to investigate to what extent an eventual structure of the melt is of importance. It is well known from the study of fused alkali halides, nitrates and other stable salt melts that very often ion association occurs and, thus, the melts can no longer be considered as an aggregate of simple, randomly distributed cations, and anions. Such a "melt structure", however, must exert an influence on the physical properties of the melt: in the case of azides, it cannot be without consequence for the stability of the melt, whether the azide ion is surrounded by fairly small, simple metal cations or by large, associated ions.

We, therefore, will include in this study measurements of the electric conductance and of ion transfer numbers. In connection with viscosity and density measurements, these data will permit us to speculate on the melt structure. Furthermore, it is planned to determine the radial ion distribution in melts by means of x-ray diffraction techniques. The combined results of these investigations will hopefully promote a better understanding of the structure of azides in the molten state and its influence on the stability of these compounds.

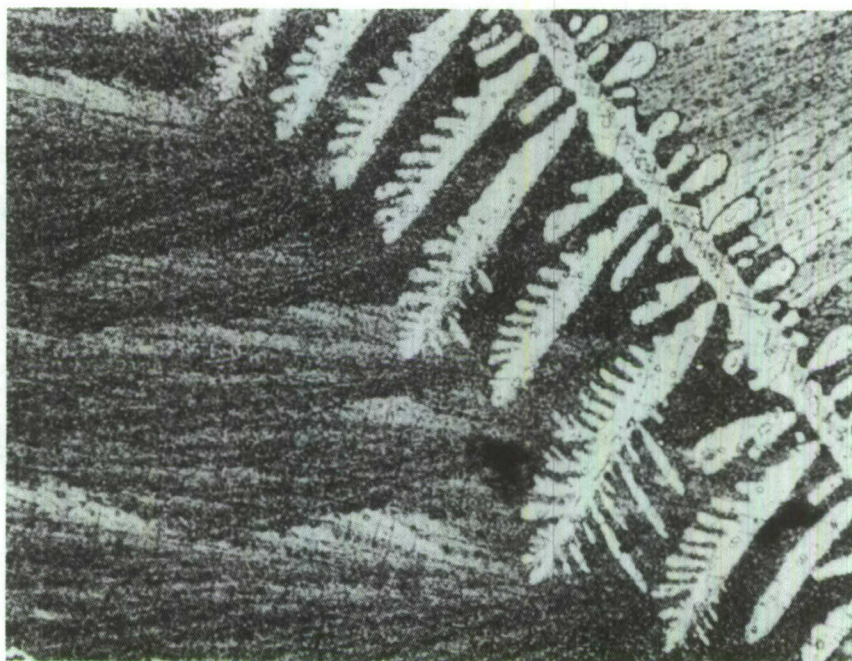


Figure 1. $\text{KN}_3\text{-NaN}_3$ (mole proportion 4:1) Dendrites of KN_3 are embedded in the eutectic mixture of both components.

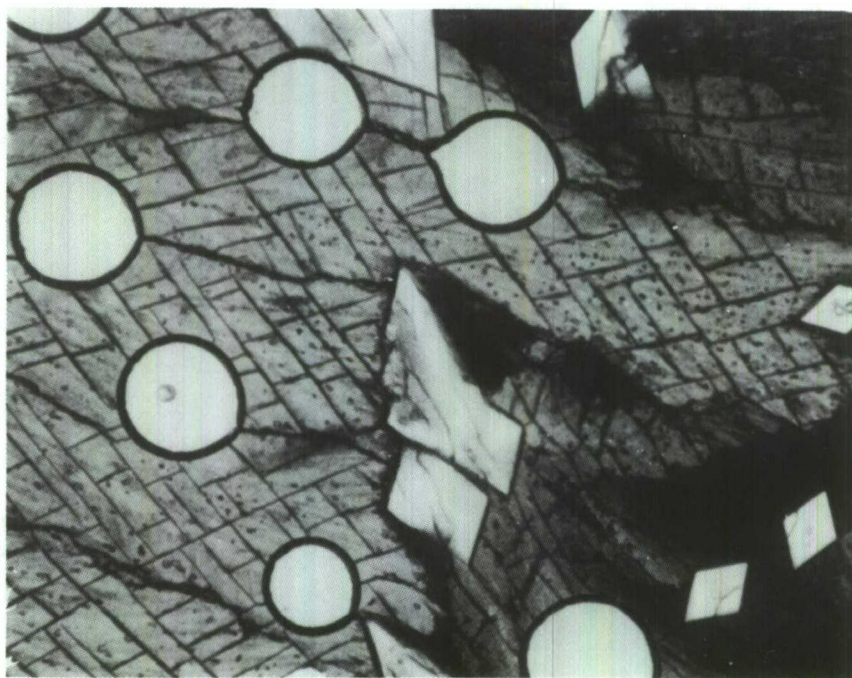


Figure 2. $\text{KN}_3\text{-NaN}_3$ (mole proportion 2:1) Crystallites of NaN_3 are grown in the eutectic matrix.

References

1. F. P. Bowden and A. D. Yoffe, "Fast Reactions in Solids," London, 1958.
2. L. Kofler and A. Kofler, "Thermo-Mikromethoden zur Kennzeichnung organ. Stoffe and Stoff-gemische," Universitätsverlag Wagner GmbH Innsbruck, Austria, 1954.
3. W. C. McCrone, "Fusion Methods in Chemical Microscopy," Interscience Publishers, Inc., New York, 1956.

SOME COMMENTS ON THE AZIDE REACTION

by

Henry Eyring
Dean, Graduate School
University of Utah
Salt Lake City, Utah

An explosion occurs whenever an exothermal reaction yielding gaseous products speeds up out of control. Most chemical reactions speed up with temperature so that the occurrence of a hot spot in an explosive system, large enough so that the heat losses are less than the heat being liberated by reaction will lead to an explosion. A reacting system which is exothermal may, however, explode because there is a branching chain reaction which goes out of control, even though the rising temperature does not itself speed the chain reactions. The atomic bomb exemplifies this situation. There are also many branching chemical chain reactions which speed up both because of the chain branching and because of the temperature rise. The hydrogen chlorine system can be set off by light which yields chlorine atoms which react with hydrogen molecules yielding hydrogen atoms. These in turn react with chlorine molecules leading to long unbranched chains which nevertheless speed out of control due to the accompanying temperature rise.

Since the azide ion acts like a halogen it is not surprising that suitable emulsions of metal azides can be used in photography to replace the metal halides. Whereas in ordinary photography the halogens are released as gases the azide radical being unstable reacts to give N_2 and some nitrides.

If hydrozoic acid is heated it can break, with the least activation energy, into HN plus N_2 . The HN then reacts with two neighboring hydrogen atoms to make ammonia and releases two more azide radicals which may either react to form three N_2 molecules or else to form two nitrogen molecules plus two nitrogen atoms. The nitrogen atoms by reacting with hydrogen may then continue the chain and indeed cause branching. The fact that when HN is released in water solution hydroxylamine is formed is only one of many bits of evidence which indicate that in thermal reactions HN is an abundant intermediate. The trapping of nitrogen atoms in solids in which the azides have been decomposed indicates that under certain circumstances these atoms are intermediates also. It would be extremely illuminating to establish how effective nitrogen atoms are in continuing the chain and whether there is branching which effectively contributes to the explosive reactions. These same considerations apply to the reactions involving metal azides where one finds

nitrogen and metal nitrides analogous to ammonia and hydrazine and even longer nitrogen chains having metals attached.

The fact that the metal azides, MN_3 , break to form $MN + N_2$ explains why the higher the ionization potential the faster is this reaction. This is because a high ionization potential for M should mean a strong MN bond and therefore a lower activation energy for the reaction $MN_3 \rightarrow MN + N_2$.

Most solid reactions occur only on the surfaces of the crystals. In any case a tight crystal lattice alters the course of homogeneous reaction so that Bowden's suggestion that melting is a necessary preliminary for anything but surface reactions is a priori likely.

The great lack of reproducibility of explosions set off with a hammer is an interesting complication. A hammer blow develops hot spots at inhomogeneities where heat is developed by slipping and compression. If the hot spot is large enough, and hot enough, the heat liberated by the chemical reactions will outrun the rate of heat dissipation. As a result the reaction rate speeds up out of control. The mechanism of reaction, i.e., whether or not it involves branching chains, etc., determines the rate of reaction and therefore determines whether or not the temperature drops or goes out of control after the hammer blow.

Because after exposure to light a picture can be developed, it follows that electrons are lifted into traps where they reduce metal ions and give small metal nuclei which can be developed further with a reducing agent. At the same time nitrogen and heat are liberated. It has been shown² that when pressure is applied to a sapphire, electrons are lifted into traps which may then drop back giving light upon subsequent heating. This process may be of some significance in developing metal nuclei which speed up subsequent reaction in a metal azide struck by a hammer. It would be of interest to see whether a hammer blow insufficient to cause reaction does nevertheless cause the formation of metal nuclei.

Because there is considerable study of azide decomposition in the molten state it should be of some interest to understand the theory of the liquid state³ and of reaction rates in solution⁴. The very extensive literature survey made for the "Department of the Army Corps of Engineers" Report 1551-TR with the two supplements reveals an amount of literature extensive enough that a theoretical study of this material with the idea of formulating a detailed verifiable theory of the rates of reaction of azides should be undertaken.

References

1. The Electrochemical Theory of Smelting and Related Reactions. Xavier de Hemptinne, H. Eyring and T. Ree, Physical Chemistry of Process Metallurgy, ed. George R. St. Pierre, Part 1, Vol. VII, pgs. 69-93. Interscience Publishers, N. Y. (1961).
2. Effects of High Pressure on the Thermoluminescence of γ -Irradiated α -Al₂O₃ Single Crystals, A. F. Gabrysh, J. M. Kennedy, H. Eyring and V. R. Johnson, The Phys. Rev., 131, 4, 1543-1548 (1963).
3. Significant Structures in Liquids, III. Partition Function for Fused Salts, C. M. Carlson, H. Eyring, T. Ree, Proc. Natl. Acad. Sci., 46, 3, 333-336 (March 1960).
4. The Equilibrium Theory of Reaction Rates, H. Eyring, The Vortex XXIV, No. 5, May 1963.

THE CRYSTAL STRUCTURE OF α -LEAD AZIDE

by

Gerald L. Glen
The Atlantic Refining Company
Glenolden, Pennsylvania

Earlier studies of lead azide were made by Miles¹, Hughes², Pfefferkorn³, Azaroff⁴, and Saha⁵. The orthorhombic unit cell has dimensions $a = 6.63$, $b = 11.31$, and $c = 16.25$ Å. With 12 molecules per unit cell, the density is 4.71 g./ml. On the basis of the diffraction effects the space group can be either Pnam or Pna2₁. The latter was chosen because a three-dimensional refinement⁵ of the lead parameters showed that the R-factor comes down considerably if the non-centrosymmetric space group is assumed.

Azaroff⁴ determined the lead positions from a two-dimensional x-ray analysis, but failed to locate the nitrogen atoms because the lead atoms dominate the intensities of the x-ray data. Neutron data for the $0kl$ reflections were collected by Danner and Kay at the Brookhaven National Laboratory. Although the neutron scattering lengths for lead and nitrogen are approximately equal, an attempt to obtain a trial structure from a Patterson synthesis of this data failed, due to a considerable overlap of vector peaks.

Three-dimensional x-ray data using $\text{CuK}\alpha$ radiation were collected by Saha⁵ at Penn State University. However, considerable experimental difficulties were encountered while taking the data. The linear absorption coefficient for $\text{CuK}\alpha$ radiation was found to be extremely high ($K = 819 \text{ cm.}^{-1}$), hence it was necessary to correct for absorption. A uniform cylindrical absorption correction was applied even though the crystals could not be made into cylinders because of the danger of detonation. Furthermore, after 3 to 4 days of radiation, the crystals started to disintegrate; therefore, more than one crystal had to be used for the collection of complete three-dimensional data. Nevertheless, Saha was able to determine the position of the nitrogen atoms in the three-dimensional Fourier sections, although further difficulties were encountered because of the presence of ripples around the lead peaks. He was able to obtain an R-value ($R = \sum |1F_0| - |F_{C1}| / \sum |F_0|$) of 0.21.

Equipped with this information, plus the two-dimensional neutron data, a two-dimensional refinement of the atomic coordinates was begun at Picatinny Arsenal. The neutron scattering density projected on a point (y, z) in the (100) face of the unit cell is represented by:

$$\rho(y, z) = 1/A_C \sum_K \sum_L F_O(Ok\ell) \exp[-2\pi i(ky + \ell z)]$$

where A_C is the area of the projected cell and $F_O(Ok\ell)$ is the observed structure factor for the crystal plane with Miller indices 0, k and ℓ . For the space group $Pna2_1$, the above equation reduces to:

$$\rho(y, z) = 4/A_C \sum_{O=0}^K \sum_{O=0}^L |F_O(Ok\ell)| \cos 2\pi ky \cos[2\pi\ell z - \alpha(Ok\ell)]$$

for k and ℓ even, and

$$\rho(y, z) = -4/A_C \sum_{O=0}^K \sum_{O=0}^L |F_O(Ok\ell)| \sin 2\pi ky \sin[2\pi\ell z - \alpha(Ok\ell)]$$

for k and ℓ odd, where K and L are the maximum observable values of k and ℓ , $|F_O(Ok\ell)|$ is the magnitude of the observed structure factor and $|\alpha(Ok\ell)|$ is the phase angle.

The magnitude of the observed structure factor was obtained from the integrated intensity of the neutrons reflected by the $Ok\ell$ plane and since approximate parameters of all the atoms were known, it was possible to calculate an approximate phase angle for each plane. Again for the space group $Pna2_1$ it can be shown that⁶

$$A_C(Ok\ell) = 4 \sum_{m=1}^N b_m \exp[-B_m \sin^2 \theta / \lambda^2] \cos 2\pi ky_m \cos 2\pi\ell z_m$$

$$B_C(Ok\ell) = 4 \sum_{m=1}^N b_m \exp[-B_m \sin^2 \theta / \lambda^2] \cos 2\pi ky_m \sin 2\pi\ell z_m$$

for k and ℓ even, and

$$A_C(Ok\ell) = -4 \sum_{m=1}^N b_m \exp[-B_m \sin^2 \theta / \lambda^2] \sin 2\pi ky_m \sin 2\pi\ell z_m$$

$$B_C(Ok\ell) = 4 \sum_{m=1}^N b_m \exp[-B_m \sin^2 \theta / \lambda^2] \sin 2\pi ky_m \sin 2\pi\ell z_m$$

for k and ℓ odd, and

$$\alpha(Ok\ell) = \tan^{-1} [B_C(Ok\ell)/A_C(Ok\ell)]$$

where N = the number of atoms in the asymmetric unit of the unit cell,

y_m and z_m define the position of the n th atom in the (100) projection of the unit cell in terms of fractional unit cell constants,

B_m is a thermal parameter for the n th atom which modifies the structure amplitude to take account of the thermal vibration of the atom,

θ is the Bragg angle of the $Ok\ell$ plane,

λ is 1.042, the wavelength of the radiation used,

b_m is the neutron scattering factor for the n th atom.

With these phase angles, a neutron density map, $\rho(yz)$, can be calculated. From this map more accurate atomic parameters can be obtained, and thereby more accurate phase angles. These new phase angles can then be used to calculate another density map; thus the Fourier refinement process continues on.

However, the projected density maps were considerably overlapped, thereby making an accurate determination of all atomic coordinates difficult. This overlapping is illustrated in Figure 1. In an attempt to overcome this difficulty a "difference map"⁷ was calculated, that is $|F_O - F_C|$ were used as Fourier coefficients instead of the observed structure factor, F_O . The calculated structure factors, F_C , were obtained as follows:

$$F_C (Ok\ell) = [A_C^2 (Ok\ell) + B_C^2 (Ok\ell)]^{\frac{1}{2}}$$

This type of synthesis suggests what changes should be made in the atomic parameters between successive Fourier cycles.

After two such cycles the conventional R-value, which is used to indicate the credibility of a postulated structure, dropped from its initial value of 0.340 to 0.238. One more cycle dropped it to 0.231.

At this point it became apparent that further refinement using Fourier projections would be difficult because of the considerable overlap of lead and nitrogen peaks. Least squares refinement was not satisfactory either, since there was also the possibility that the data contained systematic errors, i.e., absorption and extinction errors. Finally, it was decided to use a combination of these two analyses. The y- and z- coordinates for each cycle were determined by averaging the values obtained from each type of analysis.

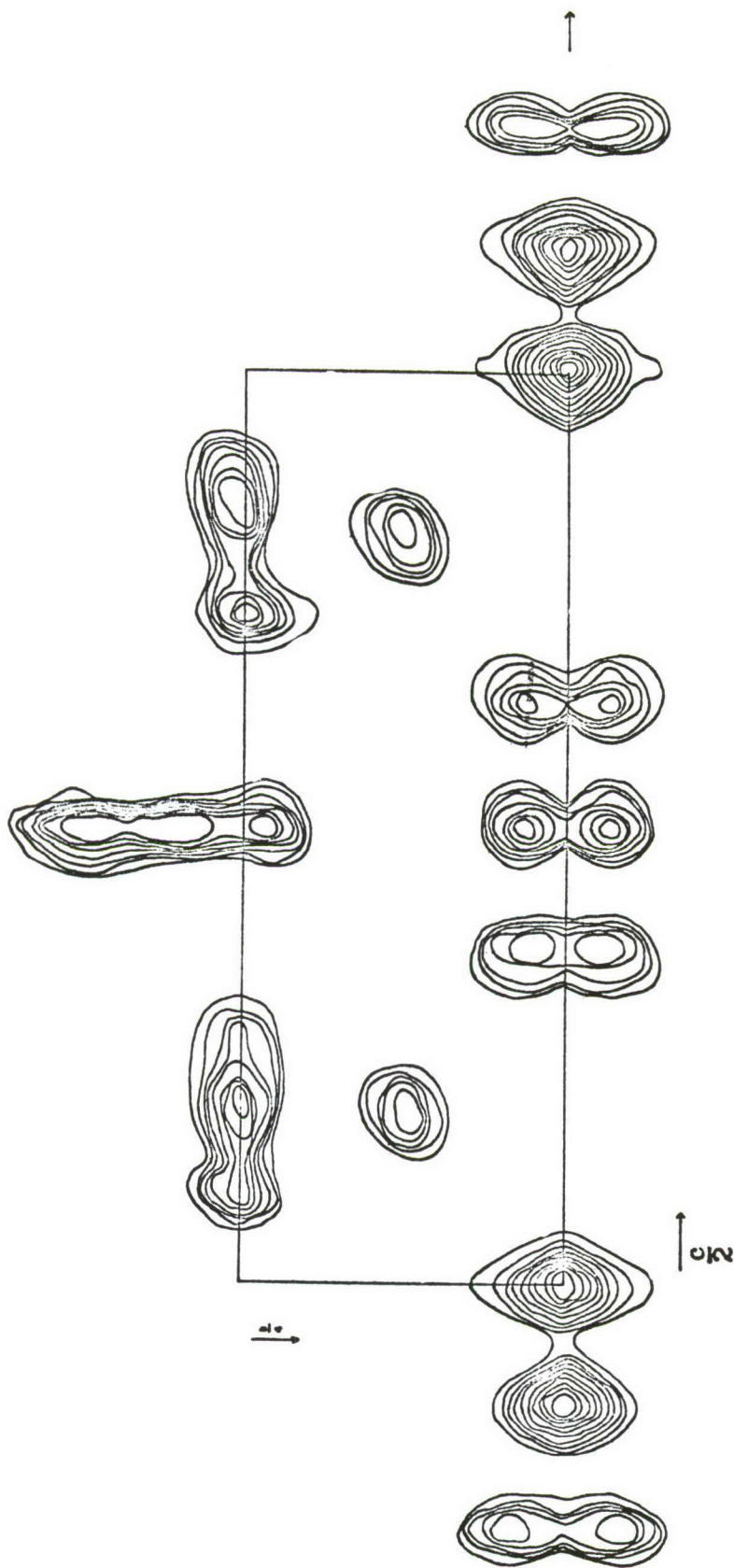


Figure 1. $0k\ell$ neutron scattering density map for one asymmetric unit. Contours are at arbitrary intervals.

In addition, the nitrogen coordinates (including the x parameters) were adjusted further, assuming that all azide groups were linear. The thermal parameters, B_m , were determined by the least squares refinement.

The least squares regression was carried out by expanding the formulae for obtaining F_c with Taylor series. Neglection of all non-linear terms and, in the thus formed least squares matrix of all non-diagonal terms results in the following equation for the shift of the nth variable parameter:

$$\Delta y_m = \sum w (F_o - F_c) (\partial F_c / \partial y_m) / \sum w (\partial F_c / \partial y_m)^2$$

where the sum includes all the contributions of the reflections used. No general weighting was applied, therefore, the weighting factor, w , was set equal to one.

This refinement procedure was continued until the change in coordinates was approximately equal to the estimated standard deviations of the coordinates. At this point the R-factor was reduced to a value of 0.07. The agreement of each reflection is illustrated in Table I. The initial and final parameters are listed in Table II. The unprimed values are those determined by Saha and the primed ones are the values obtained by the present refinement.

The standard deviations of the atomic coordinates were calculated according to Cruickshank's formulae⁷:

$$\sigma(y_m) = 2\pi [\sum k^2 \Delta F^2]^{\frac{1}{2}} / bV (\partial^2 \rho_m / \partial y_m^2)$$

$$\sigma(z_m) = 2\pi [\sum l^2 \Delta F^2]^{\frac{1}{2}} / cV (\partial^2 \rho_m / \partial z_m^2)$$

where $\partial^2 \rho_m / \partial y_m^2$ and $\partial^2 \rho_m / \partial z_m^2$ are the central curvatures at the center of the nth atom.

The average standard deviation of the y- and z-coordinates is 0.06Å. This value is high in view of the fact that the R-factor is 0.07. There are a number of factors⁷ contributing to these rather large standard deviations, namely: 1) the central curvatures of the atoms are rather small (see Figure 1), 2) the structure does not have a center of symmetry and all atoms are in general positions, and 3) the number of refined parameters (63) is not much less than the number of independent reflections (102).

The lead atoms, designated 2 and 3 in Table II, have seven nearest nitrogen neighbors and the remaining lead atom has eight. The Pb-N distances range from 2.48-2.92 Å. The packing of the molecule is illustrated in Figure 2 and some of the important bond distances are listed in Table III.

Table I

H=0

<u>K</u>	<u>L</u>	<u>F_O</u>	<u>A_C</u>	<u>B_C</u>	<u>F_C</u>
2	0	2.05	-2.12	0.	2.12
4	0	37.12	38.39	0.	38.39
6	0	3.74	1.97	0.	1.97
8	0	36.50	36.83	0.	36.83
10	0	12.75	12.39	0.	12.39
12	0	3.75	3.17	0.	3.17
14	0	13.45	14.48	0.	14.48
16	0	7.66	7.39	0.	7.39
1	1	0.	1.14	0.02	1.14
3	1	5.36	6.08	0.86	6.14
5	1	1.03	0.11	0.85	0.86
7	1	0.	1.00	0.68	1.21
9	1	0.	-0.30	-0.15	0.34
11	1	6.92	-5.58	2.78	6.24
13	1	0.	-0.15	-0.18	0.23
15	1	4.38	-5.79	-0.47	5.81
0	2	0.	0.38	-0.17	0.41
2	2	2.90	-2.13	0.24	2.14
4	2	10.71	11.02	-0.36	11.02
6	2	0.	-0.41	-0.42	0.59
8	2	13.15	13.07	1.68	13.17
10	2	1.33	-1.24	1.49	1.94
12	2	12.39	12.77	1.20	12.82
14	2	2.66	-3.06	0.24	3.07
16	2	10.51	10.73	3.38	11.25
1	3	5.91	4.94	-0.28	4.94
3	3	26.40	-27.02	0.75	27.04
5	3	15.33	16.09	0.72	16.11
7	3	1.12	-0.74	0.94	1.19
9	3	3.20	-2.36	1.68	2.90
11	3	4.50	-5.19	-0.32	5.20
13	3	4.67	3.99	2.12	4.51
15	3	6.97	7.47	0.19	7.47
0	4	1.60	1.53	0.40	1.58
2	4	4.99	-5.18	0.90	5.26
4	4	2.43	-2.60	1.63	3.07
6	4	12.12	-11.21	1.82	11.36
8	4	2.76	-1.26	2.74	3.02
10	4	13.14	-12.74	5.23	13.77
14	4	6.30	-5.67	3.91	6.88
16	4	5.41	-2.69	4.84	5.53
1	5	4.63	4.93	-1.31	5.10
3	5	4.41	4.83	-0.48	4.86
5	5	5.79	5.50	-1.22	5.64

Table I (cont'd)

H=0

<u>K</u>	<u>L</u>	<u>F_O</u>	<u>A_C</u>	<u>B_C</u>	<u>F_C</u>
7	5	2.17	-2.34	0.97	2.54
9	5	7.24	7.81	-0.90	7.86
11	5	4.81	-5.44	-1.25	5.58
13	5	3.83	4.02	0.00	4.02
0	6	22.63	-23.56	2.75	23.72
2	6	22.14	-22.38	3.49	22.65
4	6	3.14	3.62	3.16	4.80
6	6	11.78	-10.51	4.26	11.34
8	6	17.39	-17.15	2.44	17.32
10	6	5.72	-3.27	4.37	5.46
1	7	6.39	-6.15	1.17	6.26
3	7	0.86	0.44	-0.82	0.93
5	7	3.30	-3.25	-1.66	3.65
7	7	2.30	-2.24	-0.07	2.24
9	7	4.60	4.11	-2.88	5.02
0	8	14.58	13.85	-0.78	13.87
2	8	3.66	2.86	-1.66	3.31
4	8	2.10	1.15	1.48	1.87
6	8	1.55	0.54	-0.38	0.66
1	9	11.52	11.73	-0.74	11.75
3	9	9.18	9.38	0.26	9.38
5	9	7.37	-6.74	-1.50	6.91
7	9	4.54	-2.87	-1.40	3.20
0	10	11.17	-11.97	1.65	12.08
2	10	6.79	-5.79	1.27	5.93
4	10	7.20	-7.44	-0.28	7.44
6	10	3.60	-4.15	-0.31	4.16
1	11	5.61	-6.18	1.53	6.37
3	11	3.55	-3.51	1.29	3.74
0	12	24.48	24.06	-0.20	24.06
2	12	8.15	-8.10	-0.40	8.11
4	12	1.34	0.14	-1.24	1.25
1	13	18.83	-18.11	0.97	18.13
3	13	18.29	18.30	-2.51	18.47
0	14	3.70	-3.04	2.72	4.08
2	14	11.31	-10.58	2.40	10.85
4	14	7.82	7.15	-1.12	7.24
1	15	0.	0.10	-0.04	0.11
3	15	15.53	-14.01	-0.57	14.02
0	16	27.14	24.77	-9.53	26.54
2	16	12.32	-10.78	-1.42	10.87
4	16	22.91	21.13	-5.95	21.95
1	17	7.64	6.63	-2.70	7.16
3	17	2.35	1.75	-0.58	1.85

Table I (cont'd)

H=O

<u>K</u>	<u>L</u>	<u>F_O</u>	<u>A_C</u>	<u>B_C</u>	<u>F_C</u>
0	18	12.66	-11.57	-4.09	12.27
2	18	6.89	-7.43	-0.12	7.43
4	18	6.28	5.23	-2.65	5.86
1	19	0.	1.93	-0.42	1.97
0	20	9.66	8.95	-2.79	9.38
2	20	6.55	4.82	-4.90	6.88
4	20	0.	0.63	0.20	0.66
1	21	6.47	5.47	-1.27	5.62
0	22	9.09	8.92	1.94	9.13
4	22	4.73	4.71	-0.47	4.73
1	23	3.87	-2.60	2.56	3.65
0	24	14.85	13.75	0.93	13.79
0	26	15.64	-10.95	8.29	13.73

Table II
Parameter Data

<u>Atom</u>	<u>xx10³</u>	<u>x'x10³</u>	<u>yx10³</u>	<u>y'x10³</u>	<u>zx10³</u>	<u>z'x10³</u>	<u>B</u>	<u>B'</u>
N-1	663	665	219	214	184	178	2.50	1.30
N-2	654	654	224	214	251	250	2.50	1.35
N-3	646	646	229	214	326	321	2.50	1.69
N-4	598	596	272	266	488	498	2.50	1.24
N-5	608	607	233	235	560	567	2.50	1.51
N-6	616	616	200	205	624	632	2.50	3.07
N-7	622	621	216	210	-140	-137	2.50	1.23
N-8	610	610	238	237	-076	-068	2.50	1.09
N-9	600	599	261	266	-004	002	2.50	1.66
N-10	1000	993	010	001	365	368	2.50	1.23
N-11	862	831	002	-005	407	412	2.50	3.41
N-12	713	685	-006	-011	443	449	2.50	4.15
N-13	375	378	032	014	243	249	2.50	1.75
N-14	525	524	-028	-047	240	249	2.50	1.00
N-15	663	670	-092	-110	237	249	2.50	2.91
N-16	975	975	005	006	117	121	2.50	3.75
N-17	837	835	011	003	084	087	2.50	1.04
N-18	688	677	019	000	048	049	2.50	0.20
Pb-1	1064	1064	-133	-140	240	247	3.53	2.08
Pb-2	344	344	119	121	406	415	3.25	2.23
Pb-3	333	333	131	122	084	092	3.84	0.68

Table III
Bond Distances

<u>Pb-N</u>	<u>Distance (Å)</u>	<u>Pb-N</u>	<u>Distance (Å)</u>
1-10	2.58	3-1	2.81
1-15	2.63	3-9	2.81
1-16	2.70	3-13	2.84
1-13	2.72		
1-7	2.82	N-N	
1-6	2.83	1-2	1.17
1-7'	2.92	2-3	1.16
1-6'	2.92	4-5	1.18
		5-6	1.11
2-4'	2.48	7-8	1.16
2-18	2.58	8-9	1.19
2-3'	2.67	10-11	1.29
2-4	2.70	11-12	1.14
2-3	2.73	13-14	1.19
2-12	2.76	14-15	1.20
2-13	2.97	16-17	1.08
3-9'	2.48	17-18	1.22
3-1'	2.58		
3-12	2.64		
3-18	2.76		

From bond energy considerations Pauling and Brockway⁹ have shown that the linear azide groups will be assymetric if the bonding is homopolar. Evidence for this appears in the Okl neutron density map (Figure 1) and also in the calculated N-N distances. However, it is not possible to determine the direction of the covalent bonds since the differences⁷ in the interatomic distances are not significant in most cases. This is so because the x-coordinates were not directly refined and also because the standard deviations of the remaining coordinates are rather large. An accurate determination of bond distances will have to wait until three-dimensional neutron data can be obtained.

Acknowledgment: Thanks are due to Dr. J. V. R. Kaufman for bringing this problem to my attention and to Mr. I. Kluger for performing all the computer calculations. I am also grateful to Dr. H. Danner for the neutron data and for the information on the work done at Penn State and to Dr. J. H. Van den Hende for supplying me with all the computer programs.

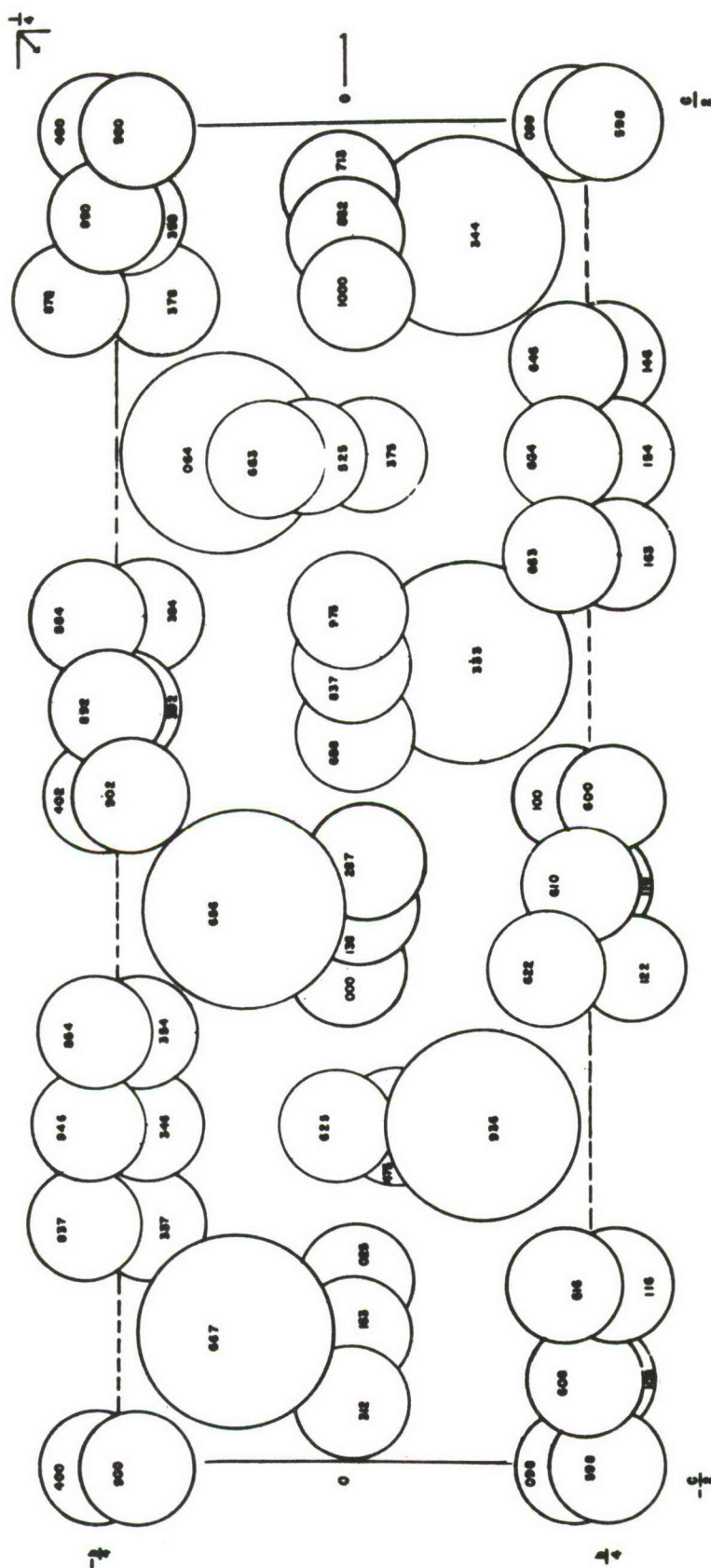


Figure 2. Diagram to illustrate the packing arrangement within the crystal. The lead atoms are represented by the large circles and the nitrogen by the small circles.

References

1. F. D. Miles, J. Chem. Soc., 2532 (1931).
2. E. W. Hughes, Ph. D. Thesis, Cornell University (1935).
3. G. Pfefferkorn, Z. Naturforsch, 3, 364 (1948).
4. L. V. Azaroff, Z. fur Krist., 107, 362 (1956).
5. P. Saha, private communication.
6. N. F. M. Henry and K. Lonsdale, ed., International Tables for X-ray Crystallography, Volume I, Symmetry Groups; The Kynoch Press, Birmingham, England (1952).
7. H. Lipson and W. Cochran, The Crystalline State: Volume III, The Determination of Crystal Structures; G. Bell and Sons, Ltd., London, England (1953).
8. J. H. Van den Hende, ERBRL Crystallographic Structure Factor and Least Squares Refinement Program for The IBM 7090 Computer, Esso Research and Engineering Co., Linden, New Jersey (1961).
9. L. Pauling and L. O. Brockway, J. Am. Chem. Soc., 59, 13 (1937).

CRYSTAL STRUCTURE CHANGE OF SODIUM AZIDE AT 19°C

by

B. S. Miller and G. J. King
Basic Research Laboratory

U. S. Army Engineer Research and Development Laboratories
Fort Belvoir, Virginia

Abstract

A loss of crystal symmetry in sodium azide at $19 \pm 1^{\circ}\text{C}$ is demonstrated by changes in the ESR signal from Mn^{++} doped crystals. X-ray powder diffraction and optical interference figures indicate a change from the normal hexagonal (rhombohedral) symmetry to orthorhombic.

Experimental

Sodium azide is rhombohedral¹ with a rhombohedral angle $\alpha = 38^{\circ}43'$ and $a_0 = 5.44 \text{ \AA}$. The alternate hexagonal cell¹ has $A_1 = A_2 = 3.637 \text{ \AA}$ and $A_3 = 15.209 \text{ \AA}$. Slow crystallization from aqueous solution yields hexagonal basal plates. Doping growth solutions with trace amounts of Mn^{++} (5 ppm) causes a modification of the crystal growth habit but the crystal structure is unchanged at room temperature.

Paramagnetic resonance measurements were made on such doped crystals over a temperature range of 270 to 300°K using a Varian X-band spectrometer with 100 kc modulation and variable temperature unit. Temperatures were measured by a cooper constantan thermocouple glued to the sample.

X-ray powder diffraction patterns were taken with a Norelco X-86-N high temperature, high vacuum diffractometer attachment with cold water circulating through the sample holder to obtain temperatures below ambient.

Results and Discussion

Paramagnetic resonance of Mn^{++} in rhombohedral (hexagonal) sodium azide at room temperature and above has been reported² and compared to the similar resonances observed for Mn^{++} in NaCl ³. The Mn^{++} resonance spectra observed show the effect of a large crystal field in a manner very similar to the effects observed in NaCl . At least three sets of 30 line resonance spectra are observed and each set of 30 lines consists of five groups of six lines each. Each group of six is a single fine structure line split up by the Mn^{++}

nuclear spin interaction. The splitting of the fine structure lines is a direct and very sensitive measure of the internal electric fields of the host crystal. For NaN_3 containing Mn^{++} , the resonance structure undergoes a sharp, reversible and reproducible transition at $19 \pm 1^\circ \text{C}$.

As in sodium chloride containing Mn^{++} , the large crystal field effects in the sodium azide Mn^{++} resonance have been attributed to the inclusion of cation vacancies to permit charge compensation³. Compensation appears to occur in the sodium ion plane and the hexagonal symmetry allows three sets of orientationally nonequivalent sites around the Mn^{++} . With the C axis of the crystal aligned with the dc magnetic field these sets are nearly equivalent and the resonance lines are superimposed (Figure 1). Without changing crystal orientation, the slight cooling through the 19°C transition temperature abruptly destroys the near equivalence and removes the superposition of the lines. The resulting spectrum has a much lower symmetry and the large multiplicity of lines can now interfere with each other (derivative detection). This type of change in crystal field is a good indication of structural changes in the host crystal.

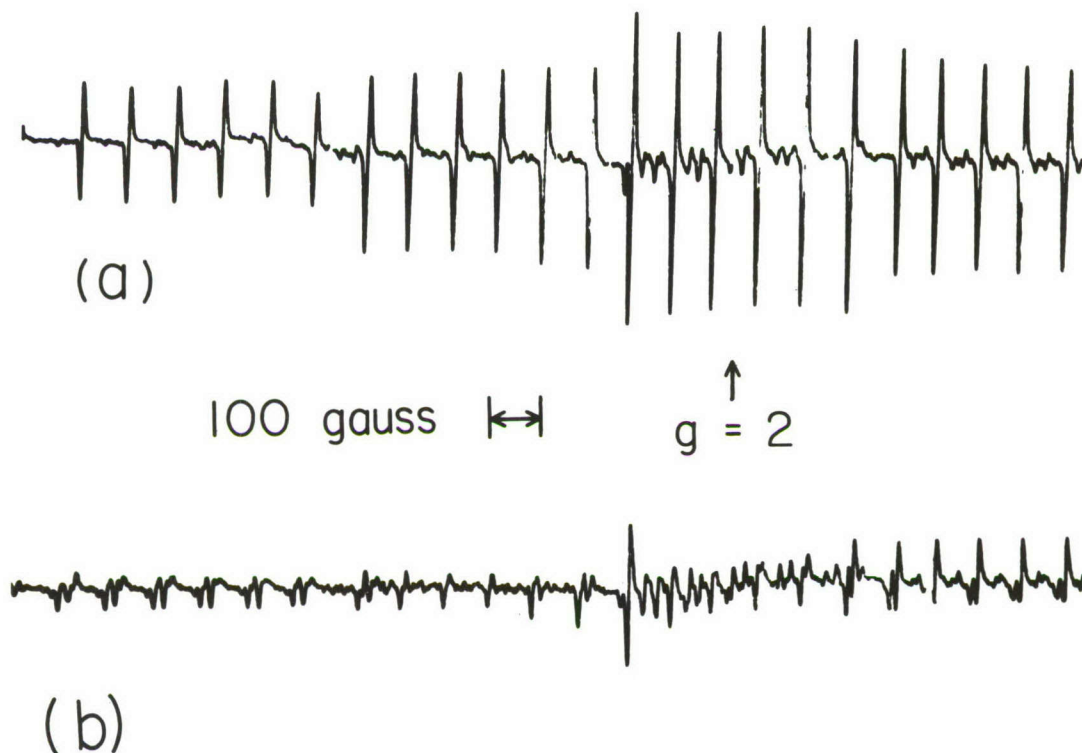


Figure 1. (a) ESR spectrum of NaN_3 with dc magnetic field closely parallel to hexagonal C axis at 22°C (incomplete spectrum), (b) same field scan and instrument gain settings with sample at 17°C .

In order to verify the interpretation of the paramagnetic resonance results, x-ray diffraction and optical polarization experiments were performed.

X-ray powder diffraction patterns were taken of finely ground pure sodium azide. At room temperature three lines could be easily identified as the $(10\cdot2)$, $(01\cdot4)$, and $(10\cdot5)$ reflections. The sample was cooled by circulating water at 5°C through the copper sample holder. The lower temperature spectrum showed line pairs with intensity ratios of 2/1 in the positions of the former reflections (Figure 2). The angular splitting of the pairs increased at higher 2θ angles. This diffraction data, although meager, is consistent with a reduction in symmetry from hexagonal to orthorhombic.

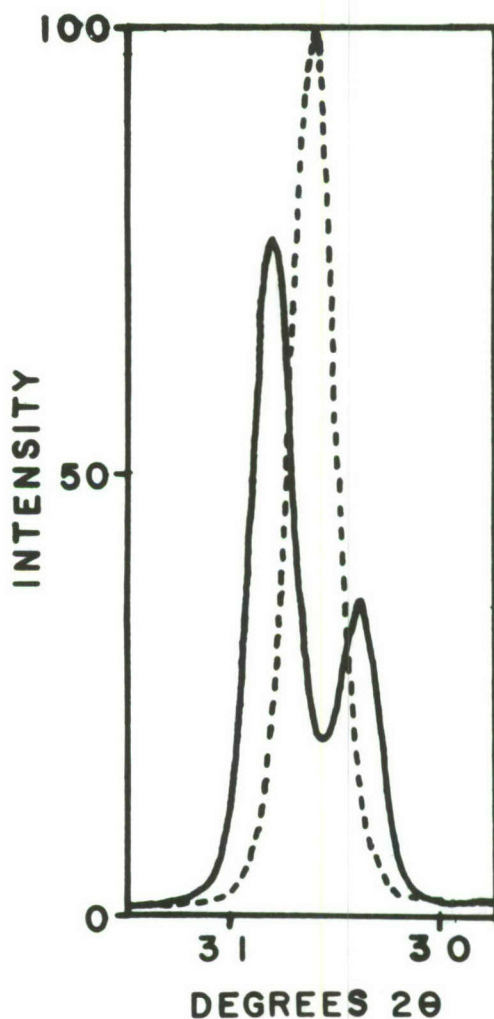


Figure 2. Portion of x-ray diffraction pattern of NaN_3 . Dotted line: $(10\cdot2)$ reflection at 22°C . Solid line: cooled to 5°C .

Small basal plates of undoped sodium azide were examined with the polarizing microscope and yielded good uniaxial interference figures⁴ at room temperature. Upon cooling the crystal slightly by flowing cool gas across the microscope stage, the interference figure was observed to swiftly become biaxial. This is again in agreement with a change to orthorhombic symmetry.

Further structural determinations have not been carried out and are not contemplated.

A limited amount of differential thermal analysis has been done on sodium azide by other workers⁵ and an indication of a transition at 18° C was noted. This is very close to the 19° C observed in ESR measurements and is probably the same phenomena. Similar x-ray diffraction patterns were reported previously but were not interpreted as due to a structure change.

It should be noted that the transition temperature of 19° C is approximately equal to the "room temperature" found in many laboratories. This may account for previously reported⁶ difficulties with structure determinations of sodium azide.

Indications of domain structure may be seen in some sodium azide crystals as colored "patches" on cooling. These color phenomena are likely associated with the structure change when poorly crystallized or multi-domain crystals are used.

Acknowledgments

The authors wish to thank Dr. Walter Lawson of Warfare Vision Branch, ERDL, for use of x-ray equipment and Dr. Howard T. Evans of the Geological Survey, Washington, D. C., for helpful discussions.

References

1. S. B. Hendricks and L. Pauling, J. Amer. Chem. Soc. 47, 2904 (1925).
2. G. J. King and B. S. Miller, Bull. Am. Phys. Soc. Ser. II, 8, 344 (1963).
3. George D. Watkins, Phys. Rev. 113, 79 (1959).
4. Hartshorne and Stuart, "Crystals and the Polarising Microscope," (Edward Arnold & Co., London, Second Ed., 1950).
5. J. Petz, University of Arkansas (1957), unpublished data.
6. M. Bassiere, J. Chim. Phys. 36, 71 (1939).

NITROGEN NMR CHEMICAL SHIFTS IN THE AZIDE ION

by

R. A. Forman
National Bureau of Standards
Washington, D. C.

As part of an investigation of bonding in the azides, the NMR chemical shifts of N^{14} in sodium azide solution have been measured. The spectrum, as expected, consists of two lines, one from the central nitrogen, and one from both of the end nitrogens in the N_3^- ion. Both lines were at higher field than the resonance in NO_3^- ion. Identification with the nuclei involved was made by integration of the spectrum.

The work was performed on a Varian DP-60 spectrometer system equipped with a V-4311 rf unit operating at 4.33 mc/sec. The measurements of the chemical shifts were made by use of the sideband-modulation technique¹.

The solution used was a saturated aqueous solution of sodium azide which had been carefully purified. Sodium azide was chosen because its solubility is high, and it is the most readily available commercially. It is expected that all of the ionic azides would give identical results. The sodium azide purchased as a purified grade from Fisher Scientific Company was purified in the following manner. A solution was prepared and filtered, and then evaporated to dryness. It was then redissolved to make a saturated solution and then sodium azide was precipitated by adding acetone. The precipitate was then redissolved in water and passed through a sodium ion exchange column to remove paramagnetic ions. A saturated solution was then prepared.

The shifts and linewidths measured are summarized in Table I. All measurements were made at a fixed frequency of 4.334610 mc/sec at a field of about 14100 G. The shifts were measured relative to a saturated solution of $NaNO_3$ contained in a small tube concentric with the sample tube. The sample tube was 15 mm o.d. and the central tube 8 mm o.d. A reversal of the position of sample and standard produced the same results within the limits of the experiment. No effect of solution concentration was noted on the chemical shifts. This combined with the width of the lines is probably a good indication of the absence of paramagnetic impurities.

The difference in the widths of the resonances from the central and end nitrogens is an indication of the different quadrupole couplings experienced by each. Previous work² on the microwave spectrum

of HN_3 indicates that the quadrupole coupling constant of the central atom should be much smaller than those of the ends; this is also indicated by the NMR results. Further work on the quadrupole coupling in the azides is currently in progress.

Table I

Nucleus	Shift (ppm)	Linewidth (milligauss)
End N^{14} in N_3^-	277.5 ± 2.6	244 ± 12
Central N^{14} in N_3^-	128.7 ± 1.2	73 ± 1.5
NO_3^-	0	52 ± 3

The author wishes to thank Dr. Harry Allen of the Analytical and Inorganic Chemistry Division of the National Bureau of Standards for allowing him the use of the spectrometer, and H. Rosenwasser of ERDL, Fort Belvoir, for information on sample preparation.

References

1. J. T. Arnold, S. S. Dharmatti, and M. E. Packard, J. Chem. Phys. 19 507 (1951).
2. R. A. Forman and D. R. Lide, Jr., J. Chem. Phys. (15 August 1963).

THE PHOTOCHEMICAL DECOMPOSITION OF SODIUM AZIDE

by

P. W. M. Jacobs, A. R. T. Kureishy and F. C. Tompkins

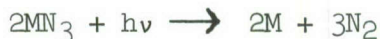
Department of Chemistry

Imperial College

London, S.W.7, England

Introduction

When a crystal of an inorganic azide is irradiated with light of wavelength corresponding to the absorption band of the solid, photochemical decomposition takes place. The reaction can be written down as:



and may be studied, kinetically, by measuring the pressure of evolved nitrogen as a function of time. The photolysis of barium, strontium, potassium and sodium azides has been studied by Thomas and Tompkins^{1,2,3}, Jacobs and Tompkins^{4,5}, Tompkins and Young⁶, Jacobs, Tompkins and Young⁷, Cunningham⁸, Jacobs, Tompkins and Pai Verneker⁹ and Sheppard¹⁰. When irradiated by the light from a low pressure (L.P.) mercury lamp (largely 2537 Å) the rate of photolysis decreases initially. For NaN_3 the rate becomes constant after the initial decay but with the Ba, Sr and K salts it increases after reaching the minimum value, eventually becoming constant. Jacobs, Tompkins and Pai Verneker⁹ and Sheppard¹⁰ have shown that this acceleratory period is due to radiation of shorter wavelength specifically the 1849 Å line present in the emission from the L.P. lamp and that it is not observed if the radiation from this source is filtered through a water filter, which absorbs strongly radiation of $\lambda < 2000 \text{ Å}$.

It is generally agreed that the first step in the photolysis of these azides is the creation of excitons rather than positive holes. The excitons thus formed can be trapped at imperfections in the azide lattice and react with other excitons to produce nitrogen. The electrons located at the traps are then transferred to metal ions to produce metal atoms. The acceleratory reaction in Ba, Sr and K azides is associated with the metal produced during the initial deceleratory reaction.

The results reported in this paper form a continuation of previous work on the thermal decomposition of sodium azide. It was found that the kinetics of the thermal decomposition of this salt are affected considerably by the method of its preparation and by

the presence of impurities. Similar differences are found in the photochemical behaviour of these preparations.

Experimental

(a) Apparatus

The rate of photolysis was measured by observing the increase in pressure in a constant volume system, using a Pirani gauge. The sample was spread uniformly in a silica cell with a flat window (area 11.3 cm²). The initial pressure before starting a run was $<10^{-6}$ mm of mercury and the outgassing rate of the order of 10^{-5} mm/hr. The source of irradiation was a low pressure mercury lamp with strong emission at 2537 Å and a number of weaker components at 1849, 2345, 2482, 2650, 2967, 3130, 4047, 4358, 5770 and 5991 Å. The intensity of irradiation was varied by changing the current in the primary circuit of the power supply to the lamp. The lamp was calibrated using a Kipp thermopile.

(b) Preparation of sodium azide

(i) 'Alkaline' sample: The commercial grade sodium azide (from Hopkin and Williams) twice recrystallised from an aqueous solution, filtered and dried in vacuo over silica gel. It was stored in vacuo over silica gel for at least two days before use.

(ii) 'Acid' sample: This was prepared and stored in a similar manner to that described in (i) but the solution of NaN₃ was made acid by adding HN₃ (pH ~ 6.5) before each reprecipitation.

(iii) '0.05 M% Fe' and '1 M% Fe' samples: These were prepared in a similar manner from NaN₃ solutions containing 0.05 M% and 1 M% FeCl₃ solution. The solution containing 1 M% FeCl₃ was acid due to hydrolysis of FeCl₃ but that containing 0.05 M% FeCl₃ was made acid by adding to it a small amount of HCl.

Results

(a) Effect of impurities

Figure 1 shows the plots of the rate of photochemical decomposition against the total number of nitrogen molecules evolved, for 200 mg samples of the different preparations of NaN₃. The runs were carried out at the room temperature (22°-26° C) and the light intensity was 12.3×10^{14} quanta cm⁻² sec⁻¹ (calculated on the basis of a 2537 Å monochromatic source). The rate decreases with the increasing degree of decomposition, settling down at a constant value (R_F) for the 'Acid', 'Alkaline' and '0.05 M% Fe' samples (Figure 1, curves A, B, C). For '1 M% Fe' sample the rate rises initially

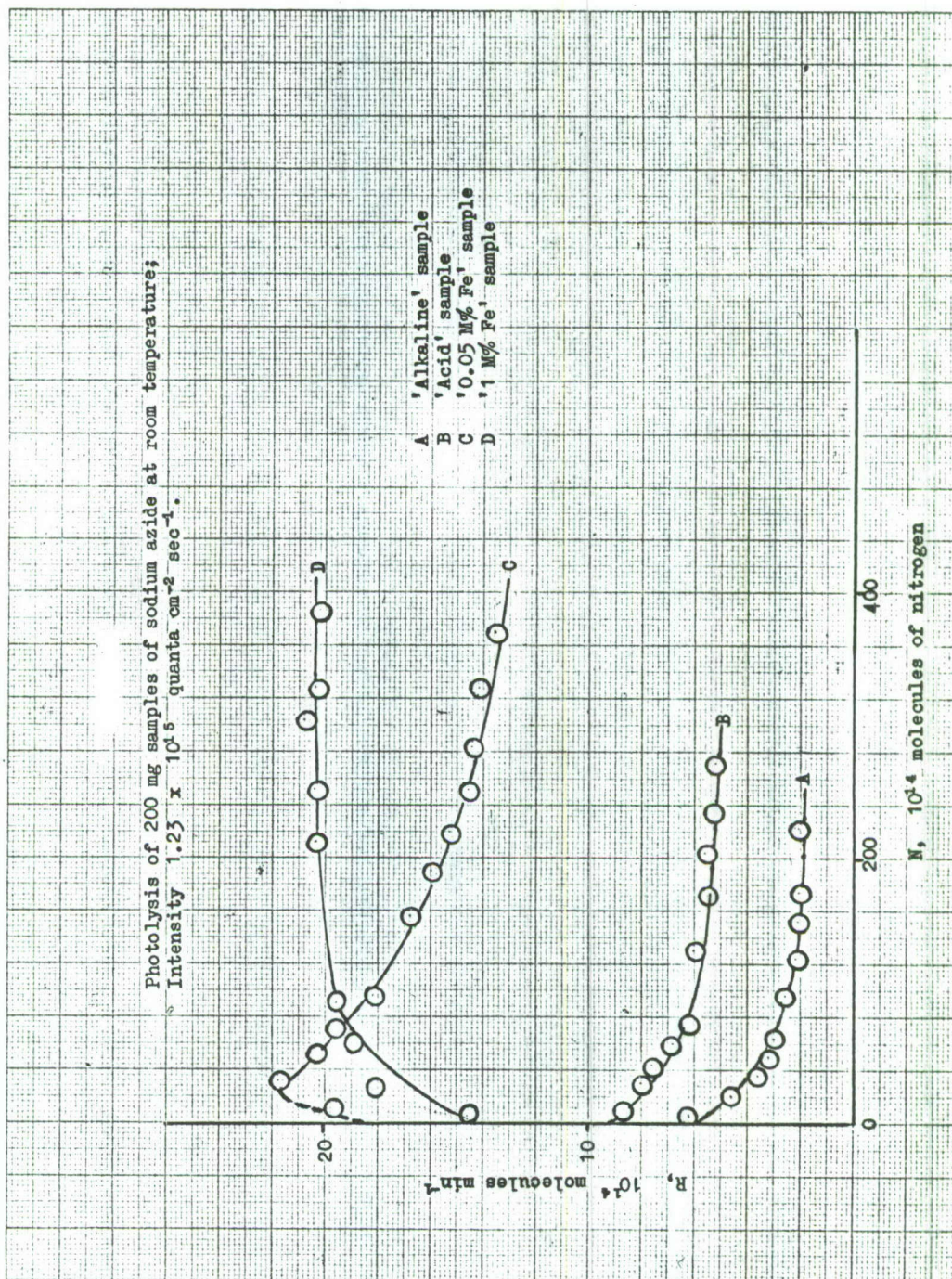


Figure 1

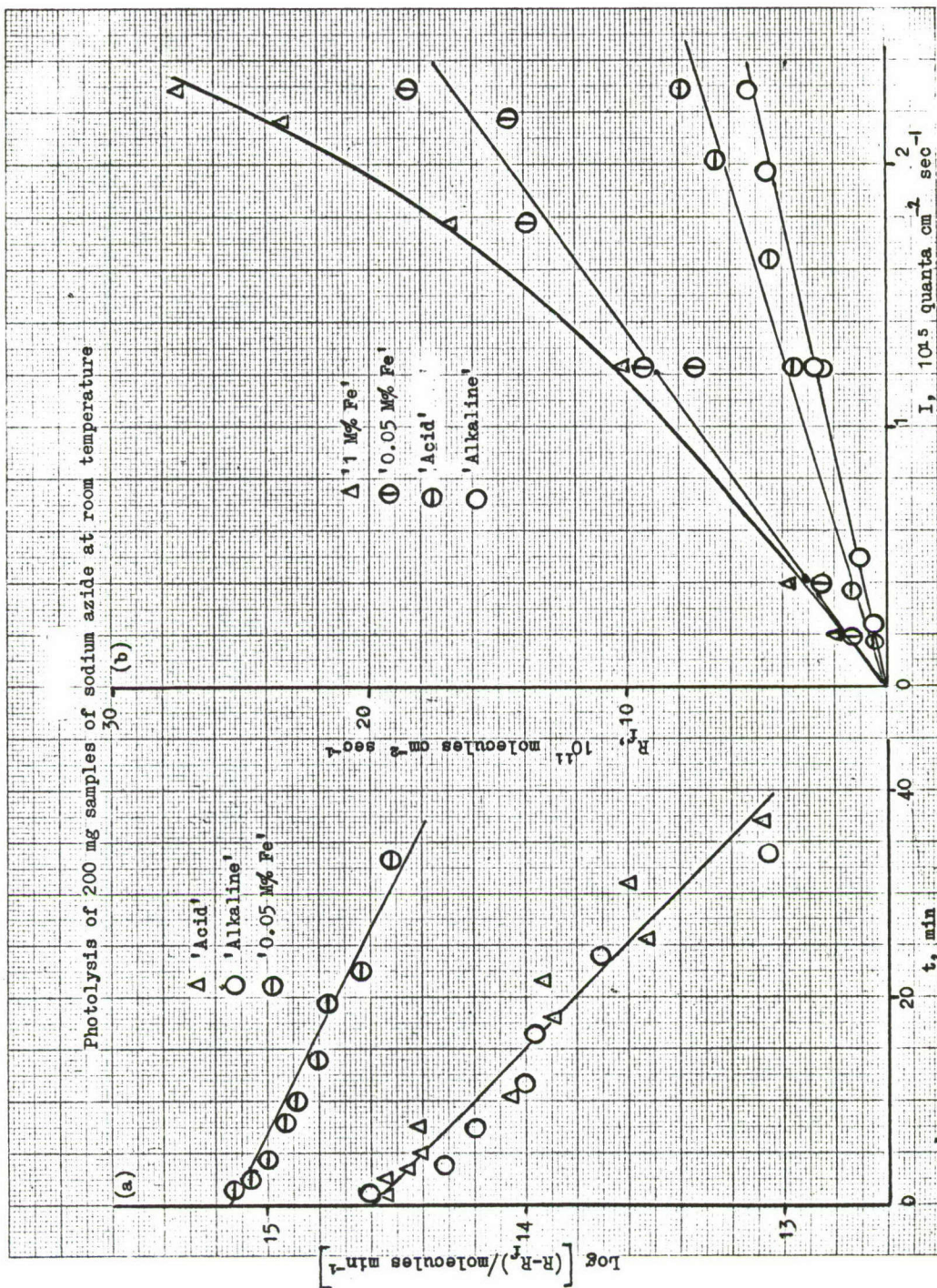


Figure 2

(Figure 1, curve D) reaching a maximum value and then decreases slowly (not shown in the figure) in a manner similar to the other preparations.

The intensity dependence of the constant rate, R_f , is shown in Figure 2B. For 'Alkaline', 'Acid' and '0.05 M% Fe' samples R_f varies linearly with the intensity. The plot for a '1 M% Fe' sample is not linear.

By measuring the value of the constant rate, R_f , also at ice temperature the values of the activation energy, E , for various preparations were found to be: 'Alkaline' sample, 4.1 kcal mole⁻¹; 'Acid' sample, 1.1 kcal mole⁻¹; '0.05 M% Fe' sample, 1.2 kcal mole⁻¹; '1 M% Fe' sample, too small to determine with any degree of accuracy.

The plots of $\log (R - R_f)$ against time, where R is the rate at time t and R_f the constant rate, are shown in Figure 2A.

(b) 'Acid' sample

Reproducible results were obtained when 400 mg samples of this preparation were decomposed photochemically at room temperature. Figure 3A shows the rate versus time plots for two different 'Acid' samples under the same conditions of temperature and intensity. A series of runs at different intensities showed that both the initial and the final rates, R_0 and R_f , are proportional to the first power of intensity (Figure 4B). The quantum yields for R and R_f are 1.45×10^{-3} and 0.48×10^{-3} molecules of N_2 per quantum. Figure 4A shows a plot of $\log (R - R_f)$ against time for the two runs at the same intensity.

(c) Effect of nitrogen

The effect of N_2 on the photochemical decomposition of sodium azide has been demonstrated by the following experiment: a sample of sodium azide was photolysed until it reached the constant rate (Figure 3A). The decomposed sample was then left in contact with nitrogen for about 17 hours in the dark. The rate against time plot after this treatment is shown in Figure 3B. The rate starts at zero and reaches a constant value which is slightly lower than the previous constant value. The lamp was then switched off and the sample left open to the pumps for two hours; the subsequent photolysis commences at a rate which is slightly higher than the previous value and it remains constant at this value (Figure 3C). Figure 3D shows that if the sample is left in contact with N_2 only for one hour the initial rate is lower but it does not start at zero (as in Figure 3B) while it rises to the constant value more quickly.

Photolysis of 400 mg samples of 'Acid' sodium azide at room temperature;
Intensity, 1.23×10^{15} quanta $\text{cm}^{-2} \text{sec}^{-1}$

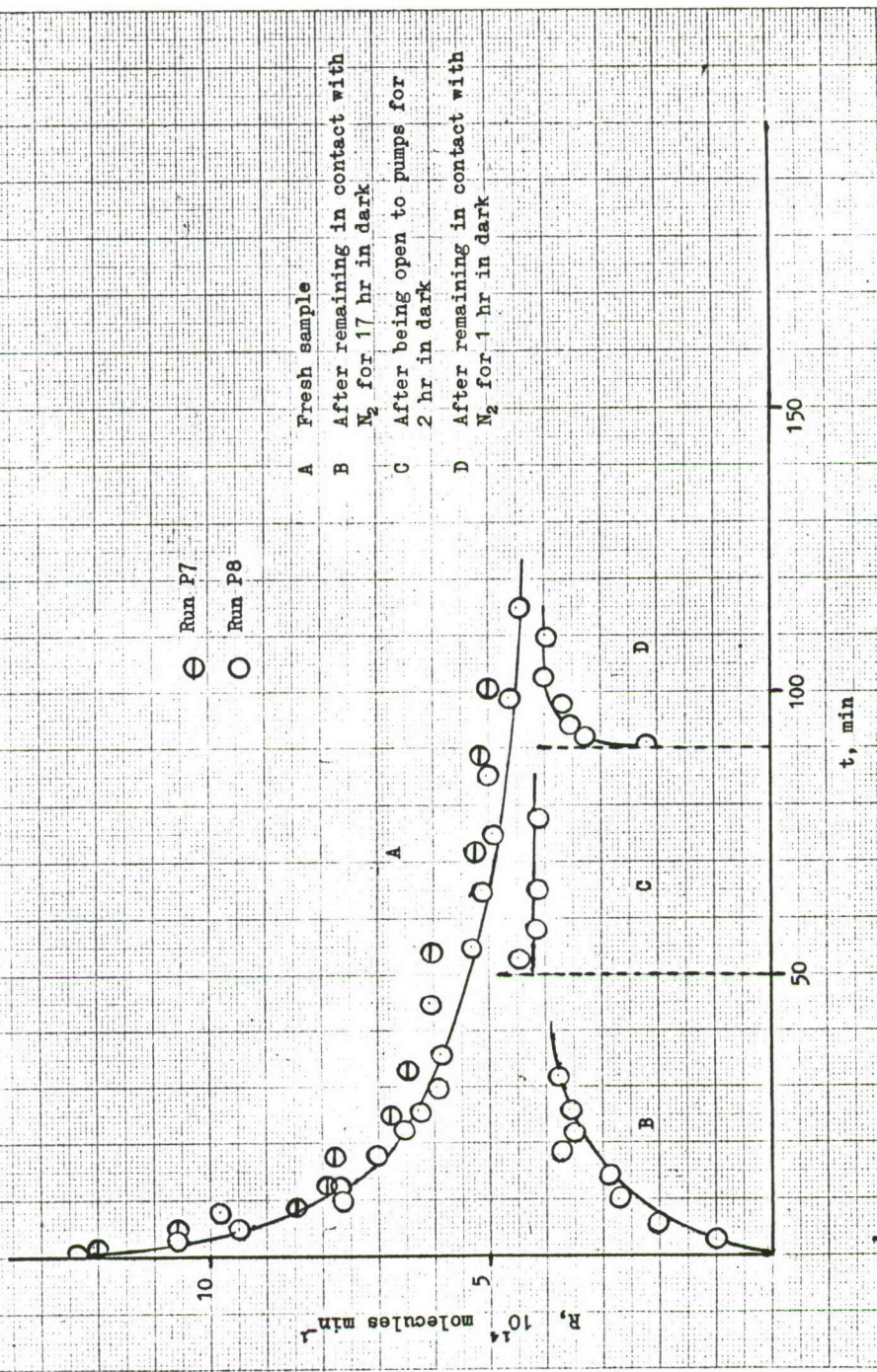


Figure 3

Discussion

(a) Mechanism

Cunningham and Tompkins¹¹ and Deb's¹² work have shown that 2537 Å line lies within a broad absorption band, which has its maximum at around 2225 Å¹². It has been suggested¹² that this band is due to formation of a low-lying excited state of the azide ion. Cunningham and Tompkins¹¹ have concluded from their measurements of absorption coefficients and F-centre formation in Na and K azides that while exciton production occurs predominantly within the lattice of KN₃, in NaN₃ these are formed only at special sites where the deformation potential is high, e.g., in the neighbourhood of dislocations. Jacobs and Tompkins⁴, from their failure to observe photoconductivity in KN₃ irradiated with a L.P. mercury lamp, concluded that free electrons were not formed. From the above information the following mechanism can be written down for the initial photolysis of NaN₃:

Process (a)



where $\text{S}' = \text{S} + 2\Box + 2e$

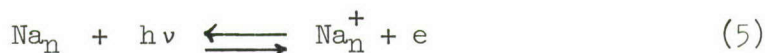
It is reasonable to assume (i) that the equilibrium in equation (1) is very rapidly reached and therefore that the concentration of N_3^{-*} does not vary with time; and (ii) that the sites, S, where the reaction can take place are being consumed, i.e., sites, S', regenerated by the reaction represented by equation (3) cannot take part in process (a). As the rate of N₂ production decreases with time it follows that the probability p_2 is very high and that the concentration of species N₃Se reaches its maximum value virtually instantaneously, which therefore will be the same as N₀, the number of sites at zero time. If N_{S'} is the number of sites consumed by reaction (3):

$$\begin{aligned} (dN_{S'}/dt) &= p_3 [\text{N}_3^{-*}] [\text{N}_3\text{Se}] \\ &= (p_3 \cdot p_1 / p_{-1}) I [\text{N}_3^-] (N_0 - N_{S'}) \end{aligned} \quad (4)$$

Equation (4) predicts that for the process (a) the initial rate, R_0 , will be proportional to the first power of intensity, I , as observed (Figure 4B) and that there will be a unimolecular decay of the number of sites at which this reaction can occur.

If the photolysis of sodium azide involved only process (a) one would expect the rate to become zero eventually, which is not so (Figure 1). The final constant rate period suggests a linear growth of a constant number of sites. If we assume that the sites S' produced during process (a) can take part in further photolysis after first losing their electrons to Na^+ ions, which thus become specks of sodium metal (Na_n), the mechanism for this process can be written as follows:

Process (b)



During the initial stages of decomposition the number of S' (and hence of sites Na_n) is varying and one cannot apply a steady state analysis to these processes. However, once all the original sites S have been consumed, number of S' , which is the same as that of Na_n becomes constant and $Ng' = [Na_n] = N_0$. Although these aggregates of metallic sodium are growing in size according to equation (8) their number remains the same and, until some large value of n , Na_{n+2} is equivalent to Na_n for the purpose of this reaction. During the constant rate period, therefore, a steady state may exist. Thus:

$$d[Na_n^+] / dt = p_5[Na_n][h\nu] - p_{-5}[Na_n^+][e] - p_6[Na_n^+][N_3^{-x}] = 0 \quad (9)$$

$$d[Na_nN_3] / dt = p_6[Na_n^+][N_3^{-x}] - p_7[Na_nN_3][N_3^{-x}] = 0 \quad (10)$$

$$d[N_2] / dt = p_7 [Na_nN_3] [N_3^{-x}] \quad (11)$$

The second term in equation (9) may be dropped because the high concentration of excitons relative to free electrons means reaction (6)

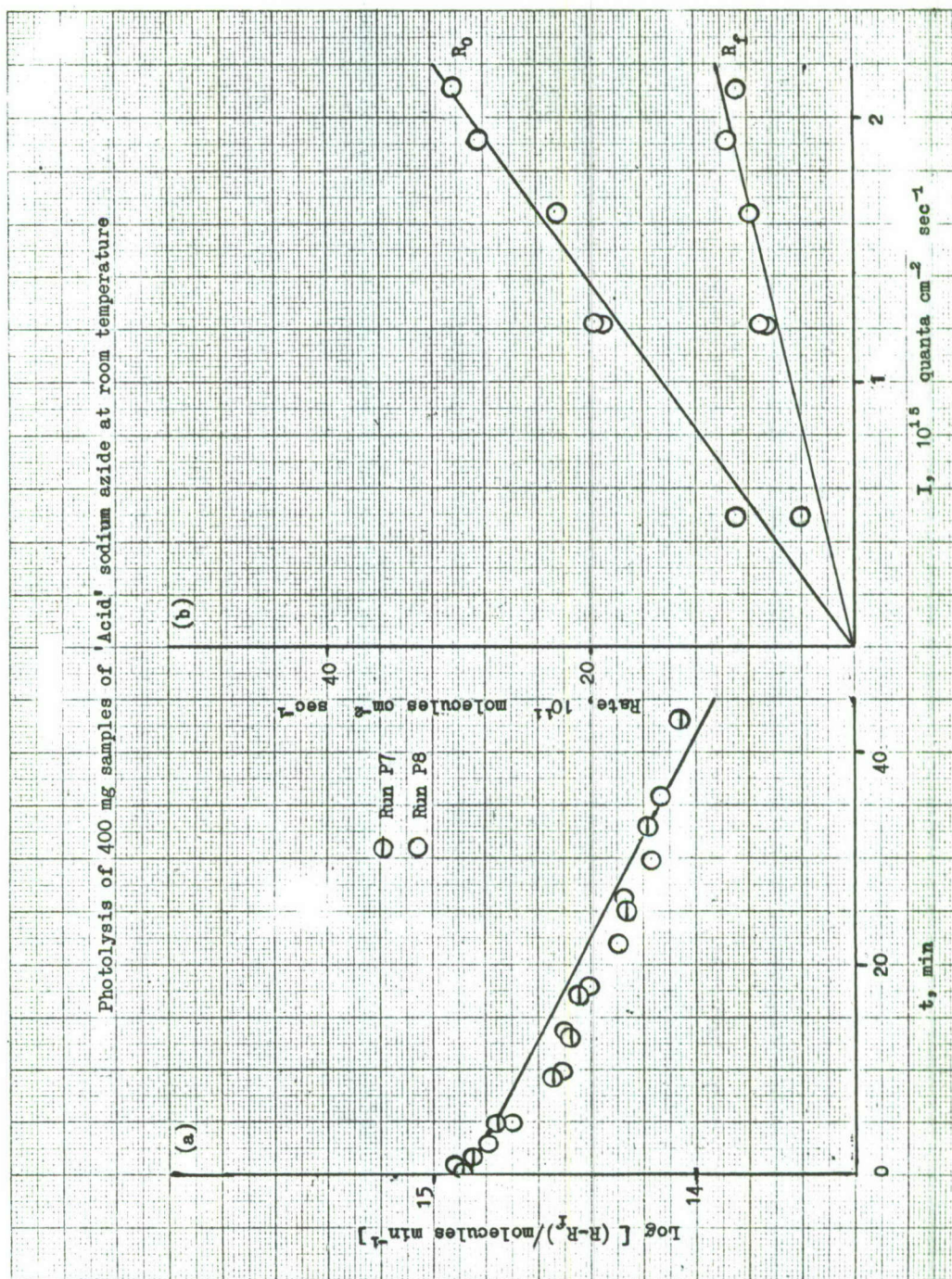


Figure 4

is preferred to reaction (-5). Neglecting this term then, equation (9) becomes

$$d[Na_n^+] / dt = p_5[Na_n][hv] - p_6[Na_n^+][N_3^-] \quad (12)$$

Adding equation (10), (11), (12) and substituting $[Na_n] = N_0$,

$[hv] = I$ gives:

$$d[N_2] / dt = p_5 N_0 I \quad (13)$$

Equation (13) predicts the observed behaviour that the constant rate, R_f , is proportional to I (Figure 4B).

(b) Nucleation and growth

If the mechanism discussed above is considered on a macroscopic scale, it is observed that it confirms to the classical concepts of nucleation and growth as applied to decompositions in the solid state. The photolysis of sodium azide can, therefore, be regarded as composed of two steps, i.e., nucleation according to a unimolecular decay law (process (a)) and the subsequent one dimensional growth of these nuclei (process (b)). When considering the thermal decomposition of solids, the product evolved in the nucleation process is generally ignored in the quantitative treatment because of its small contribution to the total. However, in photochemical decomposition both the nucleation and growth processes are of the same order of magnitude and take place simultaneously. Therefore, one cannot neglect the contribution made by the nucleation process.

Consider N_0 potential nucleus forming sites decomposing according to a unimolecular decay law with a rate constant, k_1 . As these sites decompose they become growth nuclei, which grow one dimensionally with a rate constant, k_2 . A nucleus which starts growing at time, y , will attain a size, $k_2(t - y)$, where t is the total time. Also there will be $N_0 k_1 \exp(-k_1 y)$ such nuclei. From equation (3) it will be seen that the decomposition of one site produces three molecules of nitrogen. If N is the total number of nitrogen molecules evolved and N_1 , N_2 the number of molecules produced by process (a) and process (b) respectively, N may be written as a function of time:

$$N = N_1 + N_2 = 3N_0(1 - e^{-k_1 t}) + \int_0^t N_0 k_1 e^{-k_1 y} \cdot k_2(t - y) dy \quad (14)$$

Integrating the growth term in equation (14) gives

$$N = 3N_0(1 - e^{-k_1 t}) + (N_0 k_2 / k_1)(e^{-k_1 t} + k_1 t - 1)$$

$$R = dN/dt = 3N_0 k_1 e^{-k_1 t} + N_0 k_2 (1 - e^{-k_1 t}) \quad (15)$$

When $t = 0$, $R_0 = 3N_0 k_1$ and when $t \longrightarrow \infty$, $R_f = k_2 N_0$. Substituting these values in equation (15) and rearranging gives

$$(R - R_f) = (R_0 - R_f)e^{-k_1 t}$$

$$\text{or } \log(R - R_f) = -(k_1/2.303)t + \log(R_0 - R_f) \quad (16)$$

The photolysis data is reasonably well fitted by this equation (Figures 2A and 4A).

The difference between different preparations of NaN_3 can be easily explained on the basis of the above model. The value of k_1 for 'Alkaline' and 'Acid' samples is the same (Figure 2A) and the difference in rates is mainly due to the difference in the value of N_0 , e.g., $0.25 \times 10^{15} \text{ cm}^{-2}$ for the 'Alkaline' sample as compared with $0.33 \times 10^{15} \text{ cm}^{-2}$ for the 'Acid' sample (the values of N_0 given in Table I for a 400 mg sample of the 'Acid' preparation are more reliable). For '0.05 M% Fe' sample k_1 is smaller and N_0 much higher, i.e., $1.4 \times 10^{15} \text{ cm}^{-2}$ (Figure 2A). The increase in N_0 is expected because additional sites where the reaction can occur are provided by Fe^{+++} ions. The value of k_2 for 'Alkaline', 'Acid' and '0.05 M% Fe' samples are 0.075 min^{-1} , 0.14 min^{-1} and 0.20 min^{-1} , respectively. The differences may not be significant but are as expected from the values of the activation energy associated with R_f for these samples, i.e., 'Alkaline' > 'Acid' = '0.05 M% Fe' > '1 M% Fe'.

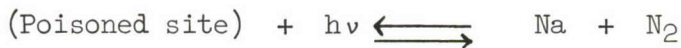
Table I
Values of constants for 400 mg samples of
'Acid' sodium azide at room temperature.

Intensity, 10^{14} quanta $\text{cm}^{-1} \text{ sec}^{-1}$	R_0 , $10^{11} \text{ molecules}$ $\text{cm}^{-2} \text{ sec}^{-1}$	R , $10^{11} \text{ molecules}$ $\text{cm}^{-2} \text{ sec}^{-1}$	k_1 , 10^{-4} sec^{-1}	N_0 , 10^{15} cm^{-2}
4.98	9.14	3.98	5.46	0.568
12.28	19.76	7.37	6.77	0.975
12.28	19.17	6.64	6.77	0.947
16.55	22.71	7.96	10.88	0.705
19.22	28.61	9.73	9.2	1.034
22.07	30.68	8.85	11.6	0.883

The initial increase in rate of the '1 M% Fe' sample can be explained in two ways. First, if $k_2 > k_1$ the rate will rise and become constant as is observed, but it is apparent from the rate-time plot (Figure 1D) that k_1 for this preparation will come out to be much higher than the value for the other preparations. Consequently, the value of N_0 will be much lower. This conclusion is inconsistent with the other observations and does not fit in with the model.

Alternatively, the initial rise in rate may be assumed to be due to increase in the number of sites. A possible reason for this can be that some of the Fe^{+++} sites are in the reduced state and that these are ionised by the u.v. light. Thus the effective number of potential nucleus forming sites increases initially. The lower value of k_1 for '0.05 M% Fe' sample indicates that the additional impurity sites due to Fe^{+++} , decay more slowly than the ones originally present in NaN_3 . At such high impurity concentrations aggregates of impurity ions will certainly be formed and these become ineffective only when completely surrounded by sodium atoms produced during the decomposition. This will account for the considerable period of constant rate at a higher value in the case of '1 M% Fe' sample and the slow decay to the ultimate value, R_f , associated with the growth process.

The effect of nitrogen described in section (c) of the results (Figure 3) is clearly due to reaction of nitrogen molecules with the sodium nuclei. The nitrogen, by chemisorption or nitride formation, uses up the donor levels which participate in the photolysis reaction by photoionisation. Hence, the decrease in the rate when the decomposed sample is left in contact with nitrogen. When subsequent photolysis is carried out the poisoned sites are regenerated by the u.v. light and the rate rises gradually to its constant value. That this rate is always slightly lower than the constant rate measured in the previous decomposition indicates that the equilibrium of the type:



exists and is continuously shifting towards an increased number of poisoned sites as the concentration of Na and N_2 increases. Thus the slow decrease observed in the 'constant rate' is explained.

References

1. Thomas and Tompkins: Proc. Roy. Soc., A209, 550 (1951).
2. Thomas and Tompkins: Proc. Roy. Soc., A210, 111 (1951).
3. Thomas and Tompkins: J. Chem. Phys., 20, 662 (1952).
4. Jacobs and Tompkins: Proc. Roy. Soc., A215, 254 (1952).
5. Jacobs and Tompkins: Proc. Roy. Soc., A215, 265 (1952).
6. Tompkins and Young: Disc. Farad. Soc., 23, 202 (1957).
7. Jacobs, Tompkins and Young: Disc. Farad. Soc., 28, 234 (1959).
8. Cunningham: Unpublished work (1958).
9. Jacobs, Tompkins and Pai Verneker: J. Phys. Chem., 66, 1113 (1962).
10. Sheppard: Ph. D. thesis, University of London (1962).
11. Cunningham and Tompkins: Proc. Roy. Soc., A251, 27 (1959).
12. Deb: J. Chem. Phys., 35, 2122 (1961).

PARAMAGNETIC RESONANCE OF Mn^{++} IN SODIUM AZIDE

by

G. J. King and B. S. Miller

Basic Research Laboratory

U. S. Army Engineer Research and Development Laboratories

Fort Belvoir, Virginia

The most remarkable feature of the resonance spectrum of Mn^{++} in NaN_3 is its similarity in behavior to Mn^{++} in NaCl. When grown slowly from aqueous solution¹ or from the melt² the Mn^{++} spectrum in NaCl crystals is primarily a single broad line with rudimentary fine structure. Heating the crystal to around 250° C, followed by quenching, produces sets of 30 line characteristic Mn^{++} spectra. The cubic structure of NaCl allows vacancy charge compensation to be energetically equivalent when the vacancy is in any one of the six nearest neighbor cation sites. The paramagnetic resonance crystal field splittings are sensitive to the direction between the vacancy and the manganese. There are at least two other inequivalent sets of spectra observed whenever one set is observed at maximum splitting and there is 90° rotation around a crystal axis separating the maximum splittings for each set.

We have observed similar effects for Mn^{++} in NaN_3 . The crystals, when first grown from solution, show a single broad resonance (Figure 1a) with an apparently disordered line structure superimposed. The similar broad line has been attributed, in NaCl, to precipitation of vacancy - Mn^{++} complexes in sites where the density of Mn^{++} is sufficient to cause exchange broadening. When $NaN_3:Mn^{++}$ is heated to 150° C the broad line vanishes and multiple sets of 30 line spectra occur which are semi-stable at 25° C. This effect is shown in Figures 1a and 1b and is qualitatively the same as that occurring in NaCl. The positive ion vacancy - Mn^{++} pair has high mobility in the lattice and heating followed by quenching causes the pair to be trapped in low concentration throughout the crystal. The spectra are then sharp lined. The Mn^{++} spectra in NaN_3 like those in NaCl, decay slowly at 25° C and return to the original broad line spectrum in several days.

The sharp line spectra of Mn^{++} in NaN_3 show the symmetry of the hexagonal structure. Sodium azide has a layer type structure³ and the symmetry in the metal plane is trigonal. The "c" axis is normal to the metal and the azide planes. Rotational studies performed with the "c" axis perpendicular to the dc magnetic field, show that a different set of lines reaches a maximum splitting every 60°. The vacancy can form a pair with equal binding energy in any one of the six nearest neighbor cation positions, which are in the metal plane.



Figure 1a. The exchange broadened resonance of Mn^{++} in sodium azide at room temperature before heating. The Mn^{++} is precipitated at preferred sites in the crystal and the density is sufficiently great to allow the exchange interaction and obliterate the line structure. The superimposed lines are from Mn^{++} in different parts of the crystal where density is low.

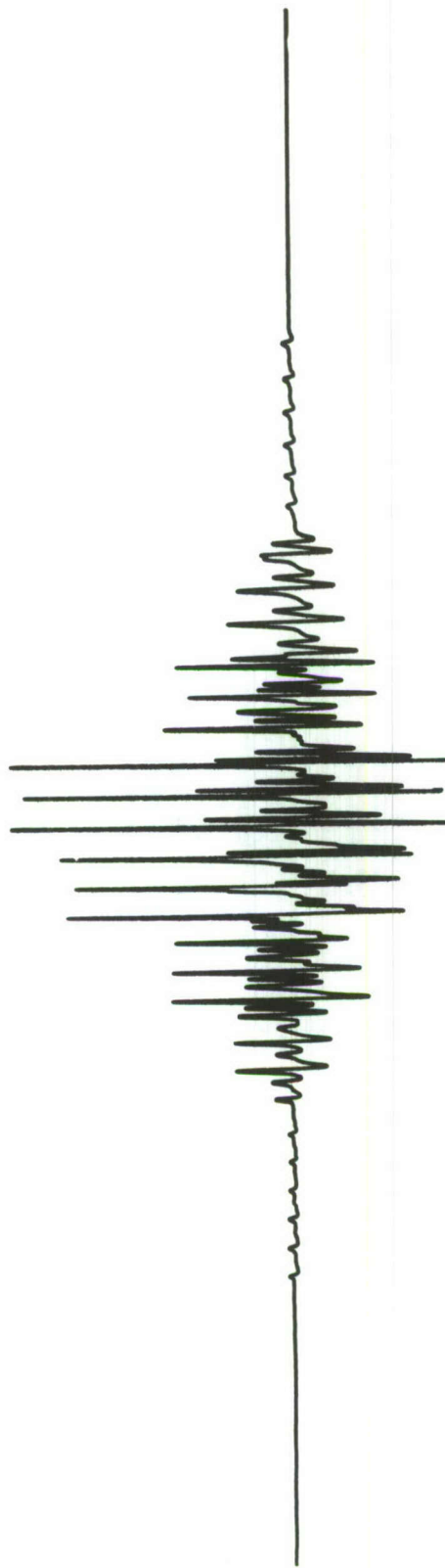


Figure 1b. The resonances of dispersed Mn^{++} - cation vacancy pairs and dissociated pairs at room temperature shortly after heating the crystal to $150^{\circ}C$. The spectrometer gain is reduced by a factor of 10 from that in Figure 1a. The magnetic field is perpendicular to the crystal $[00\cdot1]$ or "c" axis.

The resonance experiment distinguishes only three sets of 30 line spectra for a predominant axial field splitting. This coordination in NaN_3 should be compared with the coordination in KN_3 and RbN_3 . In these two compounds, there are only two possible nearest neighbor cation sites, one on either side of the Mn^{++} in the "c" axis direction. These two positions allow best charge compensation for a vacancy mechanism and, since they are equivalent in axial symmetry, we see only one axial 30 line spectrum. It is useful to note that the symmetry of the KN_3 and RbN_3 spectra seems to require a vacancy for charge compensation of the Mn^{++} . The inclusion of a compensating doubly charged negative ion would require it to be in a positive ion site, to satisfy the observed symmetry of the spectra. Vacancy - Mn^{++} complexes in alkali chlorides can exist in excited states in which, for instance, the vacancy can be removed to the next nearest cation site. In fact, the ground state separation of the complex need not be the closest separation permitted by the geometry⁴. For $\text{NaN}_3:\text{Mn}^{++}$, determinations of the relation of the crystal axes to the symmetry of the spectra indicate that vacancy compensation does occur for the nearest site, but an excited state also exists in which the vacancy and Mn^{++} are dissociated.

The dominant 30 line spectrum shown in Figure 1b is not from vacancy compensated Mn^{++} but from the dissociated vacancy - Mn^{++} complex. This differentiation is easy to make, since the line shape is roughly independent of temperature in the range 20 - 300° C. The line shapes for the vacancy compensated Mn^{++} spectra are very sensitive to temperature and broaden in a characteristic manner. These two types of spectra are in thermal equilibrium and, at temperatures above 180° C, the vacancy compensated spectra convert into the uncompensated spectrum. For NaCl the high temperature spectrum is a single six line spectrum, in accord with the cubic structure. For NaN_3 , the high temperature spectrum also shows the undistorted crystal symmetry. Following the work of Watkins², we call the high temperature spectrum, type II and the vacancy compensated spectrum, type III. Figure 1a corresponds to Watkins' type I spectrum. The relationship of the type II and III spectra in NaN_3 is obvious from the values of the parameters in the spin Hamiltonians. In both cases we use the crystal "c" axis as the major symmetry axis and the crystal field is described by:

$$\mathcal{H} = DS_1^2 + E(S_3^2 - S_2^2)$$

where 1 refers to the "c" axis, 2 refers to the trigonal axis direction between the vacancy and the manganese and the 3 axis is perpendicular to both the 1 and 2 axes. For the type II, or dissociated defect, the value of D is -240 gauss, $E = 0$ and $g = 2.002 \pm .002$. For type III spectrum, the vacancy produces a rhombic distortion and D is -265, $E = +57$ gauss and $g = 2.002 \pm .002$. In both cases A, the hyperfine coupling constant, is 87 gauss. The signs of the spin

Hamiltonian parameters are determined by observation of the second order effects in the spacing of the hyperfine lines. The type I spectrum, in NaN_3 is caused by exchange broadening resulting from the high density of Mn^{++} ions. This line is always strong in heavily doped samples and always absent in weakly doped samples. The central g value is $1.95 \pm .01$ and the line width (peak to peak on the derivative curve) is 240 gauss.

When NaN_3 is heated above 300°C the crystal decomposes and the remaining powder is dark blue. Disordered Mn^{++} spectra are evident and at $g = 2$ a strong sharp line appears. This line is resonance of the conduction electrons in sodium colloids. This result is confirmed by cooling the material through the melting point of sodium and observing the line width change in the resonance. This behavior is not typical of pure sodium azide, since ultraviolet or X irradiation are necessary, in addition to heating, to produce the colloid resonance. This is an additional complication in the Mn^{++} resonance in NaN_3 which we have not observed in KN_3 and RbN_3 . We have reported a crystal structure transformation in NaN_3 which occurs at $19 \pm 1^\circ \text{C}$. Observations have been made using optical, x ray, and paramagnetic resonance data. The transformation involves a loss of symmetry in the lattice which reduces the structure from rhombohedral (or hexagonal) to orthorhombic. The major transformation occurs sharply at 19°C but secondary changes in the Mn^{++} resonance are observed down to about 10°C . At the present time we have no definite interpretation of the effect, but the appearance of domain structure in our optical studies suggests ferro- or antiferroelectric phenomena.

The nature of the bonding of Mn^{++} to the azide ion is apparently quite different in KN_3 than that in NaN_3 . It seems that the vacancy in KN_3 provides the primary source of the crystal field splitting, since the D value averages out as vacancy jumping is activated at high temperature. In NaN_3 the vacancy provides a large electric field splitting ($E = +57$ gauss), but the main splitting comes from the undistorted crystal field, since this does not average out at higher temperatures ($D = -240$ gauss). It is likely that this difference in behavior is related to the difference in coordination of the Mn^{++} in NaN_3 and in KN_3 (or RbN_3). For the undistorted site in NaN_3 , the Mn^{++} is coordinated with six nearest neighbor azide ions and the arrangement is very nearly octahedral. This type of coordination is common for the stable complexes of the first transition series of elements.

In KN_3 the Mn^{++} has an eight-fold coordination with the azide ions. For an eight-fold cubic coordination, the first transition series of elements usually do not form stable complexes. The reason for the instability of the complexes becomes apparent from the calculation of the linear combinations of orbitals necessary to produce

bonds having symmetry properties appropriate to the eight-fold site⁵. For the first transition series, the calculation produces an extra sigma bond which cannot be satisfied by the available surrounding ligands. It is reasonable to assume that a similar situation exists for Mn^{++} in KN_3 and RbN_3 . The stability of the complex in KN_3 and RbN_3 can be explained by use of the cation vacancy. The cation vacancy in the nearest neighbor site is essentially a negative charge. This is available to satisfy the extra sigma bond and will stabilize the complex. Analysis of KN_3 by group theory is in progress.

It appears to us that the main interaction of the Mn^{++} in KN_3 is with the vacancy and other interactions are secondary. The large size of D in KN_3 and the relatively smaller value for RbN_3 is related to the increased lattice spacing in RbN_3 . In NaN_3 , the D value appears to be the result of some covalent interaction and the vacancy acts mainly to distort the local symmetry.

References

1. K. Morigaki, M. Fujimoto and J. Itoh, J. Phys. Soc. Japan 13, 1174 (1958).
2. G. D. Watkins, Phys. Rev. 113, 79 (1958).
3. S. B. Hendricks and L. Pauling, J. A. C. S. 47 2904 (1925).
4. M. P. Tosi and G. Airolidi, Nuovo Cimento 8, 584 (1958).
5. C. J. Ballhausen, "Introduction to Ligand Field Theory," (McGraw-Hill Book Co., Inc., New York, 1962).

ELECTRON PARAMAGNETIC RESONANCE
OF NITROGEN ATOMS IN ALKALI METAL AZIDES

by

Frederick F. Carlson
Basic Research Laboratory
U. S. Army Engineer Research and Development Laboratories
Fort Belvoir, Virginia

It is now well known that the irradiation of alkali metal azides with x rays at low temperatures produces a high concentration of nitrogen atoms throughout the material. Electron paramagnetic resonance, EPR, is a convenient method for studying these paramagnetic impurity atoms. We have previously reported work on nitrogen in sodium azide^{1,2}, and Wylie et al.³ have discussed similar work on potassium azide. This paper reports EPR studies of nitrogen in rubidium azide and cesium azide.

Single crystals of these materials were glued onto glass rods in desired orientations. They were immersed in liquid nitrogen and irradiated for several hours with x rays from a tube operating at 40 kv and 40 mA. The electron resonance spectra were taken at temperatures close to that of liquid nitrogen in the Varian x-band spectrometer with 100 kc modulation and phase sensitive detection.

Like KN_3 , both RbN_3 and CsN_3 are body centered tetragonal crystals. One would expect the nitrogen atoms to occupy sites analogous to those in KN_3 . One would also expect the angular variation of the spectra to be quite similar. Our study shows that these expectations are indeed fulfilled. For the three body centered tetragonal crystals, the nitrogen atoms appear to be located interstitially between alkali metal ions along the 110 and $1\bar{1}0$ directions. This is shown by the fact that there are two spectra whose major axes lie along these directions. In NaN_3 there are three spectra which indicate that the nitrogen is trapped interstitially between sodium ions along the three rhombohedral directions. All the spectra may be fit to the same spin Hamiltonian,

$$H = g\beta H \cdot S + D \left[S_z^2 - \frac{1}{3} S(S+1) \right] + E(S_x^2 - S_y^2) + A I \cdot S,$$

where g is the isotropic splitting factor, D is the fine structure parameter related to the axial crystal field, E is the fine structure parameter related to the rhombic crystal field, and A is the isotropic hyperfine interaction of the nitrogen nucleus. The table shows the values of these constants for nitrogen in the alkali metal azides.

Table I
Spin Hamiltonian Parameters for Trapped N Atoms in Alkali Azides

	Na	K*	Rb	Cs
D	0.00407 cm ⁻¹ ±0.0001 cm ⁻¹	0.0143 cm ⁻¹ ±0.0001 cm ⁻¹	0.0199 cm ⁻¹ ±0.0001 cm ⁻¹	0.0341 cm ⁻¹ ±0.0002 cm ⁻¹
E	-0.00026 cm ⁻¹ ±0.00005 cm ⁻¹	-0.00199 cm ⁻¹ ±0.00002 cm ⁻¹	-0.00463 cm ⁻¹ ± .00005 cm ⁻¹	-0.0103 cm ⁻¹ ±0.0003 cm ⁻¹
g	2.002 ± .0002	2.001 ± .0001	1.997 ± .002	1.992 ± .002
A	0.00053 cm ⁻¹ ±0.00001 cm ⁻¹	0.00051 cm ⁻¹ ±0.00002 cm ⁻¹	0.00053 cm ⁻¹ † ± 00003 cm ⁻¹	0.00054 cm ⁻¹ † ± .00005 cm ⁻¹

* Data from reference 3.

† Estimated.

In our study of RbN₃ and CsN₃ the center transition, $m = \frac{1}{2} \longleftrightarrow -\frac{1}{2}$ was not observed because of large interfering signals around the center of the resonance. The $m = \pm \frac{3}{2} \longleftrightarrow \pm \frac{1}{2}$ transitions were used to plot the angular variation of the spectrum and to determine the constants. Furthermore, the nitrogen hyperfine splittings were not well resolved. The reason for this is not known, but it may be due to the partial saturation of the signals due to high microwave power, although the bridge was operated at its lowest possible power level. In RbN₃ this broadening may also be due to the presence of two isotopes of rubidium with different magnetic moments and spin. It should also be noted that sharpness and intensity of each fine structure multiplet is a function of the angle with the static magnetic field. This effect was noted in all of the materials discussed here but was most prominent for RbN₃ and CsN₃.

We wish now to examine briefly the interrelationships among the spectra in the different alkali metal azides. First we note that the symmetry about the trapped nitrogen in all these azides is rhombic. Thus in considering the fine structure part of the spin Hamiltonian, one may use the same point charge model for the surroundings of the nitrogen atoms in all of these materials. (Strictly speaking, NaN₃ has different axes relative to the azide positions but the symmetry is the same.) This point charge model predicts that the crystal field splitting should decrease as one goes from KN₃ to CsN₃. It is observed that the splittings increase. It is clear that other factors are involved, such as covalency and overlap, which depend upon the nearest neighbor metal ion.

One of the motivations for this study was the hope that a comparative analysis going from one type of nearest neighbor alkali metals to another would lead to useful information concerning the nature of the splitting of S state ions (or atoms) in a crystalline field. The crystal field splitting or fine structure is usually considered to be the result of an interaction between the orbital angular momentum of the ion and the electrical potential of the array of point charges surrounding the ion. This interaction is manifested on the spin levels through the interaction of spin orbit coupling. However, an S state is spherically symmetrical and thus possesses no resultant orbital angular momentum, hence no crystal field splitting should be observed. In order to explain the observed fine structure of various S state spectra, theoreticians have had to assume that the splitting arose from a configuration involving a mixing of non-spherical excited states^{4,5}.

Let us consider the term D in the spin Hamiltonian. In the experiments just described it is apparent that D undergoes a large increase as one goes through the series of alkali metals from sodium to cesium. That is D increases with increasing metal ion size. We have constructed the following preliminary qualitative picture. The Hartree radial charge densities for atomic N and for Na, K, Rb, Cs ions were plotted on a common scale with origins at one-half the interionic distance of the metal ions in their respective azides (see Figure 1). The areas of common electronic charge density were measured, and a plot of the parameter D as a function of these areas of charge density was made (Figure 2). It was found that D varied in an almost precisely exponential manner. Such a variation might be expected if exchange interactions and correlation effects were being observed. That is coulomb interactions coupled with the Pauli exclusion principle induce a non-sphericity in the electron configuration of the nitrogen atom. This interaction increases approximately as an exponential function of the ion radius since the lattice constants of the azides change very little as one goes from potassium to cesium azide.

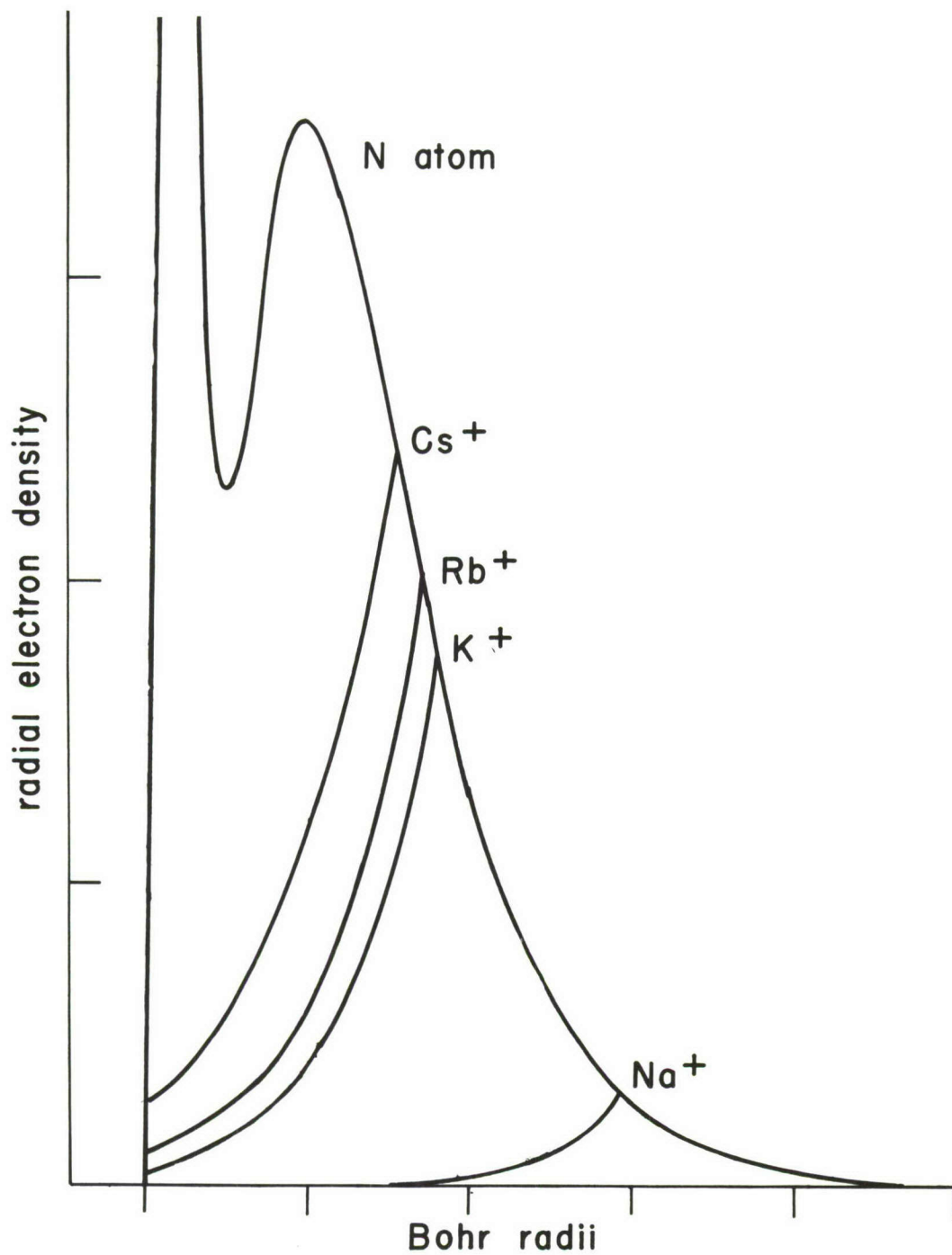


Figure 1. Hartree radical electron densities for atomic nitrogen in alkali azides showing overlapping of nearest neighbor metal ion electron densities.

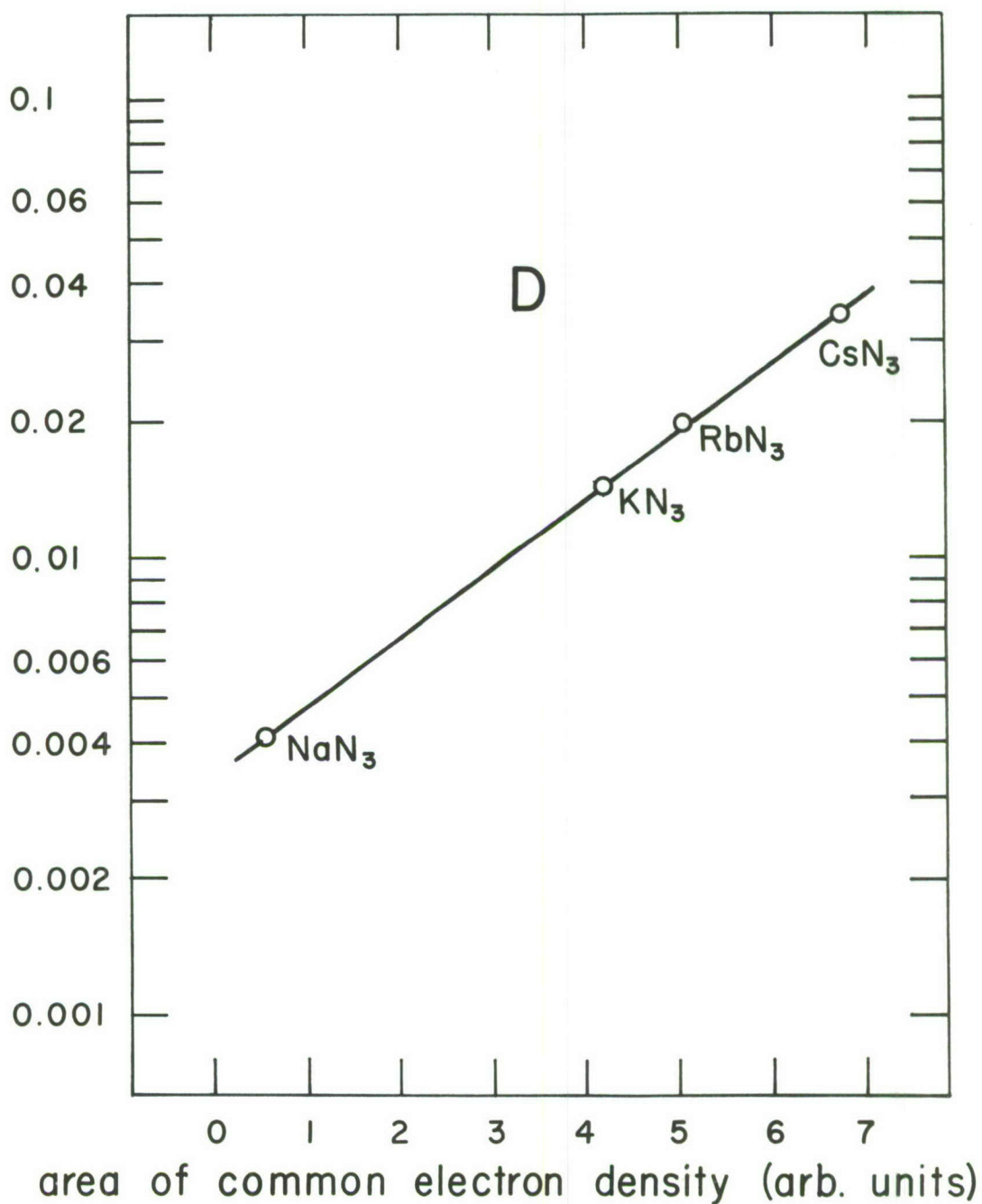


Figure 2. Spin Hamiltonian parameter, D , as a function of the squeezing effect of the nearest neighbor metal ion measured by the area of common electron density as shown on the previous figure. (The ordinate is wavenumbers.)

References

1. G. J. King, F. F. Carlson, B. S. Miller, and R. C. McMillan,
J. Chem. Phys. 34, 1499 (1961).
2. F. F. Carlson, J. Chem. Phys. 39 1206 (1963).
3. D. W. Wylie, A. J. Suskus, C. R. Young, O. R. Gilliam, and P. W.
Levy, Phys. Rev. 125, 451 (1962).
4. M. H. L. Pryce, Phys. Rev. 80, 1107 (1950).
5. H. Watanabe, Prog. in Theoret. Phys. (Kyoto) 18, 405 (1957).

ELECTRON SPIN RESONANCE OF POTASSIUM COLLOIDS IN KN_3

by

Robert C. McMillan
Basic Research Laboratory
U. S. Army Engineer Research and Development Laboratories
Fort Belvoir, Virginia

Abstract

Potassium colloids have been formed in irradiated KN_3 by heating to 300°C . A study of the ESR of the conduction electrons over the temperature range $100^\circ \text{K} < T < 450^\circ \text{K}$ shows that the width is dependent on the electrical resistivity, ρ . The resonance width at maximum slope points, ΔH , is given by: $\Delta H = 10.2 \times 10^{-6} \rho + 35.7$. Since the resistivity changes abruptly at the melting point of K, the ESR width should change. This is observed. The theory is used to estimate a particle diameter of 14\AA . The g value is measured as 1.9982 ± 0.0005 which agrees with theory.

Introduction

The decomposition of potassium azide (KN_3) by x rays and ultraviolet light has produced a variety of electron spin resonance (ESR) signals such as N_4^- , N , N_2^- , NO and NO_2^{1-3} . In sodium azide, irradiation followed by a heat treatment has produced Na colloids which have been observed by the ESR of the conduction electrons⁴ and optical absorption⁵. It was expected that a similar treatment of KN_3 should produce K colloids; however, early efforts failed to produce the resonance.

The ESR of conduction electrons in K colloids reported in this work has a temperature dependent line width which changes abruptly at the melting point of K and a g shift of $-(41 \pm 5) \times 10^{-4}$ which is in agreement with the larger spin orbit coupling of K.

Materials

In previous attempts to produce K colloids, commercially available KN_3 was used. This material contains nitrite and nitrate impurities which are probably the source of the irradiation products NO and NO_2 reported by Mergerian and Marshall³.

The KN_3 for this study was prepared by reacting KOH and NaN_3 and separating KN_3 by differential solubility in alcohol. This method produces a material free of impurities as it gives the correct melting point for KN_3 . Irradiation of crystals grown from this

material does not produce NO or NO₂ resonances. This is additional evidence that the material is free of nitrite and nitrate impurities.

Equipment

The spectrometer used in this experiment consists of a Varian 4500 EPR spectrometer, a 12 in. type 4012 magnet with a V2100A regulated power supply. The field modulation was at 100 kc. The temperature was varied using the variable temperature accessory with the Varian 4540 controller.

Klystron frequencies were measured by means of a Hewlett-Packard type 540B frequency counter system. The magnetic field was measured using a Spectromagnetic Industries model PD64S proton resonance magnetometer.

The irradiation was from a Macklett type OEG 60 x ray tube with a tungsten target operating at 40 kv and 40 mA.

Experimental

Powdered KN₃ was sealed in an evacuated quartz tube and x-irradiated for 15 hours at 30° C. The sample, which was light brown in color, changed to a dark green after heating at 300° C for two minutes.

The ESR is observed with the sample in the opposite end of the quartz tube than the one when irradiated, thus there is no interference caused by quartz resonances. The resonance has a Lorentzian shape and the width varies with the temperature. The temperature variation is shown in Figure 1. The measured g value for the resonance is 1.9982 which is constant as a function of temperature. This gives a Δg of $-(41 \pm 5) \times 10^{-4}$ to be compared with the theoretical value of 40×10^{-4} calculated by Brooks⁶.

Discussion

The ESR of the conduction electrons in colloidal metals may be examined theoretically by using the principles of spin relaxation via spin-orbit coupling developed by Elliott⁷. The relaxation time, T_L , for the conduction electrons is given by:

$$T_L = 2^{-5/3} T_R \left\{ (\Delta g)^2 [\log(q_{\max}/q_{\min}) - 2^{-5/3}] \right\}^{-1} \quad (1)$$

where Δg is the g shift from the free electron value, T_R is the relaxation time for electrical resistivity and the ratio q_{\max}/q_{\min} is approximately proportional to the particle diameter divided by the atomic diameter.

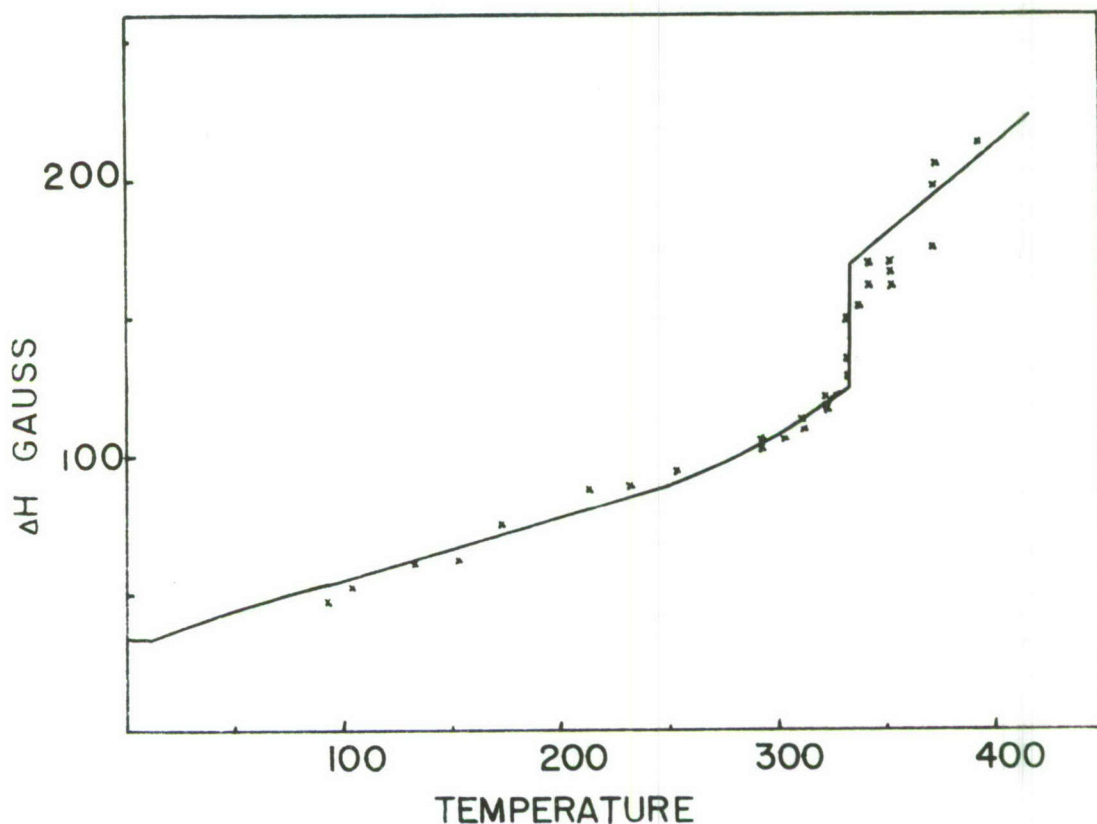


Figure 1. ESR width at maximum slope as a function of temperature. The solid line is the equation $\Delta H = 10.2 \times 10^{-6} \rho + 35.7$.

For small particles there will be an additional relaxation time, T_S , which results from surface collisions. Dyson⁸ has shown that for spherical particles this is:

$$T_S = \frac{4r}{3\varepsilon v} \quad (2)$$

where r is the radius of the particle, ε is the probability of a spin disorienting surface collision and v is the velocity of the conduction electron.

Combining these two types of relaxation the width of the resonance at the maximum slope points for a Lorentzian absorption line is

$$\Delta H = 6.34 \times 10^{-8} (T_L^{-1} + T_S^{-1}).$$

Substituting the values of T_L and T_S this becomes:

$$\Delta H = 5.7 \times 10^{-11} N(\Delta g)^2 Q \rho + 4.76 \times 10^{-8} \frac{\epsilon V}{r} \quad (3)$$

where N is the density of conduction electrons,

$$Q = \left[\ln q_{\max}/q_{\min} - 2^{-5/3} \right],$$

and ρ is the electrical resistivity in practical units.

The experimental data for K colloids are best fitted to the equation

$$\Delta H = 10.2 \times 10^{-6} \rho + 35.7. \quad (4)$$

Since N is known and Δg has been determined experimentally, Q may be calculated and an estimate may be made for the particle size. This radius may be used in the second term of equation 3 to determine the probability that a surface collision will disorient the electron spin. Table I gives the values for these calculations and other experimental data.

Table I
ESR Experimental Values of K Colloids in KN_3

Δg	$-(41 \pm 5) \times 10^{-4}$
ΔH (300° K)	105G
ΔH (100° K)	50G
Particle diameter	14Å
ϵ , Probability of surface relaxation	2.5×10^{-7}

Although the colloids are only 14Å in diameter, the ESR of conduction electrons exhibits the effects of bulk properties such as the resistivity and the melting point.

For the similar experiment with Na colloids it was found necessary to include an additional relaxation mechanism proportional to the temperature⁹. Such a relaxation mechanism is not required to explain the ESR of K colloids.

Conclusion

Previous attempts to study the temperature effects on ESR of conduction electrons of K metal have been discouraging. It has been observed only at very low temperatures and broadened rapidly so

additional information could not be obtained. This report indicates a method of producing small K colloids which can be studied at temperatures up to 450° K. Although the colloids are held in the KN_3 matrix, the ESR of the conduction electrons shows primarily the effects of the potassium.

Acknowledgments

The author wishes to thank Frank L. Harris of the Materials Branch, USAERDL, for preparation of the KN_3 and Gerard J. King for many helpful suggestions.

References

1. Shuskus, A. J., Young, C. G., Gilliam, O. R., and Levy, P. W., J. Chem. Phys. 33, 622 (1960).
2. Wylie, D. W., Shuskus, A. J., Young, C. G., Gilliam, O. R., and Levy, P. W., Phys. Rev. 125, 451 (1962).
3. Mergerian, D., Marshall, S. A., Phys. Rev. 127, 2015 (1962).
4. King, G. J., Miller, B. S., Carlson, F. F., and McMillan, R. C., J. Chem. Phys. 32, 940 (1960).
5. Miller, B. S., J. Chem. Phys. 33, 889 (1960).
6. Brooks, H., Phys. Rev. 94, 1411 (1954); see also review by Bagguley, D. M. S., and Owens, J., Rep. Progress Phys. 20, 304 (1957).
7. Elliott, R. J., Phys. Rev. 96, 266 (1954).
8. Dyson, F. J., Phys. Rev. 98, 349 (1955).
9. McMillan, R. C., King, G. J., Miller, B. S., Carlson, F. F., J. Phys. Chem. Solids 23, 1379 (1962).

THE STUDY OF TRANSIENT ABSORPTION SPECTRA OF AZIDES
BY MEANS OF A FAST RECORDING SPECTROMETER

by

G. D. Singer and H. J. Mueller
Basic Research Laboratory
U. S. Army Engineer Research and Development Laboratories
Fort Belvoir, Virginia

Thermoluminescence and absorption spectra measurements are generally made under different circumstances. The former is basically a dynamic measurement made while the temperature is changing; the latter is usually performed at a fixed temperature after processes have come to equilibrium.

A fast recording spectrometer was constructed in order to study the absorption spectra of azides under conditions similar to those in which thermoluminescence glow curves were obtained.

The spectral dispersion was achieved by means of a Farrand Double Monochromator (aperture f:5). In order to sweep the spectrum rapidly the ordinary geared drive was disconnected and the mirrors of the monochromator were driven directly by an electric motor. This arrangement is shown in Figure 1. The motor turns the eccentric disc which in turn drives the lever arm. The return is

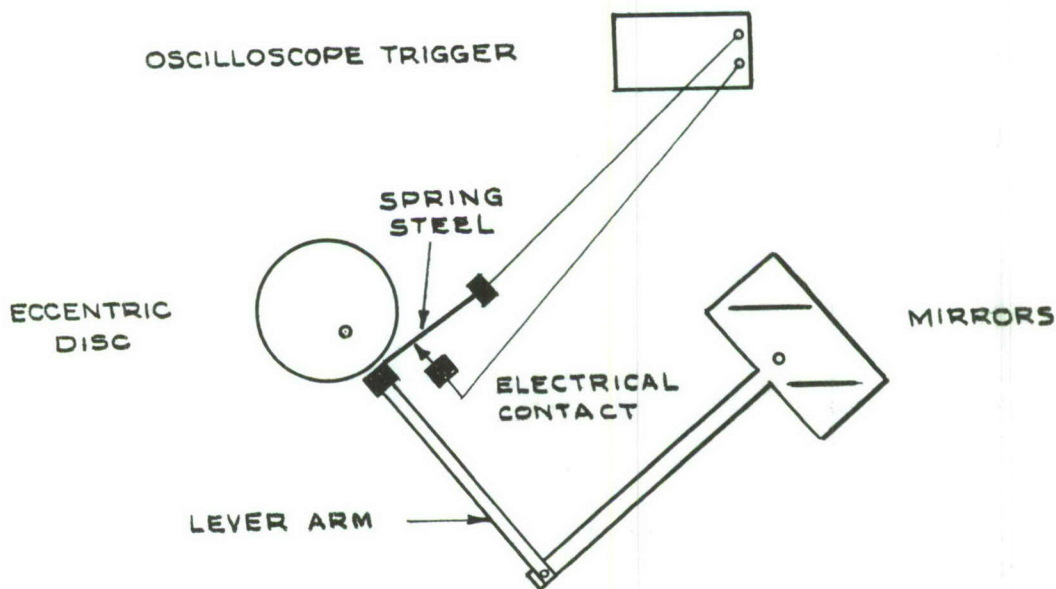


Figure 1

accomplished by a spring steel strip, causing the mirrors to oscillate. With the size disc and lever arm used, the mirrors sweep through the spectral range of about 200 to 900 m μ . The spectrometer, optical system and auxiliary equipment are shown in Figure 2.

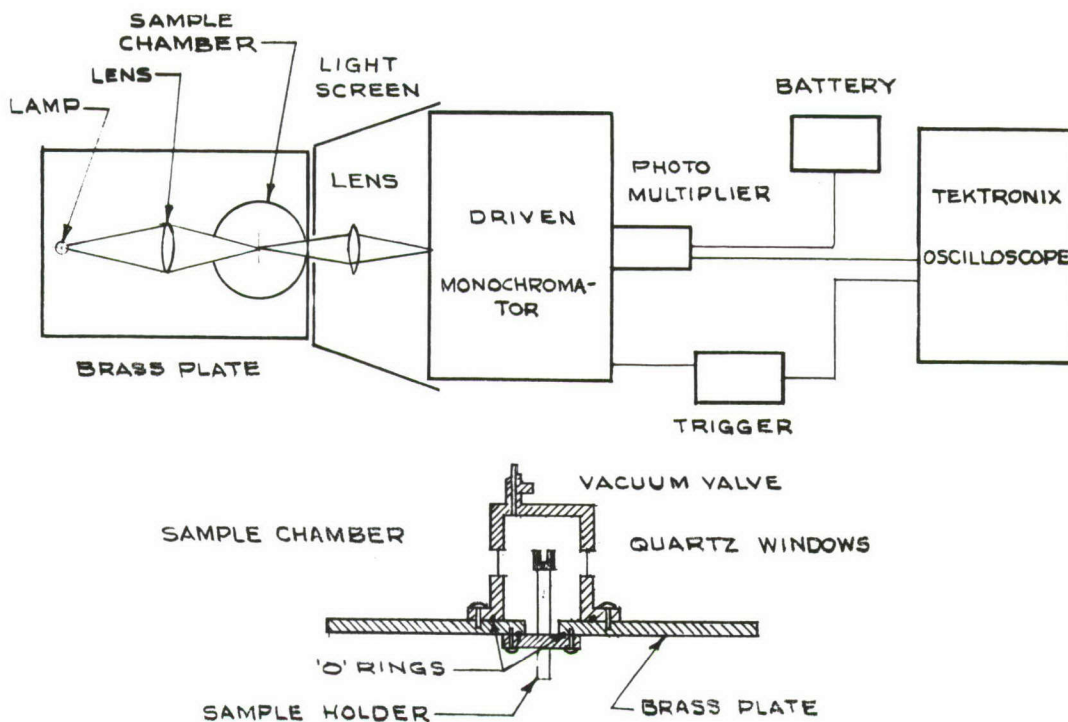


Figure 2

The sample crystal is mounted on a stage before the entrance slit of the monochromator. Figure 3 shows the sample holder. The crystal is held between the two pieces of the brass top of the holder. The sample may be cooled by pumping liquid air into the aluminum tube; the temperature may be raised by a heater inserted into the tube. A copper constantan thermocouple inside the crystal mounting and connected to a chart recorder provides a continuous record of the temperature. The sample holder is inclosed in a chamber which may be evacuated.

Light from the source is focused on a slit directly in front of the sample crystal. The light passing through the sample is again focused at the monochromator entrance slit. Quartz optics are used throughout the system.

As the spectra is scanned the output of the monochromator is detected by a photomultiplier at the exit slit and subsequently

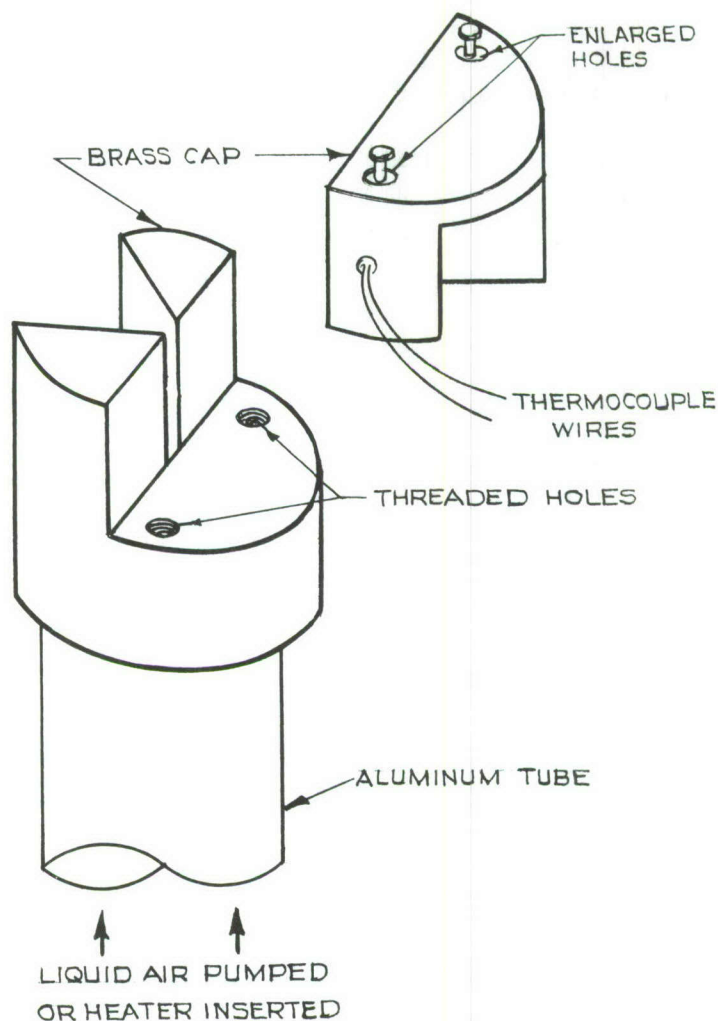


Figure 3

displayed on the screen of an oscilloscope. With each turn of the driving disc an electrical contact is made, which triggers the oscilloscope trace. For a record of the spectra, the oscilloscope screen is photographed with a Polaroid camera. The motor driven disc made one revolution per second and the full spectral range of the instrument was scanned in about $1/2$ second.

In order to take advantage of the total possible range of the instrument, two photomultipliers were employed. For the ultraviolet to visible range an RCA 7267 photomultiplier tube with S-13 response was used. The visible to infrared range was observed with an RCA 7102 tube with S-1 response.

The light source most frequently used was the PEK X-75 short arc high pressure Xenon lamp. The observed output of the Xenon lamp as seen on the oscilloscope screen is shown in Figure 4 for the two ranges of the instrument. By choice of suitable filters the spectral distribution could be made more flat for the high wavelength range.

XENON SPECTRA

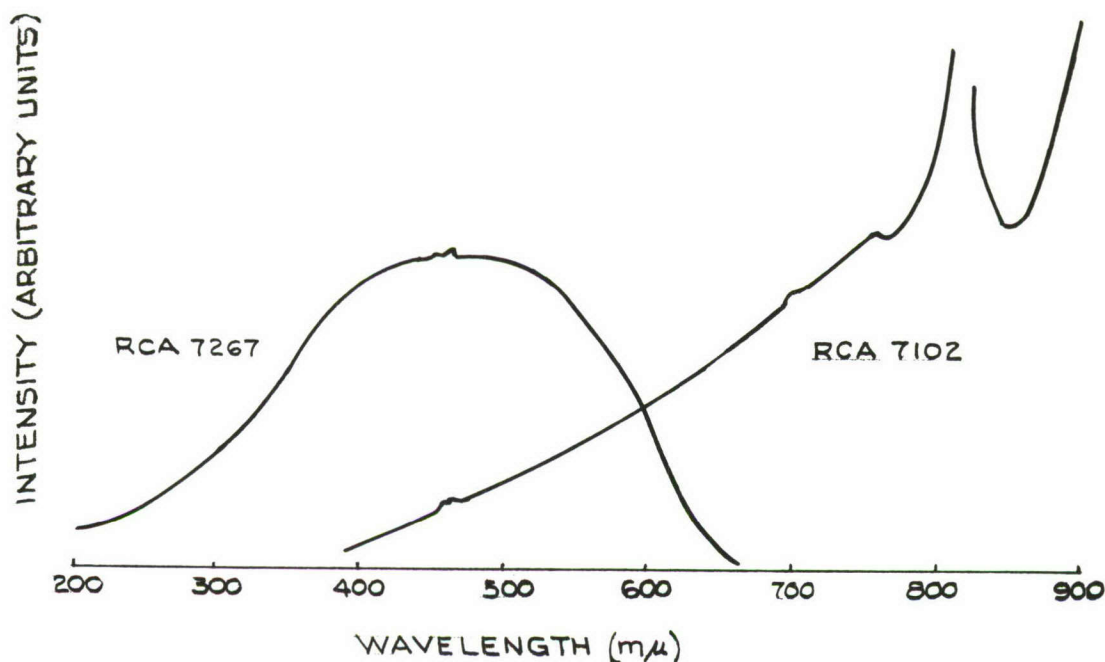


Figure 4

The dispersion of the instrument was calibrated by means of mercury lines of known wavelength. The dispersion of the spectrometer is shown in Figure 5. Wavelength is given as a function of distance on the oscilloscope screen. Since the distance could be expanded or contracted by adjustment of the sweep time, the distances in Figure 5 are given in arbitrary units.

The resolution of the instrument was limited by sweep time and photomultiplier circuit response time. In our measurements the resolving power was about 15 mμ. This resolution was sufficient for our experiments since the positions of the major absorption bands are well known from other measurements.

Measurements were made on the absorption spectra of sodium azide. Crystal platelets about 0.5 mm thick that appeared to be

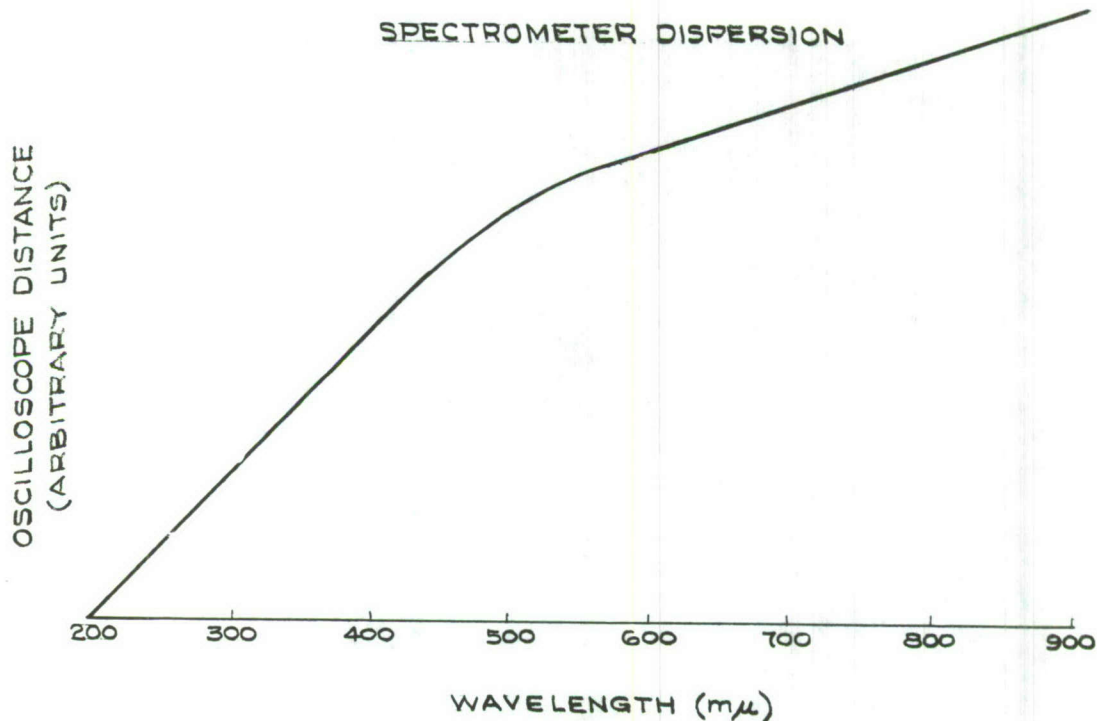


Figure 5

free from strains at low temperatures were grown in our laboratory by G. J. King. The crystals were cooled to liquid air temperature in vacuum and irradiated with a Hanovia mercury lamp until they became colored. The change in the absorption was observed by frequent photographs of the oscilloscope screen as the crystal temperature was raised. Photographs were taken as rapidly as every 10 seconds. The absorption spectra were found by normalizing the transmission of the irradiated crystal to that of the unirradiated crystal.

Even for unirradiated crystals there was considerable absorption in the short wavelength region, due to crystal quality as well as scattering outside of the critical angle as suggested by Heal and Pringle¹. This caused a reduction in light intensity in this range that made it difficult to observe absorption.

Upon irradiation at liquid air temperature several absorption bands developed. Figure 6 shows photographs of the oscilloscope screen in the 7102 tube range, before and after irradiation with the normalized curve plotted below. A more useful spectral shape was obtained by the use of a Corning glass filter No. 1-69.

At low temperature the main bands consisted of a large peak at 620 mμ, a shoulder at 730 mμ, and a small peak at 420 mμ. Most

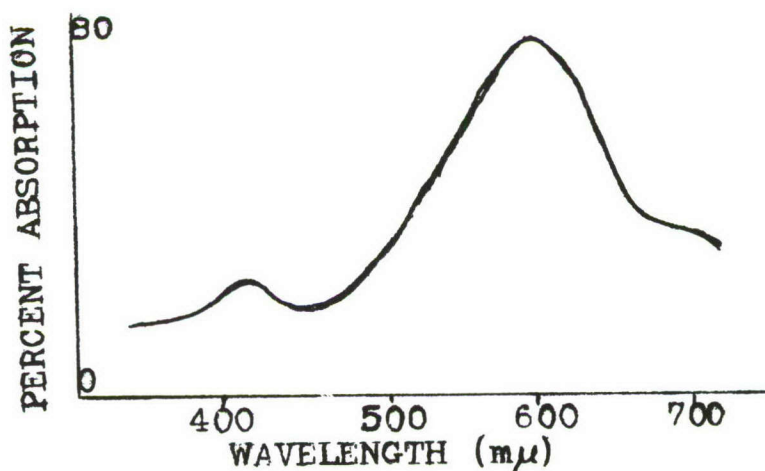
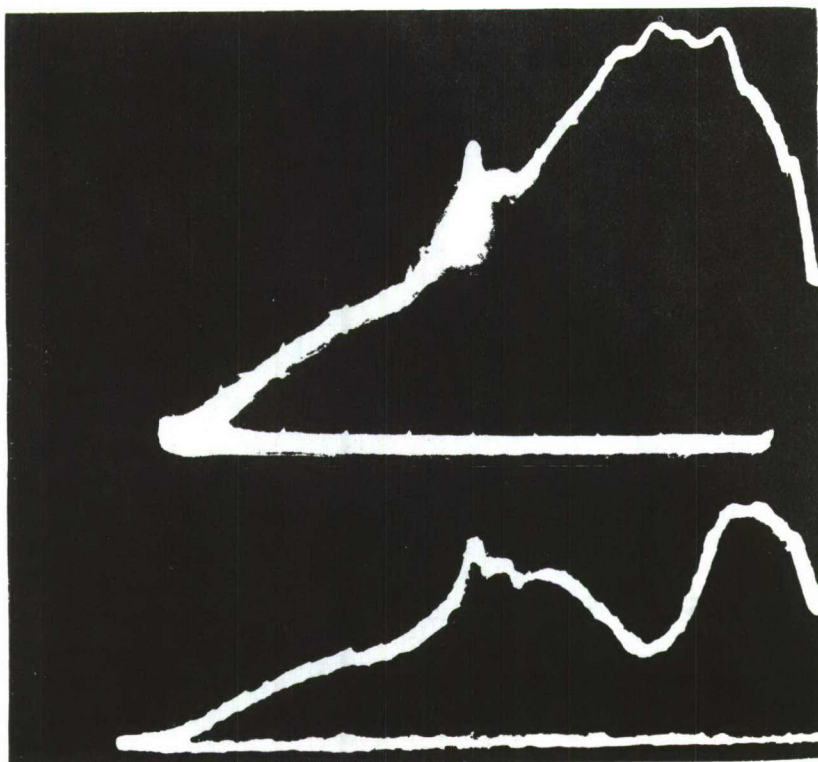


Figure 6

observers have located the large peak at $610 \text{ m}\mu$ ^{1,2,3}; however, the difference between $610 \text{ m}\mu$ and our value is within the accuracy of the experiment. The bands at $610 \text{ m}\mu$ and $730 \text{ m}\mu$ have been previously identified by King et al.³ as the F_2^+ and the F center band, respectively. The new band observed at $420 \text{ m}\mu$ may be associated with an impurity.

Due to the limitations of the instrument and the interaction of the various peaks, the effect of increasing the temperature can be given quantitatively for the large peak at $620\text{ m}\mu$ only.

The crystals were heated to room temperature at a rate of 40°C per minute. This is the same gradient used previously in our thermoluminescence and exo-electron measurements. On heating, the $730\text{ m}\mu$ band disappears while the $620\text{ m}\mu$ peak first increases and then decreases. Figure 7 shows the temperature behavior of the $620\text{ m}\mu$ peak height.

Figure 7 also shows our thermoluminescence glow curves for NaN_3 in the temperature range of interest. From a comparison of the two curves in Figure 7 one can associate the two luminescence peaks at low temperature, with the increase of the F_2^+ band and the decrease

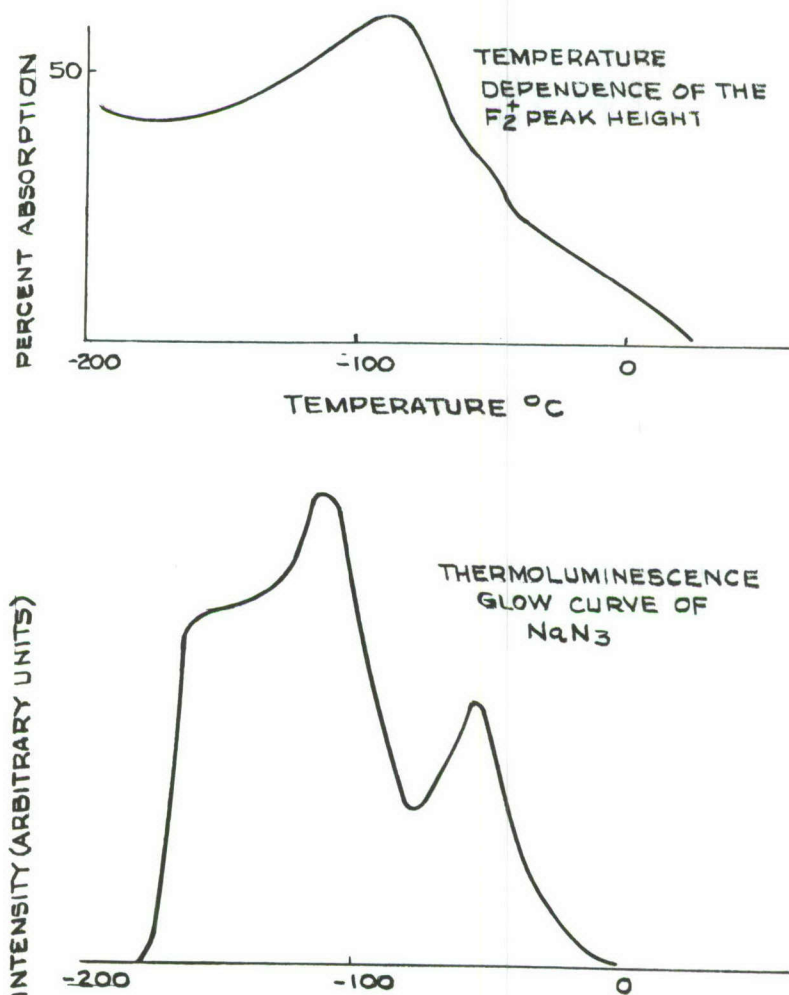


Figure 7

of the F band. The occurrence of two peaks may be due to the presence of two types of F_2^+ centers³. The thermoluminescence peak at -60°C seems to be connected with the destruction of the F_2^+ band. Deb has observed a strong release of charge in ultraviolet irradiation NaN_3 at -54°C ⁴. Considering the reproducibility of glow curve temperatures this value corresponds fairly well with our -60°C peak.

An additional thermoluminescence peak was sometimes seen at $+80^\circ$ to $+100^\circ\text{C}$. This peak was observed in samples known to contain calcium impurities and is believed to be due to this impurity. Miller and King⁵ have observed a phase transition in NaN_3 at $+19^\circ\text{C}$; however, we have seen no luminescence emission corresponding to this temperature.

An attempt was made to use the fast recording spectrometer to measure the spectrum of the thermoluminescence emission. However, even after cooling the photomultiplier to dry ice temperature the output of the monochromator was below the noise level of the tube. A rough estimate of the spectral distribution was made by using glass filters in connection with the thermoluminescence apparatus. It was found that most of the light emitted lies between 360 and 580 $\text{m}\mu$ with a maximum near 450 $\text{m}\mu$. This is similar to the fluorescence spectra of NaN_3 observed by Deb⁶ with maxima at 480 $\text{m}\mu$.

When the irradiated crystals are heated to high temperatures, broad bands develop. As the temperature is raised the bands become broader and higher and above 300°C the crystals become practically opaque. Figure 8 shows the high temperature absorption band structure obtained with our instrument a peak being exhibited between 500 $\text{m}\mu$ and 600 $\text{m}\mu$. Miller⁷ has observed an absorption band at 520 $\text{m}\mu$ in heated NaN_3 and has identified this as a colloidal band.

Absorption spectra measurements for KN_3 have also been made under the same conditions as described for NaN_3 . The results of the measurements are presently being evaluated.

Na N_3 ABSORPTION AT HIGH TEMPERATURE

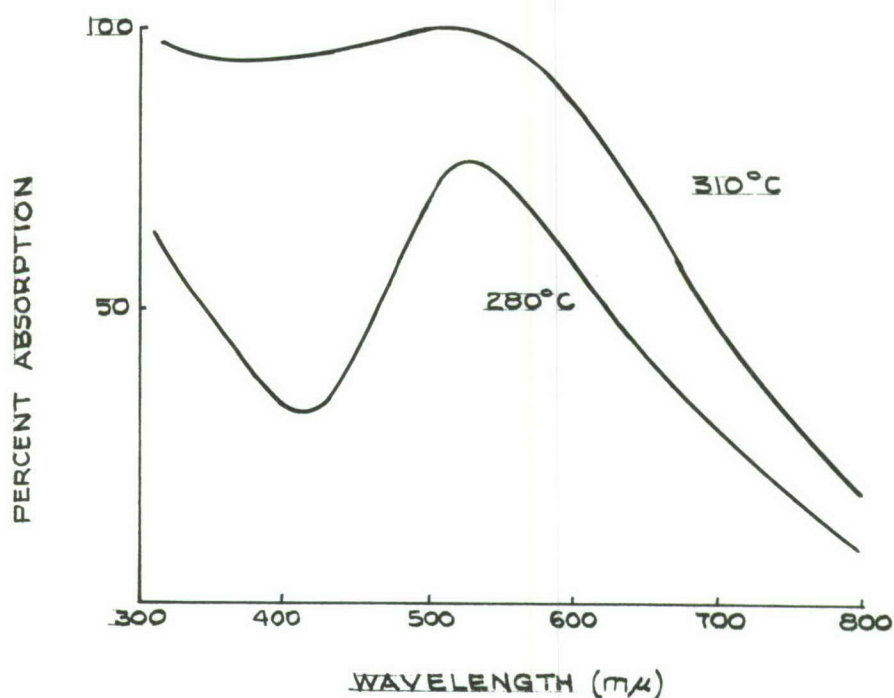


Figure 8

References

1. H. G. Heal and J. P. S. Pringle, J. Phys. Chem. Solids 15, No. 34, 261 (1960).
2. J. Cunningham and F. C. Tompkins, Proc. Roy. Soc. 251, No. 1264, 27 (1959).
3. G. J. King, B. S. Miller, F. F. Carlson, and R. C. McMillan, J. Chem. Phys. 35, No. 4, 1442 (1961).
4. S. K. Deb, Trans. of Faraday Soc. 59, No. 486, 1414 (1963).
5. B. S. Miller and G. J. King, Proceedings of the 12th Basic Research Laboratory Contractors' Conference and Symposium, 1963.
6. S. K. Deb, J. Chem. Phys. 35, No. 6, 2122 (1963).
7. B. S. Miller, J. Chem. Phys. 33, No. 3, 889 (1960).

AZIDE RESEARCH AT ARKANSAS POLYTECHNIC COLLEGE

by

Jack G. Dodd
Department of Physics
Arkansas Polytechnic College
Russellville, Arkansas

I. Structure of Lead Azide

Several years ago Azaroff was able to determine the position of the lead atoms in the unit cell of alpha lead azide by x-ray diffraction¹. However, all attempts to locate the azide radicals about each lead atom have failed. The problem which arises in x-ray work is that the cross-section of nitrogen is too small compared with that of lead; any exposure sufficient to show nitrogen loses that image in the penumbra of a vastly over-exposed lead image. In neutron diffraction the problem is different but equally severe; the scattering cross-sections of lead and nitrogen are too nearly alike, and it is not possible to tell which is which.

Macintyre has suggested a detailed x-ray study which might produce the desired result, but distortion of the crystal due to decomposition during irradiation might be sufficiently severe to smear the data beyond use, even if it were otherwise obtainable².

A very direct method which certainly should work is nuclear quadrupole resonance spectroscopy of the N^{14} in the azide groups, first suggested for the azide problem by Tantilla³. The equipment is not complicated and fairly inexpensive, the experiment is completely nondestructive, and the information presented is in fairly unambiguous form, at least for linear azide radicals. The method suffers from but two disadvantages: the only information readily obtainable is orientation information, no spacings being directly derivable from the data; and the sensitivity of the method is low. This necessitates large samples, and since the samples must be single crystals familiar old problems rear their heads.

Nothing can be done about the first disadvantage. The second we will return to in a moment, but first we will discuss an unusual quadrupole spectroscopy experiment we intend to try which is based upon the Mössbauer effect.

If it were possible to incorporate Co^{57} substitutionally for lead in a lead azide crystal, then when the Co^{57} decayed to Fe^{57*} , and the Fe^{57*} to Fe^{57} with the emission of a recoilless gamma-ray, the precise energy of the gamma-ray would depend upon the orientation

of the Fe^{57*} nuclear quadrupole moment in the crystalline electric field gradient. The resulting discrete spectrum would yield quite the same information as a pure nuclear quadrupole resonance study of such a substitutionally incorporated nuclear species; the practical difference in the methods is one of sensitivity. Nuclear radiation detectors can be made many orders of magnitude more sensitive than coherent detectors of radiation in the dekameter region because of the comparatively enormous amount of energy represented by a quantum of even a soft gamma-ray such as the 14.4 keV gamma from Fe^{57*} .

Neglecting self-absorption, even a crystal as small as 10 mg containing as little as 0.1% of Co^{57} should produce 10^6 counts/s assuming an overall counting efficiency of 0.1%. Self-absorption of the source will be very high because the source is mostly lead, and assuming even an infinite crystal we must lose two more orders of magnitude. Assume three; this still leaves 10^3 counts/s. It is hard to see what other vicissitudes could exist sufficient to make such a Mössbauer study impossible.

However, the ancillary problems surrounding a study of this kind are sufficiently severe to give us some pause. First, there is the very serious difficulty of getting the Co^{57} in the proper location in sufficient concentration. Second, there is the problem of the $\text{Co}^{57} \rightarrow \text{Fe}^{57*}$ beta decay which precedes the 14 keV isomeric transition by some 10^{-8} s, and may disrupt one of the adjacent azide groups, changing the field gradient in the vicinity of the subject nucleus. Third, there is a potential difficulty of interpretation of the data. Pure quadrupole resonance spectroscopy of N^{14} can determine the orientation of the linear azide radical axes; the Mössbauer study of nuclei located substitutionally in the lead positions reveals the field gradient at the lead position, not the nitrogen position. In general there may be more than one way to arrange azide groups to produce a given gradient at a given location: there may therefore be some ambiguity in the resulting data.

Because of these problems our best hope still seems pure nuclear quadrupole resonance spectroscopy of N^{14} in the azide groups. The only serious difficulty is that of sensitivity; it is this problem we shall now discuss.

Nitrogen is a particularly unfortunate substance with which to work for two reasons: resonances lie at low frequencies (3 - 4 mc), and relaxation times for oriented states are long (of the order of one second)⁴. Since at these frequencies quadrupole line widths are determined pretty much by inhomogeneities rather than relaxation times, cooling the sample (which simply increases T_1) does not substantially improve detectability, since the increase in T_1 will not be accompanied by much line narrowing.

Nevertheless, by choosing good circuitry and optimum operating conditions we feel we should be able to detect nitrogen resonances (by a CW absorption spectrometer of the Robinson type, and phase detection) in as little as a gram of lead azide⁵. This is still a lot of lead azide and a single crystal this large is so far pure science fiction.

But if we can locate the resonances, then other techniques may make it possible to achieve much greater sensitivity. One possibility is that of detection by nuclear induction⁶. By applying a 90° pulse to a sample we obtain a nuclear induction signal which should be detectable under optimum conditions in samples as small as several milligrams, even at room temperature. Cooling does make a difference here; the signal will be inversely proportional to T. The only difficulty is that one must wait a period of time long compared with T. between 90° pulses. This could be minutes at liquid air temperatures. A search by this method would be tedious indeed. We hope, therefore, to find the resonances using the Robinson oscillator with large powder samples, but then probably to use nuclear induction equipment to do the Zeeman study on single crystals, as we must to solve the structural problem.

It is only fair to note that the NQR data obtained, if it can be obtained, may present some problems if the azide groups in lead azide should happen not to be linear. The presence of an asymmetry parameter different from zero might result in a twelve-line spectrum rather tedious to sort out.

So far as of this date:

We have completed the Robinson oscillator and a Zeeman modulator including the necessary Helmholtz coils. We are using a lock-in amplifier and recording the output on a strip-chart recorder. The Zeeman modulator is driven from the internal oscillator of the lock-in amplifier whose frequency can be varied from about 20 to 1000 c/s with a good square-wave output into the coils.

The Mössbauer drive is designed, and in the process of being constructed. We already have on hand a single-channel analyzer and scintillation detector.

The nuclear induction apparatus is on the drawing board, but the detailed design is yet to be done.

We have just begun to set up our crystal growing apparatus. The design, adapted from a method developed by W. C. McCrone⁷, is complicated by the fact that substantial radioactivity is involved. Because of the possibility of explosion elaborate precautions must be taken to minimize possible contamination. We are therefore using

double polyethylene containers and small volumes of liquid. The only two problems remaining in this area are whether or not the crystals will grow, and whether, if they grow, they will incorporate Co⁵⁷ substitutionally for the lead.

References

1. L. Azaroff, Z. Krist. 107, 362 (1956).
2. W. M. Macintyre, Final Report, DA-44-009-ENG-3628 (July, 1959).
3. W. H. Tantilla, Ibid.
4. Watkins and Pound, Phys. Rev. 85, 1062 (1952).
5. F. N. H. Robinson, J. Sci. Inst. 36, 481 (1959).
6. Das and Hahn, Nuclear Quadrupole Resonance Spectroscopy, Chap. IV, p. 74 (Academic Press, 1958).
7. Walter G. McCrone. Private communication.

II. Explosive Sensitivity Determination by Homogeneous Heating

The "sensitivity" of an explosive is an ill-defined term, not because of any carelessness on the part of those who work with explosives, but simply because of the multiplicity of possible non-equivalent definitions of the term.

From a theoretical point of view, that test is best which yields data in the form simplest to interpret in terms of the structure and physical properties of the substance. By this criterion, the usual drop test is not very satisfactory. It is not true that nothing can be done with it, but it is true that nothing very fundamental can be done without a great deal of trouble^{1,2,3}.

The difficulty lies in the mode of energy input. It is very difficult to determine how much of the drop energy goes into the sample, what fraction of that fraction is dissipated in fracture of the crystallites, and in adiabatic compression, and in phase changes, and so forth.

We propose to develop a new sensitivity test based upon the principle of homogeneous energy input by pulse dielectric heating of the sample. This method should have the following advantages:

1. The energy goes simply into the phonon spectrum of the substance.
2. The shape and size of the sample have no first-order effect on the rate of heating.
3. Heat is generated homogeneously throughout the sample. If radiative cooling can be neglected, no thermal gradients should exist during the heating cycle.
4. "Sensitivity" can be defined simply as the length of time between the onset of the heating pulse and the moment of ignition, a parameter easily and accurately measurable and related in a fixed and reproducible manner to the total input energy.

We plan to generate the heating pulse at a frequency of a few hundred megacycles by discharging a capacitor bank into a suitable oscillator; our problem then reduces to what constitutes a suitable oscillator. The energies required are quite large, yet to meet the second part of condition #3 above, the heating period should be short.

Suppose we assume a 10 mg sample, with an explosion "temperature" of 300° C above room temperature, and a C_p of 0.1 cal/gm. The

energy required to be delivered to the sample is 0.3 cal, or about 1.3 Joules. To cause explosion in 10^{-2} s, the oscillator must deliver this energy at a mean rate of about 150 watts - a very modest requirement. The difficulty is not generating the power, but rather getting it into the sample.

We can illustrate the problem by a simple example: Since the effective impedance of the sample at any convenient frequency will certainly be high, we may imagine coupling to be obtained by making the sample the dielectric of the tank capacitor. The power dissipated in the sample will then be $V^2 C \omega \cos \delta$ where V is the rms voltage across the capacitor; ω , the angular frequency; C , the capacitance and $\cos \delta$ the power factor of the sample at the frequency ω . If we choose circuit conditions so that we may use a parallel plate capacitor of area A and separation d , the capacitance C will be

$$C = \frac{A \epsilon K}{d} \quad (1)$$

where K is the dielectric constant of the sample (presumed to fill the capacitor). The power input per unit volume to the sample will then be

$$P/Ad = E^2 \epsilon \omega K \cos \delta \quad (2)$$

where E is the rms electric field between the plates. The power input per unit mass W is obtained by dividing the above expression by the density to obtain:

$$W = \frac{E^2 \epsilon \omega K \cos \delta}{\rho} \quad (3)$$

For the sample discussed above, we require 13,000 watts/gm for explosion in 10 ms. If we assume $K \cos \delta = .05$, $W = 600$ rad/ms, $P = 5 \times 10^6$ g/m³, then

$$E = 1.5 \times 10^5 \text{ volts/cm} \quad (4)$$

By using a capacitor plate spacing of 1 mm, the rms voltage must be about 15,000 volts. This is quite possible to achieve but would require extraordinary precautions to prevent arcing across the capacitor gap.

If we allow 100 ms for explosion, the field required would only be about 5×10^4 volts/cm, which is only a little above the sparking potential in dry air. Should the quantity $K \cos \delta$ be substantially greater than 0.05, and it is very likely to be so, this will relax the insulation requirements. And if it is practical to go to higher frequencies, we may expect still further improvement.

We have also considered the possibility of using a pulsed magnetron to excite a sample placed in a suitable cavity. It would be convenient to use a cylindrical cavity excited in the $TM_{1,1}$ mode. The power required is quite within the ability of surplus radar magnetrons of the larger sizes to produce. We would prefer to be able to vary the exciting frequency over a fairly wide range; this is much more difficult to do with a magnetron than with a conventional oscillator. The much higher frequency range of the magnetron is, however, attractive.

We plan to start the firing pulse and an electronic timer simultaneously, and allow the leading edge of the light flash of the explosion to turn off the timer.

This part of the equipment, which consists of a photomultiplier feeding a fast amplifier, is virtually complete at this writing. We should be able to turn off the timer within $1 \mu\text{sec}$ of the time the optical signal is twice the dark noise. Since the timer only reads to the nearest $10 \mu\text{sec}$, this response should be adequate.

We are fortunate in having the services of Mr. Woody Gannaway whose high school science fair project was a very successful Kerr cell photography setup capable of shutter speeds in the nanosecond region. With a little modification we expect to use his equipment to take pictures of single crystals with a magnification of 50X at the instant of explosion, using exposures of less than 10^{-7}s . We hope by this means to determine if, under homogeneous heating conditions, initiation takes place at selected sites, and whether these are surface or volume distributed.

References

1. P. W. Levy, Nature 182, 37-39 (1958).
2. Africano, Adv. Cryo. Eng. 5, 533-543.
3. J. G. Dodd, Proc. Cont. Conf., Ft. Belvoir, Va. (1962).

EXCITATION OF LATTICE VIBRATIONS BY IMPACT

by

Masataka Mizushima
PEC Corporation
Boulder, Colorado

Orthogonality of Normal Coordinates

It was found in formula (35) of the Second Quarterly Report of this series that the normal coordinate Q_s of our linear finite chain is given as

$$Q_s = \alpha_s \sum_n \frac{\cos}{\sin} \left\{ \left[\frac{1}{2}(N+1) - n \right] s\pi/N \right\} q_n \quad (2-35)$$

where we take cos when s is even and we take sin when s is odd. q_n is the displacement of the n^{th} atom, n can be from one to N , s is an integer from 0 to $N-1$, and α_s is a constant.

We see that

$$\begin{aligned} & \sum_{n=1}^N \cos \left[\left\{ \frac{1}{2}(N+1) - n \right\} s\pi/N \right] \cos \left[\left\{ \frac{1}{2}(N+1) - n \right\} r\pi/N \right] \\ &= \frac{1}{2} \sum_{n=1}^N \left[\cos \left[\left\{ \frac{1}{2}(N+1) - n \right\} (s+r)\pi/N \right] + \cos \left[\left\{ \frac{1}{2}(N+1) - n \right\} (s-r)\pi/N \right] \right] \\ &= \frac{1}{2} \sin \left[(s+r)\pi/2 \right] / \sin \left[(s+r)\pi/2N \right] + \frac{1}{2} \sin \left[(s-r)\pi/2 \right] / \sin \left[(s-r)\pi/2N \right] \end{aligned} \quad (3-1)$$

where a general formula

$$\sum_{n=1}^N \cos [x + (n-1)y] = \cos \left[x + \frac{1}{2}(N-1)y \right] \frac{\sin(\frac{1}{2}Ny)}{\sin(y/2)} \quad (3-2)$$

is used. When s and r are both even integers we see the above terms in (3-1) are both zero, except when $s=r$. In the latter case the first sum is still zero but the second sum gives $N/2$. Thus

$$\sum_{n=1}^N \cos\left[\left\{\frac{1}{2}(N+1)-n\right\}s\pi/N\right] \cos\left[\left\{\frac{1}{2}(N+1)-n\right\}r\pi/N\right] = (N/2)\delta_{sr} \quad (3-3)$$

where s and r are both even.

In the same way

$$\begin{aligned} & \sum_{n=1}^N \cos\left[\left\{\frac{1}{2}(N+1)-n\right\}s\pi/N\right] \sin\left[\left\{\frac{1}{2}(N+1)-n\right\}r\pi/N\right] \\ &= \frac{1}{2} \sum_{n=1}^N \sin\left[\left\{\frac{1}{2}(N+1)-n\right\}(s+r)\pi/N\right] - \sin\left[\left\{\frac{1}{2}(N+1)-n\right\}(s-r)\pi/N\right] \\ &= 0 \end{aligned} \quad (3-4)$$

Where a general formula

$$\sum_{n=1}^N \sin[x + (n-1)y] = \sin\left[x + \frac{1}{2}(N-1)y\right] \sin\left(\frac{1}{2}Ny\right) / \sin(y/2) \quad (3-5)$$

is used. Finally

$$\begin{aligned} & \sum_{n=1}^N \sin\left[\left\{\frac{1}{2}(N+1)-n\right\}s\pi/N\right] \sin\left[\left\{\frac{1}{2}(N+1)-n\right\}r\pi/N\right] \\ &= \frac{1}{2} \sum_{n=1}^N \cos\left[\left\{\frac{1}{2}(N+1)-n\right\}(s+r)\pi/N\right] - \cos\left[\left\{\frac{1}{2}(N+1)-n\right\}(s-r)\pi/N\right] \\ &= \frac{1}{2} \sin[(s+r)\pi/2] / \sin[(s+r)\pi/2N] - \frac{1}{2} \sin[(s-r)\pi/2] / \sin[(s-r)\pi/2N] \\ &= (N/2)\delta_{sr} \end{aligned} \quad (3-6)$$

when s and r are both odd. If we take our formula (5) of the Second Quarterly Report

$$Q_s = \sum_n a_{sn} q_n \quad (2-5)$$

the above calculation showed that

$$\sum_n a_{sn} a_{rn} = \alpha_s \alpha_r (N/2) \delta_{sr} \quad (3-7)$$

Our normal coordinates are orthogonal to each other in this sense. By making n to be zero we see from (3-7) that

$$\sum_{n=1}^N a_{sn} = 0 \quad (3-8)$$

for all vibrational modes where s is not zero. Formula (2-5) and (3-7) show that another formula

$$q_n = \sum_{s=0}^{N-1} 2a_{sn} Q_s / N \alpha_s^2 \quad (3-9)$$

should hold, since this formula with the help of (3-7) gives

$$\begin{aligned} \sum_{n=1}^N a_{sn} q_n &= \sum_{n=1}^N a_{sn} \sum_{r=0}^{N-1} (2a_{rn} Q_r / N \alpha_r^2) \\ &= (2/N) \sum_{r=0}^{N-1} \sum_{n=1}^N a_{sn} a_{rn} Q_r / \alpha_r^2 = \sum_{r=0}^{N-1} \delta_{sr} Q_r = Q_s \end{aligned} \quad (3-10)$$

to satisfy (2-5) for all values of s .

Canonical Momentum

From formulas (6), (9), (3) and (5) of the Second Quarterly Report we can see canonical momentum for each normal coordinate is

$$P_s = \sum_n a_{sn} p_n = \mu \sum_n a_{sn} \dot{q}_n = \mu \dot{Q}_s \quad (3-11)$$

It is more convenient to set

$$H_s = (2\mu)^{-1}(P_s^2 + \lambda_s Q_s^2) \quad (3-12)$$

instead of formula (10) of the Second Quarterly Report. If we do this we see from the canonical equation of motion that

$$\dot{Q}_s = [Q_s, H] = [Q_s, H_s] = (2\mu)^{-1}[Q_s, P_s^2] = P_s/\mu \quad (3-13)$$

which is consistent with (3-11).

When the potential V is neglected we have

$$\dot{P}_s = \mu \ddot{Q}_s = [P_s, H_s] = -(\lambda_s/\mu)Q_s \quad (3-14)$$

also from the canonical equation of motion. Thus we see that

$$Q_s = Q_{s0} \sin(\omega_s t - \xi) \quad (3-15)$$

where

$$\omega_s = \frac{1}{2} \lambda_s / \mu = 2(k/\mu)^{1/2} \sin(s\pi/2N) \quad (3-16)$$

and ξ is a constant. We used equation (26) of the Second Quarterly Report in obtaining the last expression.

Inserting (3-16) into (3-11) we have

$$\begin{aligned} P_s &= \mu \dot{Q}_s = \omega_s \mu Q_{s0} \cos(\omega_s t - \xi) \\ &= 2(k\mu)^{1/2} \sin(s\pi/2N) Q_{s0} \cos(\omega_s t - \xi) \end{aligned} \quad (3-17)$$

Thus

$$H_s = (2\mu)^{-1} P_s^2 + \lambda_s Q_s^2 = \omega_s^2 \mu Q_{s0}^2 \quad (3-18)$$

is independent of time when V is neglected.

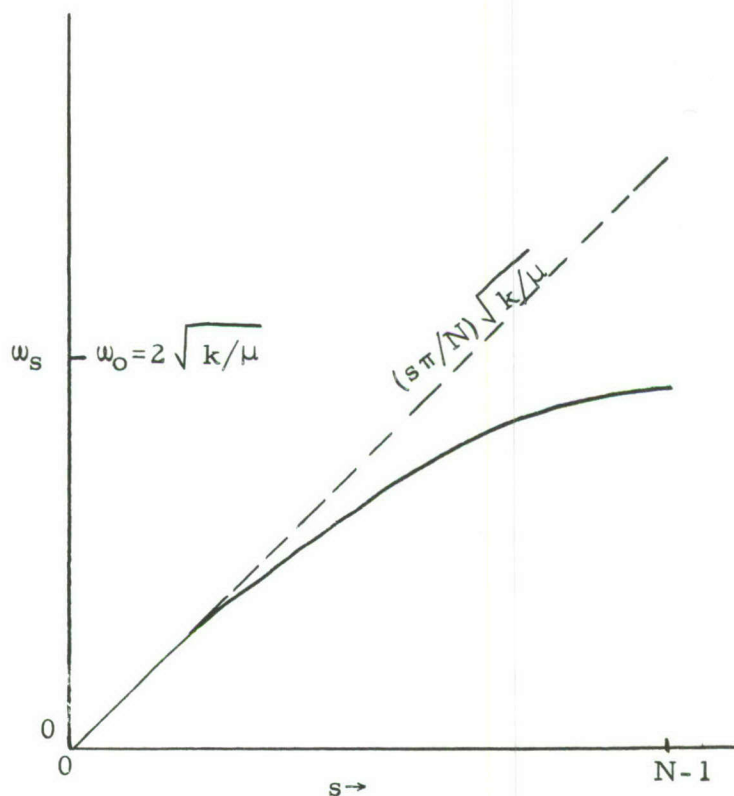


Figure 1. Frequency ω_s as a function of s .

$$\omega_s = 2(k/\mu)^{1/2} \sin(s\pi/2N)$$

Normalization of Normal Coordinate

Formula (4) of the Second Quarterly Report is

$$H_c = (2\mu)^{-1} \sum_{n=1}^N p_n^2 - (k/2) \sum_{n=2}^N (q_n - q_{n-1})^2 \quad (2-4)$$

and this formula should be equivalent to (3-12).

From (3-9) we see

$$\begin{aligned}
(2\mu)^{-1} \sum_{n=1}^N p_n^2 &= (2\mu)^{-1} \sum_{n=1}^N \sum_{s,r} a_{ns} a_{nr} P_s P_r (2/N)^2 / \alpha_s^2 \alpha_r^2 \\
&= \sum_s \alpha_s^{-2} (2/N) P_s^2 / 2\mu
\end{aligned} \tag{3-19}$$

using (3-7). Comparing this result with (3-12) we see

$$\alpha_s = (2/N)^{1/2} \tag{3-20}$$

is a suitable choice for the constant α_s . Thus we finally have

$$\begin{aligned}
Q_s &= \sum_{n=1}^N a_{sn} q_n, \quad (a) & q_n &= \sum_{s=0}^{N-1} a_{sn} Q_s, \quad (b) \\
P_s &= \sum_{n=1}^N a_{sn} p_n, \quad (c) & p_n &= \sum_{s=0}^{N-1} a_{sn} P_s, \quad (d)
\end{aligned} \tag{3-21}$$

where

$$a_{sn} = (2/N)^{1/2} \begin{cases} \cos \\ \sin \end{cases} \left[\frac{1}{2} (N+1-n) s \pi / N \right] \tag{3-22}$$

taking cos if s is even, and sin if s is odd.

Excitation of Normal Vibration

Formula (5) of our First Quarterly Report says

$$\dot{H}_s = (H_s, H] \equiv - (\partial H_s / \partial P_s) (\partial V / \partial Q_s) \tag{3-23}$$

where V is the potential energy of the interaction between the incoming particle and the chain.

From (3-12), (3-15) and (3-17)

$$\partial H_s / \partial P_s = P_s / \mu = \dot{Q}_s \tag{3-24}$$

Potential V is likely a short range one, and can be assumed to be a function of the distance between the incoming particle and the end atom of the chain. We call this distance x. Then

$$\partial V / \partial Q_s = (\partial V / \partial x)(\partial x / \partial Q_s) \quad . \quad (3-25)$$

Now

$$x = x_M - x_N = x_M - q_N + N\ell \quad (3-26)$$

using (2-2). From (3-21b) we obtain

$$\partial x / \partial Q_s = - \partial q_n / \partial Q_s = - a_{sN} \quad . \quad (3-27)$$

Putting (3-24), (3-25), and (3-27) into (3-22) we have

$$\dot{H}_s = - a_{sN} \dot{Q}_s (\partial V / \partial x) \quad . \quad (3-28)$$

Integrating both sides of this equation, we obtain the amount of energy delivered to the s^{th} normal vibration by the impact as

$$\Delta H_s = - a_{sN} \int \dot{Q}_s (\partial V / \partial x) dt \quad . \quad (3-29)$$

Strong Impulse

Our canonical equation of motion (3-13) is valid in all cases, while the second canonical equation of motion is

$$\begin{aligned} \dot{P}_s &= \mu \ddot{Q}_s = [H, P_s] = [V, P_s] - [H_s, P_s] \\ &= [P_s, H] = [P_s, V] + [P_s, H_s] \\ &= - (\partial V / \partial Q_s) - (\lambda_s / \mu) Q_s \end{aligned} \quad (3-30)$$

in general. The first term in the last expression gives the effect of the incoming particle, and exists only during the collision. In the followings of this report we will consider two typical cases

$$|\partial V / \partial Q_s| \gg |(\lambda_s / \mu) Q_s| \quad (3-31)$$

$$|\partial V / \partial Q_s| \leq |(\lambda_s / \mu) Q_s| \quad (3-32)$$

during the collision. The former case is called the case of strong impulse, while the latter is called the case of weak impulse.

In the case of strong impulse, the equation of motion during the collision is

$$\dot{\mathbf{P}}_s = - \partial V / \partial \mathbf{Q}_s = - a_{sN} \partial V / \partial \mathbf{x} \quad (3-33)$$

On the other hand the equation of motion for the incoming particle is

$$\dot{\mathbf{p}}_M = [\mathbf{p}_M, H] = [\mathbf{p}_M, V] = - \partial V / \partial \mathbf{x}_M = - \partial V / \partial \mathbf{x} \quad (3-34)$$

using (3-26). We, thus, obtain

$$\dot{\mathbf{P}}_s = - a_{sN} \partial V / \partial \mathbf{x} = a_{sN} \dot{\mathbf{p}}_M \quad (3-35)$$

or, integrating both sides over the time of collision,

$$\mathbf{P}_{s+} - \mathbf{P}_{s-} = a_{sN} (\mathbf{p}_{M+} - \mathbf{p}_{M-}) \quad (3-36)$$

where subscripts + and - means after and before the collision, respectively.

Let us call

$$\mathbf{P} = \mathbf{p}_{M+} - \mathbf{p}_{M-} \quad (3-37)$$

which is the total momentum transferred to the chain by the collision.

Suppose the chain was not vibrating before the collision, and the collision duration time is very much smaller than any vibrational period, we obtain

$$\mathbf{P}_s = a_{sN} \mathbf{P} \cos(\omega_s t) \quad (3-38)$$

and

$$\mathbf{Q}_s = (a_{sN} / \omega_s \mu) \mathbf{P} \sin(\omega_s t) \quad (3-38')$$

for the motion of the chain after the collision.

Notice that from (3-22)

$$a_{sN} = (2/N)^{1/2} \frac{\cos}{\sin} \left[\frac{1}{2}(1-N)s\pi/N \right] = (-1)^{s'/2} (2/N)^{1/2} \cos(s\pi/2N) \quad (3-39)$$

where

$$\begin{aligned} s' &= s & \text{if } s \text{ is even.} \\ s' &= s-1 & \text{if } s \text{ is odd.} \end{aligned} \quad (3-40)$$

It is worthwhile to note that the total momentum of the chain is

$$\sum_{n=1}^N p_n = (N/2)^{1/2} P_0 = (N/2)^{1/2} a_{0N} P = P \quad (3-41)$$

which gives the momentum conservation. This result also indicates that canonical momenta for vibrational modes ($s \neq 0$) are not momenta of the ordinary sense. Equation (3-36) should not be interpreted as a distribution of momentum among modes.

We see from (3-18) that

$$H_s = a_{sN}^2 P^2 / \mu \quad (3-42)$$

Since

$$\sum_{s=0}^{N-1} a_{sN}^2 = 1 \quad (3-43)$$

as can easily be seen from (3-39), the coefficient a_{sN}^2 gives the fraction of energy distributed to the s -th mode. Particularly, the motion of the chain as a whole obtains a_{0N}^2 or $2/N$ of the total energy. $(N-2)/N$ of the total energy goes to the lattice vibrations.

The energy conservation rule

$$p_{M-}^2 / 2M - p_{M+}^2 / 2M = \sum_{s=0}^{N-1} H_s = P^2 / \mu = (p_{M+} - p_{M-})^2 / \mu \quad (3-44)$$

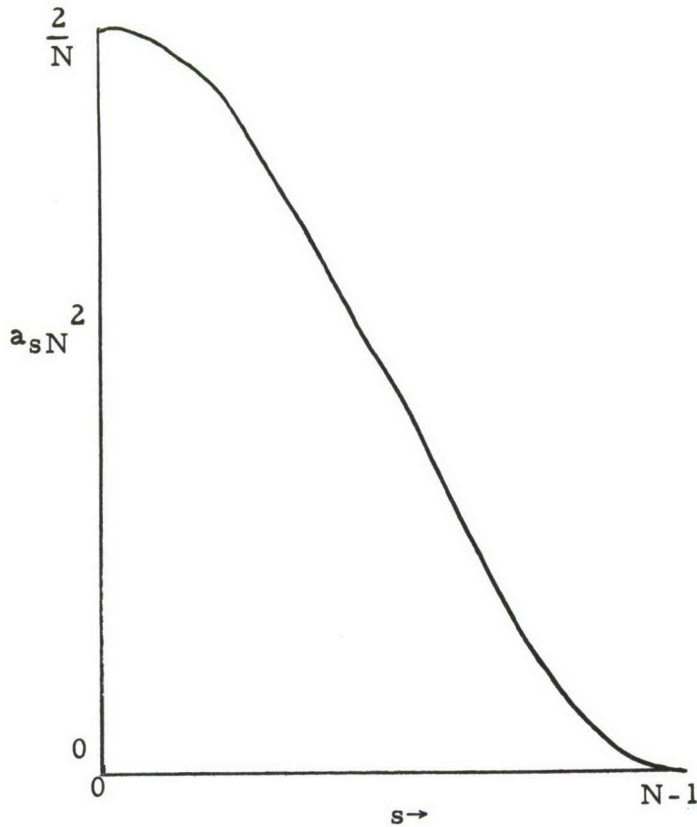


Figure 2. Energy distribution function for strong impulse $a_s N^2$ as a function of s . $s=0$ is the translational motion.

$$a_s N^2 = 2 \cos^2(s\pi/2N)/N$$

gives

$$p_{M+} = p_{M-}(2M-\mu)/(2M+\mu) \quad \text{if } 2M > \mu \quad (3-45)$$

$$\text{or } p_{M+} = p_{M-} \quad \text{if } 2M \leq \mu$$

or

$$\begin{aligned} P &= p_{M-} 2\mu/(2M+\mu) & \text{if } 2M > \mu \\ &= 0 & \text{if } 2M \leq \mu. \end{aligned} \quad (3-46)$$

The ratio of the transferred energy to the incident energy is

$$\begin{aligned} (P^2/\mu)/(p_{M-}^2/2M) &= 2M(2\mu)^2/\mu(2M+\mu)^2 \quad \text{if } 2M > \mu \\ &= 0 \quad \text{if } 2M \leq \mu. \end{aligned} \quad (3-47)$$

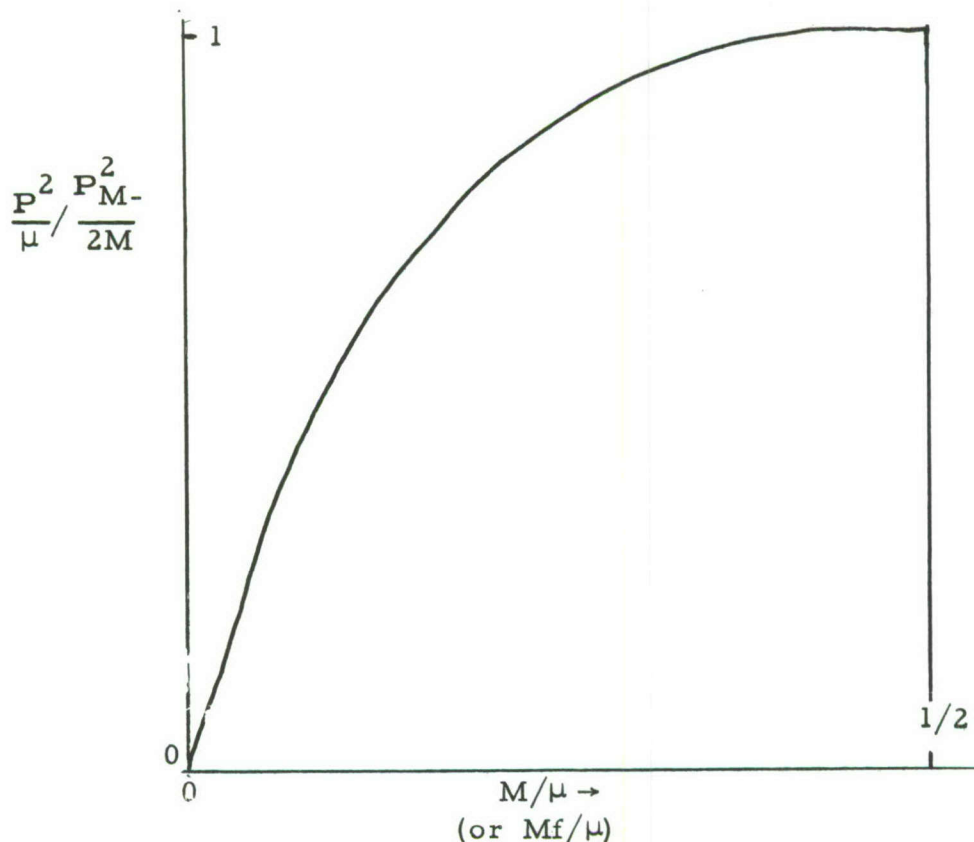


Figure 3. Efficiency of energy transfer as a function of mass ratio M/μ . ratio = $8x/(2x+1)^2$, where $x = M/\mu$.

Weak Impulse

Let us now turn to another case of weak impulse, which is given by condition (3-32). In this case the first approximation is obtained by neglecting $\partial V/\partial Q_s$ term in (3-30), or

$$Q_s = Q_{s0} \exp(i\omega_s t) \quad (3-48)$$

In order to take into account the effect of the collision, we assume

that Q_{s0} is slightly time dependent, but its second time derivative is still negligible. In that case (3-30) gives

$$2\omega_s \mu \dot{Q}_{s0} \exp(i\omega_s t) = -a_s N \partial V / \partial x \quad (3-49)$$

from which we obtain

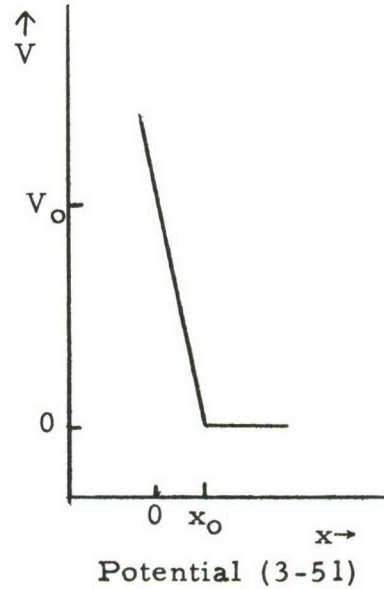
$$Q_{s0+} - Q_{s0-} = -(a_s N / 2\omega_s \mu) \int (\partial V / \partial x) \exp(-i\omega_s t) dt \quad (3-50)$$

where subscripts + and - mean after and before the collision, respectively, and the integral is to be done through the collision time.

Suppose we take a simple potential

$$\begin{aligned} V &= 0, & \text{if } x > x_0 \\ &= V_0(x_0 - x)/x_0, & \text{if } x \leq x_0 \end{aligned} \quad (3-51)$$

Figure 4



we can calculate the integral in (3-50) to obtain

$$Q_{s0+} - Q_{s0-} = -(a_s N / 2i\omega_s^2 \mu) (V_0 / x_0) [\exp(-i\omega_s t_1) - \exp(-i\omega_s t_2)] \quad (3-52)$$

where t_1 and t_2 are the times when the particle pass through x_0 before and after the collision, respectively, defining the time at the collision to be $t=0$. Thus we see

$$t_1 = (M/2)^{1/2} \int_0^{x_0} (T_+ - V)^{-1/2} dx = (2MT_+)^{1/2} x_0 / V_0$$

$$t_2 = -(M/2)^{1/2} \int_0^{x_0} (T_- - V)^{-1/2} dx = -(2MT_-)^{1/2} x_0 / V_0 \quad (3-53)$$

with the lower limit of integral such that $T-V$ is zero in each case.

When t_1 and t_2 are both small so that

$$\omega_s t_1 \ll 1, \quad \omega_s t_2 \ll 1 \quad (3-54)$$

our formula (3-52) reduces to

$$\begin{aligned} Q_{s0+} - Q_{s0-} &= -(a_s N / 2i\omega_s \mu) (V_0 / x_0) i\omega_s (t_2 - t_1) \\ &= (a_s N / 2\omega_s \mu) [(2MT_+)^{1/2} + (2MT_-)^{1/2}] \\ &= (a_s N / 2\omega_s \mu) P \end{aligned} \quad (3-55)$$

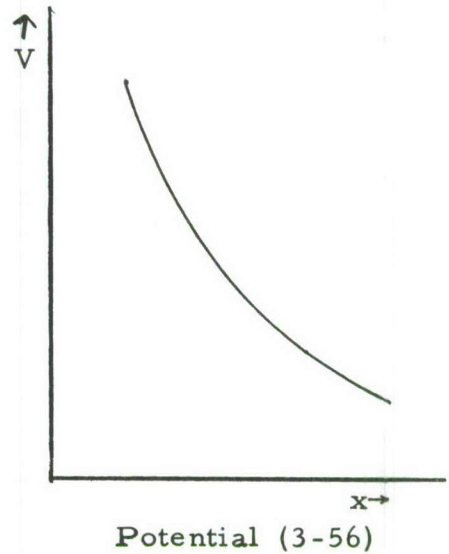
using (3-53). This result is almost identical to (3-38), which is the result of the strong impulse case.

When t_1 and t_2 are large, namely, when $\partial V / \partial x$ is small or the momentum is large, (3-52) shows that the excitation of the s -th normal vibration is much smaller than in the case of strong impulse.

Another potential such that

$$\partial V / \partial x = -T_0 \exp(-v|t|/x_0) x_0 \quad (3-56)$$

Figure 5



may be interesting. In this formula we take T_+ , v_{M+} , and T_- , v_{M-} for T , v , when t is positive and negative, respectively. We obtain from (3-50) that

$$Q_{s0+} - Q_{s0-} = -(a_{sN}/2\omega_s \mu x_0) [T_+ \{-(v_{M+}/x_0) - i\omega_s\}^{-1} + T_- \{-(v_{M-}/x_0) + i\omega_s\}^{-1}] \quad (3-57)$$

When

$$\omega_s \ll v_{M+}/x_0, \quad v_{M-}/x_0 \quad (3-58)$$

this formula reduces to

$$Q_{s0+} - Q_{s0-} = (a_{sN}/2\omega_s \mu) [(T_+/v_{M+}) - (T_-/v_{M-})] (a_{sN}/4\omega_s \mu) P \quad (3-59)$$

which corresponds to the case of strong impulse. Note that condition (3-58) corresponds to (3-54) of the previous potential. Note, however, that the critical frequency for ω_s is

$$\omega_c = 1/t = (V_0/Mv_{M\pm})/x_0 \quad (3-60)$$

in the first case, while it is

$$\omega_c = v_{M\pm}/x_0 \quad (3-61)$$

in the second case.

In both potentials one can say that normal vibrations with frequency higher than certain critical frequency will not be excited as much as predicted by the strong impulse assumption. This critical frequency is lower when the range of potential is larger.

Critical Frequency

Let us examine conditions for strong and weak impulses (3-31) and (3-32) more carefully. We see from (3-27) and (3-39)

$$|\partial V/\partial Q_s| = |(\partial V/\partial x) a_{sN}| = |\partial V/\partial x| (2/N)^{1/2} \cos(s\pi/2N) \quad (3-62)$$

while (3-16) gives

$$\cos(s\pi/2N) = [1 - (\omega_s/\omega_0)^2]^{1/2} \quad (3-63)$$

where

$$\omega_0 = 2(k/\mu)^{1/2} \quad (3-64)$$

On the other hand we have from (3-16) and (3-64)

$$|(\lambda_s/\mu)Q_s| = |\mu\omega_s^2 Q_s| = 4k(\omega_s/\omega_0)^2 |Q_s| \quad (3-65)$$

Criteria (3-31) and (3-32) are thus

$$(\omega_s/\omega_0)^2 [1 - (\omega_s/\omega_0)^2]^{-1/2} \lesseqgtr |\partial V/\partial x| (2/N)^{1/2} / 4k |Q_s| \quad (3-66)$$

where upper and lower inequality signs correspond to (3-31) and (3-32), respectively.

Since ω_s goes to zero as s goes to zero, our expression (3-66) shows the excitation of normal coordinates with small s values can always be treated by the strong impulse approximation. This is particularly true for the translational motion $s=0$, under any condition. The momentum conservation law (3-41), for example, is thus always valid.

In order to see when the assumption of strong impulse becomes invalid, we take the maximum value of Q_s calculated for the strong impulse in (3-38) to calculate the right-hand side of (3-66). Thus

$$(\omega_s/\omega_0)^2 \lesseqgtr |\partial V/\partial x| / P\omega_s \quad (3-67)$$

gives the criterion. We see from this expression that if

$$|\partial V/\partial x| > P\omega_0 \quad (3-68)$$

the assumption of strong impulse is valid for all normal vibrations. One might think that the condition (3-68) will be satisfied more easily by a weak impulse where the momentum transfer P is expected to be small. Such impression is true if $\partial V/\partial x$ does not depend on the energy of the collision. In most cases, however, interatomic potential V is such that $\partial V/\partial x$ increases rapidly as V increases. In the case of V between He atoms, for example,

$$V = 8 \exp(-2.48x)/x \quad (\text{in a.u.}) \quad (3-69)$$

is found to be a good approximation.* For such exponential potential we have as an order of magnitude

* R. A. Buckingham, Trans. Faraday Soc., 54, 453 (1958).

$$\partial V / \partial x \approx P^2 / x_0 M \approx P v_M / x_0 \quad . \quad (3-70)$$

Thus our condition (3-68) can be expressed as: if the critical frequency

$$\omega_c = v_M / x_0 \quad (3-71)$$

is larger than the maximum frequency ω_0 the assumption of strong impulse is valid for all normal vibration, but if not we have

$$\begin{aligned} \text{strong impulse for modes which have } \omega_s < \omega_c \\ \text{weak impulse for modes which have } \omega_s > \omega_c \end{aligned} \quad (3-72)$$

Excitation by a weak impulse depends on the potential V , but our results (3-52) and (3-57) indicate that

$$Q_{s0+} - Q_{s0-} \propto a_{sN} / \omega_s^2 \quad (3-73)$$

instead of a_{sN} / ω_s for the strong impulse. The energy distribution function which is a_{sN}^2 in the case of strong impulse should therefore look like the curve shown in Figure 6 in general.

The actual situation beyond the critical frequency is quite complicated and depends on each atom we take.

Inelasticity of General Collision

Since the range of potential x_0 is about 10^{-10} m, velocity v_M of about 10^3 m/sec will make the critical frequency ω_c about the same as the maximum frequency ω_0 which is about 10^{13} m/sec. Such velocity is rather fast as a macroscopic motion, while it is common as an atomic velocity at room temperature. Thus in microscopic collisions most of the normal vibrations are excited by the strong impulse, but in many macroscopic collisions (hitting by a hammer, etc.) only lower frequencies are excited by the strong impulse.

In this section we investigate what happens when ω_c is smaller than ω_0 . For the purpose of simplicity we assume that normal vibrations with frequency larger than ω_c are not excited at all. In other words we assume that the energy distribution function is

$$\begin{aligned} a_{sN}^2 & \quad \text{for } \omega_s \leq \omega_c \\ 0 & \quad \text{for } \omega_s > \omega_c \end{aligned} \quad (3-74)$$

This is shown by a chain line in Figure 6.

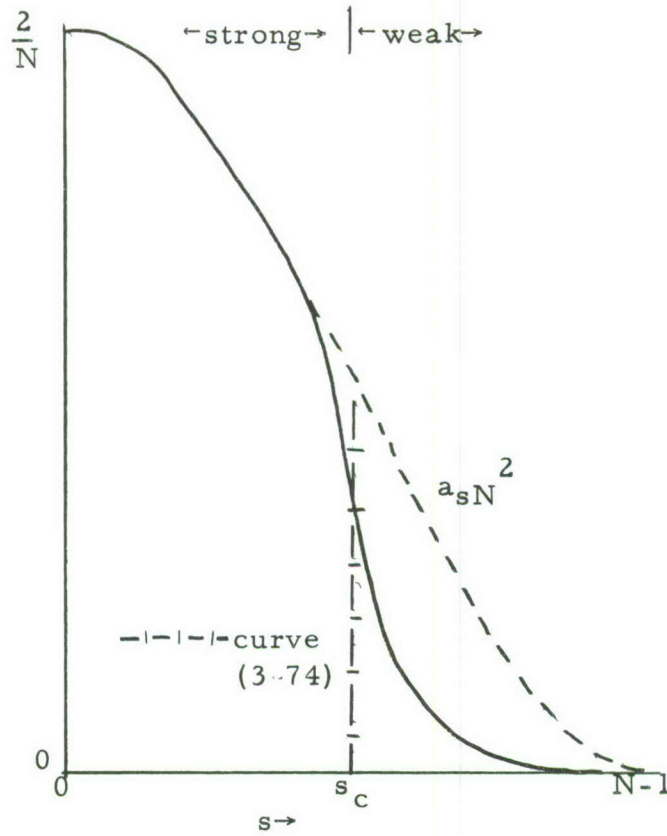


Figure 6. Energy distribution function.
 s_c is the value of s where
 $\omega_s = \omega_c$.

The total energy transferred to the chain is, using (3-42)

$$\begin{aligned}
 \sum_0^{s_c} H_s &= (P^2/\mu) \sum_0^{s_c} a_s N^2 \\
 &= (P^2/\mu)(2/N) \sum_0^{s_c} \cos^2(s\pi/2N) \\
 &= (2P^2/\mu N) \left[\frac{1}{2}s_c + \cos\{(s_c+1)\pi/2N\} \sin(s_c\pi/2N) / 2\sin(\pi/2N) \right]
 \end{aligned}
 \tag{3-75}$$

where (3-39) and

$$\sum_{r=0}^n \cos^2(rx) = \frac{1}{2}n + \cos[(n-1)x] \sin(nx) / 2 \sin x \quad (3-76)$$

is used.

From (3-16) and (3-74) we have

$$\omega_c = \omega_o \sin(s_c \pi / 2N) \quad (3-77)$$

or

$$s_c = (2N/\pi) \sin^{-1}(\omega_c/\omega_o) \quad (3-78)$$

From (3-75)

$$\begin{aligned} \sum_0^{s_c} H_s &= (2P^2/\mu\pi) [\sin^{-1}(\omega_c/\omega_o) - (\omega_c/\omega_o) \{1 - (\omega_c/\omega_o)^2\}^{1/2}] \\ &= (P^2/\mu) f(\omega_c/\omega_o) \end{aligned} \quad (3-79)$$

for the total energy transfer. The function $f(\omega_c/\omega_o)$ is tabulated in Table I.

Table I

$f(\omega_c/\omega_o)$

ω_c/ω_o	f
1.0	1.00
0.9	0.63
0.8	0.49
0.7	0.39
0.6	0.31
0.5	0.24
0.4	0.18
0.3	0.13
0.2	0.09
0.1	0.045

We see that when ω_c/ω_0 is very small

$$f(\omega_c/\omega_0) \rightarrow (2/3)(\omega_c/\omega_0)^3 \quad (3-80)$$

The ratio of the total energy given to the chain to the energy given to the translational motion of the chain as a whole is

$$\begin{aligned} \sum_0^{s_c} H_s/H_0 &= (P^2/\mu)f(\omega_c/\omega_0) / P^2/N\mu \\ &= Nf/2 \xrightarrow{\omega_c \rightarrow 0} N(\omega_c/\omega_0)^3/3 \quad (3-81) \end{aligned}$$

Since the critical frequency ω_c is expected to be proportional to the velocity of the incoming particle, the above ratio is proportional to the third power of that velocity if the latter is small enough. The ratio (3-81) is illustrated in Figure 7.

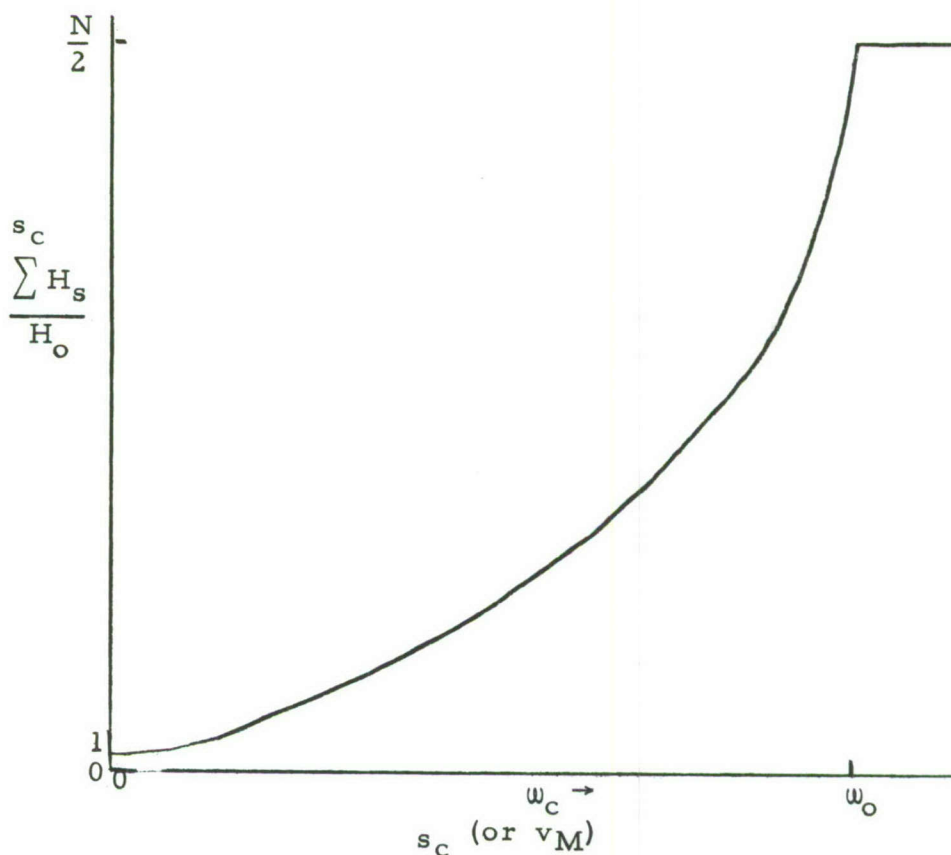


Figure 7. Ratio $\sum_0^{s_c} H_s/H_0 = Nf/2$.

Comparing our formula (3-79) with previous one (3-44), we see formulas (3-45), (3-46), and (3-47) can be applied to the present case only if we replace M by fM . Thus for the ratio of the transferred energy to the incident energy, Figure 3 holds if we take Mf/μ instead of M/μ .

Interatomic Distance

In this section we are going to investigate the distance between neighboring atoms in the chain after the chain is excited by an impact. We assume that the excitation is expressed by the energy distribution function (3-64).

From (3-21b) and (3-38)

$$q_n - q_{n-1} = (P/\mu) \sum_{s=0}^s (a_{sn} - a_{sn-1}) a_{sN} \sin \omega_s t / \omega_s \quad (3-82)$$

From (3-22) and (3-16) we see

$$\begin{aligned} (a_{sn} - a_{sn-1}) / \omega_s &= (\mu/2kN)^{1/2} \left[\frac{\cos}{\sin} \left[\left\{ \frac{1}{2}(N+1) - n \right\} s\pi/N \right] \right. \\ &\quad \left. - \frac{\cos}{\sin} \left[\left\{ \frac{1}{2}(N+1) - n + 1 \right\} s\pi/N \right] \right] / \sin(s\pi/2N) \\ &= (2\mu/kN)^{1/2} \frac{\sin}{-\cos} \left[\left(\frac{1}{2}N - n + 1 \right) s\pi/N \right] \\ &= -(-1)^{s'/2} (2\mu/kN)^{1/2} \sin[(n-1)s\pi/N] \end{aligned} \quad (3-83)$$

where s' is defined by (3-40).

Using (3-39) for a_{sN} we see

$$\begin{aligned} a_{sN} (a_{sn} - a_{sn-1}) / \omega_s &= -(2/N)(\mu/k)^{1/2} \cos(s\pi/2N) \sin[(n-1)s\pi/N] \\ &= -N^{-1}(\mu/k)^{1/2} \left[\sin\{(2n-1)s\pi/2N\} + \sin\{(2n-3)s\pi/2N\} \right] \end{aligned} \quad (3-84)$$

If we make an approximation

$$\omega_s \approx (s\pi/N)(k/\mu)^{1/2} \quad (3-85)$$

which is not so bad as shown in Figure 1, we obtain from (3-45) that

$$\begin{aligned} q_n - q_{n-1} &= -(P/N)(\mu k)^{-1/2} \sum_{s=1}^{s_c} [\cos\{(2n-1)s\pi/2N\} + \sin\{(2n-3)s\pi/2N\}] \\ &\quad \times \sin\{(s\pi/N)(k/\mu)^{1/2}t\} \\ &= P(2N)^{-1}(\mu k)^{-1/2} \sum_{s=1}^{s_c} [\cos\{[(2n-1)-2t(k/\mu)^{1/2}](s\pi/2N)\} \\ &\quad + \cos\{[(2n-3)-2t(k/\mu)^{1/2}](s\pi/2N)\} - \cos\{[(2n-1)+2t(k/\mu)^{1/2}](s\pi/2N)\} \\ &\quad - \cos\{[(2n-3)+2t(k/\mu)^{1/2}](s\pi/2N)\}] \\ &= P(2N)^{-1}(\mu k)^{-1/2} \left[\cos\{[\pi(s_c+1)/4N]g(n, t)\} \sin\{[\pi s_c/4N]g(n, t)\} / \sin\{(\pi/4N)g(n, t)\} \right. \\ &\quad \times \{(\pi/4N)g(n, t)\} \\ &\quad + \cos\{[\pi(s_c+1)/4N]g(n-1, t)\} \sin\{[\pi s_c/4N]g(n-1, t)\} / \sin\{(\pi/4N)g(n-1, t)\} \\ &\quad - \cos\{[\pi(s_c+1)/4N]g(n, -t)\} \sin\{[\pi s_c/4N]g(n, -t)\} / \sin\{(\pi/4N)g(n, -t)\} \\ &\quad \left. - \cos\{[\pi(s_c+1)/4N]g(n-1, -t)\} \sin\{[\pi s_c/4N]g(n-1, -t)\} / \right. \\ &\quad \left. \sin\{(\pi/4N)g(n-1, -t)\} \right] \end{aligned} \quad (3-86)$$

where

$$g(n, t) = 2n-1-2t(k/\mu)^{1/2} = 2n-1-t\omega_0. \quad (3-87)$$

Our formula (3-86) shows that the distance between neighboring atoms in the chain deviates from the equilibrium value by about $P/N\mu\omega_0$ where ω_0 is the maximum frequency of the chain, defined by (3-74).

If we hit a chain by another identical chain with the velocity of 10 m/sec, this means that the interatomic distance can change by about 10^{-2} Å since ω_0 is about 10^{13} m/sec. Such change is too small to initiate a chemical reaction in the chain.

Formula (3-85), however, also shows that when any of equations

$$\begin{aligned}\sin[(\pi/4N)g(n, t)] &= 0 \\ \sin[(\pi/4N)g(n-1, t)] &= 0 \\ \sin[(\pi/4N)g(n, -t)] &= 0 \\ \sin[(\pi/4N)g(n-1, -t)] &= 0\end{aligned}\tag{3-88}$$

is satisfied, the deviation is

$$|q_n - q_{n-1}| = Ps_c / 2N(\mu k)^{1/2} = (P/\mu\omega_0)(s_c/N)\tag{3-89}$$

which is larger than the above normal value by a factor of s_c . When s_c is sufficiently large a chemical reaction in the chain can occur between the n -th and $(n-1)$ -th atom at that time. Using (3-78) and (3-61)

$$s_c \approx (2N/\pi)(\omega_c/\omega_0) \approx v_M(2N/\pi\omega_0 x_0)\tag{3-90}$$

which shows that the maximum deviation (3-89) is proportional to Pv_M or the square of the velocity of the impact. If we need certain values for the deviation in order to start a chemical reaction in the chain, this result shows that the impact should be given with a velocity higher than some critical velocity. Velocity is more important than momentum in this case.

Conditions (3-88) are satisfied when $g/4N$ is an integer. From (3-88) we see that the maximum deviation (3-89) occurs when time t is given by either of

$$\begin{aligned}t &= (2n-1-4Nm)/\omega_0 \\ t &= (2n-3-4Nm)/\omega_0 \\ t &= (4Nm-2n+1)/\omega_0 \\ t &= (4Nm-2n+3)/\omega_0\end{aligned}\tag{3-91}$$

where m is an integer which can be negative as well as positive. For a given n or a location in the chain, such time t first occurs at about $2n/\omega_0$ and then repeats with the interval of $4N/\omega_0$. This

means that such maximum deviation propagate through the chain with the velocity of $\ell\omega_0/2$, where ℓ is the equilibrium distance between neighboring atoms. This is about 10^3 m/sec. The maximum value given by (3-89) does not depend on n in this approximation. This is because by taking the approximation (3-86) we neglected the dispersion. Actually the velocity of wave depends on its frequency. The maximum value (3-89) is expected to decrease as we go further from the end of the chain where the collision takes place, if we take into account the dispersion.

Important Formulas

In this section some of the important formulas obtained in this report are accumulated.

Normal coordinates:

$$Q_s = \sum_{n=1}^N a_{sn} q_n \quad (3-21a)$$

$$q_n = \sum_{s=0}^{N-1} a_{sn} Q_s \quad (3-21b)$$

$$a_{sn} = (2/N)^{1/2} \frac{\cos}{\sin} \left[\left\{ \frac{1}{2}(N-1) - n \right\} s\pi/N \right] \quad (3-22)$$

$$\omega_s = \omega_0 \sin(s\pi/2N) \quad (3-16)$$

$$\omega_0 = 2(k/\mu)^{1/2} \quad \text{: maximum frequency} \quad (3-64)$$

Strong impulse:

$$P_s = a_{sN} P \cos(\omega_s t) \quad (3-38)$$

$$Q_s = (a_{sN}/\omega_s \mu) P \sin(\omega_s t) \quad (3-38')$$

$$a_{sN} = (-1)^{s'/2} (2/N)^{1/2} \cos(s\pi/2N) \quad (3-39)$$

$$\begin{aligned} s' &= s & \text{if } s \text{ is even} \\ &= s-1 & \text{if } s \text{ is odd} \end{aligned} \quad (3-40)$$

$$H_s = a_{sN}^2 P^2 / \mu \quad (3-42)$$

Weak impulse:

$$\omega_c = v_M / x_o \quad \text{:critical frequency} \quad (3-61)$$

Normal modes with $\omega_s > \omega_c$ are not much excited,

$$\text{or} \quad Q_{so} \propto a_{sN} / \omega_s^2 \quad (3-73)$$

Inelasticity:

$$\sum_{s=0}^{s_c} H_s / H_o = N f(\omega_c / \omega_o) / 2 \quad (3-81)$$

$$f(\omega_c / \omega_o) = (2/\pi) [\sin^{-1}(\omega_c / \omega_o) - (\omega_c / \omega_o) \{ 1 - (\omega_c / \omega_o)^2 \}^{1/2}]$$

Table I for numerical values. (3-79)

Interatomic distance:

$q_n - q_{n-1}$ is about $P / N \mu \omega_o$ except when

$$t \approx \pm (2n - 4Nm) / \omega_o \quad (3-88)$$

m:integer

at which time

$$|q_n - q_{n-1}| \approx (P / \mu \omega_o) (s_c / N) \quad (3-89)$$

$$\approx P v_M / \mu \omega_o^2 x_o \quad (3-90)$$

FURTHER DEVELOPMENTS IN THE STATISTICAL THEORY OF EXPLOSION INITIATION

by

Daniel S. Ling, Jr.
PEC Corporation
Boulder, Colorado

I. Introduction and Summary

In this paper we will present a generalization of the "single-point" model. This generalization involves a more realistic treatment of the spatial aspects of the initiation problem. Much of the development presented here will closely parallel the development of the "single-point" model and for this reason the reader is urged to refer to the Proceedings of the 11th Basic Research Group Contractors' Conference and Symposium, 30 October - 1 November 1962 where the "single-point" model is discussed in detail.

Section II of this paper introduces the concept of a probability functional. This concept is fundamental to the entire discussion of this report and it is this concept which allows the treatment of the spatial aspects of the problem. The development is formulated in terms of one spatial dimension but it is clear that the generalization to three spatial dimensions is trivial.

Section III presents the derivation of the basic equation satisfied by the probability functional. This is the generalization of the equation satisfied by the function $P(T,t)$ of the "single-point" model.

In the treatment of the "single-point" model the introduction of the moments of the probability distribution was essential. Similarly, here we must introduce the moments of the probability functional. This is accomplished in Section IV.

Section V outlines the prospects for the future development of the theory presented in this paper.

II. Concept of a Probability Functional

We will consider, for simplicity, a linear system. We imagine a system consisting of individual molecules spaced at equal intervals along the x axis from minus to plus infinity. The temperature of the " i "th molecule is denoted by T_i . The probability that the " i "th molecule will react in the time interval " dt " is given by

$p(T_i)dt$. $p(T)$ will normally be taken to be of Arrhenius' form, i.e., $p(T) = Ae^{-E/kT}$.

Now we don't really know the temperature of a particular molecule. The best we can possibly know is the probability with which various temperatures may occur. For this reason we introduce the function

$$P(\cdots, T_{i-1}, T_i, T_{i+1} \cdots, t) \quad (1)$$

which has the property that

$$P(\cdots, T_{i-1}, T_i, T_{i+1} \cdots, t) \cdots dT_{i-1} dT_i dT_{i+1} \cdots \quad (2)$$

gives the probability that the " $i-1$ "st molecule has a temperature lying between T_{i-1} and $T_{i-1}+dT_{i-1}$, the " i "th molecule has a temperature lying between T_i and T_i+dT_i , etc. This is all at the specific time " t ". The index " i " ranges from $-\infty$ to $+\infty$. It is clear that P is a function of an infinite number of variables, the T_i for i ranging from minus to plus infinity, as well as being a function of time. This is what is sometimes called a "functional".

The preceding paragraph has been formulated in discrete language--isolated molecules a discrete distance apart. If we imagine the molecules getting closer and closer together we are led to a concept which we may denote by

$$P\{T(x), t\} \quad . \quad (3)$$

By this we mean an entity whose value depends on what functional value is used for $T(x)$. It is evident that both (1) and (3) describe the same concept and we shall call this the "probability functional". Since (3) is the more compact notation, we shall use it regardless of whether we are viewing the problem from the discrete or the continuous point of view. The distinction between the two points of view is not an essential one. Occasionally we shall use notation (1) when we wish to emphasize the dependence of P on T_i .

We shall also use the symbol $[dT]$ to stand for $\cdots dT_{i-1} dT_i dT_{i+1} \cdots$. Thus (2) would now be written

$$P\{T(x), t\} [dT] \quad . \quad (4)$$

It is clear that a knowledge of the functional $P\{T(x), t\}$ constitutes complete information about the system. The functional $P\{T(x)\}$ is subject to the following boundary conditions

$$P\{T(x), t\} = 0 \quad \text{if } T(x) = \infty \text{ for any } x. \quad (5)$$

$$P\{T(x), t\} = 0 \quad \text{if } T(x) < T_0 \text{ for any } x. \quad (6)$$

where T_0 is the ambient temperature.

Our next problem is the determination of the functional equation satisfied by $P\{T(x)\}$. We address ourselves to this question in the next section.

III. Derivation of the Basic Functional Equation

A. Omission of Reaction Terms

We shall first derive the functional equation assuming that no reactions occur. It is then relatively easy to add in the reaction terms. The derivation is very similar to that of the "single-point" model.

We must express $P\{T(x), t+dt\} [dT]$ in terms of $P\{T(x), t\}$. To this end we first note that the one dimensional heat conduction equation in discrete form is equivalent to

$$T_i(t+dt) = T_i(t) + K\{T_{i+1}(t) + T_{i-1}(t) - 2T_i(t)\}dt \quad (7)$$

K is a thermal conductivity coefficient. This equation may be viewed as a change of variables from the set of variables $T_i(t), i = -\infty$ to $+\infty$, to the new set $T_i(t+dt), i = -\infty$ to $+\infty$.

We will need the Jacobian (functional determinant) of the transformation (7). This is given by

$$J = \begin{vmatrix} \cdot & \cdot & \cdot & \cdot & \cdot & \cdot & \cdot & \cdot & \cdot & \cdot & \cdot \\ \cdot & \cdot & \cdot & \cdot & \cdot & \cdot & \cdot & \cdot & \cdot & \cdot & \cdot \\ \cdot & \cdot & 1-2Kdt & Kdt & \cdot & \cdot & \cdot & \cdot & \cdot & \cdot & \cdot \\ \cdot & \cdot & Kdt & 1-2Kdt & Kdt & \cdot & \cdot & \cdot & \cdot & \cdot & \cdot \\ \cdot & \cdot & \cdot & \cdot & Kdt & 1-2Kdt & \cdot & \cdot & \cdot & \cdot & \cdot \\ \cdot & \cdot & \cdot & \cdot & \cdot & \cdot & \cdot & \cdot & \cdot & \cdot & \cdot \\ \cdot & \cdot & \cdot & \cdot & \cdot & \cdot & \cdot & \cdot & \cdot & \cdot & \cdot \end{vmatrix} \quad (8)$$

This is an infinite determinant in all directions. The diagonal elements are $1-2Kdt$. The Kdt terms are one off the main diagonal and all other elements are zero. To first order in dt we may expand the determinant to obtain

$$J = 1 - \sum_i 2Kdt \quad . \quad (9)$$

This allows us to write

$$[dT(t+dt)] = J[dT(t)] \quad . \quad (10)$$

With these preliminaries we now have

$$\begin{aligned} & P\{\cdots, T_i + Kdt(T_{i+1} + T_{i-1} - 2T_i), \cdots, t+dt\} [dT_{(t+dt)}] \\ &= P(\cdots, T_i, \cdots, t) [dT_{(t)}] \quad . \end{aligned} \quad (11)$$

We now make a Taylor-McLaurin expansion of the left side of (11) and introduce (10) to obtain

$$\begin{aligned} & \left\{ P\{T(x), t\} + \sum_i \frac{\partial P}{\partial T_i} Kdt(T_{i+1} + T_{i-1} - 2T_i) + \frac{\partial P\{T(x), t\}}{\partial t} dt \right\} \left\{ 1 - \sum_i 2Kdt \right\} \\ &= P\{(T(x), t)\} \quad . \end{aligned} \quad (12)$$

Keeping only terms of first order in dt we find

$$\boxed{\frac{\partial P}{\partial t} = 2K \sum_i P - K \sum_i \frac{\partial P}{\partial T_i} \delta^2 T_i} \quad (13)$$

where we have introduced the notation

$$\delta^2 T_i = T_{i+1} + T_{i-1} - 2T_i \quad (14)$$

which is used in the calculus of finite differences.

Equation (13) is the basic functional equation (with reaction terms omitted). Before proceeding to the consideration of the

reaction terms we shall first convince ourselves of the correctness of (13) by treating a special case where the solution is already known.

Let $Y_i(t)$ be a solution of the heat conduction equation in finite difference form, namely

$$\frac{dY_i}{dt} = K(Y_{i+1} + Y_{i-1} - 2Y_i) . \quad (15)$$

Then, in the case of no reactions, a possible solution to (13) should be given by

$$P\{t(x), t\} = \prod_j \delta\{T_j - Y_j(t)\} \quad (16)$$

where π_j is the infinite product symbol and δ is the Dirac delta function. We may now verify that (16) satisfies (13).

We compute in turn the several terms of (13)

$$\frac{\partial P}{\partial t} = \sum_i \delta'\{T_i - Y_i(t)\} \left(-\frac{dY_i}{dt}\right) \prod_j' \delta\{T_j - Y_j(t)\}$$

where the prime on δ signifies the derivative of the delta function with respect to its argument and the prime on π indicates that the $j = i$ term is omitted from the infinite product. Similarly

$$\frac{\partial P}{\partial T_i} = \delta'\{T_i - Y_i(t)\} \prod_j' \delta\{T_j - Y_j(t)\} .$$

We then have

$$\frac{\partial P}{\partial t} + K \sum_i \frac{\partial P}{\partial T_i} \delta^2 T_i = \sum_i \left\{ K \delta^2 T_i - \frac{dY_i}{dt} \right\} \delta'(T_i - Y_i) \prod_j' \delta(T_j - Y_j) .$$

We can substitute for $\frac{dY_i}{dt}$ from (15) and put the right hand side in the form

$$K \sum_i \{(T_{i+1} - Y_{i+1}) + (T_{i-1} - Y_{i-1}) - 2(T_i - Y_i)\} \delta'(T_i - Y_i) \prod_i' \delta(T_j - Y_j) .$$

Since $(T_{i+1} - Y_{i+1})$ is multiplied by $\delta(T_{i+1} - Y_{i+1})$ coming from the infinite product, this gives zero. Similarly for $(T_{i-1} - Y_{i-1})$.

Remembering the property of the delta function that

$$x\delta'(x) = -\delta(x)$$

we get

$$2K \sum_i \delta(T_i - Y_i) \prod_j \delta(T_j - Y_j) = 2K \sum_i \prod_j \delta(T_j - Y_j) = 2K \sum_i P.$$

Thus we have shown that

$$\frac{\partial P}{\partial t} + K \sum_i \frac{\partial P}{\partial T_i} \delta^2 T_i = 2K \sum_i P$$

which is just equation (13).

B. Inclusion of Reaction Terms

In order to consider the reaction terms, we must first determine an expression for the probability that the i^{th} molecule is still alive (has not already reacted) at time t . We will denote this probability by $S_i(t)$ and it can be seen that

$$S_i(t+dt) = S_i(t) \left[1 - dt \int [dT] p(T_i) P\{T(x), t\} \right]. \quad (17)$$

Equation (17) says that the probability that the i^{th} molecule is still alive at time $t+dt$ equals the probability that it was still alive at time t multiplied by the probability that it does not react in the time dt . In order to be sure that there is no confusion regarding the notation used, we will write out in detail the integral on the right hand side of (17).

$$\int [dT] p(T_i) P\{T(x), t\} = \int \cdots dT_{i-1} dT_i dT_{i+1} p(T_i) P(\cdots T_{i-1}, T_i, T_{i+1}, \cdots, t).$$

From (17) we obtain the differential equation

$$\frac{dS_i}{dt} = -S_i(t) \int [dT] p(T_i) P\{T(x), t\}. \quad (18)$$

This can be readily integrated to give

$$S_i(t) = S_i(0) \exp \left[- \int_0^t dt \int [dT] p(T_i) P\{T(x), t\} \right]. \quad (19)$$

We will now assume that if the i^{th} molecule reacts, the temperature of that molecule is raised immediately by an amount Q and that no other molecules have their temperature raised. It is then readily seen that we must add to the right hand side of (13) the following two terms

$$- \sum_i p(T_i) S_i(t) P\{T(x), t\} + \sum_i p(T_i - Q) S_i(t) P(\cdots T_i - Q \cdots, t) \quad .$$

The first term represents the probability that the temperature distribution was already given by $T(x)$ and that some molecule reacted to produce a new temperature distribution. The second term represents the probability that the temperature distribution was too low at some molecule by an amount Q but that in the time dt this molecule reacted to bring the temperature distribution up to the value $T(x)$.

Thus we obtain for the basic functional equation of this theory,

$$\begin{aligned} \frac{\partial P\{T(x), t\}}{\partial t} = & 2K \sum_i P\{T(x), t\} - K \sum_i \frac{\partial P}{\partial T_i} \delta^2 T_i - \sum_i p(T_i) S_i(t) P\{T(x), t\} \\ & + \sum_i p(T_i - Q) S_i(t) P(\cdots T_i - Q \cdots, t) \end{aligned}$$

(20)

Our problem now is to solve, or at least approximately solve, this equation. To this end it is convenient to obtain the moment equations. This is considered in the next section.

IV. Calculation of the Moment Equations

The zeroth moment of our probability functional is defined as

$$M_0(t) = \int [dT] P\{T(x), t\} \quad . \quad (21)$$

In order that we shall be dealing with a consistent probability theory, this moment should be time independent. Indeed, we can prove from equation (20) that $\frac{dM_0}{dt} = 0$. Thus we may normalize our probability functional so that $M_0 = 1$.

To show that $\frac{dM_0}{dt} = 0$, we integrate equation (20) over all temperature functions $T(x)$. This is equivalent to integrating over all T_i from T_0 to ∞ . Actually since we will wish to make use of boundary condition (6) we will integrate from a value of T_i just slightly

less than T_0 to ∞ , i.e., from $T_0 - \infty$ to ∞ where ε is arbitrarily small. We shall not bother to show this for the lower limit of integration since this will always be understood.

We will consider separately the various terms of (20) in the same order in which they appear.

First,

$$\int_{T_0}^{\infty} [dT] \frac{\partial P\{T(x), t\}}{\partial t} = \frac{d}{dt} \int_{T_0}^{\infty} [dT] P\{T(x), t\} = \frac{dM_0}{dt}.$$

Next,

$$\int_{T_0}^{\infty} [dT] 2K \sum_i P\{T(x), t\} = 2K \sum_i \int [dT] P\{T(x), t\} = 2K \sum_i M_0.$$

Then,

$$\begin{aligned} & \int_{T_0}^{\infty} [dT] \left\{ -K \sum_i \frac{\partial P}{\partial T_i} \delta^2 T_i \right\} \\ &= -K \left(\cdots \int_{T_0}^{\infty} dT_j \cdots \right) \left(\sum_{(i \neq j)} \frac{\partial P}{\partial T_i} \delta^2 T_i + \frac{\partial P}{\partial T_j} (T_{j-1} + T_{j+1} - 2T_j) \right) \\ &= -K \int [dT] \sum_{(i \neq j)} \frac{\partial P}{\partial T_i} \delta^2 T_i - K \left(\cdots \int dT_{j-1} \int dT_{j+1} \cdots \right) \int_{T_0}^{\infty} dT_j \frac{\partial P}{\partial T_j} (T_{j-1} + T_{j+1} - 2T_j) \\ &= -K \int [dT] \sum_{(i \neq j)} \frac{\partial P}{\partial T_i} \delta^2 T_i - K \left(\cdots \int dT_{j-1} \int dT_{j+1} \cdots \right) \left[T_{j-1} P \right]_{T_j=T_0}^{T_j=\infty} \\ & \quad + T_{j+1} P \Big|_{T_j=T_0}^{T_j=\infty} - 2(T_j P) \Big|_{T_j=T_0}^{T_j=\infty} + 2 \int_{T_0}^{\infty} dT_j P \Big] \end{aligned}$$

If we use the boundary conditions (5) and (6) we find

$$= -K \int [dT] \sum_i \frac{\partial P}{\partial T_i} \delta^2 T_i - 2K \int [dT] P \quad .$$

(i ≠ j)

Now we can remove a second term from the \sum_i . Doing so we obtain

$$= -K \int [dT] \sum_i \frac{\partial P}{\partial T_i} \delta^2 T_i - 4K \int [dT] P \quad .$$

(i ≠ j, k)

Continuing this we can remove all the terms from \sum_i , obtaining thereby

$$= -2K \sum_i \int [dT] P = -2K \sum_i M_o \quad .$$

Finally, if we replace T_i by $T_i - Q$ as an integration variable in the 5th term it exactly cancels the 4th term. We end up finally with

$$\frac{dM_o}{dt} = 2K \sum_i M_o - 2K \sum_i M_o = 0 \quad .$$

The first moments of our probability functional are defined as

$$\theta_j(t) = \int [dT] T_j P\{T(x), t\} \quad . \quad (22)$$

It may sometimes be convenient to define a function $\theta(x, t)$ such that $\theta(x = x_j, t) \equiv \theta_j(t)$ where x_j is the position of the j^{th} molecule along the x axis. This is an appropriate notation if we wish to give a continuous, rather than discrete, formulation of the problem. We find the equation satisfied by the first moments by multiplying (20) by T_j and integrating. Again we will treat the terms in order as they occur.

First we have:

$$\int [dT] T_j \frac{\partial P}{\partial t} = \frac{d}{dt} \int [dT] T_j P = \frac{d\theta_j(t)}{dt} = \frac{\partial \theta(x_j, t)}{\partial t} \quad .$$

The next term is:

$$2K \int [dT] T_j \sum_i P\{T(x), t\} = 2K \sum_i \theta_j(t) = 2K \sum_i \theta(x_j, t) \quad .$$

The third term is rather complicated and is treated as follows:

$$\begin{aligned}
& -K \int [dT] T_j \sum_i \frac{\partial P}{\partial T_i} \delta^2 T_i = -K \sum_i \int [dT] T_j \frac{\partial P}{\partial T_i} \delta^2 T_i \\
& = -K \sum_i \int \prod_k \left(\int dT_k \int dT_i T_j \frac{\partial P}{\partial T_i} (T_{i+1} + T_{i-1} - 2T_i) \right. \\
& \quad \left. (i \neq j) \right) (k \neq i) \\
& \quad -K \int \prod_k \left(\int dT_k \int dT_j T_j \frac{\partial P}{\partial T_j} (T_{j+1} + T_{j-1} - 2T_j) \right. \\
& \quad \left. (k \neq j) \right) \\
& = -K \sum_i \int \prod_k \left(\int dT_k \left\{ T_j T_{i+1} P \Big|_{T_i=T_0}^{T_i=\infty} + T_j T_{i-1} P \Big|_{T_i=T_0}^{T_i=\infty} - 2T_j (T_i P) \Big|_{T_i=T_0}^{T_i=\infty} \right. \right. \\
& \quad \left. \left. (i \neq j) \right) (k \neq i) \right. \\
& \quad \left. + 2 \int dT_i T_j P \right\} \\
& \quad -K \int \prod_k \left(\int dT_k \left\{ T_{j+1} (T_j P) \Big|_{T_j=T_0}^{T_j=\infty} - T_{j+1} \int dT_j P \right. \right. \\
& \quad \left. \left. (k \neq j) \right) \right. \\
& \quad \left. + T_{j-1} (T_j P) \Big|_{T_j=T_0}^{T_j=\infty} - T_{j-1} \int dT_j P \right. \\
& \quad \left. - 2(T_j P) \Big|_{T_j=T_0}^{T_j=\infty} + 4 \int dT_j T_j P \right\}
\end{aligned}$$

Using boundary conditions (5) and (6), we are left with

$$\begin{aligned}
&= -2K \sum_i \int [dT] T_j P + K \int [dT] (T_{j+1} + T_{j-1} - 2T_j) P \\
&\quad (i \neq j) \\
&= -2K \sum_i \int [dT] T_j P + K \int [dT] (T_{j+1} + T_{j-1} - 2T_j) P \\
&= -2K \sum_i \theta_j(t) + K \{ \theta_{j+1}(t) + \theta_{j-1}(t) - 2\theta_j(t) \}
\end{aligned}$$

We will treat the fourth and fifth terms together.

$$\begin{aligned}
& - \int [dT] T_j \sum_i p(T_i) S_i(t) P\{T(x), t\} + \int [dT] T_j \sum_i p(T_i - Q) S_i(t) P(\dots T_i - Q \dots, t) \\
&= \sum_i S_i(t) \int [dT] T_j \{ -p(T_i) P(T) + p(T_i - Q) P(\dots T_i - Q \dots, t) \} \\
&= \sum_i S_i(t) \int [dT] T_j \{ -p(T_i) P + p(T_i - Q) P(\dots T_i - Q \dots, t) \} \\
&\quad (i \neq j) \\
&+ S_j(t) \int [dT] T_j \{ -p(T_j) P + p(T_j - Q) P(\dots T_j - Q \dots, t) \}
\end{aligned}$$

By making a shift in the integration variable of $T_i - Q \rightarrow T_i$ in the $p(T_i - Q)$ term and of $T_j - Q \rightarrow T_j$ in the $p(T_j - Q)$ term we obtain

$$\begin{aligned}
&= \sum_i S_i(t) \int [dT] T_j \{ -p(T_i) P + p(T_i) P \} \\
&\quad (i \neq j) \\
&+ S_j(t) \int [dT] \{ -T_j p(T_j) P + (T_j + Q) p(T_j) P \} \\
&= QS_j(t) \int [dT] p(T_j) P\{T(x), t\}
\end{aligned}$$

Putting these terms all together we find

$$\frac{d\theta_j}{dt} = K(\theta_{j+1} + \theta_{j-1} - 2\theta_j) + QS_j(t) \int [dT] p(T_j) P\{T(x), t\}$$

(23)

In continuous notation this equation becomes

$$\frac{\partial \theta(x, t)}{\partial t} = K' \frac{\partial^2 \theta(x, t)}{\partial x^2} + QS(x, t) \int [dT] p\{T(x)\} P$$

(24)

We obtain (24) from (23) by noting that

$$\theta_{j+1} + \theta_{j-1} - \theta_j = \theta(x_{j+1}, t) + \theta(x_{j-1}, t) - 2\theta(x_j, t)$$

is essentially the finite difference approximation to $\left. \frac{\partial^2 \theta(x, t)}{\partial x^2} \right|_{x=x_j}$.

The conductivity constant K is changed to a slightly different constant K' in order to permit the replacement of $(\theta_{j+1} + \theta_{j-1} - 2\theta_j)$ by $\frac{\partial^2 \theta}{\partial x^2}$. $S(x, t)$ is interpreted as the probability that the molecule located at x is still alive at the time t .

The second moments are defined as follows:

$$\Delta_{jk} = \int [dT] (T_k - \theta_k)(T_j - \theta_j) P\{T(x), t\} \quad (25)$$

It is first of all clear that $\Delta_{jk} = \Delta_{kj}$. To find the equations satisfied by the second moments we proceed exactly as we have done for the earlier moments. We will omit the details of the calculation and quote only the final result.

$$\frac{d\Delta_{jk}}{dt} = K(\Delta_{j+1, k} + \Delta_{j-1, k} - 2\Delta_{jk})$$

$$+ K(\Delta_{j, k+1} + \Delta_{j, k-1} - 2\Delta_{jk})$$

$$+ QS_j(t) \int [dT] (T_k - \theta_k) p(T_j) P$$

$$+ QS_k(t) \int [dT] (T_j - \theta_j) p(T_k) P$$

$$+ Q^2 \delta_{jk} S_j(t) \int [dT] p(T_j) P$$

(26)

We may introduce a function $\Delta(x, x', t)$ such that $\Delta_{jk} \equiv \Delta(x=x_j, x'=x_k, t)$ and then (26) can be written

$$\frac{\partial \Delta(x, x', t)}{\partial t} = K \frac{\partial^2 \Delta}{\partial x^2} + K \frac{\partial^2 \Delta}{\partial x'^2}$$

$$+ QS(x, t) \int [dT] \{T(x') - \theta(x')\} p\{T(x)\} P$$

$$+ QS(x', t) \int [dT] \{T(x) - \theta(x)\} p\{T(x')\} P$$

$$+ Q^2 \delta(x-x') S(x, t) \int [dT] p\{T(x)\} P$$

(27)

We could continue to compute higher moments but we anticipate no need to go beyond the second moments.

It is worth noting that equation (24) is just the one dimensional heat conduction equation plus reaction terms.

It is evident that it is a trivial matter to generalize to three dimensions. For example, we need only replace $\theta(x, t)$ by $\theta(x, y, z, t)$; $S(x, t)$ by $S(x, y, z, t)$; $\frac{\partial^2}{\partial x^2}$ by the Laplace operator and think of the probability functional $P\{T(x), t\}$ as replaced by a new functional $P\{T(x, y, z), t\}$.

V. Conclusion

We now face the problem of solving equations (23) and (26) or if we prefer equations (24) and (27). This is exactly the position in which we found ourselves with the "single-point" model prior to the introduction of the "bump" hypothesis. We have reason to believe that a similar "bump" approach will also work to solve this more general problem. The details of this are not yet completely worked out.

SOME FACTORS AFFECTING IMPACT SENSITIVITY

by

W. C. McCrone
McCrone Associates, Inc.
Chicago, Illinois

Impact sensitivities on high as well as primary explosives have been carried out for several years on an impact machine designed and constructed by our personnel. It has performed extremely well and we have gradually built up a reasonable degree of confidence in the results obtained.

Figures 1 and 2 show two views of the present arrangement; one a close-up of the striker-anvil assembly. The most important feature of this machine aside from the simplicity and ease of use is the small explosive sample size; the dropweight is also, of course, proportionately smaller. Whereas the Bruceton and NOL machines use samples in the 20 - 35 mg. range and 2 - 5 kg weights we use a 0.5 kg weight and 6 mg. samples. This fact, alone, makes possible lighter apparatus especially striker and anvil during the shots. To further ensure a mechanical system that will not change with time and shooting we have carefully sealed the apparatus to a 1 ton concrete block through a 1" thick steel plate. Finally the striker and anvil have been especially machined from a hard steel and further finished after final heat treatment. The measured hardness of these pieces is 53 Rockwell C (522 Brinell). The result of this is a surface unaffected by repeated detonation of high explosive samples. A single striker and anvil combination can be used almost indefinitely. In several instances a given pair has been used for several thousand shots with no observable effect on the surfaces.

As a result of the simple design and the very hard striker-anvil combination excellent results are obtained on high explosives.

For example, the following series of 80 shots taken on a given sample of β -HMX are shown to illustrate reproducibility.

Drop-height, Cm.	-20 shots-										% fired	50% Pt.
35												
30		+			+				+	+	100	
25	-	+	+	-	+	+	+	-	-	+	60	24
20	-		-	-		-	-	-			0	
25	+	+	+	+	+	+	+	+	+	+	100	23
20	-	-	-	-	-	-	-	-	-	-	0	
30			+	+					+		100	
25	+	-	-	+	+	+	+	-	+	-	60	24
20	-	-			-	-	-	-		-	0	
30	+	+	+								100	
25	-	-	+	+	+	+	+	+	+	+	80	23
20				-	-	-	-	-	-	-	0	

Quite pleased with such data we commenced a long series of shots using PETN and a recrystallized sample of β -HMX as standards for occasional calibration. After some months of operation the 50% points of both samples were observed to be slowly decreasing. The 50% point of the standard β -HMX was found to have decreased gradually over the 5 month test period from 37 to 30 cm. After considerable soul-searching the only clue that could be found was a very shiny top surface on the volumetric scoop used to measure out the sample. It seemed possible that this scoop (made of copper) was being gradually worn down by the leveling operation carried out with a razor blade. If this were true the volume of the scoop had been slowly decreasing over the test-period and the impact energy necessary to detonate the resulting smaller volumes of β -HMX would also be smaller.

This variation in 50% point with sample weight was immediately checked for a variety of explosives by making up a series of spoons (incidentally using a hard steel for the scoop) to hold different volumes. Starting with standard PETN we obtained the following data.

Table I
Effect of sample weight on 50% point of PETN

Weight of PETN, mg.	50% Point, cm.
0.75	17
1.8	23
2.4	26
3.1	28
4.9	37
7.8	50
12.8	73

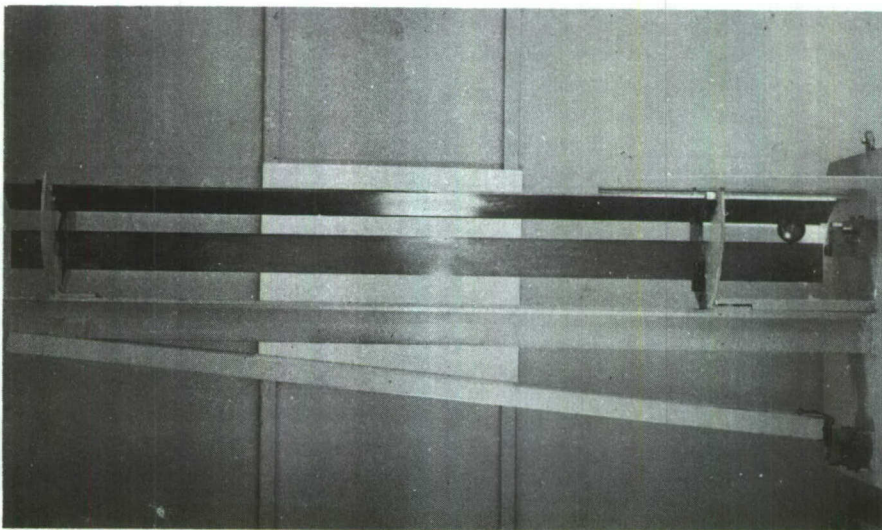


Figure 1. McCrone Associates Impact Machine

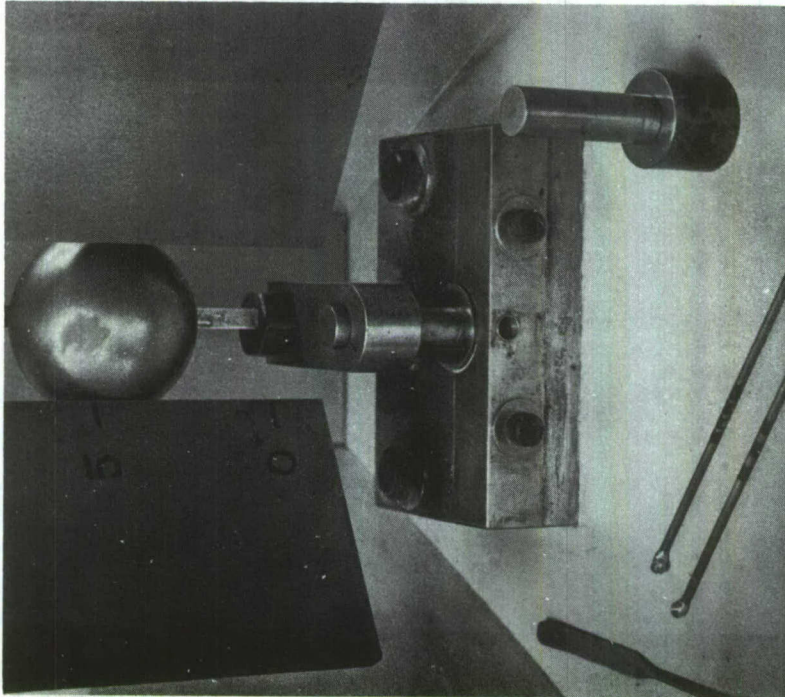


Figure 2. Striker, anvil, ball weight and lower assembly of McCrone Associates Impact Machine, volumetric sample measuring spoons and a striker-anvil pair in foreground.

Similar results were obtained for other explosives (Figure 3). This effect is, therefore, a very important variable in impact testing of explosives.

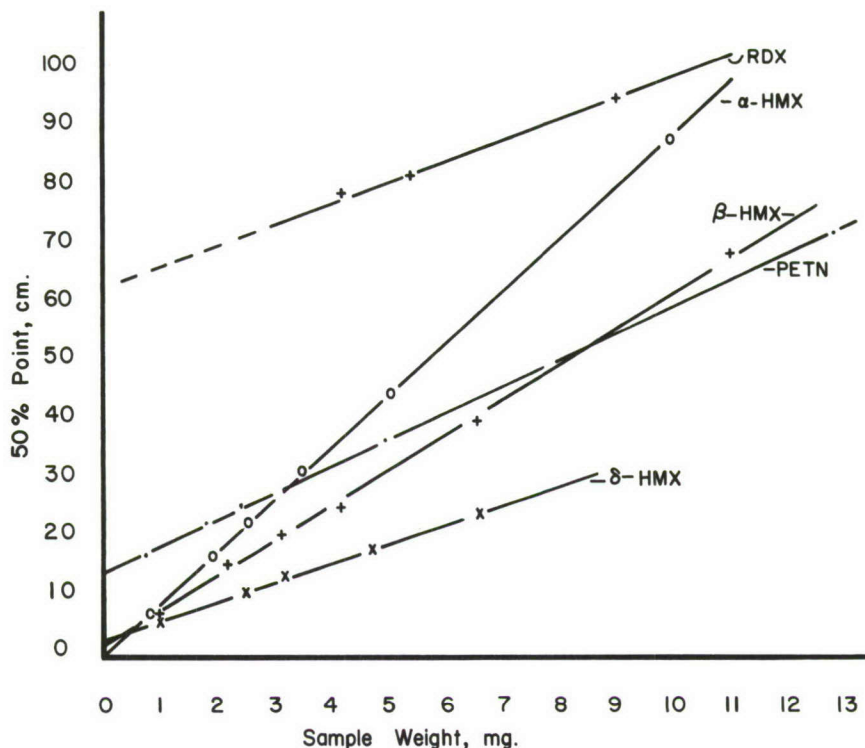


Figure 3. Impact sensitivity for various explosives as a function of sample weight.

It is interesting to consider these curves for a moment. Obviously each explosive has its own slope and often two curves will cross so that reversals in sensitivity occur. Alpha HMX, for example, is more sensitive than PETN for sample weights below about 3.3 mg, and less sensitive for larger samples. We think this difference in slope is a function mostly of the specific heat of the explosive: A high specific heat corresponding to a high slope. We don't know what the positive intercept means. It could be partly a machine characteristic since all of the drop-height energy doesn't contribute directly to the explosion. It could also be a result of inaccurate data at low weights of sample or it could be, partly at least, a result of the mechanical loss of some of the explosive on impact. This would differ with the brittleness, particle size, etc. of the explosive and would be worse at high impact levels.

In any case, the weight of sample must be controlled and we have chosen 6 mg. as our standard weight of sample. Table II shows

the sensitivities of some of our standard samples under this weight restriction.

Table II
Impact sensitivities of several standard
explosives measured with 6 mg. samples

Explosive	50% Point, cm.
RDX	85
-HMX	54
-HMX	45
PETN	42
-HMX	38
-HMX	23

Let us emphasize immediately that these data represent the relative sensitivities of these particular samples of these explosives only. Many samples of δ - and γ -HMX, and even α -HMX fire as low as 23 cm.; β -HMX and some α -HMX samples fire at 40 cm. The sensitivity of all the HMX polymorphs varies considerably from sample to sample depending on crystal size and habit as well as lattice strain.

Once we had settled on 6 mg. samples we expected our results to be completely consistent forever after. Such was not the case. In May this year it was noted that PETN was again misbehaving and the following data were reported in Table III.

Table III
Variation in 50% point for PETN

Date	50% point, cm.
February 25, 1963	41
May 8	53
May 10	49
May 22	47

A similar set of data was obtained for a sample of β -HMX (Table IV).

Table IV
Variation in 50% point for β -HMX

Date	50% point, cm.
February 21, 1963	35
March 26	40
April 23	46
May 8	49
May 10	53
May 15	45

One or two clues exist in these data: 1) the two samples are roughly parallel in behavior, and 2) the sensitivity was lower in the winter than in the spring. We concluded from the first clue that the effect was real and from the second that it was weather dependent. Since our machine is in the laboratory at a constant 75° F all year and with air conditioning from about May 15 on we elected to consider relative humidity as the variable causing the observed variation. Figure 4 is the result. The excellent relationship clearly substantiates the reality of the effect of relative humidity on impact sensitivity. Each data point is labeled with the date of measurement. The good fit of these data taken over nearly a six month period suggests that no other variables of consequence remain and that this machine can now be used for the direct comparison of one explosive with another. At present, we are correcting all data to a 6 mg. sample and 50% relative humidity. We have chosen a middle value of relative humidity because we suspect this effect to be surface, and therefore particle size, dependent. The range of 50% points for coarse particles should be less on this basis than the range for fine particles and maybe some day we'll learn more about this.

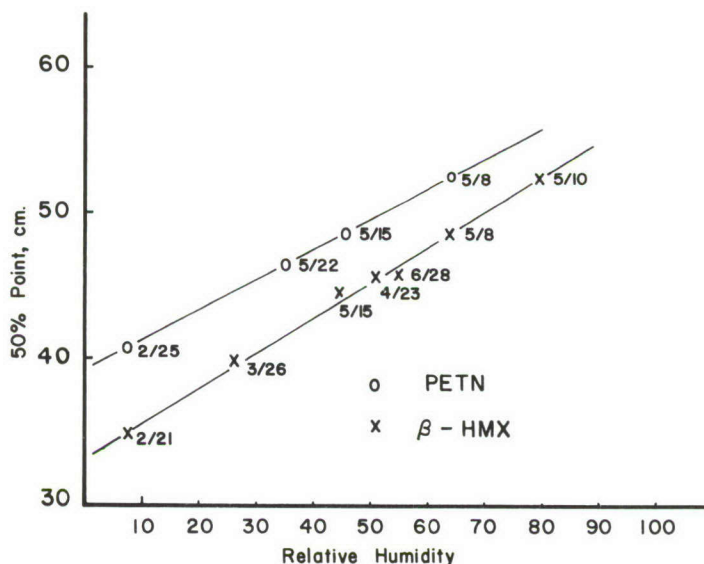


Figure 4. Effect of relative humidity on the impact sensitivity of PETN and β -HMX.

Most of the sensitivity data was taken by Anna Teetsov though Warner Hudson took some of the early weight variation data. Frequent discussions with Jack Dodd from the Arkansas Polytech and a consultant to us on several projects were most helpful and finally, the work was supported in part by the Navy Bureau of Weapons through Hercules Powder Co. and Allegheny Ballistics Laboratory.

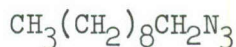
INFRARED STUDIES OF ORGANIC AZIDES

by

Eugene Lieber and C. N. R. Rao
Roosevelt University
Chicago, Illinois

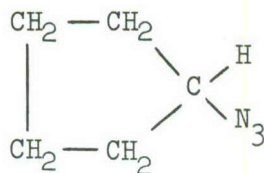
At the Eleventh Basic Research Group Contractors Conference, Lieber and coworkers¹ (superscripts are to references at end section) presented the results of their detailed studies on the infrared spectroscopy and configuration of the azido group. These studies were mainly concerned with the anomalous splitting of the bands due to the asymmetric and symmetric stretching of the azido group. A manuscript entitled INFRARED SPECTRA OF ACID AZIDES, CARBAMYL AZIDES AND OTHER AZIDO DERIVATIVES: ANOMALOUS SPLITTINGS OF THE N₃ STRETCHING BANDS and containing the detailed experimental data obtained in previous investigations has been published². The present investigation has carried out further studies on the infrared spectra of organic azides with particular reference to the band splitting.

The infrared spectra of organic azides of relatively simple structure were reexamined. Aliphatic and alicyclic azides do not show the band splittings. Thus, n-decyl azide (I):



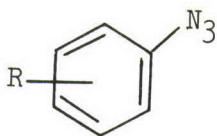
I

and cyclopentyl azide (II):



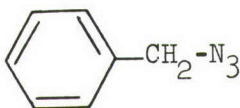
II

were prepared and the infrared spectra taken. They did not exhibit band splitting. On the other hand, a series of substituted phenyl azides (III)



III

All showed splittings of the azide asymmetric stretching bands. On the other hand, when the azido group is insulated from the benzene ring by a methylene group (CH_2), as in benzyl azide (IV):



IV

the azide stretching bands are found as singlets. The data obtained are summarized in Table I.

Table I
Important Infrared Frequencies of Organic Azides, RN_3

R	ν_1^{asym}	ν_2^{sym}	ν_x	ν_y	$2\nu_y$	δ_{N_3}
$n\text{-C}_4\text{H}_9$	2092	1263	-	-	-	-
$n\text{-C}_{10}\text{H}_{21}$	2041	1242	-	-	-	-
cyclo- C_5H_{11}	2037	1245	-	-	-	-
$\text{C}_6\text{H}_5\text{CH}_2$	2037	1242	1190	1068 1022	2136 2044	-
C_6H_5	2110 2089*	1291 1279*	1172 1126	1070 1024	2140 2048	669
$p\text{-CH}_3\text{C}_6\text{H}_4$	2053 1996*	1280 1271* 1245*	1120 1109	1032 1011	2064 2022	694
$p\text{-Br C}_6\text{H}_4$	2066 2033*	1280 1258*	1166 1119	1063 1003	2126 2006	689
$m\text{-ClC}_6\text{H}_4$	2141* 2096	1290* 1285	1159 1139	1092 1073	2184 2146	673
$p\text{-NO}_2\text{C}_6\text{H}_4$	2123 2096*	1299* 1287	1176 1110	1079	2158	681

*Appears as a shoulder or a less intense peak.

These results clearly demonstrate THAT THERE IS AN INTERACTION BETWEEN THE AZIDO-GROUP VIBRATIONS AND THE C-N STRETCHING VIBRATIONS. The assignments are made as follows: In the case of phenyl and substituted phenyl azides (III), in addition to the asymmetric (ν_1) and symmetric (ν_2) stretching vibrations, relatively intense bands are found in the regions 1110-1190 cm^{-1} (ν_x) and 1030-1070 cm^{-1} (ν_y). ν_x is probably associated with phenyl-N stretching and ν_y probably arises from a substituent sensitive aromatic ring vibrations in phenyl azides. All the substituted phenyl azides show weak absorption around 680 cm^{-1} due to N_3 bending vibration (δ). The aliphatic and alicyclic azides do not show absorption in these regions (ν_x and ν_y). Benzyl azide (IV) shows absorption in the region ν_x and ν_y , but the N_3 asymmetric and symmetric stretching bands appear as sharp single bands. DIRECT CONJUGATION OF THE AROMATIC RING WITH THE AZIDO-GROUP IS NECESSARY FOR SPLITTING. Further aspects of this conclusion are considered below.

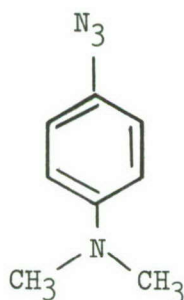
The splitting of the azide asymmetric stretching bands of phenyl azides of structure (III) may be due to the interaction of the fundamental with the combination tone ($\nu_x + \nu_y$) or the first overtone $2\nu_y$. The latter appears more likely. The splitting of the symmetric stretching bands may possibly be due to interaction with the first overtone of the azide bending mode ($\sim 680 \text{ cm}^{-1}$).

The magnitude of the azide band splitting in para-substituted phenyl azides (V):



V

IS STRONGLY DEPENDENT ON THE ELECTRICAL PROPERTY OF THE PARA-SUBSTITUENT (R in structure V). For example, para-dimethylaminophenyl azide (VI) shows maximum splitting, while para-nitrophenyl azide (VII) shows the least splitting. The dependence of the



VI



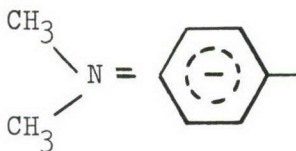
VII

The nitro-group (O_2N^- as in VII) is an electron withdrawing group and as such tends to deplete the electron density of the benzene ring, represented diagrammatically as follows (VIII)



VIII

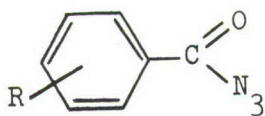
On the other hand, the dimethylamino-group ($(\text{CH}_3)_2\text{N}-$ as in VI) is an electron denoting group and as such tends to increase the electron density of the benzene ring, represented as follows (IX):



IX

In all cases, the transposition of a methylene group ($-\text{CH}_2-$) markedly diminishes the transmission of electrical effects to the azido group. The dependence of the magnitude of band splittings on the nature of the substituent is similar to that found in the case of the aryl carboxylic acid azides (X) discussed below.

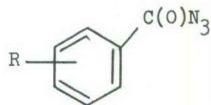
While the splittings of N_3 stretching bands have been examined in detail by Lieber and co-workers^{1,2}, the data obtained were of a qualitative or semi-quantitative nature. The extension of this aspect of the investigation has, accordingly, been directed to the quantitative aspects of the band splittings for a series of substituted benzazides (X):



X

The data obtained are summarized in Table II.

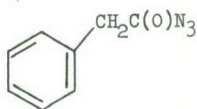
Table II
Quantitative Data on the Asymmetric
Stretching Band of Acid Azides



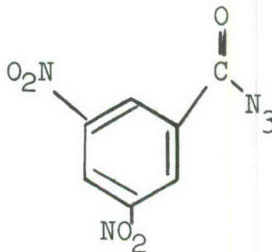
<u>R</u>	<u>ν_{\max}</u>	<u>ϵ_{\max}^a</u>	<u>$\Delta \nu_{\frac{1}{2}} (\text{cm}^{-1})$</u>
4-CH ₃ O ⁻	2193* 2137	78.9 353.6	53 10
H-	2179* 2141	132 412	38 18
4-O ₂ N ⁻	2193 2146	77.5 185.3	36 19
3,5-di-O ₂ N ⁻	2227 2165	55 295	25 28
**	2143	303.9	15

* Appears as a shoulder or a less intense peak.

** Compound is:

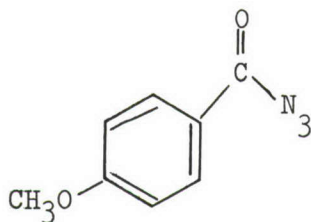


The molecular extinction coefficients of the bands were determined by keeping the concentrations of X nearly the same in order to minimize errors. Maximum separation between the peaks and perturbation of band intensity was observed for the 3,5-dinitro derivative (XI):



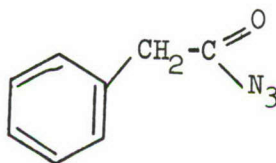
XI

Indeed, the extent of splitting of ν_1 (asym), varied with the nature and position of R in structure X, interaction being greatest in the case of groups which decrease the electron density of the benzene ring (VIII) and least for the groups which increase the electron density of the benzene ring (IX). On the other hand the band intensity of the principle ν_1 (as measured by ϵ max) is highest for the para-methoxy derivative (XIII):



XIII

corresponding closely to that of benzyl azide (XIV) which shows no ν_1 band splitting:



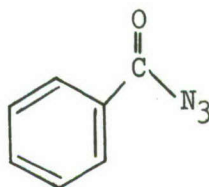
XIV

In addition to the data recorded in Table II, the azide asymmetric stretching band of benzazide (R = H in structure X) was quantitatively recorded in chloroform as well as carbon tetrachloride. There was little or no difference between the spectra, indicating that band splitting is not very sensitive to solvents (see also: Proceedings of the 9th Annual Base Research Contractors Conference, 4-7 October 1960, page 275). The ϵ^a values of the N_3 asymmetric stretching bands in chloroform and carbon tetrachloride are quite close. The data obtained are summarized in Table III.

Table III
Extinction Values of Benzazide
(I, R = C_6H_5) in Different Solvents

Solvent	ϵ^a of the peak at	
	2141 cm^{-1}	2179 cm^{-1}
Carbon Tetrachloride	490	120
Chloroform	412	132

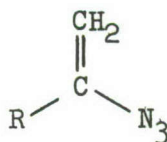
An important phase of the present investigation comprised the determination of the infrared spectra at low temperatures concentrating on the azide asymmetric stretching band. After considerable effort a suitable low temperature cell was devised. Benzazide (XV; R = H in structure X)



X

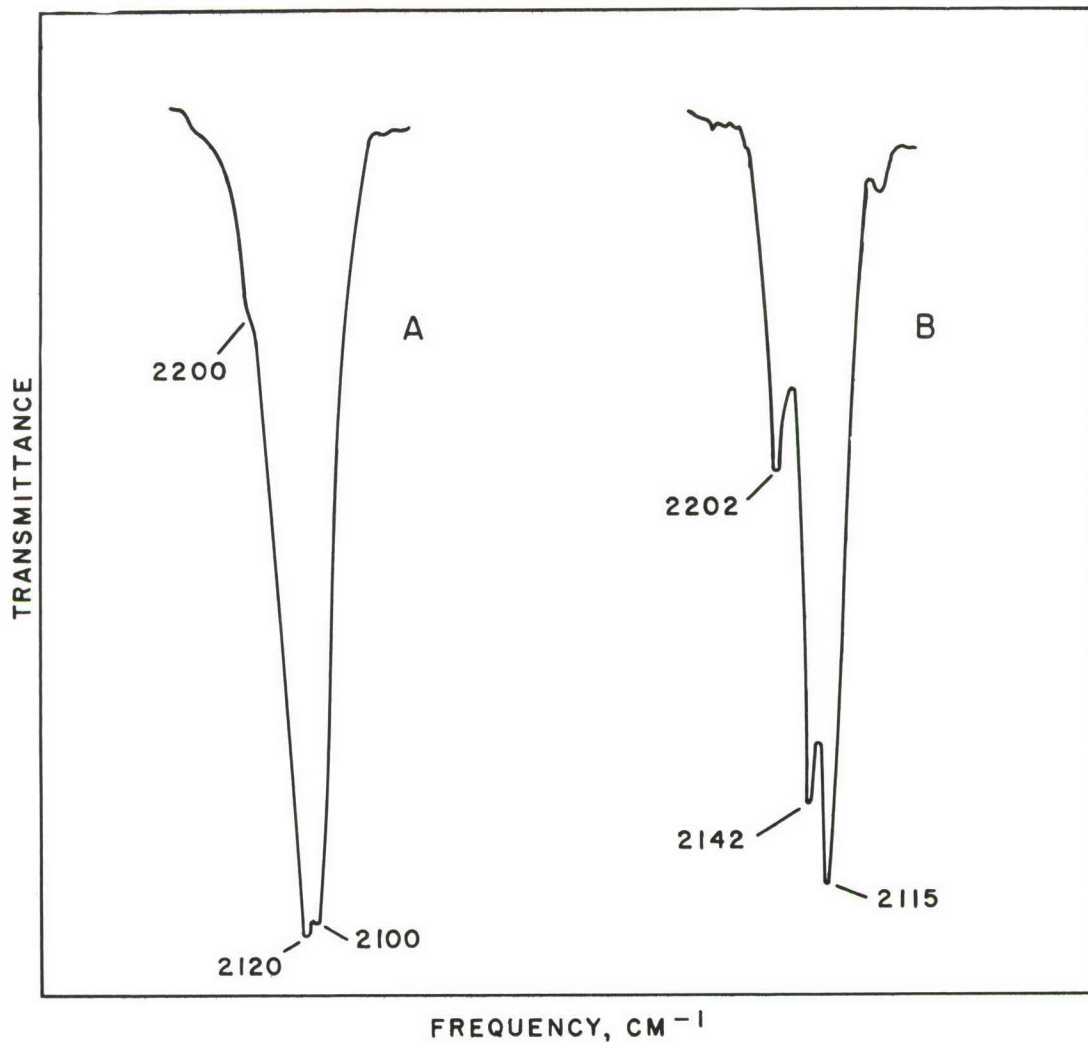
was chosen for the initial studies. The sample of benzazide was prepared in the pellet form employing potassium bromide as the matrix material. The spectra were recorded using dry ice-acetone and liquid air as refrigerants. The accuracy of the temperature control is estimated to be $\pm 10^\circ$ K, due to imperfect contact between the thermocouple and the effective absorbing region of the sample. IT WAS FOUND THAT THE BAND SPLITTING PERSISTS WITHOUT LOSS OF INTENSITY TO 125° K (the lowest temperature studied thus far) AND THAT THE SPECTRA AT 298° K, 220° K AND 125° K WERE PRACTICALLY SUPERIMPOSABLE. The results demonstrate, that whatever the mechanism of band splitting may be, that it is insensitive to temperature.

Dr. G. Smolinsky, of the Bell Telephone Laboratories, Murray Hill, N. J., has kindly furnished us the infrared absorption spectral maps of two specimens of vinyl azides having the structure (XV):



XV

where R is n-butyl (C_4H_9 -) and phenyl (C_6H_5). Both of these derivatives show splitting of the asymmetric stretching band of the azide group. The phenyl derivative (XV, R = C_6H_5) shows the splitting of the asymmetric stretching band of the azide group to a triplet THE FIRST OBSERVATION OF THIS TYPE. This is illustrated in the accompanying figure, showing the sharp contrast in band splitting between the n-butyl derivative (XV, R = C_4H_9 -) and the phenyl derivative. The assignments for the important bands are given in Table IV. It is suggested that the splitting is due to Fermi interaction of ν_1



The Asymmetric N₃ Stretching Band of (A) n-butyl vinyl azide (XV, R = n-C₄H₉-) (B) styryl azide (XV, R = C₆H₅)

with ($\nu_3 + \nu_4$) or ($\nu_4 + \nu_x$). The 940 and 1028 cm^{-1} bands (ν_x) are probably due to the C-C stretching vibrations.

Table IV
Important Frequencies (in cm^{-1}) of Vinyl Azides (VIII)(a)

<u>R</u>	<u>2 ν_4 or ($\nu_3 + \nu_4$)</u>	<u>ν_1</u>	<u>ν_2</u>	<u>ν_3</u>	<u>ν_4</u>	<u>ν_x</u>
n-C ₄ H ₉	2485 2440	2100 2120 2200	1627	1275	1225	940
C ₆ H ₅	2505 2440	2115 2142 2202	1612	1297	1223	1028 905

(a) ν_1 , N₃ asymmetric stretching; ν_2 , C=C stretching;
 ν_3 , C-N stretching; ν_4 , N₃ symmetric stretching and
 ν_x , other bands.

Conclusions

The present investigation has demonstrated that all unsaturated or conjugated azides show splitting of the azide stretching bands. The extent of splitting varies with the nature of the group (or groups) adjacent to the azide, the interaction being greatest for groups which decrease the electron availability to the neighboring azido group. The intensity of the ν_1 principal band, on the other hand, is highest when groups which increase electron availability are adjacent to the azido group. Further, the splitting is independent of nature of solvent and of temperature. These conclusions support the hypothesis^{3,4} of the important contribution of the "bent structure" of the azido-group. The recent quantitative study by Roberts⁶ of the energy difference between the linear and bent state of the azide group also offers firm support, while intramolecular vibrational effects appear to satisfactorily explain the origin of the band splittings, it does not explain "why" these effects vary with the structural environment of the molecule (see Figure).

References

1. Proceedings of the Eleventh Basic Research Group Contractors Conference, USAERDL, Department of the Army, U. S. Army Mobility Command, Fort Belvoir, Virginia, 30 October - 1 November 1962, page 139.
2. Lieber, et.al., Spectrochimica Acta, 19, 1135 (1963).
3. See reference 1, page 143.
4. Proceedings of the Tenth Basic Research Group Contractors Conference, USAERDL, Department of the Army, Corps of Engineers, Fort Belvoir, Virginia, 24-26 October 1961, page 52.
5. Lieber, Technical Report "Investigations Concerning the Possible Existence of N, N₂ and N₃ Radicals," Contract No. DA-44-009 ENG-4142, Project No. 8-07-11-440, ERDL, Fort Belvoir, Virginia, 1 July 1961, page 50.
6. Roberts, J. D., Chem. Ber., 94, 273 (1961).

AZIDO-COMPLEXES IN NON-AQUEOUS SOLUTIONS

by

V. Gutmann, G. Hampel and O. Leitmann

Technical University

Vienna, Austria

It has been shown that coordination equilibria between metal ions and chloride ions can be followed in non-aqueous solutions. Analogous studies on azide ions have not been reported and seemed to be of interest in order to

1. establish the species formed in solution
2. determine their formation constants and
3. compare the stabilities of azide complexes with those of the halide complexes.

The present investigation deals with spectrophotometric measurements on cobalt and copper (II) perchlorate with azide ions in certain non-aqueous solutions.

The solvent should have a reasonable dielectric constant in order to allow the formation of ionic species and also reasonable donor properties. Qualitative observations on the solubilities of sodium and potassium azides in various solvents have shown that dimethylformamide, dimethylsulfoxide, trimethyl phosphate and acetonitrile may be used as solvents. Conductometric studies showed somewhat higher conductivities for potassium azide than for sodium azide. It proved unfortunate that the former could not be used in the present spectrophotometric studies since insoluble potassium perchlorate was formed.

The tetraalkylammonium azides were prepared by reacting the respective hydroxide with hydrazoic acid. After recrystallization from organic solvents, they were obtained as colorless crystals which could be melted without any apparent signs of decomposition. Tetraalkylammonium azide was used in the first place in this study, the conductivity of which in some solvents is shown in Table I.

The anhydrous perchlorates were obtained by reacting anhydrous cobalt- or copper chlorides in the solvent under investigation with silver perchlorate. Silver chloride was precipitated and removed by filtration. The solutions contained the metal cations probably in the hexasolvated form. On addition of tetraethylammonium chloride as a chloride ion donor in trimethyl phosphate as a solvent the

Table I
Specific Conductivities at 10^{-3} mol/l [$\text{cm}^{-1}\Omega^{-1}$]

solvt. salt	TMP	AN	DMSO
Et_4NCl	$3,23 \cdot 10^{-5}$	$1,35 \cdot 10^{-4}$	$4,76 \cdot 10^{-5}$
NaCl	$4,73 \cdot 10^{-6}$	$7,12 \cdot 10^{-6}$	$4,52 \cdot 10^{-5}$
Et_4NN_3	$4,52 \cdot 10^{-5}$	$2,32 \cdot 10^{-4}$	$5,13 \cdot 10^{-5}$
NaN_3	$2,47 \cdot 10^{-5}$	$5,17 \cdot 10^{-5}$	$5,13 \cdot 10^{-5}$

changes of the spectra were followed. At a molar ratio $\text{Co}^{++}:\text{Cl}^- = 1:0.2$ indications for the formation of the solvated octahedral $[\text{CoClL}_5]^+$ ion (L = ligand solvent) were obtained (Figure 1). On further addition of chloride ions the characteristic spectrum of tetrahedral $[\text{CoCl}_2\text{L}_2]$ appeared, which was changed to those of $[\text{CoCl}_3\text{L}]^-$ and $[\text{CoCl}_4]^{--}$ on further successive additions of chloride ions (Figure 2).

In trimethyl phosphate similar results are obtained for the cobalt (II)-azido system (Figures 3 and 4). At a molar ratio $\text{Co}^{++} : \text{N}_3^- = 1:1$, the monoazido complex is formed which appears to be octahedral $[\text{CoN}_3(\text{TMP})_5]^+$. This is converted to tetrahedral $[\text{Co}(\text{N}_3)_2(\text{TMP})_2]$ by further addition of azide ions. Figure 4 shows that a molar ratio of $\text{Co}^{++} : \text{Et}_4\text{NN}_3 = 1:4$ is sufficient to produce the spectrum of the tetraazido complex ion, which is also achieved by adding an excess of sodium azide. The sodium azide provided a smaller concentration of free azide ligands than did the equivalent amount of tetraethylammonium azide.

In a similar way reactions of copper (II) solutions were investigated in anhydrous trimethylphosphate. The $[\text{CuCl}]_{\text{sv}}^+$ is formed by adding an equimolar amount of tetraethylammonium chloride, while with sodium chloride, which is dissociated to a lesser extent a ten-fold excess appears to be necessary (Figure 5). Stoichiometric amounts of tetraethylammonium chloride were found to be sufficient to form copper (II) chloride and trichlorocuprate $[\text{CuCl}_3]^-$.

respectively, but a much larger excess is necessary to completely form tetrachlorocuprate (II) $[\text{CuCl}_4]^{--}$ (Figure 6).

In a similar way the azido-complexes are formed. While a large excess of the sodium salt is necessary in order to form the respective complexes, a stoichiometric amount of the tetraalkylammonium salt is sufficient (Figure 7).

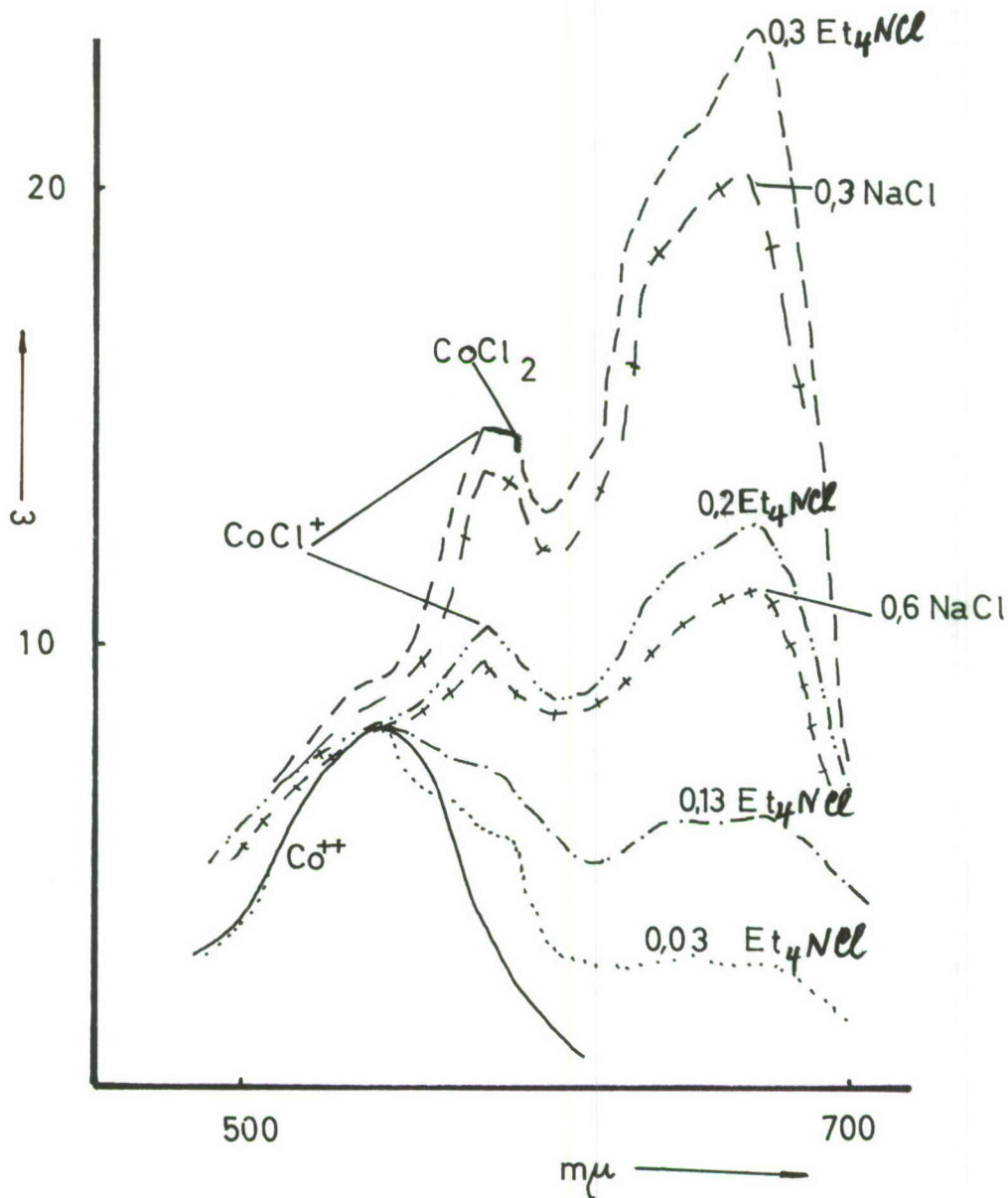


Figure 1. Co (II) chlorosystem in TMP.

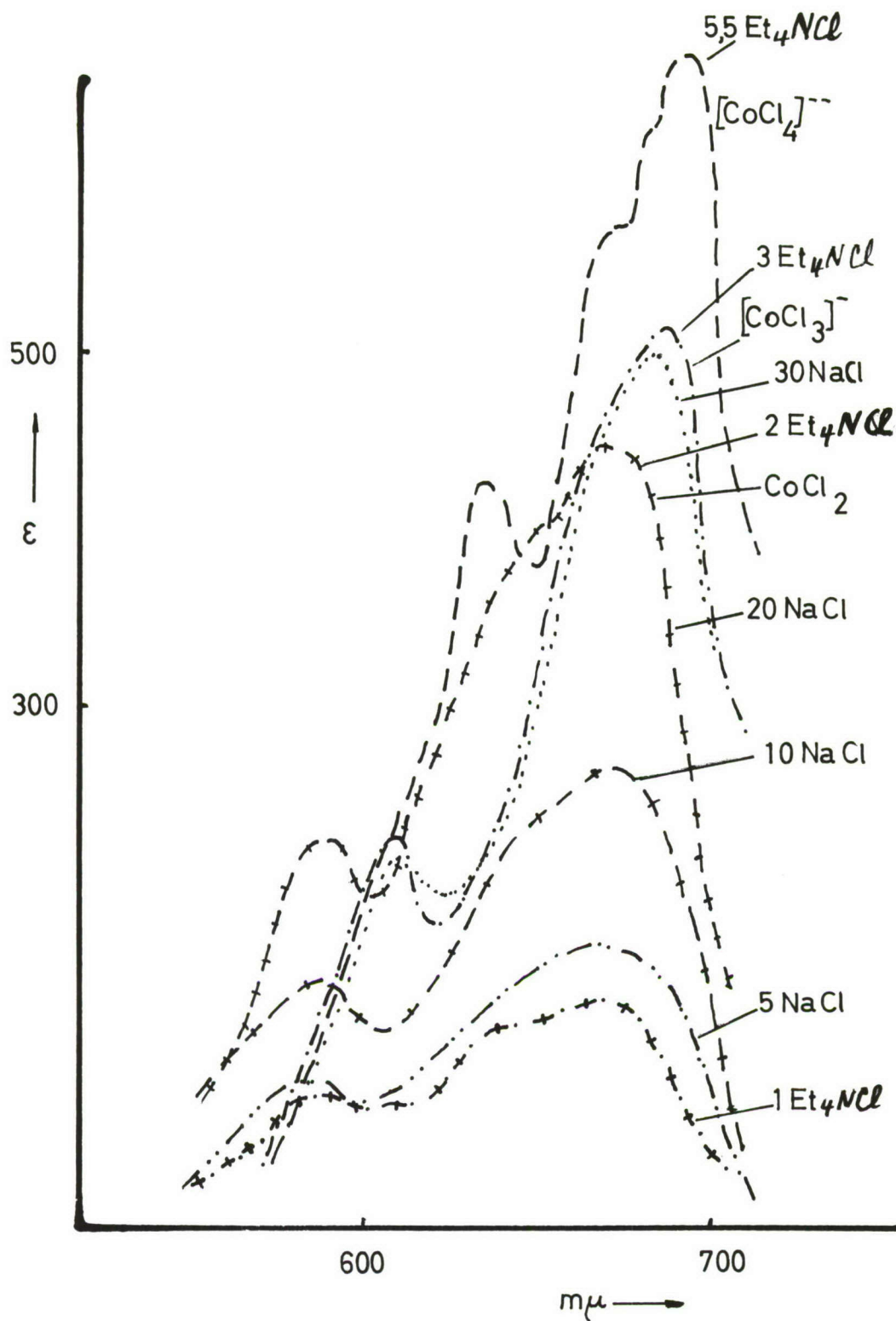


Figure 2. Co (II) chlorosystem in TMP.

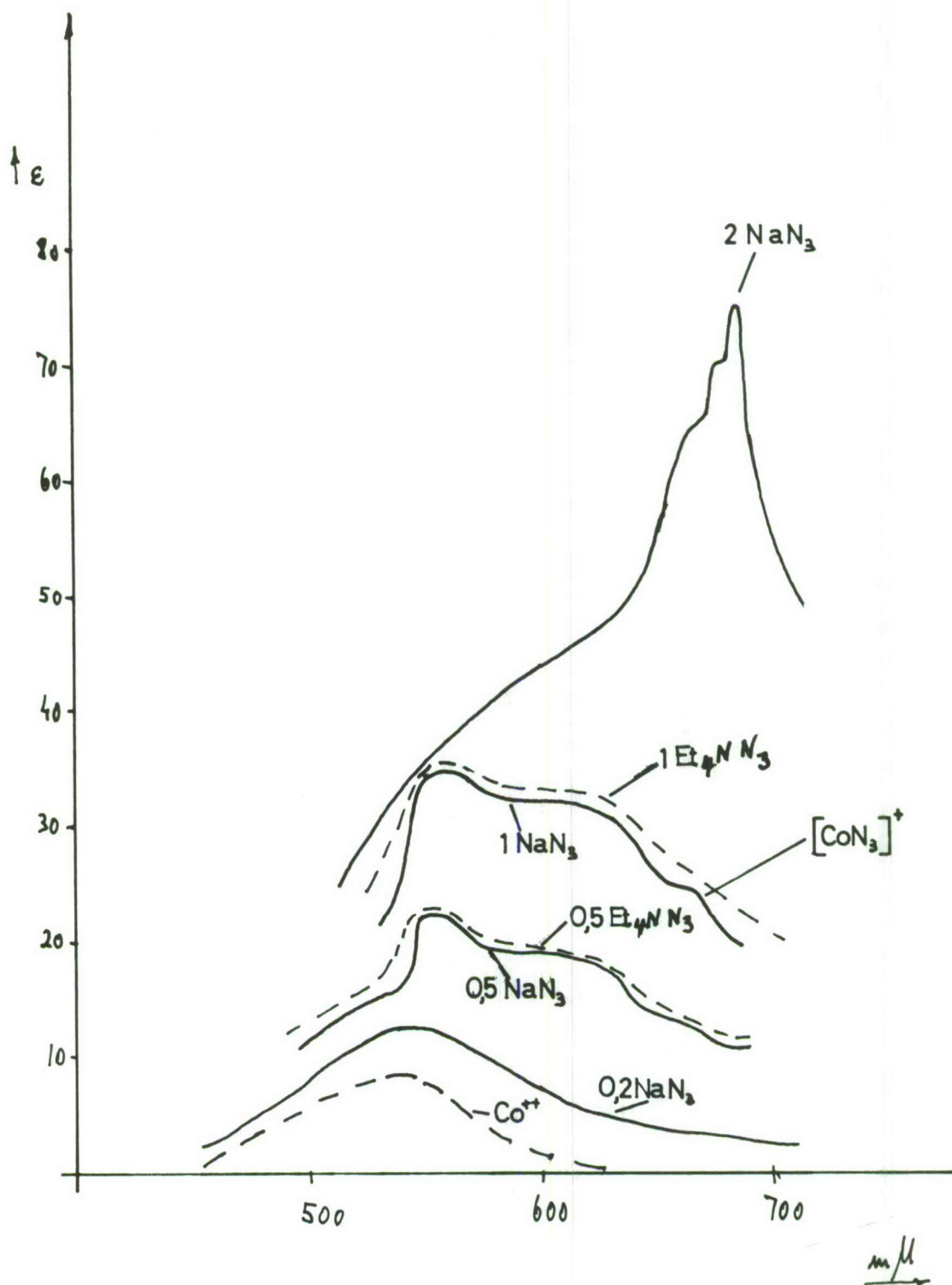


Figure 3. Co (II) azidosystem in TMP.

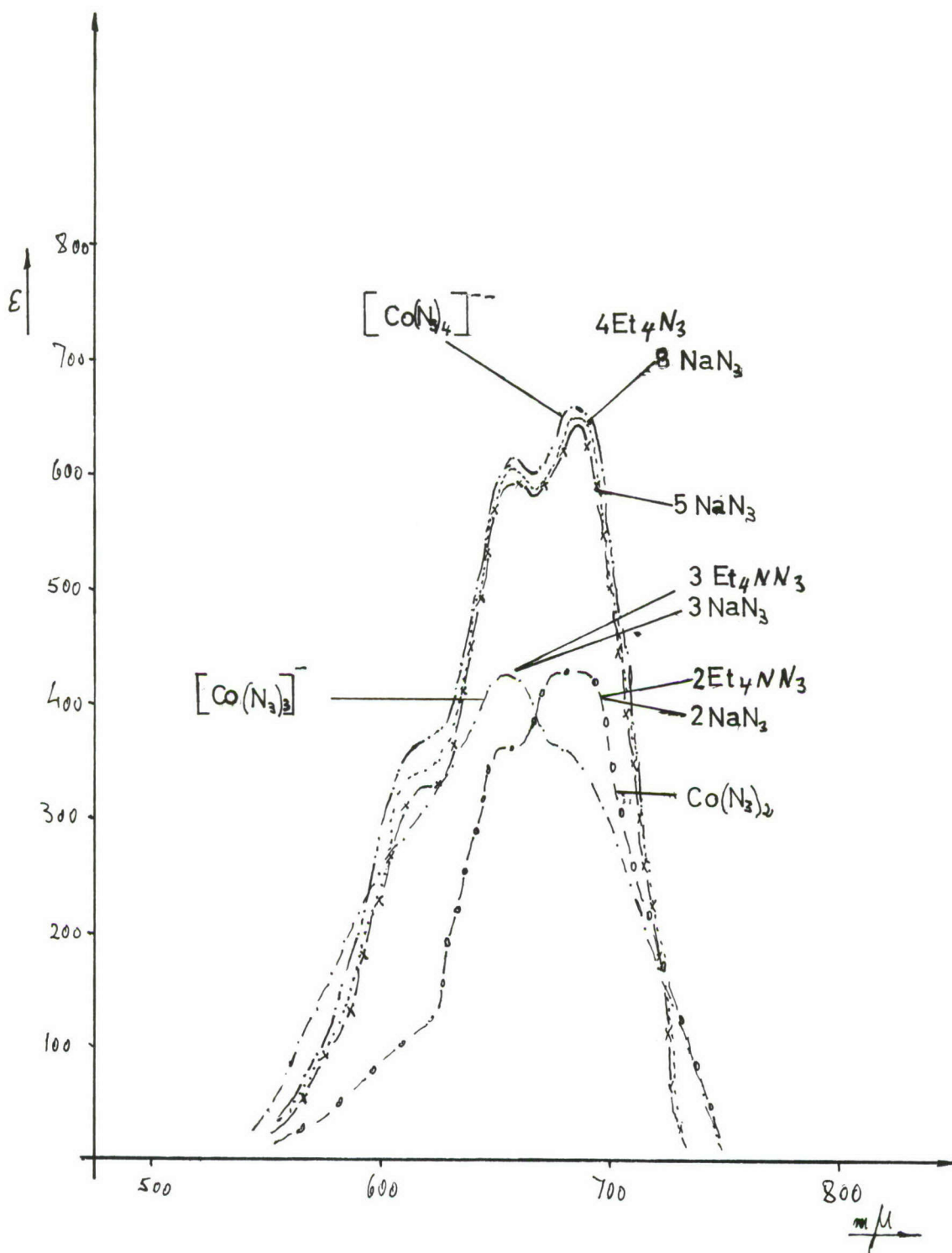


Figure 4. Co (II) azidosystem.

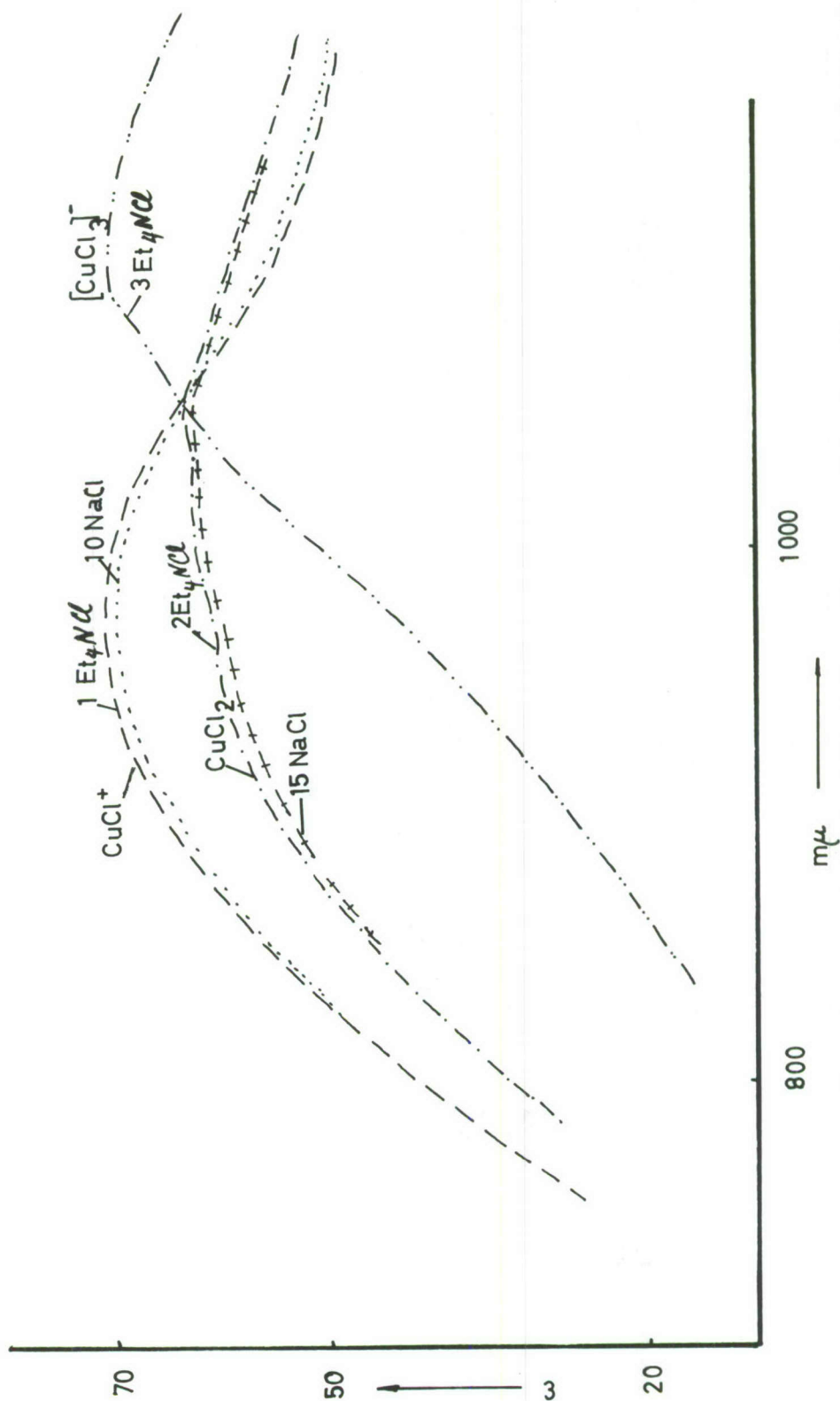


Figure 5. Cu (II) chlorosystem in TMP.

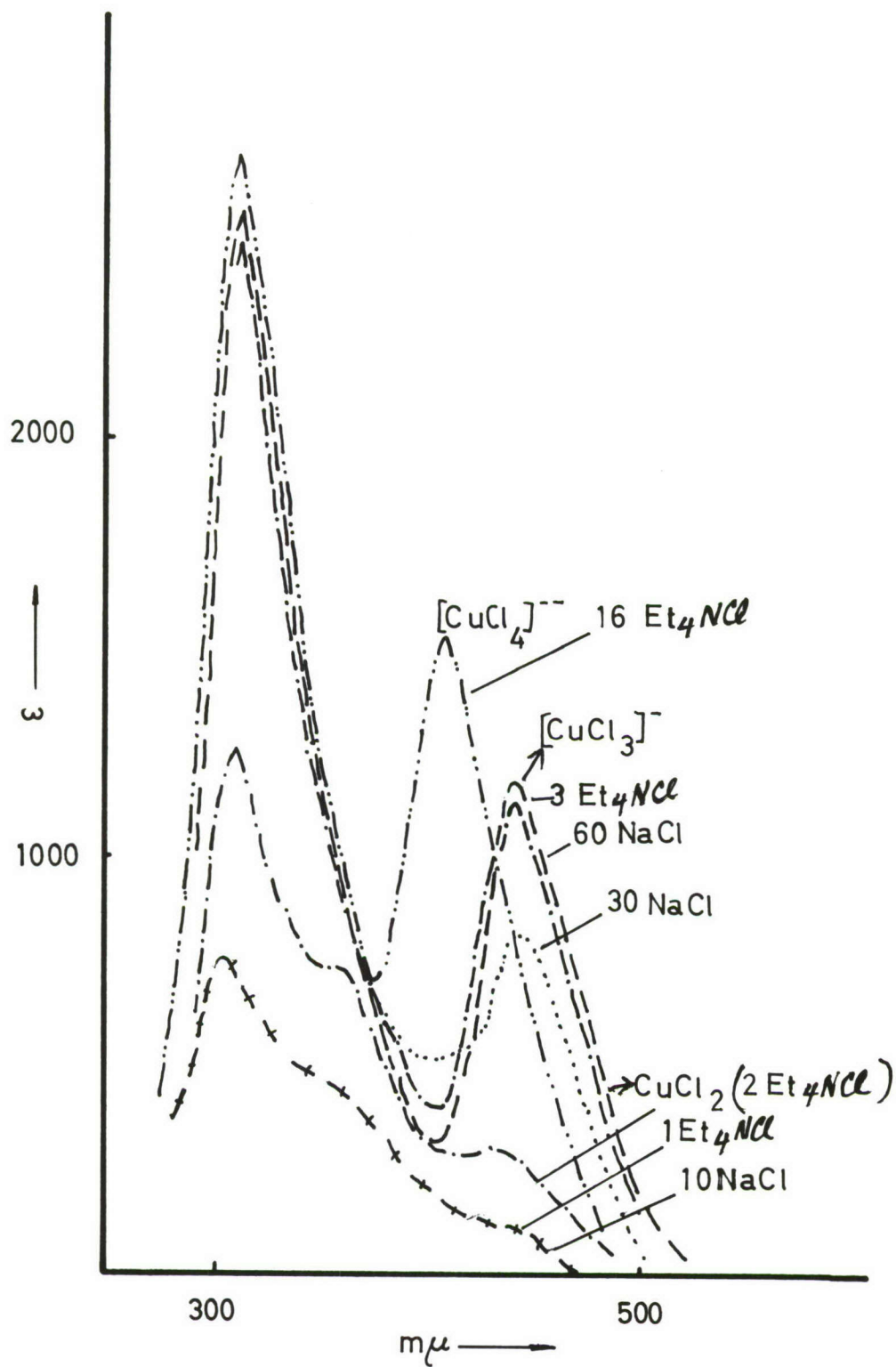


Figure 6. Cu (II) chlorosystem in TMP.

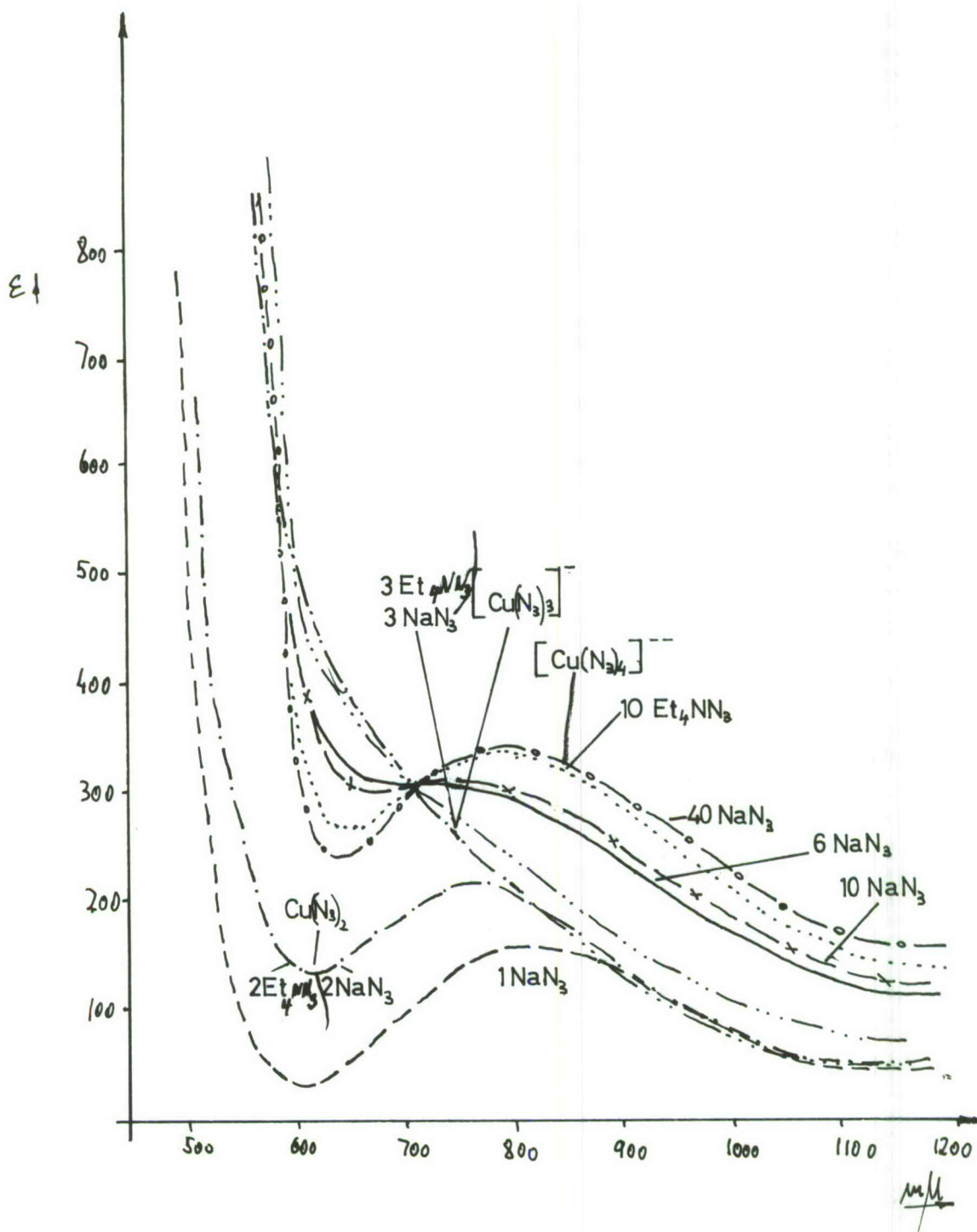


Figure 7. Cu (II) azidosystem in TMP.

Table II gives a comparison of the readiness to form the corresponding chloro- and azido-complexes for cobalt (II). Considering the formation $[\text{CoX}_4]^{--}$, a smaller amount of tetraethylammonium azide is necessary than that of tetraethylammonium chloride, which is an indication that the azido-complexes may be more stable than the chloro-complexes.

Table II
Coordination Forms of Co (II) Chloro- and
Azido-complexes in TMP

	Et_4NCl	NaCl		Et_4NN_3	NaN_3
$[\text{CoCl}]^+$	1	3	$[\text{CoN}_3]^+$	1	1
$[\text{CoCl}_2]$	2	20	$[\text{Co}(\text{N}_3)_2]$	2	2
$[\text{CoCl}_3]^-$	3	30	$[\text{Co}(\text{N}_3)_3]^-$	3	3
$[\text{CoCl}_4]^{--}$	5,5		$[\text{Co}(\text{N}_3)_4]^{--}$	4	8

Table III gives the results for copper (II) compounds from which similar conclusions may be drawn.

Table III
Coordination Forms of Cu (II) Chloro- and
Azido-complexes in TMP

	Et_4NCl	NaCl		Et_4NN_3	NaN_3
$[\text{CuCl}]^+$	1	10	$[\text{CuN}_3]^+$		
$[\text{CuCl}_2]$	2	15	$[\text{Cu}(\text{N}_3)_2]$	2	2
$[\text{CuCl}_3]^-$	3	60	$[\text{Cu}(\text{N}_3)_3]^-$	3	3
$[\text{CuCl}_4]^{--}$	16		$[\text{Cu}(\text{N}_3)_4]^{--}$	10	40

Finally, Table IV contains the stability constants of chloro-complexes, but analogous figures for the azido-complexes have not been obtained due to lack of data of the free ligand azide concentration. However, by comparing the conductivities of solutions of tetraethylammonium chloride and tetraethylammonium azide, the conclusion seems justified that formation constants of the azido-complexes will be somewhat higher than that for the chloro-complexes.

Table IV
Stability Constants of Co (II) and
Cu (II) Chlorocomplexes in TMP

k_1	$[\text{CoCl}]^+$	$5.0 \cdot 10^6$	$[\text{CuCl}]^+$	$5.5 \cdot 10^6$
k_2	$[\text{CoCl}_2]$	$3.0 \cdot 10^5$	$[\text{CuCl}_2]$	$3.7 \cdot 10^4$
k_3	$[\text{CoCl}_3]^-$	$1.3 \cdot 10^4$	$[\text{CuCl}_3]^-$	$3.6 \cdot 10^3$
k_4	$[\text{CoCl}_4]^{--}$	$1.4 \cdot 10^3$	$[\text{CuCl}_4]^{--}$	$1.1 \cdot 10^3$

INFRARED SPECTROSCOPIC EVIDENCE FOR THE SPECIES NH^*

by

Dolphus E. Milligan and Marilyn E. Jacox
National Bureau of Standards
Washington, D. C.

The matrix isolation technique, first applied to infrared observations by Pimentel and coworkers^{1,2}, has been particularly useful for the study of the photolysis of simple azides. Using this technique, a dilute gaseous mixture of the species of interest in a diluent such as argon or nitrogen is frozen on a cold window, typically at 4 or at 20° K. The infrared spectrum of the resulting film is characterized by sharp absorptions, since in most such samples the molecules are no longer free to rotate and since association with like molecules is minimized. The sample is photolyzed using a medium-pressure mercury arc, and the infrared spectrum of the product species is scanned. Photolysis of various azides suspended in a matrix environment has been found to be relatively efficient, since molecular nitrogen is characteristically eliminated, and there is a high activation energy for recombination.

Becker, Pimentel, and Van Thiel^{3,4} have extensively studied the photolysis of HN_3 suspended in Ar and N_2 matrices at 20° K. They reported NH_3 , NH_4N_3 , and incompletely characterized species with infrared absorptions at about 1290 and 1325 cm^{-1} among the products of the photolysis.

Milligan⁵ has found that the photolysis of CH_3N_3 in a matrix produces in good yield the previously unobserved species $\text{CH}_2=\text{NH}$. Milligan and Jacox⁶ have studied this system after prolonged photolysis and have identified the species HNC , also unstable under ordinary conditions. Milligan and Jacox⁷ have also studied the matrix isolation spectra of FN_3 , ClN_3 , and BrN_3 and of their respective infrared-active photolysis products, NF , NCl , and NBr . In supplementary attempts to observe the ultraviolet spectrum of NF , an absorption was observed near 3360 Å. This band has been found to be associated with the $^3\Pi_1 - ^3\Sigma^-$ transition of NH , demonstrating the presence of NH ($^3\Sigma^-$) in the system. Since this species must have arisen from the photolysis of excess HN_3 present in the preparation of the FN_3 , it appeared worthwhile to make further observations on the photolysis of matrix-isolated HN_3 .

* Partial support by ARPA (Order No. 395, Project Code No. 3910) and by AFOSR (Contract No. AF 49(638)542) is gratefully acknowledged.

The high resolution infrared spectrometer (Beckman IR-9) used for the present experiments, together with improved thermal contact between coolant can and cold window, have been essential factors in the infrared identification of NH. The NH_3 and NH_4N_3 found in the earlier experiments were not observed in the present experiments. In experiments using Ar or N_2 matrices, at either 4 or 20° K, a weak absorption has been observed following photolysis at 3137 cm^{-1} . This absorption does not diminish on prolonged photolysis, as the 1290 and 1325 cm^{-1} peaks do. When a sample enriched to 97% $\text{H}(\text{N}^{15}\text{N}^{14})_2$ is photolyzed, peaks of equal intensity appear at 3130 and 3137 cm^{-1} . The calculated isotopic shift is 7.5 cm^{-1} . A peak at $2323 \pm 2\text{ cm}^{-1}$ appears following photolysis of an Ar:DN₃ sample. The new peak disappears when the sample is warmed to a temperature at which diffusion through the matrix can occur.

From his studies of the ultraviolet absorption spectrum of NH produced by the flash photolysis of gaseous HNCO , Dixon⁸ has estimated the vibrational constant of NH ($3\Sigma^-$) as 3125.6 cm^{-1} . Thus, the weight of evidence appears to support the assignment of the 3137 cm^{-1} absorption to ground state ($3\Sigma^-$) NH. Since spin conservation requires that NH be initially produced in an upper singlet state, ready collisional deactivation of this species must occur in the matrix. Corresponding to the vibrational fundamental at 3137 cm^{-1} , the force constant for NH would be 5.41 mdyn/\AA .

It is noteworthy that two distinct phosphorescences have been observed when irradiation of an Ar:HN₃ or of a N_2 :HN₃ sample is interrupted. During the first few minutes, a purple glow is seen. This purple glow has not yet been successfully photographed. After about five minutes of photolysis, the purple glow is supplanted by a green glow which has been identified as arising from the N atom $2D - 4S$ transition near 5229 \AA . Since the spectral output of the mercury discharge (AH-4) is insufficient to dissociate N_2 , the source of these N atoms deserves further consideration.

Beckman and Dickinson⁹ have established that the primary photolytic reaction in the gas phase photolysis of HN_3 is



The high intensity photolysis studies of Thrush¹⁰ on HN_3 also yielded a diffuse ultraviolet absorption which may be associated with the species N_3 , which Thrush suggested might be formed by the secondary reaction



It is possible that some N_3 is produced in the matrix by this mechanism, and that this N_3 may be a source of N atoms upon either

spontaneous or photolytic decomposition.



However, the matrix isolation in the present experiments is such that reaction (2) could occur to an appreciable extent only during the early stages of photolysis, when an appreciable number of HN_3 molecules are situated on adjacent or nearly adjacent sites. Hence, it is necessary to consider other photolytic reactions by which N atoms may be produced. One possible reaction is



Since the NH intensity does not appear to diminish on prolonged photolysis, reaction (4) appears to be a relatively unlikely source of N atoms. It is also possible that photolytic decomposition of HN_3 according to reaction (5) occurs to a small extent.



followed by reaction (3).

Since HN_3 and HNCO are isoelectronic, some parallels in their behavior on photolysis may be possible. Dixon¹¹ has observed NCO in good yield in the same experiments in which he produced NH by the flash photolysis of gaseous HNCO . Although the predominant primary photolytic reaction is known to produce $\text{NH} + \text{CO}$, possibly some of this NCO may have been produced by the analog of reaction (5). Our recent studies of the photolysis of HNCO in Ar and N_2 matrices have led to the identification of five of the six vibrational fundamentals of the previously unobserved tautomer, HOCN . Experiments on DNCO have provided confirmation of this identification. Unfortunately, it is not certain whether HOCN results from the recombination of matrix-isolated $\text{H} + \text{NCO}$, as we have found that both HNCO and HOCN appear when NH (produced by the photolysis of HN_3) reacts with CO in a matrix. Very little CO results from the matrix photolysis of HNCO , and no NH has been observed. However, in view of the relatively low activation energy for the recombination of NH with CO, infrared observation of NH in this system would not be anticipated.

In summary, evidence has been presented supporting the identification of the weak 3137 cm^{-1} absorption appearing following photolysis of matrix-isolated HN_3 as the vibrational fundamental of ground state NH. The observation of N atoms in this system has led to a consideration of possible reactions by which they may be produced.

References

1. E. Whittle, D. A. Dows, and G. C. Pimentel, J. Chem. Phys. 22, 1943 (1954).
2. E. D. Becker and G. C. Pimentel, J. Chem. Phys. 25, 224 (1956).
3. E. D. Becker, G. C. Pimentel, and M. Van Thiel, J. Chem. Phys. 26, 145 (1957).
4. M. Van Thiel and G. C. Pimentel, J. Chem. Phys. 32, 133 (1960).
5. D. E. Milligan, J. Chem. Phys. 35, 1491 (1961).
6. D. E. Milligan and M. E. Jacox, J. Chem. Phys. 39, 712 (1963).
7. D. E. Milligan and M. E. Jacox, To be published.
8. R. N. Dixon, Can. J. Phys. 37, 1171 (1959).
9. A. O. Beckman and R. G. Dickinson, J. Am. Chem. Soc. 50, 1870 (1928); J. Am. Chem. Soc. 52, 124 (1930).
10. B. A. Thrush, Proc. Roy. Soc. (London) A235, 143 (1956).
11. R. N. Dixon, Phil. Trans. Roy. Soc. (London) A252, 165 (1960).

GROUP THEORETICAL ANALYSIS OF THE VIBRATIONAL SPECTRUM OF IMPURITIES IN CRYSTALS

by

L. A. Veguilla-Berdecia and George C. Turrell
Department of Chemistry
Howard University
Washington, D. C.

Introduction

In recent publications, creditable use has been made of the unit cell method of Bhagavantam and Venkatarayudu in interpreting the vibrational spectra of crystals¹. This approach is a special case of a more general method due to Sir C. V. Raman. In 1943 and 1947 Raman and coworkers published a series of papers in the Proceedings of the Indian Academy of Sciences outlining in great detail the rationale of their approach and giving several examples of the application of the method to real systems, e.g., diamond and rock-salt. From their results one might be led into believing that the introduction of the Raman unit cell as the basis for calculations was a "tour de force". However, such is not the case, for Raman himself points out in the opening papers of the 1943 and 1947 symposia that the introduction of the "larger than usual" unit cell for vibrational analysis is a logical consequence of the periodicity of the lattice. When the translational symmetry of the lattice is taken into account, together with the dynamical equations of motion of the system, a substantial simplification results in the calculations of force constants and in the interpretation of the observed lines in the spectra obtained in the laboratory. In order to appreciate the reduction in labor one need only compare the more sophisticated work of Born² on NaCl with the calculations of Raman³ and Ramanathan⁴ on the same system. A critique of these two schools of thought is not intended here, but suffice to say that both approaches lead to usable results⁵. The group theoretical background requirements necessary to the understanding of the Raman method are not unusually high, and in any case they have been admirably presented by Chelam⁶ in papers appearing in the 1943 symposium. Chelam's papers do not seem to have reached many readers.

When the crystal under consideration contains substitutional impurities, it appears that Raman's unit cell method must be entirely forsaken since the periodicity of the lattice has been destroyed by the presence, at a lattice site, of a foreign body. There are indications that this is not the case; the paper presented here intends to show how a simple extension of Raman's ideas leads to a reasonably simple treatment of the vibrational spectrum of crystals

containing impurities. The initial step in this direction was taken by Turrell⁷, who proposed to use the perturbed spectrum of the impurity in a lattice as a "probe" to measure interionic forces. In a formal way, Turrell introduced the factoring of the unit cell group into an orientation group and an impurity group, thus leading to the result that the lattice vibrations can be classified according to the irreducible representations of an effective unit cell group, whereas the internal vibrations of the impurity transform according to the irreducible representations of the impurity group. Since these two sets of irreducible representations are related to each other by the usual correlation diagram, the vibrational selection rules for the entire system can be established in principle. The choice of the inequivalent atoms in Raman unit cell and a suitable potential function is all that is needed to characterize the system completely.

The effect of impurities on the vibrational spectrum of crystals is mainly threefold:

- 1) modification of the distribution of normal mode frequencies,
- 2) appearance of localized modes,
- 3) alteration of the atomic displacements in the neighborhood of the impurities.

The exact manner in which these effects occur has been thoroughly discussed by Montroll et al.⁸, Asahi and Hori⁹, Lifshitz¹⁰, and many others. Of particular interest to the spectroscopist is the excellent paper by Wallis and Maradudin¹¹ on impurity-induced infrared lattice-vibration absorption. The details of their analysis are long and complicated and are not repeated here. The essential results are that absorption can occur at frequencies associated with localized modes and that these frequencies may be higher than that of the main maximum. When more than one impurity exists in the system, the important criteria are the nature of the impurities and their separation distance. Naturally, if the impurities are widely separated they can be considered to act independently of each other.⁸ With these results available in the literature, one considers now the case in which the impurity is a polyatomic species with its own particular structure. For example, one might consider a 0.01% solution of azide ion (N_3^-) in NaCl. This system is substantially different from the systems investigated in the aforementioned papers because the azide ion is a three particle impurity and as such destroys the "topology" of the lattice. Furthermore, the azide ion has its own characteristic spectrum independent of that of the lattice. If the internal vibrations of the azide ion are of much higher frequency than those of the lattice, then one can re-establish a similarity between this system and those

treated by Lifshitz, Montroll, and others, by considering the azide ion to be a sphere and placing its center of mass at the lattice site. Within this high-low frequency approximation the results on localized modes can be carried over to this system. In order to investigate the complete spectrum of such a system one can then proceed to a Raman unit cell analysis. In the following discussion of the Raman model the NaCl lattice will be used.

The NaCl lattice is a face centered lattice with a basis. Associated with each Na atom there exists a corresponding Cl atom, thus leading to two particles per Bravais cell. The crystallographic unit cell contains 27 particles but of these only 4 Na and 4 Cl are "not shared" with the other cells. Similarly the Raman unit cell contains 8 Na and 8 Cl. Starting with a sodium atom at the (0,0,0) position one can arrive at the other seven sodium atoms by the application of the operations of the translation group for the Raman cell which in this case turns out to be a group of order 8. The space group for NaCl is therefore a finite group of order 384. The coordinates of the eight sodiums are: $(0,0,0)$, $(0,\frac{1}{2},\frac{1}{2})$, $(\frac{1}{2},\frac{1}{2},0)$, $(\frac{1}{2},0,\frac{1}{2})$, $(1,1,1)$, $(\frac{1}{2},1,\frac{1}{2})$, $(1,\frac{1}{2},\frac{1}{2})$, and $(\frac{1}{2},\frac{1}{2},1)$. One way of finding the coordinates of the corresponding chlorines is to add $(\frac{1}{2},0,0)$ to each of the above locations. The resulting structure, however, does not possess the symmetry O_h , which identifies NaCl. In order to satisfy this last requirement and, simultaneously, the requirements of the Raman unit cell, one can build a Wigner-Seitz type unit cell which in this case turns out to be a rhombic dodecahedron. This cell has the required volume (eight times that of the Bravais cell), the required 8 Na and 8 Cl, as well as the required O_h symmetry. Although the total number of particles in this Wigner-Seitz cell is 33 (19 chlorines and 14 sodiums), the nineteen chlorines contribute only eight and the 14 sodiums only eight due to the sharing with other cells. A normal coordinate analysis of this cell can yield only 48 independent normal coordinates, including three for translation. The transformation properties of these normal coordinates are to be classified according to the irreducible representations of the full space group. Since the character tables for space groups are not readily available, a method is needed by which such a classification can be accomplished without having to work with a group of order 384. Such a procedure is available and the details are to be found in Chelam's paper. In less digestible manner it is also found in Lomont's monograph¹².

The space group for NaCl can be written as

$$S = \tau_8 \otimes O_h$$

where $S \equiv$ space group of NaCl according to Raman

$\tau_8 \equiv$ the Abelian, invariant translation subgroup of order 8

$O_h \equiv$ the crystallographic point group of order 48

$\otimes \equiv$ semi-direct product.

The calculation of the force constants for NaCl on the basis of the Raman model has been effected by K. G. Ramanathan.⁴ When the NaCl lattice contains a small concentration of azide ions (for chloride), the O_h symmetry of the unit cell is reduced because the azide is linear symmetric, $D_{\infty h}$. However, it matters how one orients the N_3^- with respect to the surrounding ions. If the azide is oriented along the cube diagonal of the crystallographic unit cell, the symmetry operations which apply are those of D_{3d} . If oriented along the C_4 axis, then the resulting symmetry is D_{4h} , etc. In other words, the presence of the structure N_3^- in the lattice alters the symmetry of the space. The resulting symmetry for each particular orientation of the impurity is called the "impurity group", \mathcal{G} . The internal vibrations of the impurity are classified according to the impurity group, \mathcal{G} , and not according to O_h . However, the external (lattice) vibrations are not grossly affected by the presence of the impurity and hence are classified according to the irreducible representations of the unit cell group O_h , which one calls now "an effective unit cell", since the crystal is not pure. Clearly \mathcal{G} must be a subgroup of O_h ; therefore, a correlation diagram can be written down relating the symmetry species of O_h with those of \mathcal{G} . Formally one can write

$$O_h = \mathcal{G} \times \mathcal{O}$$

where $\mathcal{O} \equiv$ orientation group

$\times \equiv$ strong direct product.

For N_3^- along the body diagonal one has

$$O_h = D_{3d} \times C_{2v} .$$

From the correlation diagrams $S \rightarrow O_h \rightarrow D_{3d}$ one can obtain in principle the selection rules for the system. In this manner, perhaps, the satellite bands and other substructure observed in the spectra of impurity systems can be explained. An actual calculation of N_3^- in NaCl is in progress designed to test the model proposed here.

References

1. James I. Bryant, J. Chem. Phys. **38**, 2845 (1963).
2. M. Born and K. Huang, Dynamical Theory of Crystal Lattices, Oxford, Clarendon Press (1954).
3. C. V. Raman, Proc. Indian Acad. Sciences **18**, 237 (1943).
4. K. G. Ramanathan, Proc. Indian Acad. Sciences **18**, 493 (1943).
5. S. S. Mitra, Vibrational Spectra of Solids, Vol. 13, page 1, Solid State Physics, Academic Press, New York, (1962).
6. E. V. Chelam, Proc. Indian Acad. Sciences **18**, 283 (1943).
7. G. C. Turrell, Proceedings of the Eleventh Basic Research Group Contractors' Conference and Symposium, Fort Belvoir, Virginia, November, 1962.
8. A. A. Maradudin, E. W. Montroll and G. H. Weiss, Theory of Lattice Dynamics in the Harmonic Approximation, Solid State Physics, Supplement 3, Academic Press, New York (1963).
9. J. Hori and T. Asahi, Prog. Theor. Phys. **17**, 523 (1957).
10. I. M. Lifshitz, Nuovo Cimento, Suppl. A1 **3**, 716 (1956).
11. R. F. Wallis and A. A. Maradudin, Prog. Theor. Physics **24**, 1055 (1960).
12. J. S. Lomont, Application of Finite Groups, Academic Press, New York (1959).

MOLECULAR SPECTROSCOPY IN THE BASIC RESEARCH LABORATORY

by

James I. Bryant
Basic Research Laboratory
U. S. Army Engineer Research and Development Laboratories
Fort Belvoir, Virginia

I. Introduction

At this conference last year, efforts were made to report in some detail the theoretical and experimental technicalities involved in the studies of the vibrational spectroscopy of azide single crystals. The group theoretical analysis of the selection rules for a single crystal of potassium azide and the subsequent assignments of experimentally observed vibrational absorptions were made in terms of the unit cell model. Investigations of this nature are being continued with other azide crystals. However, this year instead of discussing the results of the more recent studies, I'd like to explain something of the long range objectives of the investigations in this area and also mention something of the information which can, in general, be obtained from studies of vibrational spectra of metastable substances.

II. Vibrational Spectra of Azide Single Crystals

Very little fundamental information on the internal energetics or solid structure of many initiator-type materials is available even today. It is one of the principal objectives of the Basic Research Laboratory to carry out activities to gain knowledge of this type. Over the last few years the relationship between the observed vibrational spectrum of a crystalline material and its internal structure has been clarified. Thus, it is fairly well accepted today that the unit cell or factor group model provides an effective method of describing the first order vibrations of a pure crystal.

Investigations of the vibrational spectra of the metallic azides have been carried out for a number of years. Sutherland and Penny¹ discussed the vibrational spectra on several metallic azides on which data was available in 1936, but were unable to reach any conclusions as to their symmetry. Later Delay, Duval and Lecompt² measured spectra of a series of azides by a powder technique and because of bands observed in the 1500-1600 wavenumber region, concluded that the two forms of the azide ion



were in resonance in the crystal. They suggested that each form produced independent fundamental vibrations. For example, an absorption at 2080 wavenumbers was assigned as ν_3 for the symmetric form and one at 1600 wavenumbers as ν_3 for the asymmetric form. Pauling³ showed that by considering resonance between symmetric and asymmetric structures for the azide ion of sodium azide, the bond length between the nitrogen atoms is 1.15 Å. However, resonance of this nature requires only one form for the azide ion. Tautomerism must exist between the two forms to produce two independent spectra, in the event of which the calculations of Pauling would not apply. The conclusions of Delay et. al. are, therefore, in doubt and the present view is that the bands observed in the 1500-1600 wavenumber region can be attributed to lattice combinations and/or impurities.

It is of interest to determine whether the change in explosive property of the metallic azides is due to increasing asymmetry of the azide ion as the bonding provided by coordination between the azide and the surrounding metallic ions changes. For the heavy metal azides, interpretations of this type from the results of x-ray diffraction experiments are difficult since the diffracting efficiency of an atom is proportional to its atomic weight. Therefore, the x-rays are absorbed by the heavy cations. Little structural work in this area has been completed.

If the vibrational assignments of the free ions are known, it may be possible to use spectroscopic data to indicate crystal structure. It may also be possible to obtain data regarding the crystal-line field. In the measurement of the vibrational spectra of crystalline materials, the use of single crystal samples appears extremely desirable. Single crystal spectra have the advantage of avoiding the high degree of light scattering obtained when powdered samples are used and the complications arising from lack of knowledge of the environment of the vibrating species when pressed disk or solution samples are measured. Halford⁴ has pointed out that the number of infrared-active absorptions is dependent on the physical state of the sample, more absorptions being observed for liquid samples than for gaseous, and more for solid than for liquid. On the other hand, in the past, single crystal samples have been avoided because of the numerous overlapping bands they produce which are difficult to resolve. It seems, however, that if such spectra can be effectively interpreted, they should afford the most information obtainable concerning the vibrational energy of the materials concerned. Due to recent advances in technology, such as higher resolution grating spectrometers, capabilities for obtaining spectra over wide temperature ranges, and the use of polarized radiation, more effective interpretations than ever before can now be made of single crystal spectra.

Fairly recently, infrared studies of single crystals of various azides have been carried out by Moore⁵ in England and by Papazian⁶ in this country. Both of these studies are of a survey nature, although the former investigation is a much more detailed study than the latter. Neither of the investigators measured the Raman and far infrared spectra of the single crystals or made use of polarized radiation in their studies.

The purpose of the investigations in this laboratory is to carry out detailed studies of the vibrational spectrum of single crystals of the metallic azides and to relate the observed spectrum to the vibrations of the crystal as described by the unit cell or factor group model.

At present, the investigations of the vibrational spectra (infrared and Raman) of potassium⁷ and sodium⁸ azides have been completed. From this point on, I would like to present some data from these studies which demonstrate some of the approaches to, complications of, and results obtainable from the vibrational studies of single crystals.

The results of the infrared study of single crystals of potassium azide were presented in detail at this conference last year. At that time, investigations of the Raman spectrum had not been carried out. Figure 1 shows the Raman spectrum of a single crystal of potassium azide. For convenience, the spectrum can be divided into two regions; the region of the lattice vibrations (approximately from 100 to 200 wavenumbers) and the symmetric stretching region (approximately from 1250 to 1350 wavenumbers). Two rotatory and one translatory lattice modes are predicted for the KN_3 crystal by the unit cell selection rules. In the actual spectrum, two lines are observed at 107 and 151 cm^{-1} . These lines are very likely due to the rotatory lattice vibrations since Halford has pointed out that the intensity of rotatory lattice lines are expected to be greater than translatory. In the symmetric stretching region, the unit cell selection rules allow Raman activity for two species of ν_1 ($A_{1g} + B_{2g}$) and for five species of $2\nu_2$ ($3A_{1g} + B_{1g} + B_{2g}$). Since Fermi resonance can only occur between identical species, four lines are expected to be observed for $2\nu_2$ corresponding to the four species ($3A_{1g} + B_{2g}$) which can resonate with the two species of ν_1 . It is assumed that only species of $2\nu_2$ which resonate with ν_1 will borrow sufficient intensity to be observed. In the observed spectrum, the one strong and one weak line observed in the 1350 cm^{-1} regions were assigned as species of ν_1 and the three weak and one strong lines in the 1270 cm^{-1} region as species of $2\nu_2$. On the basis of similarities of intensities, the four weak lines were assigned as A_{1g} symmetry and the two intense lines as B_{2g} .

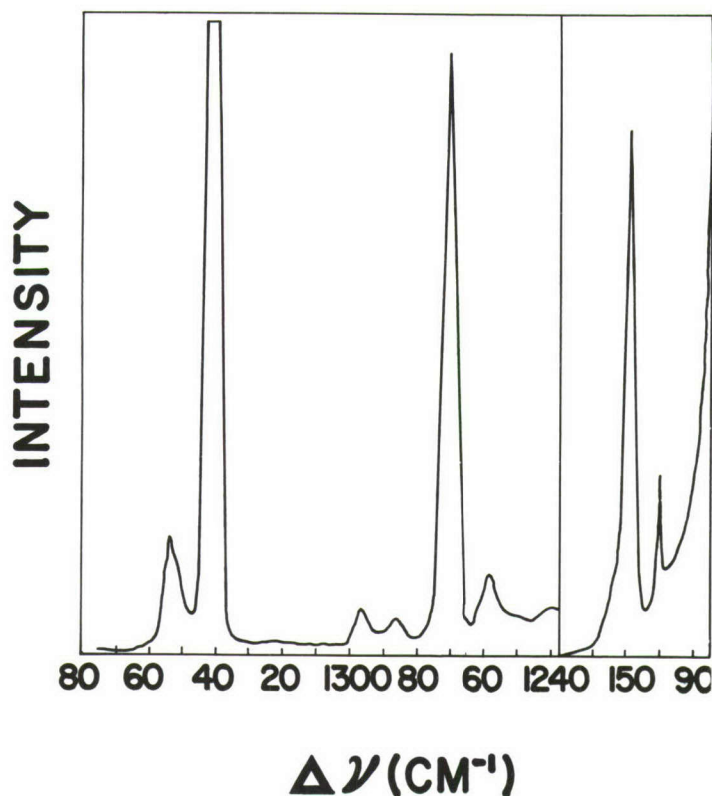


Figure 1. Raman spectrum of a single crystal of potassium azide.

The theoretical and experimental investigation of the vibrational spectrum of a single crystal of sodium azide served as an effective test for the suitability of the unit cell (factor group) model for interpreting the vibrational spectrum of single crystals. Because of the relative simplicity of the NaN_3 unit cell structure (Figure 2) (only one molecule per unit cell) and azide ion (linear and symmetric), a relatively uncomplicated single crystal spectrum is obtained. For such a spectrum, a more rigorous treatment can be given to assignments and more precise and accurate correlations between theoretical and observed spectra are possible.

The complete results of the application of the unit cell model to a single crystal of sodium azide are shown in Table I. Since there is only one molecule per unit cell, crystal field splittings of fundamental absorptions do not occur. The basic spectrum is thus that of the free ion. However, two translatory and one rotatory lattice modes are allowed and these can combine with fundamental absorptions to modify considerably the features of the basic spectrum. Only vibrations of species A_{2u} and E_u are infrared active for

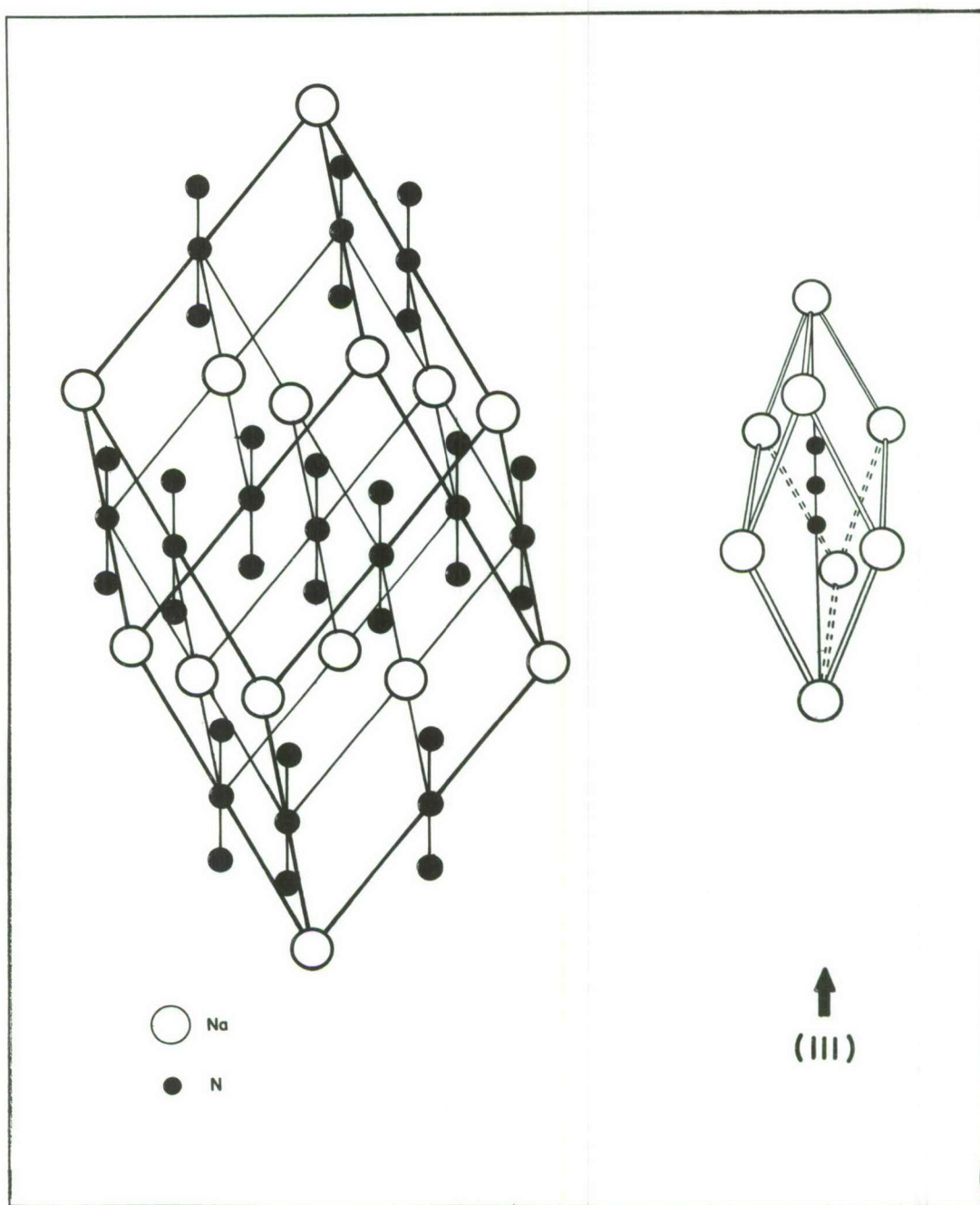


Figure 2. Models of the structure and unit of structure of a sodium azide single crystal.

the space group D_{3d} and the active combination and overtone levels and lattice combinations may be calculated using the multiplication properties of irreducible representations.

Table I
Vibrational Species of NaN_3 Single Crystals

D_{3d}	Σn_i	T_i	T_i'	R'	n_i'	Activity
A_{1g}	1	0	0	0	1	R ν_1
A_{2g}	0	0	0	0	0	
E_g	1	0	0	1	0	R
A_{1u}	0	0	0	0	0	
A_{2u}	3	1	1	0	1	IR ν_3
E_u	3	1	1	0	1	IR ν_2

The measuring of the Raman spectrum of a single crystal of sodium azide at the time the infrared investigation was being carried out aided considerably in the analysis of the spectrum of the latter. The Raman spectrum, shown in Figure 3, consisted of three distinct lines, all of which are essentially depolarized. The intense line at 122 cm^{-1} is due to a rotatory motion of the azide ion as a rigid unit. Medium strength absorptions repeatedly occurring on either side of fundamental absorptions in the infrared could thus be assigned with confidence as sums and differences of the fundamental and the Raman rotatory lattice mode. The strong line at 1358 cm^{-1} in the Raman spectrum is the symmetric stretching frequency, ν_1 . This mode undergoes only a slight Fermi resonance perturbation with the A_{1g} species of the first overtone of the bending mode, $2\nu_2$. The resulting weak line due to $2\nu_2$ appears at 1267 cm^{-1} . In the infrared spectrum, a group of absorptions were observed symmetrically situated about the 1358 cm^{-1} frequency. These bands were assigned as sums and differences of ν_1 and the two translatory lattice modes predicted by the unit cell selection rules. The values of 1501 and 1208 cm^{-1} can be inferred from the Raman-active fundamental and the infrared-active lattice combinations for the frequency of the two translatory lattice modes.

Figure 4 shows the infrared spectrum of the asymmetric stretching region for a sodium azide single crystal. This region is probably the most interesting one in the spectrum since it can illustrate the possibility of the occurrence of misleading complications in

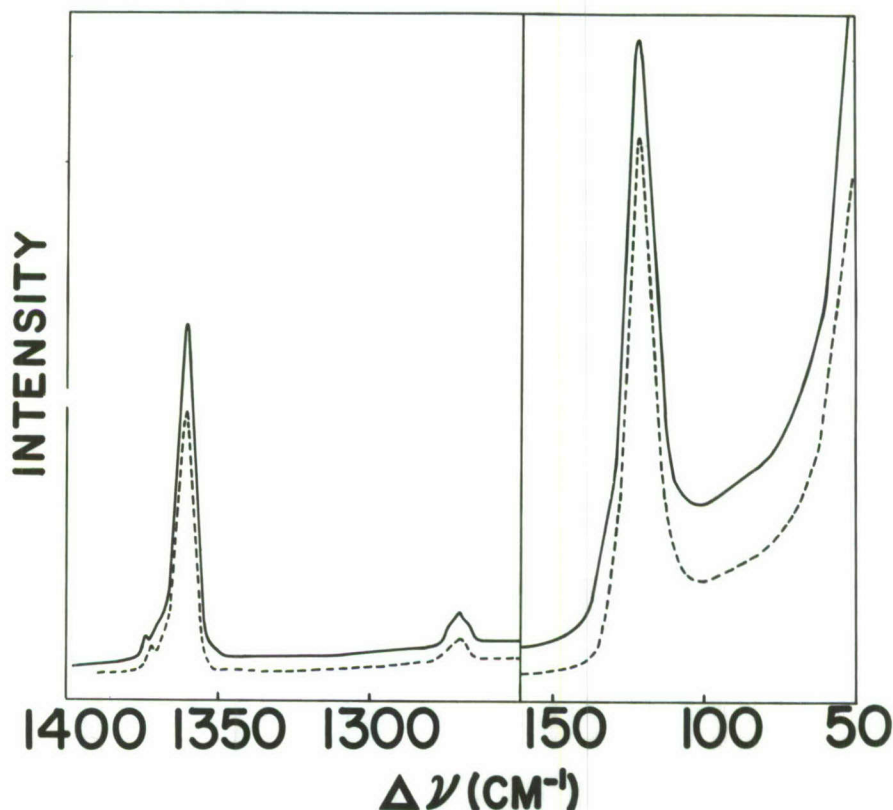


Figure 3. Raman spectrum of a single crystal of sodium azide.

spectra of single crystals. When the spectrum of a sodium azide crystal was measured, the azide ions, which are all aligned perpendicular to the flat faces of the crystals, are parallel to the incident beam. Thus, in this spectral region, the normally intense ν_3 fundamental is not highly absorbing because the azide ions are oriented so that the A_{2u} vibrations cannot interact appreciably with the incident beam. Only combination bands of E_u symmetry should appear in this region. However, with crystals of any appreciable thickness, A_{2u} absorptions can appear weakly because of crystal imperfections, discrepancies in orientation, convergence of the light beam, and the like. The center of the ν_3 fundamental was, therefore, taken as 2043 cm^{-1} . The two most intense bands in this region occurring at 122 cm^{-1} on either side of this frequency are lattice combinations with ν_3 . Superimposed on the broad envelope of the fundamental and the lattice combinations are sharp bands of medium to weak intensity which could confidently be assigned as the combinations $\nu_1 + \nu_2$ at 2000 cm^{-1} and $2\nu_2 + \nu_2$ at 1898 cm^{-1} . On the

outer fringe of the envelope are two broad, medium strength bands at 2336 and 1846 cm^{-1} whose disposition was considered in terms of higher order absorptions (possible multiphonone absorptions).

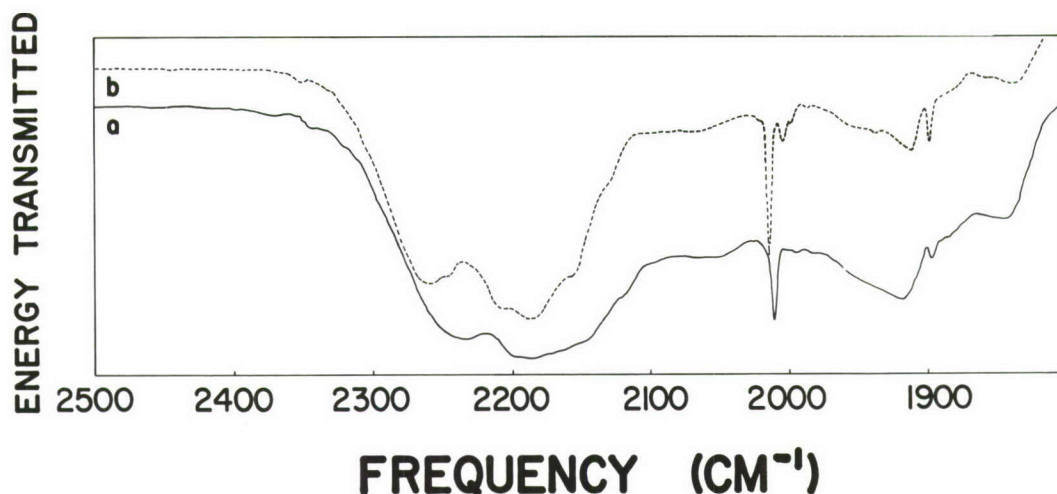


Figure 4. Infrared spectrum of a 0.1 mm thick sodium azide single crystal in the asymmetric stretching region: (a) 298° K, (b) 90° K.

In summary, the study of the vibrational spectra of sodium and potassium azides indicates that effective correlations can be made between the theoretical vibrations of the alkali metal azides and their spectra by application of the unit cell model. At present, survey spectra of thin silver azide crystals are being measured. Efforts are also being made to obtain thick crystals of silver azide needed to observe the fine structure of the spectrum. From silver azide, plans are to proceed to investigate the vibrational spectrum of lead azide. From these studies, efforts will be made to determine the relationship of chemical bonding and metastability of the metallic azides.

III. Infrared Absorptions of UV Irradiated Azides

The secondary area of investigation in molecular spectroscopy is the study of crystalline azides which contain impurities due to ultraviolet and x-ray irradiation by observing their vibrational spectra. This study must, of necessity, follow the investigation of the vibrations of pure (unirradiated) crystals, since interpretation of spectra of damaged crystals cannot effectively be made until thorough and accurate assignments of pure crystals are available. The mechanism of decomposition by irradiation may be made clearer by detection of intermediate products stabilized at low

temperatures. Thus, in the vibrational spectrum, new bands may appear, the assignment of which would allow characterization of decomposition intermediates.

Several models have been proposed to account for the visible and ESR absorptions of irradiated azide crystals. Since these models are related to electronic transitions, they are inadequate to account for absorptions in the infrared. In this laboratory, consideration has been given to the interpretation of the infrared absorptions in terms of the theory of molecular vibrations. Some aspects of the results of these investigations are presented below.

Figure 5 shows changes in the spectrum of a single crystal of sodium azide before and after UV irradiation for 1.5 hours at 90° K. The medium strength absorption at 1721 cm^{-1} disappeared when the crystal was bleached by heating. Similar infrared absorptions were observed for irradiated crystals of potassium, rubidium, and cesium azides.

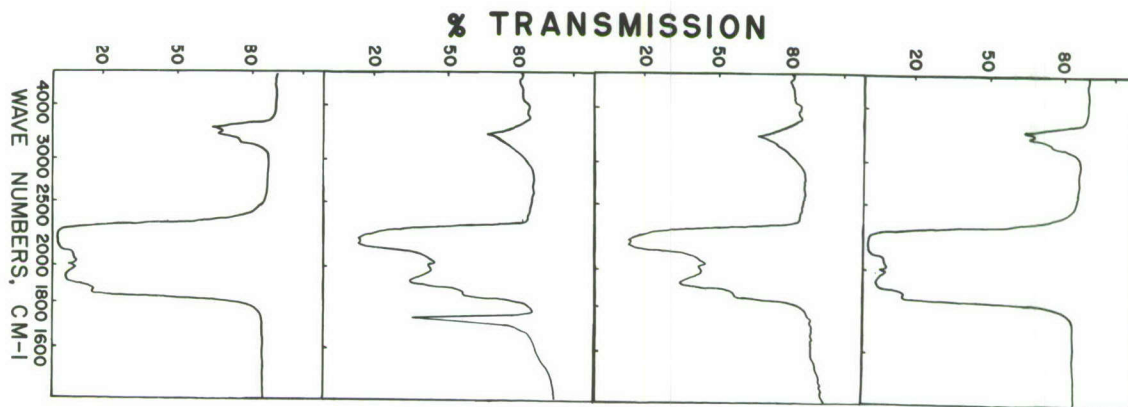


Figure 5. Infrared spectrum of a single crystal of sodium azide before and after UV irradiation: (a) sample temperature 298° K, (b) temperature lowered to 90° K, (c) after 1.5 hrs. UV irradiation at 90° K, (d) temperature returned to 298° K.

Early in these investigations it was determined that the infrared absorptions due to UV irradiation could also be observed using KBr pressed disk samples of the azides. This fact permitted the investigation of a number of metallic azides since the difficult task of obtaining large single crystals was eliminated. A series of azide samples prepared by this technique were irradiated with UV light and their infrared spectra examined. The results of this study are shown in Table II. Finally, using pressed disk samples, three different isotopic species of potassium azide were irradiated and the frequency of the bands due to irradiation was recorded. The results are shown in Table III.

Table II
Infrared Absorptions of UV Irradiated
Azides in KBr Pressed Disk

Azide	Irradiation time (hours)	Frequency of irradiation band (cm^{-1})
LiN_3	4.5	None observed
NaN_3	4.5	1721
KN_3	1.5	1620
RbN_3	3.5	1625
CsN_3	4.5	1630
$\text{Ca}(\text{N}_3)_2$	4.5	None observed
$\text{Ba}(\text{N}_3)_2$	4.5	1682
AgN_3	4.5	None observed
$\text{Pb}(\text{N}_3)_2$	4.5	None observed

Table III
Frequency of Infrared Absorption Due to UV
Irradiation of Various Isotopic Species of KN_3

Isotopic species	Observed frequency (cm^{-1})
KN_3^{14}	1620
* KNNN^{15}	1610
* KNN^{15}N	1605

* Enriched to 95% in N^{15} in the indicated position.

Although the above studies do not permit an unambiguous characterization of the center responsible for the infrared absorption, they do furnish useful information which can help to achieve this goal. The regular frequency shifts for the different isotopic species of KN_3 strongly indicate that the center responsible for the infrared vibrations is some configuration of vibrating nitrogen atoms. These observations and resulting conclusion are significant since one can dispense with such arguments as charge transfer and the possible infrared absorption of color centers and deal with the more straight forward problem of searching for a nitrogen configuration which can produce the observed vibrational frequency. The results of the pressed disk study are interesting since the metallic azides which were studied are divided into a relatively stable and relatively unstable group corresponding to the azides which respectively produce and do not produce a new infrared absorption band when irradiated. This suggests that the configuration responsible for the irradiation band in the infrared is present in the decomposition mechanism of the stable azides which do produce a new band and absent in those of the unstable azides which do not. At present, approximate force constant calculations are being carried out in order to relate the frequency of the irradiation band to various centers which have been proposed as intermediates in the photolysis of various metallic azides.

IV. Infrared Spectra of Isotopically Enriched NaN_3 and KN_3

In order to effectively interpret the fine structure in spectra of azide single crystals, assignments must be made for weak absorptions due to vibrations of various N^{15} isotopic species occurring at natural abundance. Although the carrying out of approximate force constant calculations can aid considerably in making isotopic assignments, the direct observation of the absorption in spectra of isotopically enriched samples provides a more convenient and accurate means of accomplishing this goal. In addition to confirming the assignments of the various isotopic absorptions in the single crystal studies, the results permitted observation of the symmetric stretching vibration, ν_1 , which is infrared active for NaN_3^{14} and KN_3^{14} . Experimental values of the isotopic effect were also obtained and compared with the theoretical values determined by isotopic mass calculations. Figures 6, 7, and 8 show the isotopic shifts for KN_3 in the bending, asymmetric stretching, and 3300 cm^{-1} regions, respectively. As expected in each region, the shift is greater for the end N^{15} isotopic species than for the center. The largest numerical shifts with change of isotopic mass were observed for the combination bands $\nu_1 + \nu_3$ and $2\nu_2 + \nu_3$ in the 3300 cm^{-1} region. The smallest shifts were shown for the bending fundamental near 640 cm^{-1} . In Figure 7, the constancy of the

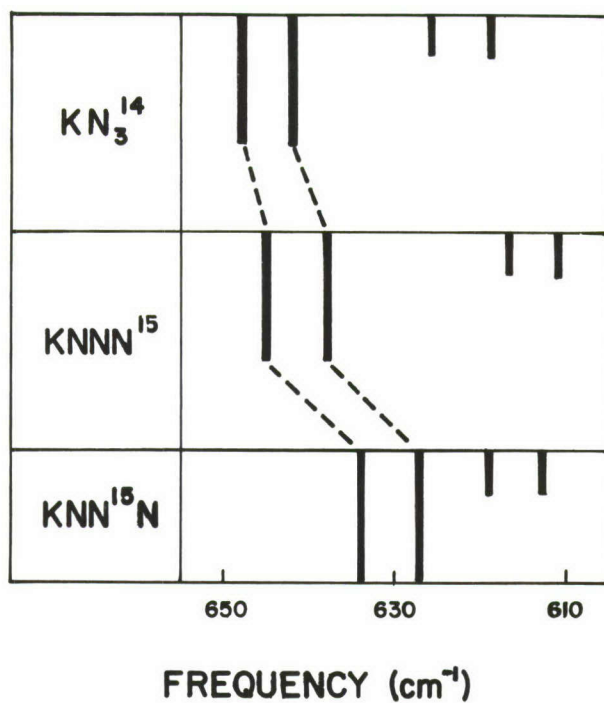


Figure 6. Isotopic shifts for potassium azide in the bending region of the infrared spectrum.

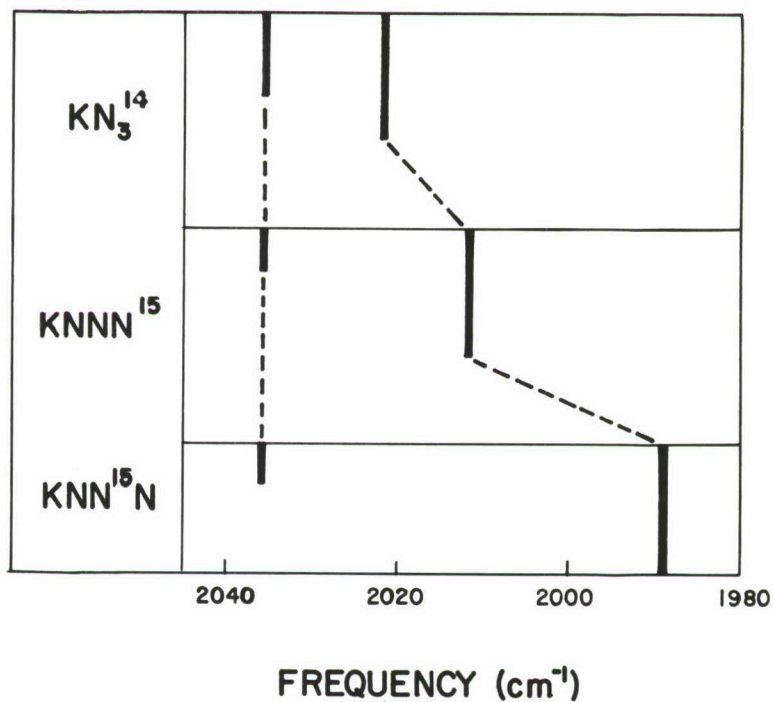


Figure 7. Isotopic shifts for potassium azide in the asymmetric region of the infrared spectrum.

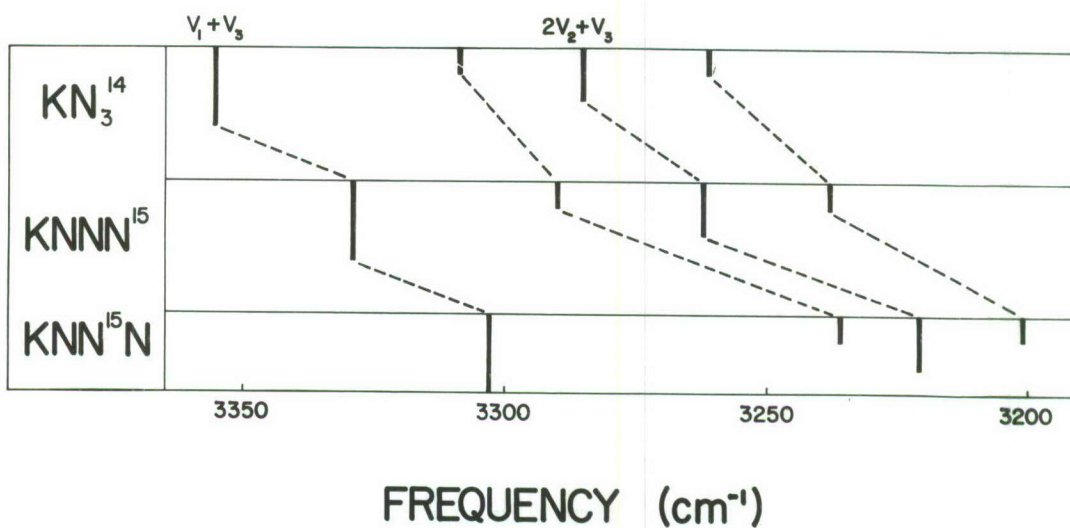


Figure 8. Isotopic shifts for potassium azide in the 3300 combination region of the infrared spectrum.

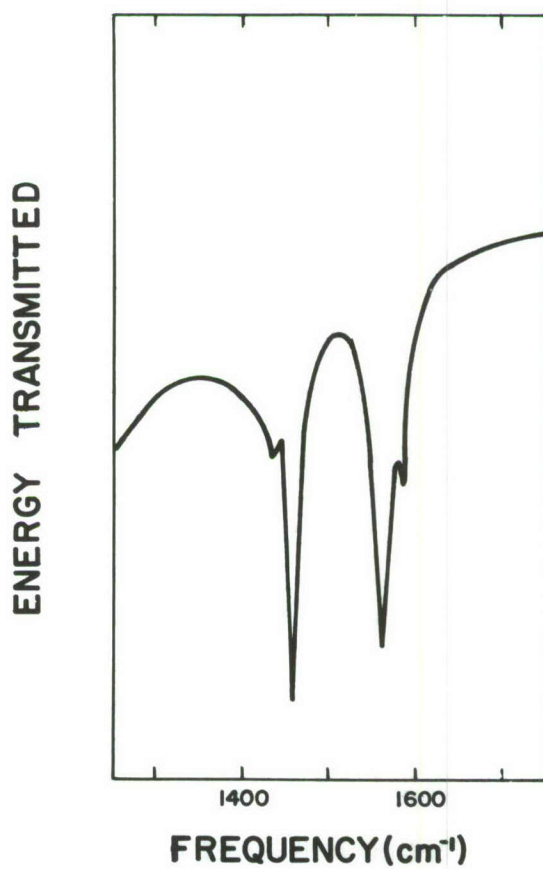


Figure 9. Symmetric stretching region of the infrared spectrum of KNNN^{15} showing Fermi resonance between ν_1 and $2\nu_2$.

frequency of the band at 2038 cm^{-1} is in agreement with the assignment of this absorption as ν_3 for N_3^{14} at a substitution site in the KBr lattice. Figure 9 shows the symmetric stretching region for KNNN^{15} where Fermi resonance between ν_1 and $2\nu_2$ is much in evidence. Observed and calculated isotopic effects of sodium azide are shown in Table IV.

Table IV

Observed and Calculated Isotopic Effect of Sodium Azide

	$\frac{\nu_1^i}{\nu_1}$	$\frac{\omega_1^i}{\omega_1}$	$\frac{\nu_2^i}{\nu_2}$	$\frac{\omega_2^i}{\omega_2}$	$\frac{\nu_3^i}{\nu_3}$	$\frac{\omega_3^i}{\omega_3}$
	observed	calculated	observed	calculated	observed	calculated
NaNNN^{15}	0.994552	0.984419	0.992329	0.992540	0.994638	0.992540
NaNN^{15}N	n. m.	1.000000	0.977458	0.977559	0.980952	0.977559
$\text{NaN}^{15}\text{N}^{15}\text{N}^{15}$	n. m.	0.966195	0.964778	0.966195	0.965705	0.966195

n. m. = not measured

The agreement of observed and calculated values is quite satisfactory, the small difference being due to the use of observed fundamental frequencies rather than zero order frequencies. Finally, in order to determine observed isotopic effect values accurate values of the fundamental frequencies of KN_3^{14} were required from which bond force constants can be determined. The frequencies measured and the force constants determined in this study are listed in Table V and compared with values reported by Gray and Waddington⁹.

Table V

Fundamental Frequencies and Force Constants for Sodium Azide

	ν_1 (cm^{-1})	ν_2 (cm^{-1})	ν_3 (cm^{-1})	k_1 (dynes/cm)	k_{12} (dynes/cm)	$k\delta/l^2$ (dynes/cm)
Reference A ¹	1358.4 ²	639	2128	13.92	1.30	0.56
This work	1358.4 ²	638.6	2126.2	13.82 ₆	1.39 ₅	0.56 ₁

¹Reference A; P. Gray and T. C. Waddington, Proc. Roy. Soc., (London) A235, 106 (1956)

²L. Kahovec and K. Kohlrausch, Monatsh. 77, 180 (1947)

In both studies, the values for the frequency of the stretching vibration was taken from the work of Kohavec and Kohlrausch.¹⁰ The difference in the frequency values measured in this study modify only to a small extent the values of the force constants determined by Gray and Waddington.

In summary, it can be said that the investigations which have been carried out so far indicate that studies of vibrational spectra can provide useful information concerning the internal and crystal structure of metallic azides. They also show promise, as detailed vibrational data is accumulated on a cross-section of the metallic azides, of providing insight into the relationship of structure to the stability of these materials.

References

1. W. G. Penny and G. B. M. Sutherland, Proc. Roy. Soc A156, 678 (1936).
2. Delay, Duval and Lecompt, Bull. Soc. Chim. France 12, 581 (1945).
3. S. Hendricks and L. Pauling, J. Am. Chem. Soc. 47, 2904 (1925).
4. R. S. Halford, J. Chem. Phys. 14, 8 (1946).
5. P. W. J. Moore, unpublished.
6. H. Papazian, J. Chem. Phys. 34, 1614 (1961).
7. J. I. Bryant, J. Chem. Phys. 38, 2845 (1963).
8. J. I. Bryant, J. Chem. Phys. (in press).
9. P. Gray and T. Waddington, Trans. Faraday Soc. 53, 901 (1957).
10. L. Kohavec and K. Kohlrausch, Monatsh. 77, 180 (1947).

APPENDIX I

ATTENDANCE LIST

Brower, Dr. Frank M., Dow Chemical Co., Midland, Michigan
Bryant, Dr. James I., USAERDL Fort Belvoir, Virginia
Burkhard, Dr. Donald G., PEC Corporation, Boulder, Colorado
Carlson, Frederick F., USAERDL, Fort Belvoir, Virginia
Coleman, Amos J., USAERDL, Fort Belvoir, Virginia
Cook, Dr. Charles J., Stanford Research Inst., Menlo Park, California
Corey, H., USAERDL, Fort Belvoir, Virginia
Dando, J. D., USAERDL, Fort Belvoir, Virginia
Darwent, Dr. B. deB., Catholic University, Washington, D. C.
Davis, V. M., USAERDL, Fort Belvoir, Virginia
Deb, Dr. S. K., American Cyanamid Co., Stamford, Connecticut
Dickinson, N. K., USAERDL, Fort Belvoir, Virginia
Dodd, Dr. J. G., Arkansas Polytechnic College, Russellville, Arkansas
Egghart, Dr. H. C., USAERDL, Fort Belvoir, Virginia
Elser, Dr. Wolfgang, USAERDL, Fort Belvoir, Virginia
Eyring, Dr. Henry, University of Utah, Salt Lake City, Utah
Fisher, Dr. Howard, Aerojet General Corporation, Downey, California
Forman, Richard A., National Bureau of Standards, Washington, D. C.
Forsyth, Dr. A., U. S. Army Munitions Command, Dover, New Jersey
Gelerinter, Dr. E., Cornell University, Ithaca, New York
Glen, Dr. Gerald L., The Atlantic Refining Co., Glenolden, Pennsylvania
Grieve, W. I., AFSC-STLO, Washington, D. C.
Gutmann, Dr. Viktor, Institute of Vienna, Vienna, Austria
Harvalik, Dr. Z. V., USAERDL, Fort Belvoir, Virginia
Howard, Dr. Fred, Eglin Air Force Base, Florida
Jacox, Dr. Marilyn, National Bureau of Standards, Washington, D. C.
Jobstl, Dr. J. A., USAERDL, Fort Belvoir, Virginia
Jorgensen, Wilhelm, U. S. Army Research Office, Durham, North Carolina
Kallmann, Dr. H. P., New York University, New York, New York
Kemney, Dr. P. J., U. S. Army Munitions Command, Dover, New Jersey
Kemp, M. D., USAERDL, Fort Belvoir, Virginia
King, G. J., USAERDL, Fort Belvoir, Virginia
Kronick, Paul L., Franklin Institute, Philadelphia, Pennsylvania
Krueger, Colonel Philip G., USAERDL, Fort Belvoir, Virginia
Kureishy, Dr. A. R. T., Imperial College, London, England
Lieber, Dr. Eugene, Roosevelt University, Chicago, Illinois
Ling, Dr. D. S., PEC Corporation, Boulder, Colorado
McCrone, Dr. W. C., McCrone Associates, Chicago, Illinois
McGill, Dr. R., U. S. Naval Ordnance Laboratory, White Oak, Silver
Spring, Maryland
McMillan, R. C., USAERDL, Fort Belvoir, Virginia
Magrum, Dr. S. J., OCR&D, Washington, D. C.
Manno, Dr. R., U. S. Army Munitions Command, Dover, New Jersey

Marinkas, P., U. S. Army Munitions Command, Dover, New Jersey
Mergerian, Dr. D., Westinghouse Electric Corp., Baltimore, Maryland
Miller, B. S., USAERDL, Fort Belvoir, Virginia
Mizushima, Dr. M., PEC Corporation, Boulder, Colorado
Moriarty, Dr. R. M., Catholic University, Washington, D. C.
Mueller, Dr. H. J., USAERDL, Fort Belvoir, Virginia
Norberg, Dr. R. E., Washington University, St. Louis, Missouri
O'Dell, M. S., USAERDL, Fort Belvoir, Virginia
Okamoto, Dr. Y., New York University, New York, New York
Paca, F. B., USAERDL, Fort Belvoir, Virginia
Pai-Verneker, Dr. V. R., Picatinny Arsenal, Dover, New Jersey
Poole, H. D., Defense Research Staff, British Embassy, Washington, D. C.
Ranganathan, Dr. R., Howard University, Washington, D. C.
Rosenwasser, H., USAERDL, Fort Belvoir, Virginia
Seaton, Dr. D. L., Lawrence Radiation Laboratory, Livermore, California
Silverstein, M. S., Frankford Arsenal, Philadelphia, Pennsylvania
Singer, George D., USAERDL, Fort Belvoir, Virginia
Taylor, J. L., USAERDL, Fort Belvoir, Virginia
Terada, Dr. K., Dow Chemical Co., Midland, Michigan
Theophanides, Dr. T., Howard University, Washington, D. C.
Torkar, Dr. K., Institute of Technology, Graz, Austria
Turrell, Dr. G. C., Howard University, Washington, D. C.
Vandersluis, H. J., USAERDL, Fort Belvoir, Virginia
Veguilla-Berdecia, Dr. L. A., Howard University, Washington, D. C.
Wawner, F. E., Texaco Experiment Inc., Richmond, Virginia
Weber, Dr. H. C., Chief, Scientific Advisor, OCR&D, Washington, D. C.

APPENDIX II

PROGRAM

Conference Chairman and Co-chairmen
M. D. Kemp, R. C. McMillan, and A. J. Coleman

Wednesday, 6 November 1963

0830-0900 Registration

SESSION I - Chairman: N. K. Dickinson, Ch., Mil Dept

0900-1000 Opening (CLASSIFIED)

Harvalik, Z. V., USAERDL, "Field Theory of Initiation"

1000-1015 Coffee Break

SESSION II - Chairman: Dr. H. J. Mueller

1015-1200 Weber, H. C., Chief Scientific Advisor, U. S. Army,
Title to be announced

Forsyth, A., Kemmey, P. J., Manno, R., and Pai-Verneker,
V. R., Picatinny Arsenal, Dover, N. J., "Study of
Preparation and Properties of Azides"

Torkar, K., Institute of Technology, Graz, Austria,
"Properties and Reactivities of Different Prepared
 NaN_3 and $\text{Ba}(\text{N}_3)_2$ "

1200-1215 Group Picture

1215-1315 Lunch

SESSION III - Chairman: Dr. E. Lieber

1315-1500 Terada, K., Erbel, J. A., and Brower, F. M., The Dow
Chemical Co., Midland, Michigan, "The Preparation and
Properties of Some Novel Light Metal Azides"

Taylor, J. L., USAERDL, "Further Studies on the Three
Component System in Purification"

Kemp, M. D., USAERDL, "Further Observations on the Growth
of Alpha Lead Azide Crystals"

Blais, M., and Pai-Verneker, V. R., Picatinny Arsenal,
Dover, N. J., "The Mechanism of Uptake of Impurities
by Azide Crystals"

1500-1510 Coffee Break

1510-1600 Joebstl, J. A., USAERDL, "An Electron Microscopic
Investigation of the Thermal Decomposition of NaN_3
and KN_3 Crystals"

O'Dell, M. S., and Darwent, B. deB., Catholic University,
Washington, D. C., "The Gas Phase Decomposition of
Simple Organic Azides"

*Goss, Frank A., Sandia Corp., Albuquerque, New Mexico,
Fisher, H. J., and Kenworthy, H. M., Aerojet-General
Corp., Downey, California, "Ignition Temperature of
Lead Styphnate as a Function of Rate of Energy Input"

Thursday, 7 November 1963

SESSION IV - Chairman: Dr. Z. V. Harvalik

0830-0945 Okamoto, Y., Goswami, J. C., and Brenner, W., New York
University, New York, "Decomposition of Alkaline Earth
Azides Under Organic Solvents"

Egghart, H. C., USAERDL, "Kinetic Studies on the Reaction
Between Azides and Metal Ions"

Mueller, H. J., and Joebstl, J. A., USAERDL, "Properties
of Molten Azides: Data on Binary Systems of Monovalent
Inorganic Azides"

0945-1000 Coffee Break

1000-1215 Eyring, H., University of Utah, Salt Lake City, Utah,
Title to be announced

Glen, G. L., The Atlantic Refining Co., Glenolden, Pa.,
"The Crystal Structure of Alpha Lead Azide"

Miller, B. S., and King, G. J., USAERDL, "Crystal
Structure Change of Sodium Azide at 19°C "

Forman, R. A., NBS, Washington, D. C., "Nitrogen NMR
Chemical Shifts in the Azide Ion"

Jacobs, P. W. M., Kureishy, A. R. T., and Tompkins, F. C.,
Imperial College of Science and Technology, London,
England, "The Photochemical Decomposition of Sodium
Azide"

1215-1315

Lunch

SESSION V - Chairman: Dr. D. G. Burkhard

1315-1500 King, G. J., and Miller, B. S., USAERDL, "Paramagnetic
Resonance of Mn^{++} in Sodium Azide"

Carlson, F. F., USAERDL, "Electron Paramagnetic Resonance
of Nitrogen Atoms in Alkali Metal Azides"

McMillan, R. C., USAERDL, "Electron Spin Resonance of
Potassium Colloids in KN_3 "

1500-1510

Coffee Break

1510-1615 Singer, G. D., and Mueller, H. J., USAERDL, "The Study
of Transient Absorption Spectra of Azides by Means of
a Fast Recording Spectrometer"

Dodd, J. G., Arkansas Polytechnic College, Russellville,
Arkansas, "Azide Research at Arkansas Polytechnic
College"

Mizushima, M., PEC Corporation, Boulder, Colorado,
"Classical Treatment of Excitation of Lattice Vibration
by External Impact"

Friday, 8 November 1963

SESSION VI - Chairman: Mr. G. J. King

0830-1000 Ling, D. S., PEC Corporation, Boulder, Colorado, "Further
Developments in the Statistical Theory of Explosion
Initiation"

McCrone, W. C., McCrone Associates, Inc., Chicago, Ill.,
"Measurement of Impact Sensitivity of Explosives"

Lieber, E., and Rao, C. N. R., Roosevelt University,
Chicago, Ill., "Infrared Studies of Organic Azides"

1000-1015

Coffee Break

- 1015-1200 Gutmann, V., Institute of Technology, Vienna, Austria,
"Azido-complexes in Nonaqueous Solutions"
- Milligan, D. E., and Jacox, M. E., NBS, Washington, D. C.,
"Infrared Spectroscopic Evidence for the Species NH"
- Veguilla-Berdecia, L. A., and Turrell, G. C., Howard
University, Washington, D. C., "Group Theoretical
Analysis of Impurities in Solids"
- Bryant, J. I., USAERDL, "Vibrational Spectroscopy in the
Basic Research Laboratory"
- 1200-1215 Summaries, future plans.

* Paper not received by deadline, preprint not available.

AUTHOR INDEX

	<u>Page</u>		<u>Page</u>
Blais, M.	65	Leitmann, O.	235
Brenner, W.	91	Lieber, E.	225
Brower, F. M.	21	Ling, D. S., Jr.	205
Bryant, J. I.	257	Manno, R.	5
Carlson, F. F.	151	McCrone, W. C.	219
Darwent, B. deB.	89	McMillan, R. C.	157
Dodd, J. G.	173	Miller, B. S.	125, 145
Egghart, H. C.	95	Milligan, D. E.	247
Erbel, A. J.	21	Mizushima, M.	181
Eyring, H.	109	Mueller, H. J.	103, 163
Forman, R. A.	129	O'Dell, M. S.	89
Forsyth, A.	5	Okamoto, Y.	91
Glen, G. L.	113	Pai-Verneker, V. R.	5, 65
Goswami, J. C.	91	Rao, C. N. R.	225
Gutmann, V.	235	Singer, G. D.	163
Hampel, G.	235	Taylor, J. L.	39
Jacobs, P. W. M.	131	Terada, K.	21
Jacox, M. E.	247	Tompkins, F. C.	131
Joebstl, J. A.	73, 103	Torkar, K.	11
Kemmey, P. J.	5	Turrell, G. C.	251
Kemp, M. D.	49	Veguilla-Berdecia, L. A.	251
King, G. J.	125, 145	Weber, H. C.	1
Kureishy, A. R. T.	131		

DISTRIBUTION LIST FOR

12th BASIC RESEARCH GROUP CONTRACTORS' CONFERENCE AND SYMPOSIUM

ADDRESSEE

University of Utah
Attn: Dr. Henry Eyring
207 Park Building
Salt Lake City, Utah

Princeton University
Attn: Dr. R. Smoluchowski
School of Engineering
Princeton, New Jersey

The Catholic University of
America
Attn: Dr. B. deB. Darwent
Chemistry Department
Washington 17, D. C.

Howard University
Attn: Dr. G. C. Turrell
Chemistry Department
Washington, D. C.

PEC Corporation
Attn: Dr. Donald G. Burkhard
1001 Mapleton Avenue
Boulder, Colorado

Roosevelt University
Attn: Dr. Eugene Lieber
Chemistry Department
Chicago 5, Illinois

Stanford Research Institute
Attn: Dr. Charles J. Cook
Chemical Physics Division
Menlo Park, California

National Bureau of Standards
Attn: Dr. Te-Tse Chang
1040 Industrial Building
Washington 25, D. C.

ADDRESSEE

National Bureau of Standards
Attn: Mr. Richard Forman
1038 Industrial Building
Washington 25, D. C.

National Academy of Sciences
Attn: Dr. J. H. Probus
2101 Constitution Avenue, NW
Washington 25, D. C.

Office, Chief Research &
Development
Room 3D442, Pentagon
Washington 25, D. C.
Attn: Dr. R. Weiss (1)
Dr. H. C. Weber (1)
Dr. S. J. Magrum (1)
Dr. Ivan R. Hirshner, Jr (1)

Technical Library
Office, Asst Secretary of Defense
Washington 25, D. C.

Command & General Staff College
Fort Leavenworth, Kansas

Commanding General
U. S. Army Mobility Command
Attn: AMSMO-R
Center Line, Michigan

Commanding Officer
Ordnance Materials
Research Office
Watertown Arsenal
Watertown 72, Mass.

Commanding General
Aberdeen Proving Ground
Aberdeen Proving Ground, Maryland
Attn: Dr. R. Eichelberger (1)
Mr. M. Sultanoff (1)

ADDRESSEE

Commanding General
Frankford Arsenal
Attn: Library
Pitman-Dunn Laboratory Group
Philadelphia 37, Pa.

Commandant, Army War College
Attn: Library
Carlisle Barracks, Pa.

Chief of Naval Research
Reports Branch (Code 530)
Department of the Navy
Washington 25, D. C.

U. S. Naval Weapons Station
Attn: Mr. Ernest Mason
Yorktown, Virginia

U. S. Naval Weapons Laboratory
Attn: Mr. Peter Altman
Dahlgren, Virginia

Commander
U. S. Naval Ordnance Test Station
China Lake, California
Attn: Tech Library Branch (1)
Dr. H. D. Mallory (1)
Dr. T. B. Joyner (1)

Research and Development Dept.
Naval Propellant Plant
Indian Head, Maryland
Attn: Library (1)
Dr. Mae I. Fauth (1)

Commander
U. S. Naval Ordnance Laboratory
White Oak, Silver Spring, Md.
Attn: Library (1)
Dr. James Ablard (1)
Dr. Carl T. Zovko (1)

Director, Naval Research Lab.
Attn: Code 2021
Washington 25, D. C.

ADDRESSEE

Director
Diamond Ordnance Fuse Laboratories
Washington 25, D. C.

Bureau of Naval Weapons
Attn: Mr. Charles B. Blank
Code RMMP-223
Washington 25, D. C.

Chief
AFSC-Scientific & Technical
Liaison Office
Attn: Mr. W. I. Grieve
c/o Department of the Navy
Room 2305, Munitions Bldg
Washington 25, D. C.

Commander in Chief
Strategic Air Command
Attn: DM7D1
Offutt Air Force Base, Nebraska

United States Air Force
Attn: Mr. Fred E. Howard, Jr.
No. 4 ASD, ASQP/67-3220
Eglin Air Force Base, Florida

Air Force Office of Scientific
Research
Attn: M. Swerdlow
Solid State Sciences Division
Washington 25, D. C.

Lawrence Radiation Laboratory
Attn: Dr. Roger Anderson
Livermore, California

Bureau of Mines
Attn: Mr. M. Bowser
Pittsburgh, Pa.

Westinghouse Electric Corporation
Attn: Dr. Dickron Mergerian
Air Arm Division
Mail Stop 308
Baltimore 3, Maryland

ADDRESSEE

Brookhaven National Laboratory
Attn: Dr. Paul W. Levy
Upton, Long Island, New York

U. S. Army R&D Liaison Group
Europe (9851 DU)
Attn: Dr. Bernard Stein
APO 757
New York, New York

U. S. Army Research Office
(DURHAM)

Box CM, Duke Station
Durham, North Carolina
Attn: Dr. R. G. Ghirardelli (1)
Dr. George M. Wyman (1)
Dr. Herman Robl (1)

University of Kansas
Attn: Dr. Daniel S. Ling
Department of Physics
Lawrence, Kansas

University of Utah
Attn: Dr. M. A. Cook
Institute of Metals and
Explosives Research
Salt Lake City, Utah

The Engineer School Library
Building 270
Fort Belvoir, Va.

Tech Documents Center
USAERDL, Ft Belvoir, Va.

British Liaison Officer
USAERDL, Ft Belvoir, Va.

Canadian Liaison Officer
USAERDL, Ft Belvoir, Va.

Military Department
USAERDL, Ft Belvoir, Va.

Basic Research Group
USAERDL, Ft Belvoir, Va. (30 copies)

ADDRESSEE

U. S. Army Munitions Command
Dover, New Jersey
Attn: Library (1)
Dr. J. V. R. Kaufman (1)
Dr. V. R. Pai-Verneker (1)
Mr. L. H. Eriksen (1)
Mr. Paul L. Marinkas (1)
Mr. P. Townsend (1)
Dr. A. Forsyth (1)
Dr. P. J. Kemmey (1)
Dr. R. Manno (1)
Dr. H. J. Matsuguma (1)

University of South Dakota
Attn: Dr. Olen Kraus
Vermillion, South Dakota

Technical Library
USAERDL, Ft Belvoir, Va.

Dow Chemical Company
Attn: Dr. Frank M. Brower (1)
Dr. K. Terada (1)
Midland, Michigan

Combat Research Branch
Attn: F. B. Paca (1)
J. D. Dando (1)
USAERDL, Fort Belvoir, Va.

Combat Engineering Branch
Attn: Mr. V. M. Davis
USAERDL, Fort Belvoir, Va.

Dr. S. K. Deb
Applied Research Department
American Cyanamid Co.
Research Laboratories
1937 West Main Street
Stamford, Connecticut

Arkansas Polytechnic College
Attn: Dr. J. G. Dodd
Russellville, Arkansas

Far Infrared Branch
Attn: Dr. W. Elser
USAERDL, Ft Belvoir, Va.

ADDRESSEE

Dr. Howard Fisher
Aerojet General Corporation
11711 S. Woodruff Ave.
Downey, California

Dr. E. Gelerinter
Cornell University
Ithaca, New York

Dr. Gerald L. Glen
The Atlantic Refining Co.
Research & Development Dept.
500 South Ridgeway Ave.
Glenolden, Pa.

Dr. Marilyn Jacox
Dynamometer Building
Room 204
Conn. Ave. & Van Ness Sts., NW
Washington, D. C., 20234

Mr. Wilhelm Jorgensen
U. S. Army Research Office (Durham)
Box CM, Duke Station
Durham, North Carolina

Dr. H. P. Kallmann
New York University
100 Washington Square
New York 3, New York

Dr. Paul L. Kronick
Franklin Institute
Philadelphia, Pennsylvania

Deputy Commander
USAERDL, Fort Belvoir, Va.

Dr. Walter C. McCrone
McCrone Associates, Inc.
449 East 31st Street
Chicago 16, Illinois

Dr. Russell McGill
U. S. Naval Ordnance Laboratory
White Oak, Silver Spring, Md.

ADDRESSEE

Dr. M. Mizushima
PEC Corporation
Boulder, Colorado

Dr. R. M. Moriarty
Assistant Professor
Department of Chemistry
The Catholic University of America
620 Michigan Ave., N. E.
Washington 17, D. C.

Dr. Richard E. Norberg
Department of Physics
Washington University
St. Louis, Missouri

Dr. Y. Okamoto
New York University
College of Engineering
Research Division
University Heights
New York 53, New York

Mr. H. D. Poole
M/Research
Defense Research Staff
British Embassy
3100 Mass. Ave., N.W.
Washington 8, D. C.

Dr. Donald L. Seaton
Lawrence Radiation Laboratory
P. O. Box 808
Livermore, California

Mr. M. S. Silverstein
Chemistry Research Lab. 1330
Frankford Arsenal
Philadelphia, Pa., 19137

Combat Research Branch
Attn: Mr. H. J. Vandersluis
USAERDL, Fort Belvoir, Va.

ADDRESSEE

Dr. L. A. Veguilla-Berdecia
Department of Chemistry
Howard University
Washington, D. C.

Mr. Franklin E. Wawner
Texaco Experiment Inc.
Richmond, Virginia

Dr. A. J. Erbel
Dow Chemical Co.
Midland, Michigan

Dr. M. Blais
U. S. Army Munitions Command
Dover, New Jersey

Dr. H. M. Kenworthy
Aerojet-General Corporation
Downey, California

Dr. Frank A. Goss
Sandia Corporation
Albuquerque, New Mexico

Dr. Dolphus E. Milligan
Dynamometer Building
Room 204
Conn. Ave. & Van Ness Sts., NW
Washington, D. C., 20234

New York University
Attn: Dr. J. C. Goswami
Dr. W. Brenner
College of Engineering
Research Division
University Heights
New York 53, New York